Connectivity, Organization, and Network Coordination of the *Drosophila* Central Circadian Clock

by

Zepeng Yao

A dissertation submitted in partial fulfillment
of the requirements for the degree of
Doctor of Philosophy
(Molecular, Cellular and Developmental Biology)
in the University of Michigan
2016

Doctoral Committee:

Associate Professor Orie T. Shafer, Chair
Assistant Professor Sara J. Aton
Professor Daniel B. Forger
Professor John Y. Kuwada
Professor Haoxing Xu

DEDICATION

In Loving Memory of Grandma and Grandpa

ACKNOWLEDGEMENTS

First and foremost, I would like to express my deepest gratitude to my advisor, Dr. Orie Shafer. Orie is enthusiastic, patient, and fun. I am very fortunate to be one of his first students and have received lots of scientific training directly from him. Orie has given me tremendous freedom to explore my scientific interests and provided enormous support to my research throughout the years. Orie is very dedicated to the career development of his students. He spent countless hours helping with my presentations and editing my proposals and manuscripts. Working with Orie has always been exciting and rewarding.

I would also like to express my sincere gratitude to Dr. Rich Hume. I have collaborated with Rich on the electrophysiological characterization of clock neurons over the past two years. Rich taught me everything about electrophysiology from scratch. I am extremely fortunate again to have received training directly from him. Besides, Rich has given me lots of valuable advice on my research as well as my future career.

In addition, I would like to thank all of my committee members, Dr. John Kuwada, Dr. Haoxing Xu, Dr. Sara Aton, and Dr. Daniel Forger for their support, critiques, and insightful discussions on my thesis research. Special thanks to Sara for the millions of reference letters she has written for me over the years.

My sincere thanks go to every current and former member of the Shafer Lab. I would like to specially thank Katie Lelito, Ann Marie Macara, and Tamara Minosyan for collaborating on the neural circuit analysis project, my first research project in the Shafer Lab. I thank Amy

Bennett for working closely with me over the past few years and for her assistance on my research. I thank Qi Zhang, Charles “Andy” Williams, Aaron Talsma, Andrew Bahl, Bronson Gregory, Veronica Varela, and Swathi Yadlapalli for their friendship and helpful discussions. I thank the many technicians, programmers, and undergraduates who are working and have worked in the lab for technical assistance, especially Rebecca Mudri, Harper Jocque, Claire Palmarini, and Jonte Jones.

I thank the numerous colleagues for reagents and advice. I thank members of the Neurobiology Joint Lab Meeting for fun and intense scientific discussions. I thank the Scott Pletcher Lab for long-term collaboration. In addition, I thank Dr. Laura Olsen, Dr. Steven Clark, Dr. Daniel Klionsky, Dr. Anuj Kumar, Dr. John Schiefelbein, and Dr. Cunming Duan among others for their help with my Ph.D. studies. I also greatly appreciate all the help from Mary Carr, Diane Durfy, and other MCDB staff.

To all of my friends here at University of Michigan and all around the world: Thank you for your friendship, your support, and all the fun we had! I would also like to thank all of my teachers and mentors throughout my life. I am indebted to my parents, my sister, and other family members for their unconditional love and support. Last but not least, I thank my loving wife, Meiyan Jin, for everything that cannot be fully accounted for with words. She is the sunshine of my life.

PREFACE

This thesis describes the research I conducted in Dr. Orie T. Shafer's lab, which began in January 2011. The objective of my work was to better understand the neuronal connectivity, organizing principles, and mechanisms of network coordination of circadian clock neuron networks.

Chapter 2 was published in *Journal of Neurophysiology* (2012; 108(2):684-96), with author listed as Zepeng Yao (Z.Y.), Ann Marie Macara (A.M.M.), Katherine R. Lelito (K.R.L), Tamara Y. Minosyan (T.Y.M.), and Orie T. Shafer (O.T.S.). Z.Y., A.M.M, and K.R.L were co-first authors. Z.Y., A.M.M., K.R.L., T.Y.M., and O.T.S. designed the research; Z.Y., A.M.M., K.R.L., and T.Y.M. performed experiments; Z.Y., A.M.M., K.R.L., and T.Y.M. analyzed data; Z.Y., A.M.M., K.R.L., T.Y.M., and O.T.S. interpreted results of experiments; Z.Y., A.M.M., and K.R.L. prepared figures; Z.Y., A.M.M., K.R.L., and O.T.S. drafted manuscript; O.T.S. edited and revised manuscript; O.T.S. approved final version of manuscript. Z.Y. specifically generated the data for Figures 2.3, 2.5 and 2.7.

Chapter 3 has not yet been published. A manuscript comprising this chapter is in preparation for publication, with authors listed as Zepeng Yao (Z.Y.), Richard I. Hume (R.I.H.), and Orie T. Shafer (O.T.S.). Z.Y., R.I.H., and O.T.S. designed the research; Z.Y. performed experiments and analyzed data; Z.Y., R.I.H., and O.T.S. interpreted results of experiments; Z.Y. and O.T.S. wrote the manuscript.

Chapter 4 was published in *Science* (2014; 343(6178):1516-20), with authors listed as Zepeng Yao (Z.Y.) and Orie T. Shafer (O.T.S.). Z.Y. and O.T.S. designed the research; Z.Y. performed experiments and analyzed data; Z.Y. and O.T.S. interpreted results of experiments; Z.Y. and O.T.S. wrote the paper.

Chapter 5 has not yet been published. A manuscript comprising this chapter is in preparation for publication, with authors listed as Zepeng Yao (Z.Y.), Amelia J. Bennett (A.J.B.), Jenna L. Clem (J.L.C.), and Orie T. Shafer (O.T.S.). Z.Y. and O.T.S. designed the study. Z.Y. conducted all the experiments. A.J.B. analyzed the phase of activity peaks in light/dark cycles for individual flies; J.C. quantified the PER immunostaining intensity of the CRY^{+} $DN1_{p}$s; Z.Y. performed the remaining analyses. Z.Y. and O.T.S. wrote the paper.

TABLE OF CONTENTS

LIST OF TABLES

LIST OF FIGURES

ABSTRACT

Daily rhythms in behavior and physiology are orchestrated by a network of circadian clock neurons. Neuronal connections within this network produce coherence and robustness in circadian timekeeping that are uncharacteristic of rhythms driven by isolated neurons or non-neuronal clocks. Using *Drosophila* as a simple yet conserved model system, my thesis research aims to understand how clock neurons are physiologically connected and how their molecular oscillations are coordinated to produce coherent circadian rhythms.

I have developed an experimental approach to address functional connectivity in the fly brain that combines chemogenetic excitation of neurons of interest with simultaneous monitoring of potential postsynaptic physiology with genetically encoded fluorescent sensors. Using this method, I have mapped connections in the clock network mediated by the critical neuropeptide Pigment-Dispersing Factor. In addition, I have performed *ex vivo* patch-clamp recordings of the fly clock neurons and provided the first electrophysiological characterization of the dorsal lateral neurons (LN_ds), which constitute the so-called Evening Oscillator of the clock network. I find that the neuronal activity of LN_ds is modulated by multiple fast neurotransmitters, and that a group of dorsal clock neurons provides inhibitory synaptic input onto the LN_ds. Lastly, using genetic and behavioral approaches, I find that while GABAergic inhibition of the clock network functions to promote sleep at night, glutamatergic inhibition of the clock network functions to promote wakefulness during the day.

To study how the molecular rhythms of clock neurons are coordinated, I have genetically sped-up or slowed-down the molecular clock in specific subsets of clock neurons and determined how such manipulations affect the molecular oscillations in un-manipulated clock neuron classes and sleep/activity rhythms. I find that the various groups of clock neurons do not display uniform modes of coupling. Rather, they display unique and complex coupling relationships that vary from group to group. In contrast to the widely accepted "Master Pacemaker" model that had dominated the field for more than a decade, my results show that the clock network consists of multiple independent oscillators, each of which is unified by its neuropeptide output. Finally, I find that robust circadian rhythms require coherence of molecular clocks across a much larger proportion of the clock network than previously thought.

Collectively, my thesis research greatly advances our understanding of how the circadian clock neuron network is wired and how it is organized and coordinated.

CHAPTER 1. Introduction

1.1 Circadian clocks

Almost every living organism on this planet has an endogenous timing system, the so-called circadian clock, to help anticipate and adapt to the daily cycle of day and night (Moore-Ede et al., 1982). This endogenous clock orchestrates daily rhythms in physiology, metabolism, and various behaviors. In many animals, including humans, the master clock resides in the brain and consists of a network of so-called clock neurons, each of which contains a molecular clock that generates oscillations in gene expression with a period of approximately 24 hours (Herzog, 2007). Neuronal connections within this network allow clock neurons to coordinate their molecular clocks and produce coherent and robust circadian rhythms that are uncharacteristic of rhythms driven by isolated clock neurons or non-neuronal clocks (Welsh et al., 2010). A major interest in the field is to understand how clock neurons are physiologically connected and how their molecular oscillations are functionally coordinated.

1.2 *Drosophila* offers an excellent model for the study of circadian clocks

The fruit fly, *Drosophila melanogaster*, has proved an excellent model for the study of circadian clocks due to its genetic accessibility and relative simplicity. *Drosophila* displays robust circadian rhythms in activity and rest. Under 12h:12h light:dark cycles, *Drosophila* displays a characteristic bimodal pattern of activity centered around dawn and dusk, and is

relatively inactive in the middle of the day and throughout the night (Fig. 1.1). The rest state of *Drosophila* shares the core characteristics of mammalian sleep, including increased arousal threshold and the presence of homeostatic regulation among others (Hendricks et al., 2000; Shaw et al., 2000; Huber et al., 2004). Genetic studies in *Drosophila* have identified many of the molecular clock components and led to a transcription/translation feedback loop model of the molecular clock, which is conserved across a wide spectrum of species (reviewed by Dunlap, 1999). A brief introduction of the molecular clock will be given in Section 1.3. In addition, the clock neurons in the fly central brain have been mapped out. The anatomy and neurochemistry of clock neurons will be introduced in Section 1.4. Current models of the clock network function will be discussed in Section 1.5.

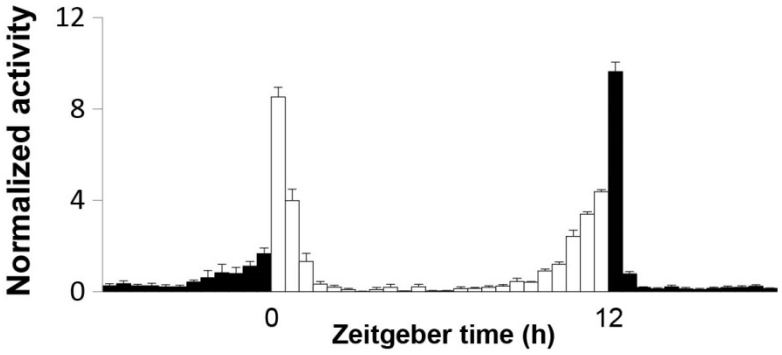

Figure 1.1. Population average activity profile of wild type Canton-S flies.
A population average activity profile (also known as an "eduction plot") of wild type Canton-S flies (n=32) under a 12h:12h light:dark cycle. Zeitgeber time (ZT) 0 indicates the time of lights-on, and ZT12 indicates the time of lights-off. Note that there is an increase of activity levels before lights-on and before lights-off, which are referred to as morning anticipation and evening anticipation, respectively.

1.3 Molecular clocks

Many components of the molecular clock are conserved between flies and mammals (reviewed by Yu and Hardin, 2006). The core components of the *Drosophila* molecular clock include CLOCK (CLK), CYCLE (CYC), PERIOD (PER), and TIMELESS (TIM), which constitute a transcription/translation feedback loop (Fig. 1.2) (reviewed by Hardin, 2011). In brief, heterodimers of CLK and CYC bind to the E-box elements (canonically 5'-CACGTG-3') in the *per* and *tim* promoters and promote the transcription of *per* and *tim* (Hao et al., 1997; Allada et al., 1998; Darlington et al., 1998; Rutila et al., 1998; McDonald et al., 2001; Wang et al., 2001). PER and TIM proteins accumulate in the cytoplasm, later translocate into the nucleus (Vosshall et al., 1994; Curtin et al., 1995; Saez and Young, 1996; Shafer et al., 2002; Meyer et al., 2006) where they act to suppress CLK/CYC function (Lee et al., 1998, 1999; Bae et al., 2000). The cytoplasmic accumulation of PER is delayed by DOUBLETIME (DBT), which phosphorylates PER and targets PER for degradation, whereas it is facilitated by TIM, which stabilizes PER–DBT complexes and enables the accumulation of DBT–PER–TIM complexes in the cytoplasm (Kloss et al., 1998, 2001; Price et al., 1998). Nuclear translocation of PER and TIM is promoted by phosphorylation of PER by CASEIN KINASE 2 (CK2) (Lin et al., 2002; Akten et al., 2003) and phosphorylation of TIM by SHAGGY (SGG) (Martinek et al., 2001). Overall, the negative feedback of PER and TIM on their own transcription results in oscillations in the abundance of their mRNAs and proteins with a period of approximately 24 hours (Hardin et al., 1990; Sehgal et al., 1995).

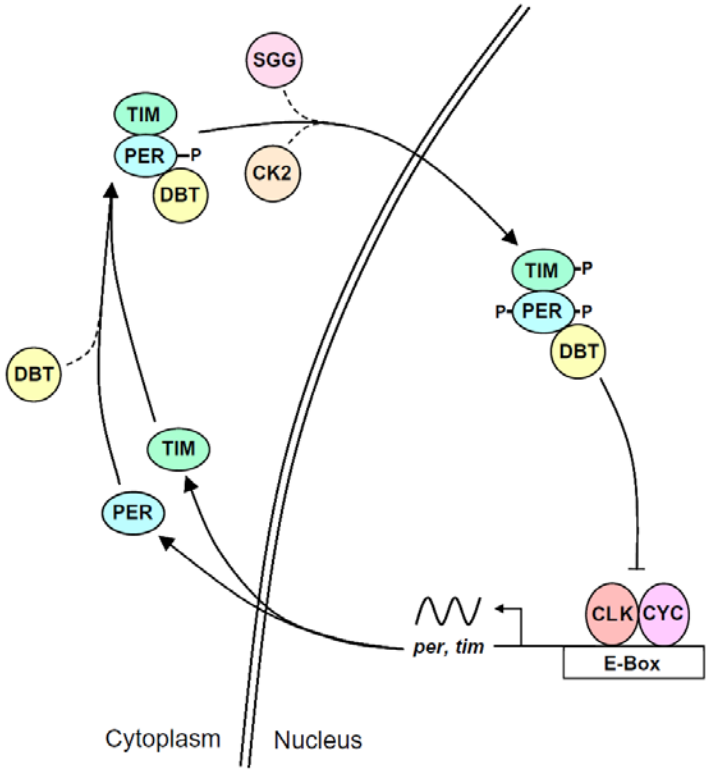

Figure 1.2. The core feedback loop of the *Drosophila* molecular clock.
All the genes, regulatory elements, and proteins are defined in the text. "P" represents phosphorylation site(s). See text for details. This figure is reprinted from *Adv. Genet.* 74. Hardin, P.E., Molecular genetic analysis of circadian timekeeping in *Drosophila*. 141–173. Copyright (2011), with permission from Elsevier.

1.4 Anatomy and neurochemistry of the *Drosophila* clock neuron network

The neuroanatomy of the *Drosophila* clock neuron network has been relatively well characterized. There are approximately 150 clock neurons in the adult fly brain, radically fewer than the tens of thousands of neurons in the mammalian clock centers (Herzog, 2007). Despite its relative simplicity, the fly clock neuron network shares both anatomical and functional similarities with that of mammals (Helfrich-Förster, 2004; Vansteensel et al., 2008). The fly's clock neurons are divided into nine groups based on their anatomy: (1) four pairs of large ventral

lateral neurons (l-LN_vs); (2) four pairs of small ventral lateral neurons (s-LN_vs); (3) one pair of so-called fifth small ventral lateral neurons (5^{th} s-LN_vs); (4) six pairs of dorsal lateral neurons (LN_ds); (5) two pairs of anterior dorsal neurons group 1 ($DN1_a$s); (6) ~15 pairs of posterior dorsal neurons group 1 ($DN1_p$s); (7) two pairs of dorsal neurons group 2 (DN2s); (8) ~40 pairs of dorsal neurons group 3 (DN3s); and (9) three to four pairs of lateral posterior neurons (LPNs) (Fig. 1.3) (Kaneko and Hall, 2000; Shafer et al., 2006). Most of the clock neurons send projections to the dorsal protocerebrum, with a notable exception of the l-LN_vs, which send a network of fibers onto the surface of the medulla and also project contralaterally to the opposite brain hemisphere (reviewed by Helfrich-Förster, 2005). The $DN1_a$s and subsets of the LN_ds, $DN1_p$s, and DN3s have additional projections towards the accessory medulla, where the l-LN_vs and s-LN_vs are located (Kaneko and Hall, 2000; Helfrich-Förster, 2005; Shafer et al., 2006; Helfrich-Förster et al., 2007). The extensive overlap of their neurites suggests that the various classes of clock neurons may be interconnected. However, the physiological connectivity within the clock neuron network remains largely uncharacterized.

The clock neurons are remarkably heterogeneous in their neurochemistry. Pigment-dispersing factor (PDF), a neuropeptide that is critical for circadian rhythms in locomotor activity, is expressed exclusively by the l-LN_vs and the s-LN_vs (together called the LN_vs) in the central brain (Fig. 1.4) (Helfrich-Förster, 1995; Renn et al., 1999). The receptor for PDF (PDFR) is expressed by about half of the clock neurons, most of which co-express a deep-brain blue light photoreceptor Cryptochrome (CRY) (Fig. 1.4a) (Yoshii et al., 2008; Im and Taghert, 2010; Im et al., 2011). Many neuropeptides are expressed in the clock network in addition to PDF, including neuropeptide F (NFP), short neuropeptide F (sNPF), ion transport peptide (ITP), and IPNamide (IPNa), each of which is expressed by only a small number of clock neurons (Fig. 1.4b)

(reviewed by Hermann-Luibl and Helfrich-Förster, 2015). The 5th s-LN$_v$ and subsets of the LN$_d$s cholinergic (Johard et al., 2009), while some DN1s and DN3s are glutamatergic (Hamasaka et al., 2007) (Fig. 1.4b). This remarkable heterogeneity in neuroanatomy and neurochemistry suggests that the various clock neurons play distinct and diverse roles in the control of circadian rhythms.

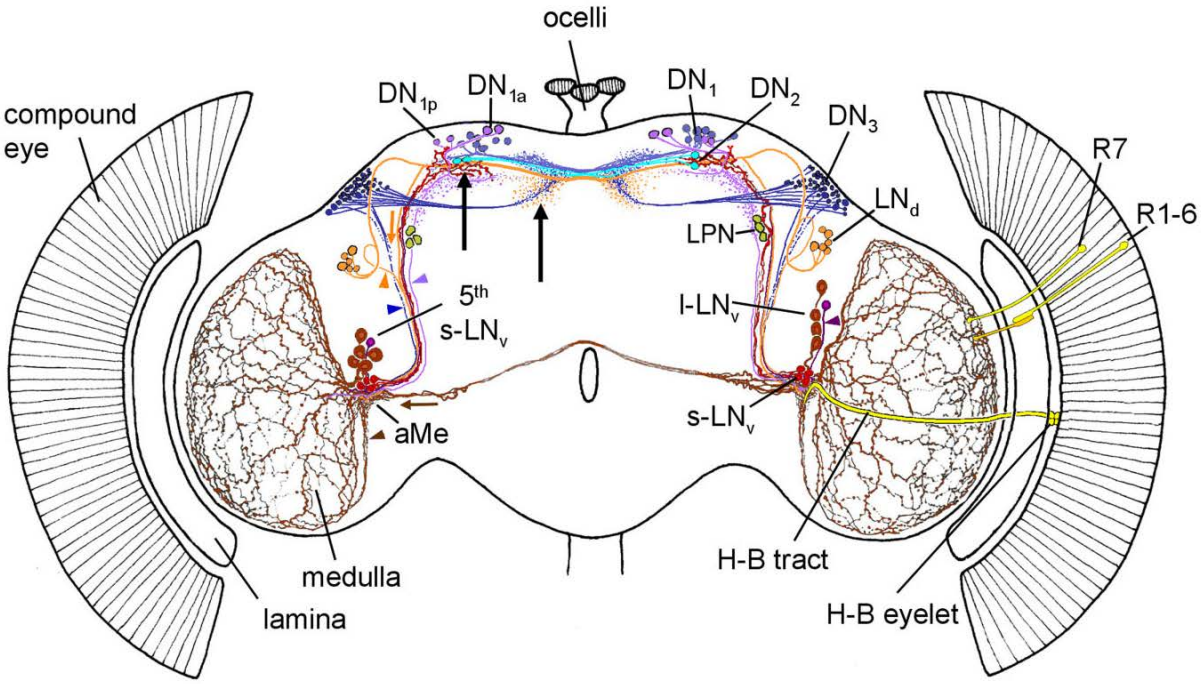

Figure 1.3. A schematic of the clock neurons and their projections in the adult fly brain. The various classes of clock neurons are described in the text and labeled in the schematic. The projections of each clock neuron class are depicted in the same color as their soma. The LPN projections have not been described. aMe, accessory medulla. See text for details. The figure is reprinted from Helfrich-Förster, C., Shafer, O.T., Wülbeck, C., Grieshaber, E., Rieger, D., and Taghert, P. (2007). Development and morphology of the clock-gene-expressing lateral neurons of *Drosophila melanogaster*. *J. Comp. Neurol.* 500, 47–70, with permission from John Wiley and Sons.

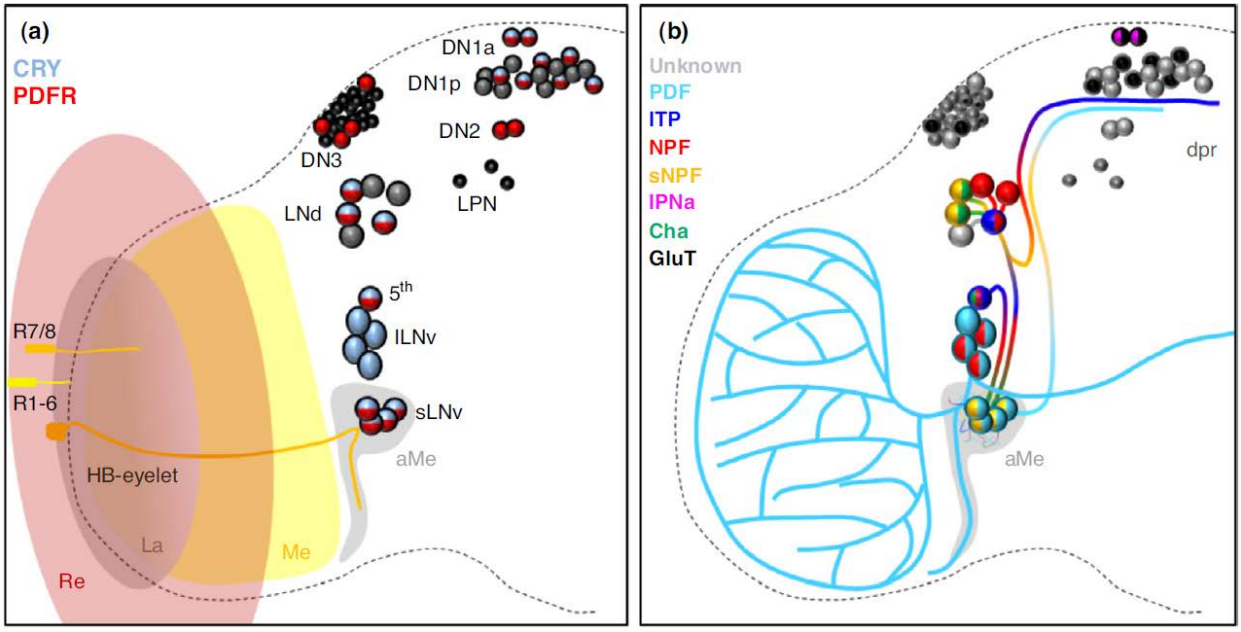

Figure 1.4. Neurochemistry of the *Drosophila* clock neuron network.
(**a**) A schematic of the expression patterns of Cryptochrome (CRY) and PDF receptor (PDFR) within the clock neuron network. Note that CRY and PDFR are co-expressed by many clock neurons. Re, retina; La, lamina; Me, medulla; aMe, accessory medulla. (**b**) A schematic of the expression of neuropeptides and neurotransmitters by the various clock neurons. PDF, pigment-dispersing factor; ITP, ion transport peptide; NPF, neuropeptide F; sNPF, short neuropeptide F; IPNa, IPNamide. The expression of choline acetyltransferase (Cha) and vesicular glutamate transporter (GluT) indicates the presence of acetylcholine and glutamate, respectively. dpr, dorsal protocerebrum. This figure is reprinted from *Curr. Opin. Insect Sci.* 7. Hermann-Luibl, C., and Helfrich-Förster, C. Clock network in *Drosophila*. 65–70. Copyright (2015), with permission from Elsevier.

1.5 Models of the *Drosophila* clock neuron network function

Studies employing cell ablation and mosaic genetic rescue approaches have suggested a dual-oscillator model of the *Drosophila* clock network function: The LN_vs function collectively as a "morning oscillator" that promotes activity around dawn, whereas the LN_ds and the 5^{th} s-LN_v function collectively as an "evening oscillator" that promotes activity around dusk (Grima et al., 2004; Stoleru et al., 2004). The LN_vs are essential for robust circadian timekeeping in the

absence of environmental cues (Renn et al., 1999), and are thought to be the dominant pacemaker of the clock network under short-day conditions and constant darkness (Stoleru et al., 2005, 2007). In contrast, it is thought that light activates output from the LN_ds/5^{th} s-LN_v, and these neurons become the dominant pacemaker under long-day conditions and constant light (Picot et al., 2007; Stoleru et al., 2007). This dual-oscillator model provides a powerful and elegant model for the functional division of the clock neuron network and the adaptation of the clock neuron network to day-length changes, but it does not account for many experimental observations (discussed by Yoshii et al., 2012).

In addition to the lateral clock neurons, recent work has highlighted the importance of another group of clock neurons, the $DN1_p$s. $DN1_p$s are capable of driving activity rhythms in the presence of light (Murad et al., 2007), and can promote activity both around dawn and dusk depending on the specific light and temperature conditions (Fujii and Amrein, 2010; Zhang et al., 2010a, 2010b). Furthermore, the $DN1_p$s have been implicated as key output neurons of the clock network in the control of activity and sleep rhythms (Cavanaugh et al., 2014; Kunst et al., 2014).

1.6 References

Akten, B., Jauch, E., Genova, G.K., Kim, E.Y., Edery, I., Raabe, T., and Jackson, F.R. (2003). A role for CK2 in the Drosophila circadian oscillator. Nat. Neurosci. *6*, 251–257.

Allada, R., White, N.E., So, W.V., Hall, J.C., and Rosbash, M. (1998). A mutant Drosophila homolog of mammalian clock disrupts circadian rhythms and transcription of period and timeless. Cell *93*, 791–804.

Bae, K., Lee, C., Hardin, P.E., and Edery, I. (2000). dCLOCK is present in limiting amounts and likely mediates daily interactions between the dCLOCK-CYC transcription factor and the PER-TIM complex. J. Neurosci. *20*, 1746–1753.

Cavanaugh, D.J., Geratowski, J.D., Wooltorton, J.R.A., Spaethling, J.M., Hector, C.E., Zheng, X., Johnson, E.C., Eberwine, J.H., and Sehgal, A. (2014). Identification of a circadian output circuit for rest: Activity rhythms in drosophila. Cell *157*, 689–701.

Curtin, K.D., Huang, Z.J., and Rosbash, M. (1995). Temporally regulated nuclear entry of the Drosophila period protein contributes to the circadian clock. Neuron *14*, 365–372.

Darlington, T.K., Wager-Smith, K., Ceriani, M.F., Staknis, D., Gekakis, N., Steeves, T.D., Weitz, C.J., Takahashi, J.S., and Kay, S.A. (1998). Closing the circadian loop: CLOCK-induced transcription of its own inhibitors per and tim. Science *280*, 1599–1603.

Dunlap, J.C. (1999). Molecular bases for circadian clocks. Cell *96*, 271–290.

Fujii, S., and Amrein, H. (2010). Ventral lateral and DN1 clock neurons mediate distinct properties of male sex drive rhythm in Drosophila. Proc. Natl. Acad. Sci. U. S. A. *107*, 10590–10595.

Grima, B., Chélot, E., Xia, R., and Rouyer, F. (2004). Morning and evening peaks of activity rely on different clock neurons of the Drosophila brain. Nature *431*, 869–873.

Hamasaka, Y., Rieger, D., Parmentier, M.-L., Grau, Y., Helfrich-Förster, C., and Nässel, D.R. (2007). Glutamate and its metabotropic receptor in Drosophila clock neuron circuits. J. Comp. Neurol. *505*, 32–45.

Hao, H., Allen, D.L., and Hardin, P.E. (1997). A circadian enhancer mediates PER-dependent mRNA cycling in Drosophila melanogaster. Mol. Cell. Biol. *17*, 3687–3693.

Hardin, P.E. (2011). Molecular genetic analysis of circadian timekeeping in Drosophila. Adv. Genet. *74*, 141–173.

Hardin, P.E., Hall, J.C., and Rosbash, M. (1990). Feedback of the Drosophila period gene product on circadian cycling of its messenger RNA levels. Nature *343*, 536–540.

Helfrich-Förster, C. (1995). The period clock gene is expressed in central nervous system neurons which also produce a neuropeptide that reveals the projections of circadian pacemaker cells within the brain of Drosophila melanogaster. Proc. Natl. Acad. Sci. U. S. A. *92*, 612–616.

Helfrich-Förster, C. (2004). The circadian clock in the brain: a structural and functional comparison between mammals and insects. J. Comp. Physiol. *190*, 601–613.

Helfrich-Förster, C. (2005). Neurobiology of the fruit fly's circadian clock. Genes. Brain. Behav. *4*, 65–76.

Helfrich-Förster, C., Shafer, O.T., Wülbeck, C., Grieshaber, E., Rieger, D., and Taghert, P. (2007). Development and morphology of the clock-gene-expressing lateral neurons of Drosophila melanogaster. J. Comp. Neurol. *500*, 47–70.

Hendricks, J.C., Finn, S.M., Panckeri, K. a, Chavkin, J., Williams, J. a, Sehgal, A., and Pack, A.I. (2000). Rest in Drosophila Is a Sleep-like State. Neuron *25*, 129–138.

Hermann-Luibl, C., and Helfrich-Förster, C. (2015). Clock network in Drosophila. Curr. Opin. Insect Sci. *7*, 65–70.

Herzog, E.D. (2007). Neurons and networks in daily rhythms. Nat. Rev. Neurosci. *8*, 790–802.

Huber, R., Hill, S.L., Holladay, C., Biesiadecki, M., Tononi, G., and Cirelli, C. (2004). Sleep homeostasis in Drosophila melanogaster. Sleep *27*, 628–639.

Im, S.H., and Taghert, P.H. (2010). PDF receptor expression reveals direct interactions between circadian oscillators in Drosophila. J. Comp. Neurol. *518*, 1925–1945.

Im, S.H., Li, W., and Taghert, P.H. (2011). PDFR and CRY signaling converge in a subset of clock neurons to modulate the amplitude and phase of circadian behavior in Drosophila. PLoS One *6*, e18974.

Johard, H.A.D., Yoishii, T., Dircksen, H., Cusumano, P., Rouyer, F., Helfrich-Förster, C., and Nässel, D.R. (2009). Peptidergic clock neurons in Drosophila: ion transport peptide and short neuropeptide F in subsets of dorsal and ventral lateral neurons. J. Comp. Neurol. *516*, 59–73.

Kaneko, M., and Hall, J.C. (2000). Neuroanatomy of cells expressing clock genes in Drosophila: transgenic manipulation of the period and timeless genes to mark the perikarya of circadian pacemaker neurons and their projections. J. Comp. Neurol. *422*, 66–94.

Kloss, B., Price, J.L., Saez, L., Blau, J., Rothenfluh, A., Wesley, C.S., and Young, M.W. (1998). The Drosophila clock gene double-time encodes a protein closely related to human casein kinase Iepsilon. Cell *94*, 97–107.

Kloss, B., Rothenfluh, A., Young, M.W., and Saez, L. (2001). Phosphorylation of PERIOD is influenced by cycling physical associations of DOUBLE-TIME, PERIOD, and TIMELESS in the Drosophila clock. Neuron *30*, 699–706.

Kunst, M., Hughes, M.E., Raccuglia, D., Felix, M., Li, M., Barnett, G., Duah, J., and Nitabach, M.N. (2014). Calcitonin gene-related peptide neurons mediate sleep-specific circadian output in Drosophila. Curr. Biol. *24*, 2652–2664.

Lee, C., Bae, K., and Edery, I. (1998). The Drosophila CLOCK protein undergoes daily rhythms in abundance, phosphorylation, and interactions with the PER-TIM complex. Neuron *21*, 857–867.

Lee, C., Bae, K., and Edery, I. (1999). PER and TIM inhibit the DNA binding activity of a Drosophila CLOCK-CYC/dBMAL1 heterodimer without disrupting formation of the heterodimer: a basis for circadian transcription. Mol. Cell. Biol. *19*, 5316–5325.

Lin, J.-M., Kilman, V.L., Keegan, K., Paddock, B., Emery-Le, M., Rosbash, M., and Allada, R. (2002). A role for casein kinase 2alpha in the Drosophila circadian clock. Nature *420*, 816–820.

Martinek, S., Inonog, S., Manoukian, a S., and Young, M.W. (2001). A role for the segment polarity gene shaggy/GSK-3 in the Drosophila circadian clock. Cell *105*, 769–779.

McDonald, M.J., Rosbash, M., and Emery, P. (2001). Wild-type circadian rhythmicity is dependent on closely spaced E boxes in the Drosophila timeless promoter. Mol. Cell. Biol. *21*, 1207–1217.

Meyer, P., Saez, L., and Young, M.W. (2006). PER-TIM interactions in living Drosophila cells: an interval timer for the circadian clock. Science *311*, 226–229.

Moore-Ede, M.C., Sulzman, F.M., and Fuller, C.A. (1982). The clocks that time us: physiology of the circadian timing system (Harvard University Press).

Murad, A., Emery-Le, M., and Emery, P. (2007). A subset of dorsal neurons modulates circadian behavior and light responses in Drosophila. Neuron *53*, 689–701.

Picot, M., Cusumano, P., Klarsfeld, A., Ueda, R., and Rouyer, F. (2007). Light activates output from evening neurons and inhibits output from morning neurons in the Drosophila circadian clock. PLoS Biol. *5*, 2513–2521.

Price, J.L., Blau, J., Rothenfluh, a, Abodeely, M., Kloss, B., and Young, M.W. (1998). double-time is a novel Drosophila clock gene that regulates PERIOD protein accumulation. Cell *94*, 83–95.

Renn, S.C., Park, J.H., Rosbash, M., Hall, J.C., and Taghert, P.H. (1999). A pdf neuropeptide gene mutation and ablation of PDF neurons each cause severe abnormalities of behavioral circadian rhythms in Drosophila. Cell *99*, 791–802.

Rutila, J.E., Suri, V., Le, M., So, W.V., Rosbash, M., and Hall, J.C. (1998). Cycle is a second bHLH-PAS clock protein essential for circadian rhythmicity and transcription of Drosophila period and timeless. Cell *93*, 805–814.

Saez, L., and Young, M.W. (1996). Regulation of nuclear entry of the Drosophila clock proteins period and timeless. Neuron *17*, 911–920.

Sehgal, A., Rothenfluh-Hilfiker, A., Hunter-Ensor, M., Chen, Y., Myers, M.P., and Young, M.W. (1995). Rhythmic expression of timeless: a basis for promoting circadian cycles in period gene autoregulation. Science *270*, 808–810.

Shafer, O.T., Rosbash, M., and Truman, J.W. (2002). Sequential nuclear accumulation of the clock proteins period and timeless in the pacemaker neurons of Drosophila melanogaster. J. Neurosci. *22*, 5946–5954.

Shafer, O.T., Helfrich-Förster, C., Renn, S.C.P., and Taghert, P.H. (2006). Reevaluation of Drosophila melanogaster's neuronal circadian pacemakers reveals new neuronal classes. J. Comp. Neurol. *498*, 180–193.

Shaw, P.J., Cirelli, C., Greenspan, R.J., and Tononi, G. (2000). Correlates of sleep and waking in Drosophila melanogaster. Science *287*, 1834–1837.

Stoleru, D., Peng, Y., Agosto, J., and Rosbash, M. (2004). Coupled oscillators control morning and evening locomotor behaviour of Drosophila. Nature *431*, 862–868.

Stoleru, D., Peng, Y., Nawathean, P., and Rosbash, M. (2005). A resetting signal between Drosophila pacemakers synchronizes morning and evening activity. Nature *438*, 238–242.

Stoleru, D., Nawathean, P., Fernández, M.D.L.P., Menet, J.S., Ceriani, M.F., and Rosbash, M. (2007). The Drosophila circadian network is a seasonal timer. Cell *129*, 207–219.

Vansteensel, M.J., Michel, S., and Meijer, J.H. (2008). Organization of cell and tissue circadian pacemakers: A comparison among species. Brain Res. Rev. *58*, 18–47.

Vosshall, L.B., Price, J.L., Sehgal, A., Saez, L., and Young, M.W. (1994). Block in nuclear localization of period protein by a second clock mutation, timeless. Science *263*, 1606–1609.

Wang, G.K., Ousley, A., Darlington, T.K., Chen, D., Chen, Y., Fu, W., Hickman, L.J., Kay, S.A., and Sehgal, A. (2001). Regulation of the cycling of timeless (tim) RNA. J. Neurobiol. *47*, 161–175.

Welsh, D.K., Takahashi, J.S., and Kay, S.A. (2010). Suprachiasmatic nucleus: cell autonomy and network properties. Annu. Rev. Physiol. *72*, 551–577.

Yoshii, T., Todo, T., Wülbeck, C., Stanewsky, R., and Helfrich-Förster, C. (2008). Cryptochrome is present in the compound eyes and a subset of Drosophila's clock neurons. J. Comp. Neurol. *508*, 952–966.

Yoshii, T., Rieger, D., and Helfrich-Förster, C. (2012). Two clocks in the brain: an update of the morning and evening oscillator model in Drosophila. Prog. Brain Res. *199*, 59–82.

Yu, W., and Hardin, P.E. (2006). Circadian oscillators of Drosophila and mammals. J. Cell Sci. *119*, 4793–4795.

Zhang, L., Chung, B.Y., Lear, B.C., Kilman, V.L., Liu, Y., Mahesh, G., Meissner, R.A., Hardin, P.E., and Allada, R. (2010a). DN1p Circadian Neurons Coordinate Acute Light and PDF Inputs to Produce Robust Daily Behavior in Drosophila. Curr. Biol. *20*, 591–599.

Zhang, Y., Liu, Y., Bilodeau-Wentworth, D., Hardin, P.E., and Emery, P. (2010b). Light and temperature control the contribution of specific DN1 neurons to Drosophila circadian behavior. Curr. Biol. *20*, 600–605.

CHAPTER 2. Analysis of functional neuronal connectivity in the *Drosophila* brain[1]

2.1 Abstract

Drosophila melanogaster is a valuable model system for the neural basis of complex behavior, but an inability to routinely interrogate physiologic connections within central neural networks of the fly brain remains a fundamental barrier to progress in the field. To address this problem, we have introduced a simple method of measuring functional connectivity based on the independent expression of the mammalian P2X2 purinoreceptor and genetically encoded Ca^{2+} and cAMP sensors within separate genetically defined subsets of neurons in the adult brain. We show that such independent expression is capable of specifically rendering defined sets of neurons excitable by pulses of bath-applied ATP in a manner compatible with high-resolution Ca^{2+} and cAMP imaging in putative follower neurons. Furthermore, we establish that this approach is sufficiently sensitive for the detection of excitatory and modulatory connections deep within larval and adult brains. This technically facile approach can now be used in wild-type and mutant genetic backgrounds to address functional connectivity within neuronal networks governing a wide range of complex behaviors in the fly. Furthermore, the effectiveness of this approach in the fly brain suggests that similar methods using appropriate heterologous receptors might be adopted for other widely used model systems.

[1] Originally published in *J Neurophysiol* 2012 Jul 15;108(2):684-96 doi: 10.1152/jn.00110.2012 with authors listed as Zepeng Yao*, Ann Marie Macara*, Katherine R. Lelito*, Tamara Y. Minosyan, and Orie T. Shafer (* denotes equal contribution).

2.2 Introduction

Despite its relative simplicity the nervous system of *Drosophila melanogaster* is capable of producing a remarkable repertoire of complex behaviors (Weiner 1999). Work on *Drosophila* has identified discrete networks of neurons that govern circadian timekeeping (Nitabach and Taghert 2008), courtship (Villella et al. 2008), memory (McGuire et al. 2005), sleep (Crocker and Sehgal 2010), feeding (Melcher et al. 2007), and decision-making (e.g., Dickson 2008; Peabody et al. 2009). The study of these and other neural networks in the fly continues to enrich and inform our understanding of the neural control of animal behavior. For many of these central brain networks the pattern and physiologic basis of their constituent connections have been proposed; however, due to the electrophysiologic inaccessibility of much of the fly CNS, many aspects of these network models remain unchallenged experimentally. The development of technically feasible methods to test for the presence and physiologic nature of connections between defined neuronal classes of the fly CNS will therefore be critical for progress in the field.

The ability to address the nature of connections between pairs of identified neurons has been one of the great strengths of large invertebrate model systems (Kandel 1976). The stereotyped and large neurons of these organisms are accessible to multiple recording and stimulating electrodes, making it possible to stimulate activity in a neuron of interest while measuring electrophysiologic responses in putative follower neurons (e.g., Kandel et al. 1967; Willows and Hoyle 1969; Fig. 2.1). Unfortunately, such multielectrode experiments are not feasible for most central neural networks of the *Drosophila*brain. The electrophysiologic inaccessibility of many central fly neurons has been surmounted somewhat by the use of genetically encoded sensors for neuronal excitation and second-messenger signaling (e.g.,

Lissandron et al. 2007; Ruta et al. 2010; Shafer et al. 2008; Tian et al. 2009; Tomchik and Davis 2009; Wang et al. 2003; Yu et al. 2003) and the physiologic responses of single deeply situated neurons can now be routinely observed in the fly brain using live imaging techniques. Combining these techniques with an ability to acutely activate subsets of neurons would allow for existing models of neural connectivity to be tested and the downstream targets of neurons of interest to be identified physiologically.

Several genetically encoded triggers of neural excitation have been successfully used in *Drosophila* in conjunction with various chemical or physical triggering methods (reviewed in Venken et al. 2011). The first instance of such triggering in the fly used the photochemical excitation of neurons expressing transgenic P2X2 receptor, a mammalian ATP receptor that is not encoded by the *Drosophila* genome (Lima and Miesenböck 2005; Littleton and Ganetzky 2000). The mammalian thermosensitive TRPV1 channel has been used to excite fly sensory neurons using its ligand capsaicin (Marella et al. 2006) and ectopic expression of the *Drosophila* thermosensitive TRPA1 channel has also been used to activate multiple neuron types with pulses of high temperature (e.g., Parisky et al. 2008). Furthermore, the mammalian cold-sensitive TRPM8 channel has been used with both low-temperature pulses and menthol vapor as exogenous excitation triggers in the fly (Peabody et al. 2009). Finally, several groups have used the bacterial opsin Channelrhodopsin-2 (ChR2) to trigger neuronal excitation in *Drosophila* with blue light (e.g., Pulver et al. 2009; Schroll et al. 2006; Zimmermann et al. 2009). The fact that ChR2 is maximally activated by blue wavelengths makes it problematic for use in live imaging experiments, since GFP-based sensors must be excited with the same wavelengths that activate opsin conductance (Guo et al. 2009). The recent development of red-shifted optogenetic controls (Yizhar et al. 2011) and Ca^{2+} sensors (Zhao et al. 2011) may

ultimately circumvent this problem, but these newly developed tools have not yet been successfully introduced to *Drosophila*. The use of temperature pulses to trigger the opening of TRPA1 or TRPM8 channels during live imaging experiments is also problematic, because acute shifts in temperature can cause significant movement of imaging targets within the explanted brain during high-resolution imaging, which makes the analysis of single-neuron somata difficult (Q. Zhang and O. Shafer, unpublished observations). For these reasons we have opted for ligand-gated triggering of transgenic receptors as a means for acute neuronal excitation. The feasibility of combining ATP excitation of P2X2-expressing fly neurons to attain biologically relevant neural excitation during behavioral and physiologic experiments has already been established for both larval and adult nervous systems (e.g., Hu et al. 2010; Lima and Miesenböck 2005). We have therefore chosen ATP/P2X2 excitation for use in our live imaging experiments.

In *Drosophila* the Gal4/UAS system is a powerful and versatile method of transgene expression that has been the tool of choice for directing sensor expression in specific neuronal classes within the fly brain (Brand and Perrimon 1993; Venken et al. 2011). The recent development of alternative binary expression systems, the LexA and Q systems (Lai and Lee 2006; Potter et al. 2010), now makes it possible to independently direct P2X2 and sensor expression within different neuronal classes. Here we have used the simultaneous use of the Gal4 and LexA systems for the independent dual binary expression of P2X2 and genetically encoded sensors of Ca^{2+} or cAMP, thereby allowing for the acute excitation of defined neuronal populations during the simultaneous live imaging of Ca^{2+} and cAMP dynamics within putative neuronal targets (Fig. 2.1).

Here we establish the feasibility of the simultaneous use of the GAL4 and LexA systems to render defined groups of neurons excitable by pulses of bath-applied ATP while

simultaneously and independently expressing the Ca^{2+} sensor GCaMP3.0 or the cAMP sensor Epac1-camps in putative follower neurons. We present proof of principle experiments that establish the efficacy of this method for detecting established and/or predicted excitatory and modulatory connections within larval and adult brains, concentrating on the well-characterized circadian clock neuron network of the fly (Nitabach and Taghert 2008), the constituent physiologic connections of which have remained largely unexamined. The *LexAop-P2X2*, *LexAop-GCaMP3.0*, and *LexAop-Epac1-camps* lines we have used for these studies, along with large and growing number of existing GAL4, UAS, and LexA lines, constitute a useful and technically facile toolkit for the interrogation of central neuronal networks in the *Drosophila* brain.

2.3 Methods

2.3.1 Fly stocks and rearing

Flies were reared on cornmeal-yeast-sucrose media at 25°C under a 12:12 light:dark cycle or under the diurnal conditions of the lab. All Gal4 and UAS lines used in this study have been previously described: *Pdf(M)-Gal4;; and ;Pdf(bmrj)-Gal4;* (Renn et al. 1999), *;UAS-GCaMP3.0;* (Tian et al. 2009), *;;UAS-P2X2*(Lima and Miesenböck 2005), ;;*Clock(4.1M)-Gal4* (Zhang et al. 2010a,b), ;*Clock(-856[8.2/2])-Gal4;* (Gummadova et al. 2009), *;c929-Gal4;* (Hewes et al. 2000), *;Rh6-Gal4;* (Pichaud and Desplan 2001), *;UAS-Epac1-camps(50A);* (Shafer and Taghert 2009), and *;Cha(7.4)-Gal4/CyO*; (Salvaterra and Kitamoto 2001). The *;Pdf-LexA;*line has also been described previously (Shang et al. 2008). The creation of the *LexAop-P2X2*, *LexAop-GCaMP3.0*, and *LexAop-Epac1-camps* lines is described in the

following text. Stable lines carrying combinations of these elements were created using standard *Drosophila* genetic techniques.

2.3.2 Creation of LexAop P2X2 and sensor lines

We used the LexA-response element containing pLOT vector (Lai and Lee 2006) for the creation of *LexAop-GCaM3.0*,*LexAop-Epac1-camps,* and *LexAop-P2X2* plasmids. GCaMP3.0 (Tian et al. 2009) was obtained in a pEGFP-N1 vector from Addgene (Cambridge, MA; plasmid # 22692) and digested with *Eag*I. The resulting GCaMP3.0-containing fragment was gel purified, digested with *Bgl*II, and subsequently PCR purified using a QIAquick PCR Purification Kit (Qiagen, Valencia, CA). In parallel, pLOT vector was digested with *Eag*I and *Bgl*II, and treated with CIP alkaline phosphatase (New England Biolabs, Ipswich, MA) following manufacturer's instructions. The GCaMP3.0 fragment was ligated with the linearized pLOT vector with a Quick Ligation Kit from New England Biolabs. Epac1-camps (Nikolaev et al. 2004) was sequentially digested from the pUAST-Epac1-camps plasmid (Shafer et al. 2008) using *Xho*I and *Bgl*II, and PCR purified. This Epac1-camps fragment was cloned into pLOT as above using sequential *Xho*I and *Bgl*II restriction digests of pLOT. The P2X2 trimer (Lima and Miesenböck 2005) was obtained as the Gateway entry clone pENTRA1_P2X2 from G. Miesenböck (Oxford University). We created a pLOT Gateway vector by cutting pLOT with KPN1, generating blunt ends using T4 DNA Polymerase (Invitrogen), and inserting the chloramphenicol/ccdB-resistant Gateway cassette A using T4 DNA Ligase following manufacturer's instructions (Invitrogen). We transformed OmniMAX 2T1R cells (Invitrogen) with the resulting pLOT-Gateway vector, selected ampicillin- and chloramphenicol-resistant clones for vector propagation, and purified the pLOT-Gateway vector using a Qiagen Mini Prep kit (Qiagen). The transfer of the P2X2 trimer from pENTRA1_P2X2 to the pLOT-Gateway

vector was accomplished via LR recombination reaction according to manufacturer's instructions (Invitrogen) using LR II clonase (Invitrogen).

All three LexAop plasmids were extracted and purified using a Qiagen Mini Prep kit. Purified plasmids were sent to Genetic Services, Inc. (Cambridge, MA), where they were injected into w^{1118} embryos. We isolated and mapped several independent transgenic lines for each LexAop element using standard fly genetic techniques. The specific lines used here were: *w;LexAop-GCaMP3.0(4B)*;, *w;LexAop-Epac1-camps(1A);*, *w;LexAop-P2X2(7);*, and *w;;LexAop-P2X2(1).*

2.3.3 Dissections, solutions, and test compound delivery

Flies were anesthetized on CO_2 and brains were dissected into room temperature hemolymph-like saline (HL3) consisting of (in mM): 70 NaCl, 5 KCl, 1.5 $CaCl_2$, 20 $MgCl_2$, 10 $NaHCO_3$, 5 trehalose, 115 sucrose, 5 HEPES; pH 7.1 (Stewart et al. 1994). For larval brain dissections, third instar (nonwandering) larvae were removed from the food and brains were dissected directly into HL3, keeping the eye disks and ventral nerve cord intact. Mouth hooks continued to move after dissections and were therefore removed to prevent brain movement during imaging experiments. All brains were allowed to adhere to the bottom of 35-mm FALCON culture dishes (Becton Dickenson Labware, Franklin Lakes, NJ) under a drop of HL3 contained within a petri dish insert (Bioscience Tools, San Diego, CA) for directing perfusion flow. Brains were imaged 5 to 10 min after dissection to allow for optimum baseline stabilization and settling of the brain to the dish. Perfusion flow was established over the brain with a gravity-fed PS-8H perfusion system (Bioscience Tools). Test compounds were delivered to mounted brains by switching perfusion flow from the main HL3 line to another channel containing diluted compound for desired durations followed by a return to HL3 flow. All test compounds were

dissolved in HL3. To control for the effects of switching channels, we perfused HL3 for 30 s from a second vehicle channel as a vehicle control. Adenosine 5[prime]-triphosphate disodium salt hydrate (ATP), guanosine 5[prime]-triphosphate disodium salt hydrate (GTP), and carbamoylcholine chloride (carbachol) were purchased from Sigma-Aldrich (St. Louis, MO).

2.3.4 Live imaging and analysis

Live imaging was performed using an Olympus FV1000 laser-scanning microscope (Olympus, Center Valley, PA) under a ×20 (0.50 N/A W, UMPlan FL N) or ×60 (1.10 N/A W, FUMFL N) objective (Olympus, Center Valley, PA). Regions of interest (ROIs) were selected over single neuronal somata or, in the case of Bolwig's nerve, over the length of a nerve. For GCaMP3.0 imaging experiments, frames were scanned with a 488-nm laser at 1—10 Hz for 5 min and GCaMP emission was directed to a photomultiplier tube by means of a DM405/488 dichroic mirror. Scanning frequencies for GCaMP3.0 imaging were kept constant within experiments, but varied between experiments. Experiments involving multiple neuronal classes demanded larger scanning areas and therefore lower scan rates. Epac1-camps FRET imaging was performed by scanning frames with a 440-nm laser at a frequency of 1 Hz for 5 min. CFP and YFP emission was separated by means of a SDM510 dichroic mirror.

For each neuron within an optical section, ROIs were drawn over somata using Fluoview software (Olympus). Raw intensity values for GCaMP3.0 emission or Epac1-camps CFP and YFP emission were recorded as mean pixel intensities (value range: 0—4,095) for each ROI at each time point and exported from Fluoview. Data transformations (see details in the following text) were conducted using custom software developed in Matlab (The MathWorks, Natick MA). For GCaMP3.0 experiments, raw intensity traces were filtered with a 10-point moving average to

remove high-frequency noise and then normalized to percentage fluorescence changes ($\Delta F/F_0$) using the following equation

$$((F_n - F_0) / F_0) \times 100\ \%$$

where F_n is a raw intensity value recorded at each point in time and F_0 is the baseline fluorescence value, calculated from the average of the raw intensity values in the first 10 s of recording from each trace. Maximum GCaMP3.0 fluorescence change values (max $\Delta F/F_0$) were determined as the maximum percentage change observed for each trace over the entire duration of each imaging experiment. Maximum values for each treatment and genotype were averaged to calculate the mean maximum change from baseline. To remove the direct excitatory effects of 488-nm light on Bolwig's Nerve (BN) (Yuan et al. 2011) from our analysis, which we observed during the start of a subset of our 488-nm scans, the F_0 for all larval BN experiments was calculated from the average fluorescent intensities observed during the 15 s preceding the stimulus onset, by which time the baseline GCaMP3.0 fluorescence had stabilized following the light-induced excitation of the nerve.

For Epac1-camps data processing, we corrected YPF intensity values for spillover from the CFP channel by the following equation

$$YFP_{SOC} = YFP - (CFP \times 0.444)$$

where YFP_{SOC} is the spillover—corrected YFP intensity, YFP and CFP are the raw intensity values, and 0.444 is the proportion of CFP emission that spills over into the YFP channel on our imaging system. The inverse FRET ratio, which is proportional to increases in cAMP, was calculated by taking the ratio of CFP/YFP_{SOC} at all time points for each ROI. Each ratio trace was filtered with a 10-point moving average. All spillover-corrected and filtered Epac1-camps inverse FRET traces were normalized to the first time point to an initial value of “1.0.” Filtered,

corrected, and normalized inverse FRET traces were expressed as percentage inverse FRET changes and averaged for each treatment and neuron type to create mean inverse FRET traces. The maximum percentage inverse FRET change was determined for every neuron based on the entire duration of the experiment. Such maximum inverse FRET changes were averaged for each treatment and neuron type to determine the mean maximum inverse FRET change. For most Epac1-camps inverse FRET traces, a spontaneous and gradual increase in inverse FRET was observed due to a slow photobleaching of YFP, as has been described previously for this sensor (Börner et al. 2011; Shafer et al. 2008). To correct for these spontaneous changes, we determined the mean inverse FRET increase for 10—20 untreated or vehicle treated neurons of a particular genotype, depending on the nature of the experiment. This mean trace was then subtracted from each individual experimental trace to generate corrected inverse FRET traces.

To statistically compare maximum changes in GCaMP3.0 fluorescence or Epac1-camps inverse FRET ratio between the vehicle and test compounds, we used a Kruskal—Wallis one-way ANOVA with a Dunn's multiple comparison test. Pairwise comparisons of maximum changes in GCaMP3.0 fluorescence or inverse Epac1-camps FRET in response to test compound or vehicle perfusion were made using the Mann—Whitney *U* test. All plots and statistical tests were generated and performed using Prism 5 (GraphPad, San Diego CA). Figures were constructed in Adobe Illustrator and Photoshop (Adobe Systems, San Jose, CA). To obtain intensity-mapped images representing select time points before, during, and after ATP/P2X2 stimulation, single frames were captured from intensity-mapped still images using Fluoview. These images were imported to Photoshop (Adobe Systems, San Diego CA), and trimmed to size.

2.4 Results

2.4.1 Controlled excitation of P2X2-expressing deep brain neurons with perfused ATP is compatible with high-resolution live imaging.

Previous work has established that neurons expressing transgenic P2X2 receptor in *Drosophila* can be excited at biologically relevant levels through the global uncaging of ATP in freely moving flies (Lima and Miesenböck 2005) or through the puffing of ATP on explanted brains during electrophysiologic recordings of superficial brain neurons (Hu et al. 2010). We wondered if the simple perfusion of ATP across the explanted brain could provide a reliable and technically facile means of exciting deeply situated adult neurons in a manner compatible with high-resolution live imaging. We therefore used a *Pdf-Gal4* driver to coexpress *UAS-GCaMP3.0* (Tian et al. 2009) and *UAS-P2X2* (Lima and Miesenböck 2005) in the small ventral lateral neurons (s-LN_vs). These cells are critical circadian pacemaker neurons whose small somata and deep position within the central brain make them difficult neurons to investigate electrophysiologically (Cao and Nitabach 2008). Compared with vehicle controls (Fig. 2.2*A*), 30-s perfusions of 1 or 2.5 mM ATP resulted in significant GCaMP3.0 fluorescence increases, thereby revealing acute excitation of the s-LN_vs (Fig. 2.2, *B, C, E, F*). In contrast, 30-s perfusions of 2.5 mM GTP did not result in significant increases in on GCaMP3.0 fluorescence, instead causing very small decreases in fluorescence during perfusion (Fig. 2.2, *D* and *E*). The latencies of the s-LN_v responses to 1 mM ATP were less consistent compared with the responses to 2.5 mM, although a few s-LN_vs did display relatively late responses to the higher dose (Fig. 2.2, *B* and *C*). Many of the GCaMP3.0 fluorescence increases displayed by the s-LN_vs following 1 mM ATP perfusion were markedly bimodal, unlike the majority of responses to 2.5 mM (Fig. 2.2, *B* and *C*). This was reminiscent of s-LN_v GCaMP3.0 responses to nicotinic acetylcholine

receptor activation. Carbachol (CCh) excitation of s-LN_v nicotinic acetylcholine receptors (nAChRs), which like P2X2 are expected to gate both Na^+ and Ca^{2+} upon ligand binding, results in bimodal GCaMP3.0 responses at low CCh concentrations but in single fluorescence peaks at high concentrations (Lelito and Shafer 2012). It is possible that, in the case of bimodal responses, the first peak reflects the direct gating of Ca^{2+} through P2X2, whereas the second peak represents Ca^{2+} entry through voltage-gated Ca^{2+} channels or the release of intracellular Ca^{2+}.

The *Drosophila* genome does not encode a P2X2 receptor homolog and previous studies suggest that there are no acute behavioral or physiologic effects of ATP in the absence of transgenic P2X2 (Lima and Miesenböck 2005; Littleton and Ganetzky 2000). Nevertheless, it is still possible that bath-applied ATP might have previously uncharacterized effects on the physiology of fly neurons, possibly through effects on the conserved ATP sensitive K^+ channel (Kim and Rulifson 2004), or might have effects on properties of the genetically encoded sensors themselves (Willemse et al. 2007). We therefore treated brains expressing *UAS-GCaMP3.0* or *UAS-Epac1-camps* in the absence of transgenic P2X2 expression with 30-s perfusions of 2.5 mM ATP to determine if ATP had measurable effects on GCaMP3.0 fluorescence or the inverse Epac1-camps FRET ratio (CFP/YFP), which are directly proportional to Ca^{2+} and cAMP levels, respectively. The 30-s perfusions of 2.5 mM ATP resulted in very small but consistent transient decreases in GCaMP3.0 fluorescence relative to vehicle controls (Fig. 2.2, *G* and *H*). Bath-applied ATP also caused a consistent increase in Epac1-camps inverse FRET values relative to vehicle controls (Fig. 2.2, *I* and *J*). However, the evaluation of raw CFP and YFP traces revealed that this change was not due to bona fide FRET changes, but rather to decreases in YFP fluorescence, reminiscent of GCaMP3.0 fluorescence loss (Fig. 2.2*J* and data

not shown). We therefore conclude that bath-applied ATP has only small and easily accounted for effects on GCaMP3.0 fluorescence and Epac1-camps inverse FRET.

Taken together, these results indicate that deeply situated P2X2-expressing neurons can be excited by the controlled perfusion of ATP across the explanted brain in a manner compatible with high-resolution GCaMP3.0 and Epac1-camps live imaging within single neuronal somata. Furthermore, the absence of ATP excitation in neurons lacking transgenic P2X2 expression confirms that, as expected from previous work (Lima and Miesenböck 2005), ATP did not excite the s-LN_vs in the absence of specifically directed P2X2 expression and had only minor effects on genetically encoded sensors.

2.4.2 LexA operator-driven sensors and P2X2 for dual binary expression experiments.

Our proposed method of circuit interrogation requires the independent expression of the P2X2 receptor and genetically encoded sensors in neurons of interest and their putative follower neurons (Fig. 2.1). To complement existing *UAS-Sensor* and *UAS-P2X2*lines and the large number of existing GAL4 and LexA drivers, we have created a series of transgenic flies containing GCaMP3.0, Epac1-camps, and P2X2 elements under the control of the LexA operator (LexAop) (Lai and Lee 2006). We tested the functionality of our *LexAop-GCaMP3.0* and *LexAop-Epac1-camps* elements within s-LN_vs using the previously described *Pdf-LexA* element (Shang et al. 2008). The adult s-LN_vs respond to the general cholinergic agonist carbachol (CCh) with rapid Ca^{2+} and cAMP increases (Lelito and Shafer 2012). LexAop-driven GCaMP3.0 and Epac1-camps were indeed capable of detecting significant increases in Ca^{2+} and cAMP in response to 30-s perfusions of 10^{-4} M CCh (Fig. 2.3, *A*—*D*). Along with evidence presented below, these results indicate that our *LexAop-*

GCaMP3.0 and*LexAop-Epac1-camps* elements are suitable for the observation of Ca^{2+} and cAMP dynamics within single somata of deeply situated neurons of the adult brain.

We tested the functionality of our *LexAop-P2X2* element by coexpressing it with *LexAop-GCaMP3.0* in the s-LN_vs using *Pdf-LexA*. The s-LN_vs of *Pdf-LexA*,*LexAop-GCaMP3.0*/+;*LexAop-P2X2*/+ brains displayed clear increases in GCaMP3.0 fluorescence in response to 30-s perfusions of 1 mM ATP, indicating that the LexAop-driven P2X2 element had rendered the s-LN_vs sensitive to bath-applied ATP (Fig. 2.3, *E* and *F*). Importantly, the *LexAop-P2X2* element rendered the s-LN_vs sensitive to ATP only when driven by the *Pdf-LexA* driver: when *UAS-GCaMP3.0* was driven in the s-LN_vs with *Pdf-GAL4* in flies carrying the *LexAop-P2X2* element, ATP had no significant effects on GCaMP3.0 fluorescence (Fig. 2.3, *E* and *F*). This observation, along with work presented in the following text, indicates that the presence of the*LexAop-P2X2* element does not cause significant P2X2 expression in the absence of LexA drivers. The same was true for the previously described *UAS-P2X2* element (Fig. 2.3, *E* and *F*; Lima and Miesenböck 2005). We conclude that, like its UAS counterpart, our *LexAop-P2X2* element is capable of specifically rendering deeply situated adult neurons excitable by bath-applied ATP.

2.4.3 Bath-applied ATP reliably and repeatedly activates P2X2-expressing neurons of the adult brain.

Having acquired the genetic elements necessary for dual binary control of P2X2 and sensor expression, we sought to determine the most reliable means of exciting deep brain neurons expressing *UAS-P2X2* and *LexAop-P2X2* elements using bath-applied ATP. We first imaged the somata of three different classes of neuron coexpressing P2X2 and GCaMP3.0: the s-LN_vs and $DN1_p$ clock neurons [using*Pdf(bmrj)-GAL4* and *Clock(4.1M)-Gal4*, respectively] and

the olfactory projection neurons [PNs; using *Cha(7.4)-Gal4*] and compared the effects of 30-s perfusions of a range of ATP concentrations on GCaMP3.0 fluorescence (Fig. 2.4*A*). For all three neuron types, 30-s perfusions of 0.1 mM ATP had no significant effects on GCaMP3.0 fluorescence. Higher concentrations resulted in dose-dependent increases in Ca^{2+} responses, with the s-LN_vs and $DN1_p$s displaying sigmoidal response curves and the PNs (the most superficial of the neurons tested) displaying a biphasic response curve with diminished response magnitudes at doses >5 mM (Fig. 2.4*A*). We also compared the effects of these ATP concentrations between s-LN_vs expressing GCaMP3.0 and P2X2 using either the GAL4 or LexA expression system. The LexA-expressing s-LN_vs displayed significant GCaMP3.0 responses over the same range of ATP concentrations as their GAL4-expressing counterparts, but did so with lower response amplitudes, most likely due to lower levels of transgene expression (Fig. 2.4*E*). Nevertheless, the LexA-expressing s-LN_vs displayed maximum fluorescence changes ($\Delta F/F_0$) approaching 100%, amplitudes on par with the GCaMP3.0 responses displayed by fly sensory neurons subjected to acute sensory excitation (Tian et al. 2009). As shown in Fig. 2.4, *C* and *D*, the excitatory responses of single P2X2-expressing neurons to a series of increasing ATP doses were proportional to the concentration of perfused ATP. Thus, the excitatory responses of single neurons can be controlled through the manipulation of ATP dose, thereby making it possible to excite neurons at a range of intensities.

Our results suggest that 30-s perfusions of 1—5 mM ATP result in significant neuronal excitation for all three neuron types we tested. To gauge the reliability of such ATP/P2X2 excitation we analyzed how often each of these 30-s ATP treatments failed to excite the P2X2-expressing s-LN_vs, $DN1_p$s, and PNs. We defined a failure conservatively as any ATP-treated neuron displaying less than a 25% maximal increase in GCaMP3.0 fluorescence. For all three

neuron types, failure rates were <50% for 1 mM ATP perfusions and approached zero at higher concentrations (Fig. 2.4*B*). Our choice of 30-s perfusions was based on previous experiments involving the bath application of neurotransmitters and receptor agonists (Lelito and Shafer 2012). We wondered if shorter applications of ATP might still yield sufficient excitation of the s-LN_vs, the most deeply situated of the neurons tested, using both the LexA and Gal4 expression systems. We therefore determined the failure rates for various durations of 2.5 mM ATP for s-LN_vs coexpressing GCaMP3.0 and P2X2 with either LexA or Gal4 drivers. For perfusion durations of 10 to 20 s, failure rates for both genotypes were all near 30%. Failure rates reached zero at perfusion durations of 25 s for LexA s-LN_vs and at 30 s for GAL4 s-LN_vs (Fig. 2.4*F*).

The ability to excite the same set of P2X2-expressing neurons repeatedly would allow for multiple sets of putative follower neurons residing in different focal planes to be investigated in the same brain preparation. We therefore asked if P2X2-mediated excitation by bath-applied ATP could be used to repeatedly stimulate deep brain neurons. Indeed, repeated 30-s perfusions of 2.5 mM ATP resulted in reliable repeated excitation of s-LN_vs expressing either GAL4- or LexA-driven P2X2 (Fig. 2.4, *G* and *H*). Although the baseline fluorescence of these neurons displayed a slow and steady drop in intensity, there was no significant difference in the mean maximum GCaMP3.0 fluorescence increases displayed in response to the first and last (fifth) 30-s perfusion of ATP, when compared with the baseline fluorescence preceding each ATP pulse. For repeated excitation using the GAL4 system to coexpress GCaMP3.0 and P2X2 expression (Fig. 2.4*G*), the first ATP perfusion caused a mean maximum GCaMP3.0 increase of 126.6 ± 32.9% and the fifth and final pulse caused a mean increase of 114.5 ± 21.9% ($P = 0.8438$ by Mann—Whitney *U* test). For repeated excitation using the LexA system (Fig. 2.4*H*) the first ATP perfusion caused a mean maximum GCaMP3.0 increase of 145.3 ± 19.1% and final pulse

caused a mean increase of 94.1 ± 18.8% (P = 0.0524 by Mann—Whitney U test). Thus, P2X2-expressing neurons can be repeatedly activated in the same dissected brain without a significant rundown in excitation.

Based on these results, we conclude that 30-s perfusions of 1—5 mM ATP result in robust, reliable, and repeatable excitation of deep brain P2X2-expressing neurons, using either the GAL4 or LexA expression system to drive the expression of P2X2. However, we note that different neuronal types display differing profiles of excitation, indicating that specific excitation parameters should be determined empirically for every neuron class and genotype to be excited.

2.4.4 Dual binary expression of P2X2 and genetically encoded sensors allow for the specific excitation of neuronal subsets during live imaging experiments.

Having confirmed the efficacy of our LexAop-driven sensor and P2X2 elements, we next sought to confirm that the simultaneous use of the GAL4 and LexA systems could render specific neuron classes excitable by ATP during high-resolution imaging experiments. We therefore used the *Pdf-LexA* element to drive *LexAop-GCaMP3.0* expression in both the s-LN_vs and the large ventrolateral neurons (l-LN_vs) of the circadian clock network, while simultaneously using the *c929-GAL4* element, which is expressed by the l-LN_vs but not the s-LN_vs, to drive P2X2 in the l-LN_vs and in the many other peptidergic neurons expressing this GAL4 driver (Fig 2.5*A*; Hewes et al. 2000). Thus, the l-LN_vs of ;*Pdf-LexA,LexAop-GCaMP3.0/c929-GAL4;UAS-P2X2*/+ brains will express P2X2, whereas the s-LN_vs will not. If the specific dual binary expression of P2X2 and GCaMP3.0 were successful, the l-LN_vs would be expected to display acute GCaMP3.0 responses to bath-applied ATP, whereas the s-LN_vs would not. As predicted, 30-s perfusions of 1 mM ATP resulted in the excitation of the l-LN_vs, but did not excite the s-LN_vs imaged within the same focal planes (Fig. 2.5, *B–D*). This result, along with the

experiments presented in the following text, indicate that the simultaneous use of the GAL4 and LexA systems for the independent expression of P2X2 and genetically encoded sensors, makes possible the specific excitation of neuronal subsets in a manner compatible with high-resolution live imaging experiments. This result also suggests that the excitation of the l-LN_vs, neurons important for the control of arousal, sleep, and the integration of circadian light input (Parisky et al. 2008;Shang et al. 2008; Sheeba et al. 2008), does not result in large acute Ca^{2+} increases in the critical s-LN_v pacemaker neurons.

2.4.5 Gal4-based excitation and LexA-based live imaging for an established excitatory connection in the larval brain.

We next sought to determine if our proposed method of addressing functional connectivity was sufficiently sensitive to detect an established neuronal connection in *Drosophila*. We were motivated to propose the present approach to circuit analysis because there are few well-established synaptic connections in our circuitry of interest, the circadian clock neuron network. One of the only fully confirmed synaptic connections in the *Drosophila* clock network is the excitatory connection between Bolwig's organ (BO), the maggot eye, and the LN_v clock neurons, which persist through metamorphosis to become the adult s-LN_vs (Fig. 2.6*A*; Helfrich-Förster et al. 2007). BO projects directly to the larval optic neuropil via Bolwig's nerve (BN), where its terminals reside in close apposition to LN_v arbors (Helfrich-Förster et al. 2002; Malpel et al. 2002). BN expresses ChAT, an enzyme required for acetylcholine (ACh) synthesis (Yasuyama and Salvaterra 1999) and ChAT is required in BN for photic resetting of larval clock neurons (Keene et al. 2011). Dissociated and cultured larval LN_vs are directly excited by bath-applied ACh and nicotine (Wegener et al. 2004). Finally, Yuan and colleagues (2011) have recently shown that blue-light stimulation of BO causes acute

Ca^{2+} increases in the larval LN_vs clock neurons. Thus, the BN to LN_v connection in the larval brain offers a well-established excitatory connection in the clock network on which to test our method for addressing connectivity.

Under our experimental conditions, we found it necessary to remove the larval mouth hooks to prevent brain movement during imaging. Mouth hook removal was associated with the loss of BO, leaving only the afferent BNs associated with the eye disks and central brain (Fig. 2.6, *A* and *B*). We therefore first confirmed that excitation of BN was possible in the absence of BO by coexpressing P2X2 and GCaMP3.0 in BN using the *Rh6-Gal4* driver, which is expressed in a subset of BN axons (Fig. 2.6*A*; Keene et al. 2011). We found that 30-s perfusions of 5 mM ATP caused reliable Ca^{2+} responses in BNs of *;Rh6-GAL4/UAS-GCaMP3.0;UAS-P2X2*/+ brains, indicating the successful excitation of BNs (Fig. 2.6, *B*, *D*, and *G*).

Having confirmed successful ATP/P2X2 excitation of BN in our preparation, we asked if the predicted excitatory responses could be detected in larval LN_vs in response to BN excitation. We therefore created *;Rh6-Gal4/Pdf-lexA, LexAop-GCaMP3.0; UAS-P2X2*/+ larvae to independently express P2X2 in BN and GCaMP3.0 in the LN_vs (Fig. 2.6*A*). Consistent with previous reports, we observed no *Rh6-GAL4* driver expression in the LN_vs or in any other central neurons of the larval brain (e.g., Keene et al. 2011 and data not shown). All 30-s perfusions of 5 mM ATP caused significant GCaMP3.0 fluorescence increases in the LN_vs of *Rh6-Gal4/Pdf-lexA, LexAop-GCaMP3.0; UAS-P2X2*/+ brains (Fig. 2.6, *C*, *E*, and *H*). To confirm that the LN_v responses to ATP perfusion were due to the specific excitation of the BN and not to the leaky expression of *UAS-P2X2* in non-BN cell types or native responses of larval LN_vs to ATP, we repeated the experiment on brains dissected from *;Pdf-lexA, LexAop-GCaMP3.0*/+*; UAS-P2X2*/+ larvae, which lacked the *R6-GAL4* element and therefore would not have driven P2X2

expression specifically in BN. The LN_vs of these flies did not display significant changes in GCaMP3.0 fluorescence following 30-s perfusions of 5 mM ATP (Fig. 2.6, *F* and *I*), indicating that nonspecific *UAS-P2X2*expression or native ATP responses had not caused the Ca^{2+} responses displayed by the LN_vs following the ATP/P2X2 excitation of BN. We conclude that our method of addressing connectivity was sufficiently sensitive to detect an established excitatory connection deep within the larval brain.

2.4.6 LexA-based excitation and GAL4-based live imaging to test a predicted peptidergic connection in the adult central brain.

The circadian clock neuron network of the adult fly consists of approximately 150 neurons that express conserved molecular clockwork (Nitabach and Taghert 2008). Understanding the connective properties of this network was our motivation for developing a means for interrogating the physiologic connections between neuronal classes deep within the fly brain. The s-LN_vs are critical neuronal pacemakers required for the maintenance of robust rhythms in sleep and activity in the fly under constant darkness and temperature (Grima et al. 2004;Renn et al. 1999; Shafer and Taghert 2009; Stoleru et al. 2004). A large and growing body of anatomic, genetic, and physiologic evidence suggests that the clock neuron network is coordinated through modulatory connections between the s-LN_vs and the various classes of dorsal clock neurons. The s-LN_vs project to the dorsal brain, where their terminals comingle with terminals from the dorsal clock neuron classes (Helfrich-Förster et al. 2007; Kaneko and Hall 2000). The s-LN_vs express the neuropeptide pigment-dispersing factor (PDF), the genetic loss of which causes a weakening or loss of free-running behavioral rhythms (Helfrich-Förster 1995; Renn et al. 1999; Shafer and Taghert 2009) and a loss of synchronization among various clock neuron classes (Lin et al. 2004). PDF signals through PDFR, a G-protein—coupled

receptor (GPCR) that signals through cAMP increases (Hyun et al. 2005; Lear et al. 2005; Mertens et al. 2005) and is expressed by dorsal clock neurons (Im and Taghert 2010). Finally, the dorsal neuron classes respond to bath-applied PDF peptide with cAMP increases (Shafer et al. 2008). Taken together, these findings provide strong evidence for a neuromodulatory connection between the s-LN_vs and dorsal clock neurons in the adult fly brain. Thus, the current prevailing model predicts that the excitation of the s-LN_vs will result in acute cAMP increases within dorsal clock neurons.

Nevertheless, the physiologic nature of this proposed connection has not been confirmed experimentally. Indeed, recent work has shown that the s-LN_vs also express*short neuropeptide F* (*sNPF*) (Johard et al. 2009), which encodes four peptides whose GPCR would likely antagonize PDFR signaling (Garczynski et al. 2007; Mertens et al. 2002; Reale et al. 2004). The coexpression of potentially antagonistic peptides in the s-LN_vs suggests that the excitation of these neurons might in fact cause cAMP decreases in dorsal clock neuron classes. Determining the functional nature of this proposed connection therefore requires the ability to experimentally interrogate its physiology. We therefore set out to determine the nature of the predicted connection between the s-LN_v pacemakers and the LN_ds, which are among the predicted neuronal targets of the s-LN_vs (Im and Taghert 2010; Shafer et al. 2008) and are thought to play a critical role in the control of the fly's evening bout of daily activity (Grima et al. 2004; Stoleru et al. 2004).

To investigate the proposed connection between the s-LN_vs and the LN_d clock neurons, we drove P2X2 expression specifically in the l-LN_vs and s-LN_vs using *Pdf-LexA*, while driving GCaMP3.0 or Epac1-camps expression with *Clock(856)-GAL4*, which is expressed throughout most of clock neuron network (Fig. 2.7*A*; Gummadova et al. 2009). Note that although *Pdf-*

LexA drives *LexAop-P2X2* in both the l-LN_vs and s-LN_vs, only the s-LN_vs send projections to the dorsal brain, whereas the l-LN_vs project to both optic lobes (Fig. 2.7*A*; Helfrich-Förster et al. 2007). For brains dissected from *;Clock(856)-GAL4,UAS-GCaMP3.0/+;Pdf-LexA,LexAop-P2X2/+* flies, excitation of the l-LN_vs and s-LN_vs with 30-s perfusions of 1 mM ATP caused clear increases in GCaMP3.0 fluorescence in the LN_vs, but had no measurable effects on the LN_ds residing in the same optical sections, suggesting that LN_v excitation does not cause large acute Ca^{2+} increases or acute excitation in the LN_ds (Fig. 2.7*B*). In contrast, 30-s perfusions of 1 mM ATP across *;Clock(856)-GAL4,UAS-Epac1-camps/+;Pdf-LexA,LexAop-P2X2/+* brains resulted in significant increases in Epac1-camps inverse FRET within the LN_ds, consistent with cAMP increases in response to LN_v excitation (Fig. 2.7, *C* and *D*). Direct ATP/P2X2 excitation of the l-LN_vs and s-LN_vs caused significant increases in Epac1-camps inverse FRET (Fig. 2.7, *E* and *F*, and data not shown), indicating a strong coupling of neuronal excitation and cAMP production in these neurons. The large increase in LN_d inverse Epac1-camps FRET was preceded by a small and transient decrease in inverse FRET (Fig. 2.7*C*). However, this decrease was not caused by LN_v excitation, because we observed a similar initial decrease in mean inverse FRET in control brains lacking the *Pdf-LexA* element for driving *LexAop-P2X2* expression in the LN_vs (Fig. 2.7*C*).

The LN_d cAMP response to bath-applied ATP required P2X2 expression in the LN_vs, because brains carrying the *LexAop-P2X2* element but lacking the *Pdf-LexA* driver failed to show cAMP increases in either the LN_ds or LN_vs (Fig. 2.7, *C–F*; "—P2X2"). Furthermore, the LN_d cAMP response to LN_v excitation required functional PDF receptor, because ATP perfusion over brains from *$PdfR^{5304}$;Clock(856-GAL4,UAS-Epac1-camps/+;Pdf-LexA,LexAop-$P2X_2$/+* flies failed to produce significant changes in LN_d Epac1-camps inverse FRET levels (Fig.

2.7, *C* and *D*; "—PDFR"), despite clear excitation of LN_vs within the same optical sections (Fig. 2.7, *E* and *F*; "—PDFR").

Our results indicate that the excitation of the l-LN_vs and s-LN_vs results in acute cAMP increases in the LN_ds and that this response requires functional PDF receptor signaling (Fig. 2.7, *C* and *D*). Thus, our method of connectivity analysis was sufficiently sensitive to experimentally confirm a predicted modulatory connection deep within the adult brain. Given the thorough vetting of GCaMP3.0 and Epac1-camps sensors in the fly CNS by previous studies (e.g., Shafer et al. 2008; Tian et al. 2009), the lack of GCaMP3.0 responses in the face of clear Epac1-camps responses in the LN_ds following LN_v excitation suggests that the LN_ds are not strongly excited by the LN_vs and that the LN_v-to-LN_d connection acts predominantly as a modulator of LN_d cAMP signaling. Thus, the connection between these neuronal classes could not have been detected with Ca^{2+} imaging alone, which argues for the use of diverse sensor types in the investigation of functional connectivity. The efficacy of this approach to circuit interrogation now makes possible a wider analysis of the patterns of clock network connections, and an investigation of how these connections might change over the course of the circadian cycle or in response to changing environmental conditions such as photoperiod and temperature. Furthermore, these experiments establish the feasibility of conducting such experiments in mutant backgrounds of choice.

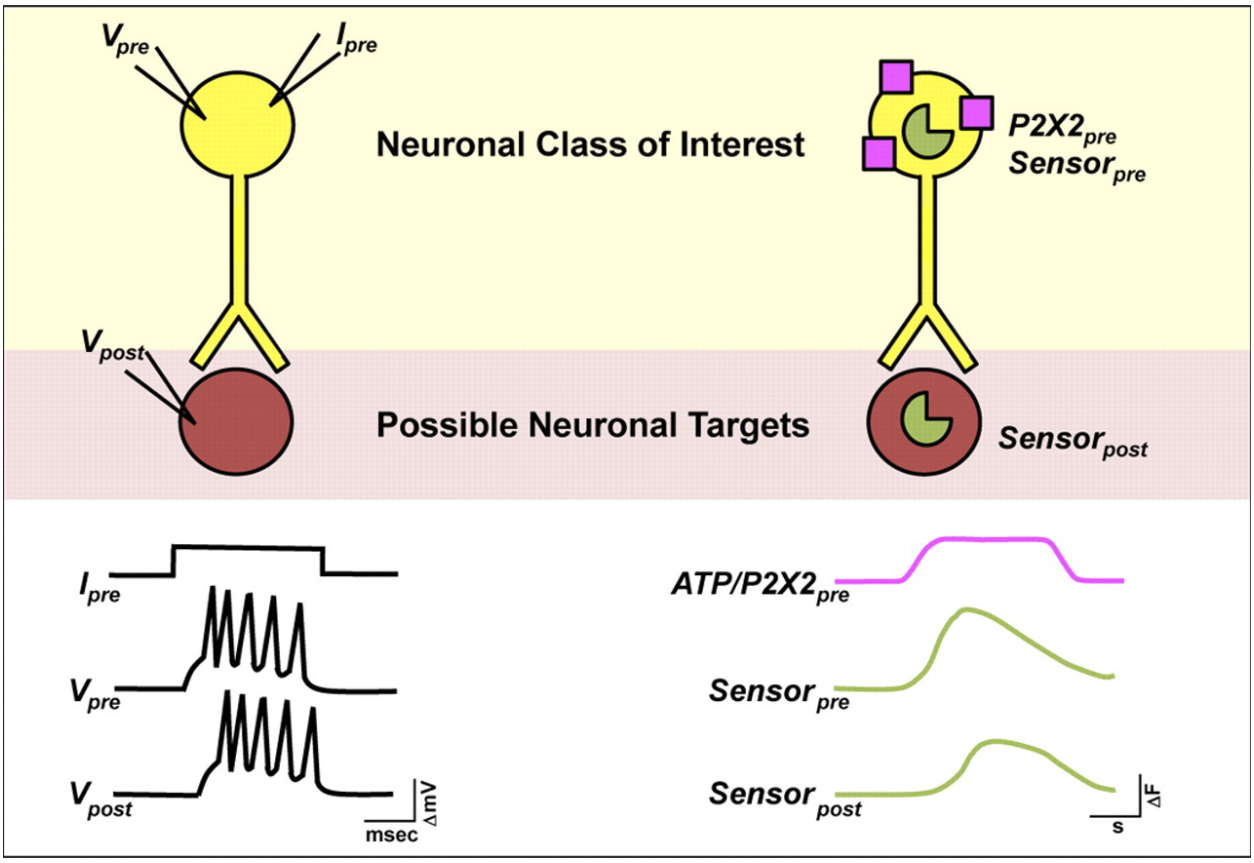

Figure 2.1 Schematic of dual binary, ATP/P2X2 excitation approach to network interrogation.
Left: an electrophysiologic approach to connectivity in invertebrate nervous systems. The investigator stimulates a neuron of interest with depolarizing current while simultaneously recording membrane voltage in putative follower neurons (e.g., Kandel et al. 1967). *Right*: a physiogenetic approach to connectivity in the *Drosophila* nervous system. Depolarizing current is induced in neuronal classes of interest through ATP gating of transgenic P2X2 receptors (shown in purple), whereas Ca^{2+} or cAMP levels are simultaneously monitored in putative follower neurons using genetically encoded sensors (shown in green). Note the differing time scales between methods.

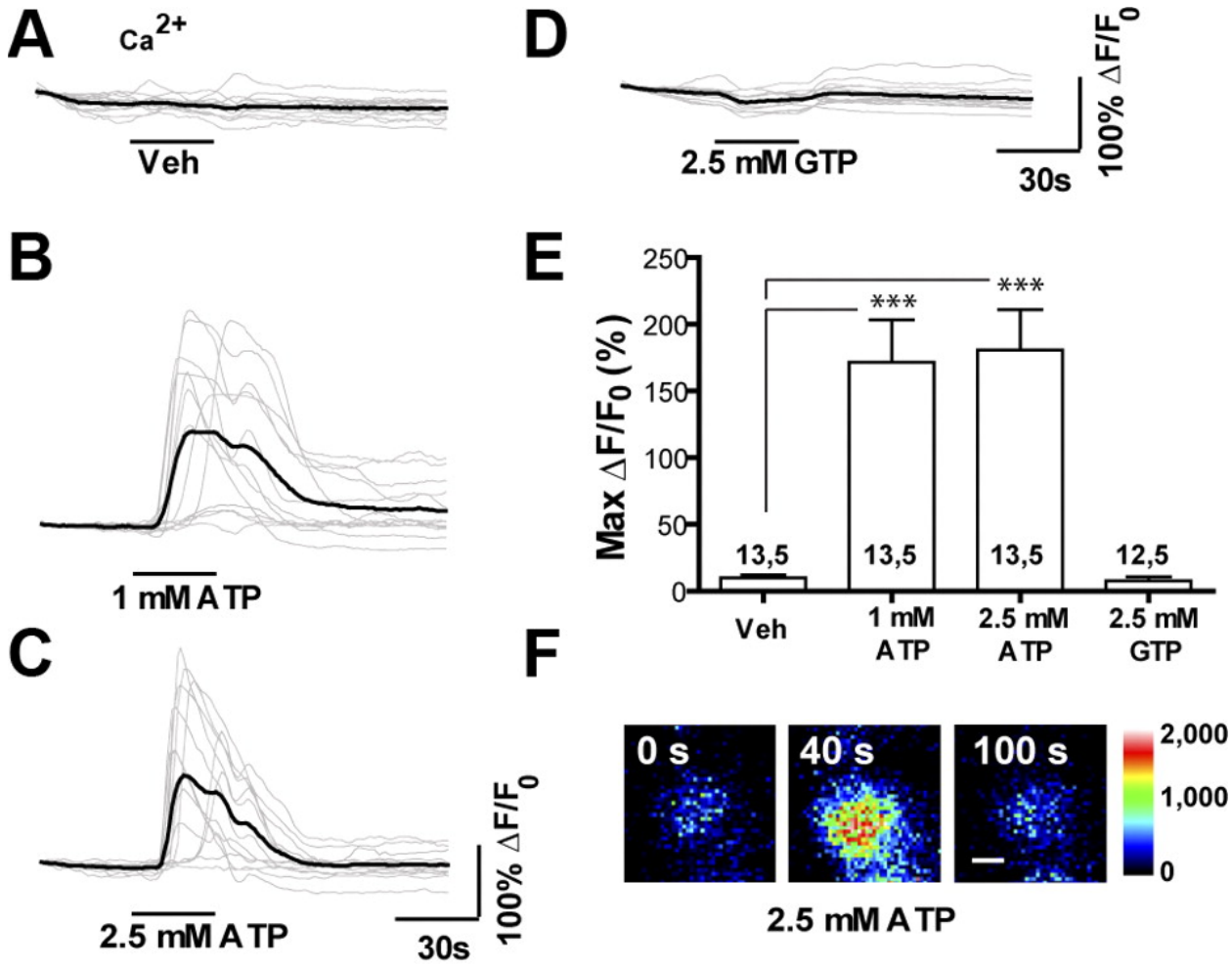

Pdf-GAL4;UAS-GCaMP3.0/+;UAS-P2X2/+

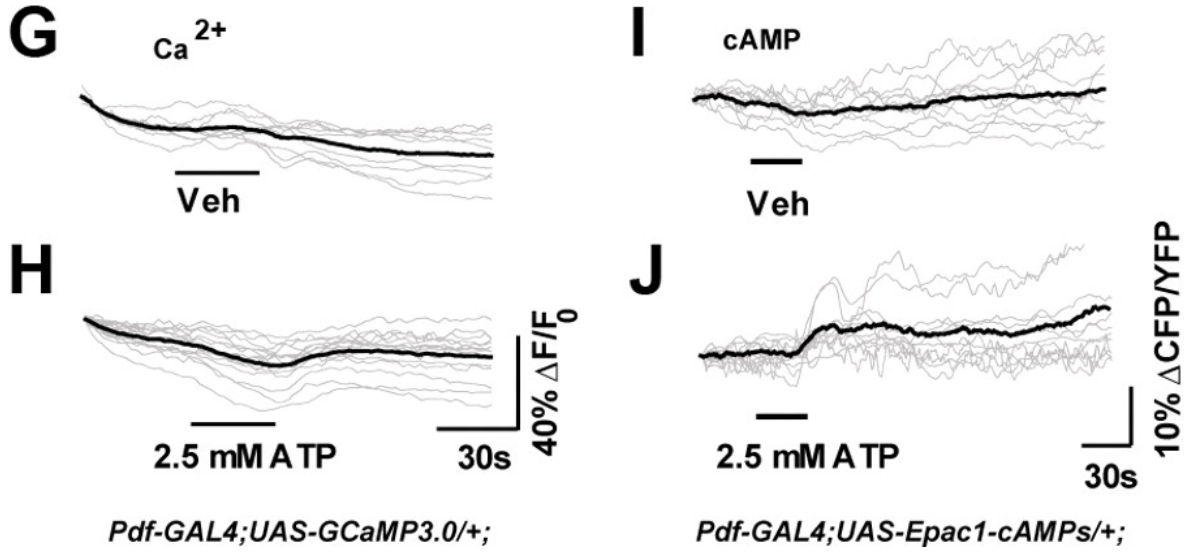

Pdf-GAL4;UAS-GCaMP3.0/+;

Pdf-GAL4;UAS-Epac1-cAMPs/+;

Figure 2.2 Bath application of ATP results in the excitation of P2X2-expressing deep brain neurons during live imaging experiments.
A–D: individual (*gray*) and mean (*black*) traces of *Pdf(M)-Gal4;UAS-GCaMP3.0/+;UAS-P2X2/+* s-LN_v responses to 30-s perfusion of (*A*) vehicle (*N* = 13 neurons from 5 brains [13,5]), (*B*) 1 mM ATP (*N* = 13,5) (*C*) 2.5 mM ATP (*N* = 13,5), and (*D*) 2.5 mM GTP (*N* = 12,5). Test compounds were perfused after a 35-s baseline interval and responses were recorded for a total of 150 s. *E*: histogram summarizing the mean maximum percentage increase in GCaMP3.0 fluorescence displayed by the neurons plotted in *A–D*. Perfusion of 1 and 2.5 mM ATP caused fluorescence increases that were significantly greater than vehicle control ($P < 0.0001$, by Mann—Whitney *U* test). The perfusion of 2.5 mM GTP did not cause significant fluorescence increases relative to the vehicle control ($P = 0.6302$ by Mann—Whitney *U* test). The two numbers displayed within or above each bar of the histogram indicate the number of neurons and the number of brains examined, respectively. *F*: representative intensity mapped micrographs of a single *Pdf(M)-Gal4;UAS-GCaMP3.0/+;UAS-P2X2/+* s-LN_v before (0 s), during (40 s), and after (100 s) its response to bath-applied 2.5 mM ATP. The scale bar in *F* = 2.5 μm. *G* and *H*: characterization of ATP's P2X2-independent effects on GCaMP3.0 fluorescence: unlike vehicle perfusion (*G*), 30-s 2.5 mM ATP perfusion (*H*) caused a slight but consistent decrease in GCaMP3.0 fluorescence. *I* and *J*: characterization of ATP's P2X2-independent effects on Epac1-camps inverse FRET levels. Unlike vehicle perfusion (*I*), 30-s 2.5 mM ATP perfusion caused a slight increase in inverse FRET (*J*), due to a decrease in YFP emission.

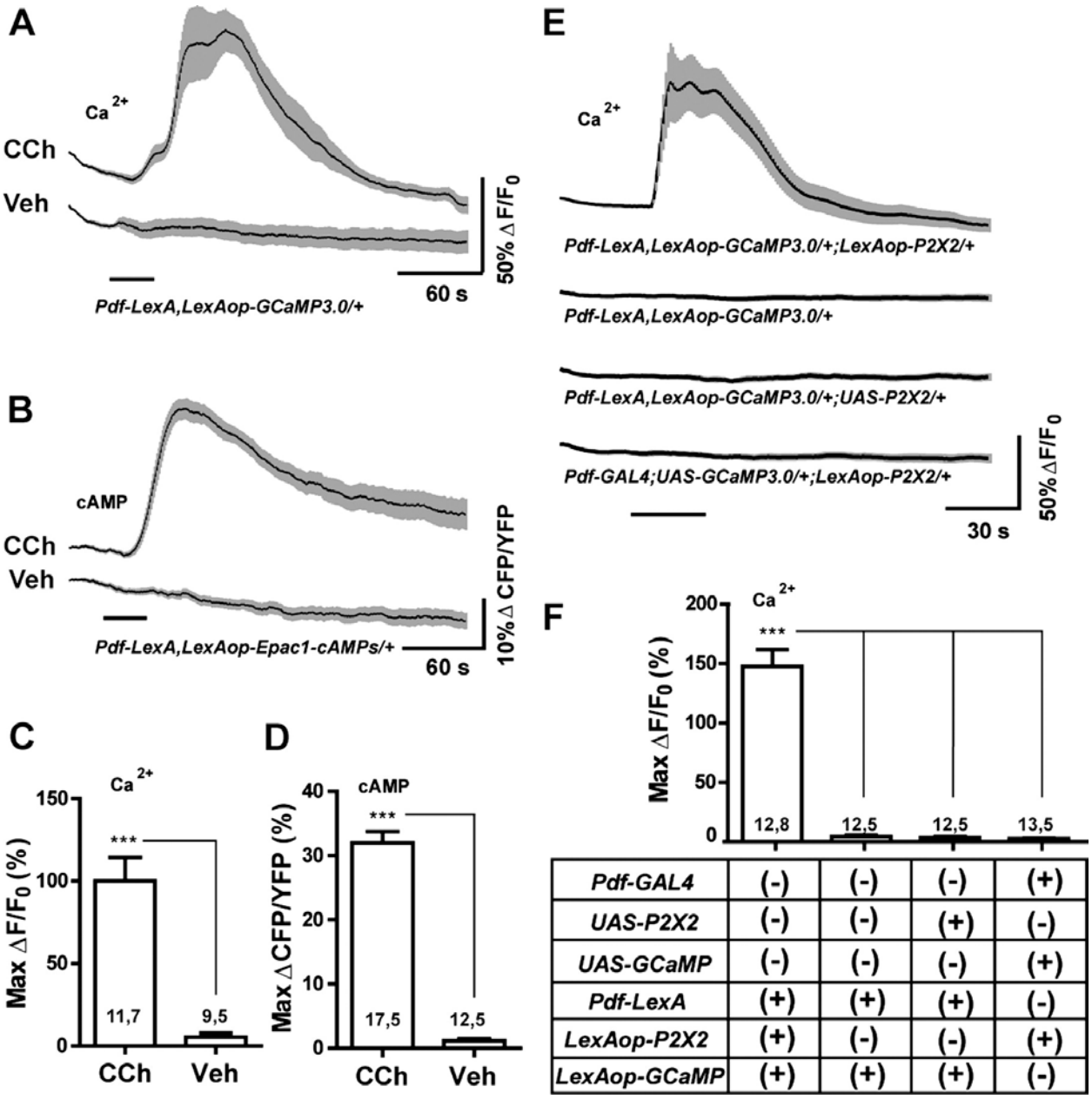

Pdf-GAL4	(-)	(-)	(-)	(+)
UAS-P2X2	(-)	(-)	(+)	(-)
UAS-GCaMP	(-)	(-)	(-)	(+)
Pdf-LexA	(+)	(+)	(+)	(-)
LexAop-P2X2	(+)	(-)	(-)	(+)
LexAop-GCaMP	(+)	(+)	(+)	(-)

Figure 2.3 LexA operator-driven P2X2 and genetically encoded sensors for excitation and live imaging.

A: mean GCaMP3.0 traces for *Pdf-LexA(7M),LexAop-GCaMP3.0(4A)/CyO* s-LN$_v$s to 30-s perfusions of 10^{-4} M carbachol (CCh) or vehicle (Veh). *B*: mean Epac1-camps inverse FRET traces for *Pdf-LexA(7M),LexAop-Epac1-camps(1A)/CyO* s-LN$_v$s to 30-s perfusions of 10^{-4} M CCh or Veh. *C* and *D*: maximum changes in GCaMP3.0 fluorescence (*C*) or Epac1-camps inverse FRET increases (*D*) of s-LN$_v$ corresponding to the data in *A* and *B*, respectively. Numbers on the histograms indicate the number of neurons and brains sampled. Both LexAop-driven sensors displayed significant responses to CCh relative to Veh controls ($P = 0.0004$ for GCaMP3.0 fluorescence and $P < 0.0001$ for Epac1-camps inverse FRET by Mann—

Whitney *U* test). *E*: mean GCaMP3.0 traces for the s-LN_vs of the genotypes indicated below the plots to 30-s perfusions of 10^{-3}M ATP. *Pdf-LexA*—driven expression of *LexAop-P2X2* rendered s-LN_vs sensitive to bath-applied ATP. *UAS-P2X2* and *LexAop-P2X2* elements did not render neurons sensitive to ATP in the absence of their appropriate Gal4 or LexA drivers. *F*: summary of maximum Ca^{2+} responses of s-LN_v in *E*. *** indicates $P < 0.001$ by Kruskal—Wallis one-way ANOVA and a Dunn's multiple comparison test. Numbers on the histogram is in*C*, *D*, and *F* indicate the number of neurons and brains sampled. For *A*, *B*, and *E*, the time of perfusion is indicated by the bars under the plots and the *gray-shaded* regions surrounding the mean plots indicate SE, as do the error bars in *C*, *D*, and *F*.

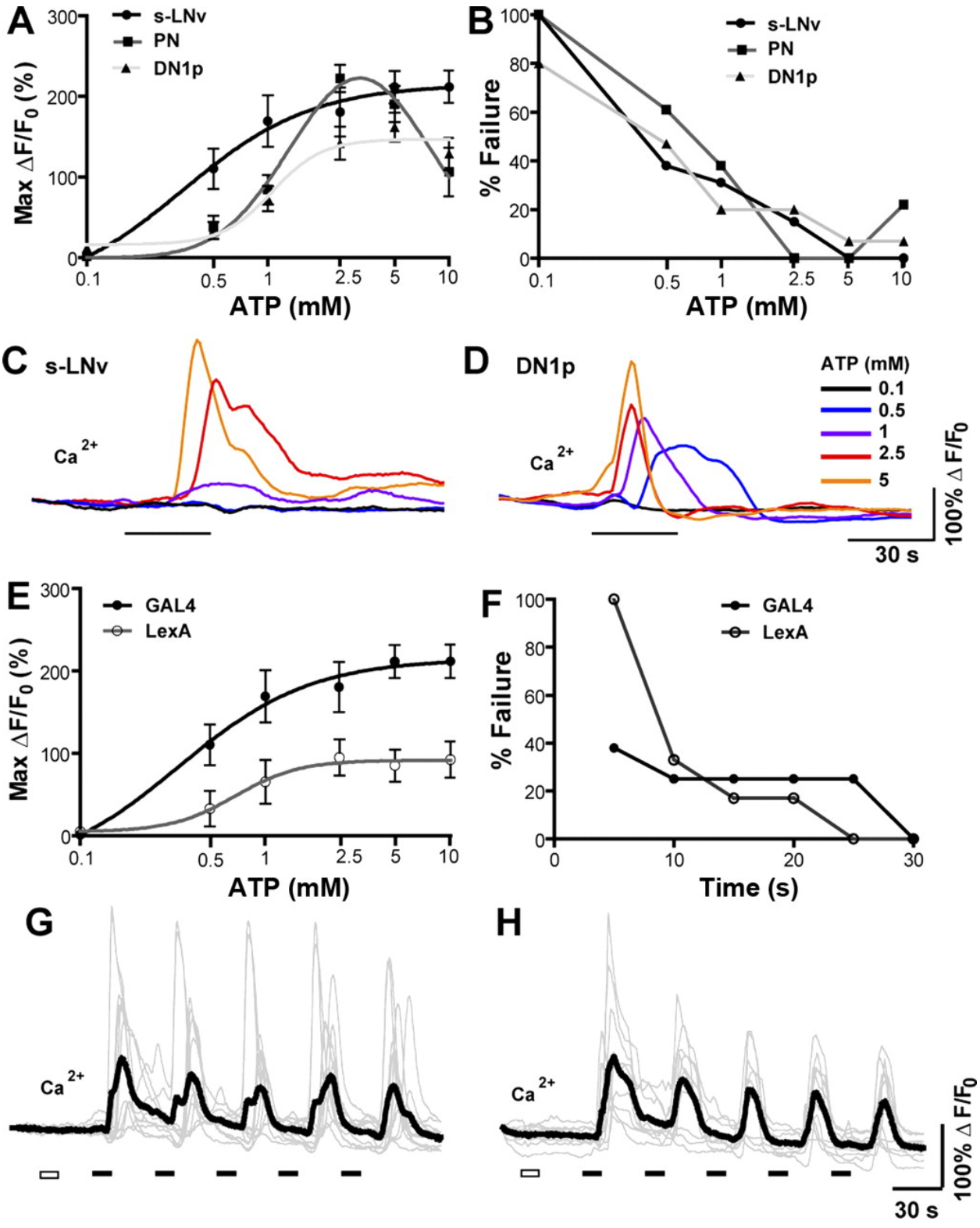
A
s-LNv
PN
DN1p
Max ΔF/F0 (%)
ATP (mM)
B
% Failure
C
s-LNv
Ca 2+
D
DN1p
ATP (mM)
0.1
0.5
1
2.5
5
100% ΔF/F0
30 s
E
GAL4
LexA
F
Time (s)
G
H

Figure 2.4 Bath-applied ATP reliably and repeatedly activates deeply situated P2X2-expressing neurons in the explanted adult brain.
A: dose—response curves for the excitation of P2X2-expressing s-LN_vs (*N* = 13,5), $DN1_p$s (*N* = 15,5), and olfactory projection neurons (PN, *N* = 18,5)) by 30-s perfusions of ATP. The genotypes used for each neuronal class where *Pdf-Gal4;UAS-GCaMP3.0/+;UAS-P2X2/+* for s-LN_vs, ;UAS-GCaMP3.0/+; *Clock(4.1M)-Gal4/UAS-P2X2* for $DN1_p$s, and *;Cha(7.4)-Gal4/UAS-GCaMP3.0;UAS-P2X2/+* for PNs. Values represent the mean maximum increase in GCaMP3.0 fluorescence ($\Delta F/F_0$) detected during the 150 s following ATP perfusion. *B*: failure rate curves for 30-s ATP perfusions over a range of concentrations for s-LN_vs, $DN1_p$s, and PNs based on the data shown in *A*. A maximum GCaMP3.0 fluorescence increase of <25% was considered a failure to excite. *C* and *D*: GCaMP3.0 responses of a single s-LN_v (*C*) and $DN1_p$ (*D*) cell body to increasing ATP concentrations (0.1–5 mM), each delivered for 30 s. Single neurons displayed graded responses to increasing ATP doses. *E*: dose—response curves for s-LN_vexcitation in response to 30-s ATP perfusions comparing s-LN_vs from *Pdf-Gal4;UAS-GCaMP3.0/+;UAS-P2X2/+* (*N* = 13,5) and ;*Pdf-LexA,LexAop-GCaMP3.0/LexAop-P2X2;* (*N* = 10,5) brains. *F*: failure rates of s-LN_v excitation by various durations of 2.5 mM ATP perfusions comparing s-LN_vs excited using the GAL4 (*N* = 8,5) and LexA (*N* = 10,5) systems. Genotypes were identical to those used in *E*. *G*: individual (*gray*) and mean (*black*) GCaMP3.0 traces for repeatedly activated s-LN_vs from *Pdf-Gal4;UAS-GCaMP3.0/+;UAS-P2X2* brains (N=11,5). *H*: individual (*gray*) and mean (*black*) GCaMP3.0 traces for repeatedly activated s-LN_vs from *Pdf-LexA,LexAop-GCaMP3.0/LexAopP2X2* brains (*N* = 10,5). For *G* and *H* the *white rectangles*indicate 30 s of vehicle perfusion and *black rectangles* indicate 30 s of 2.5 mM ATP perfusion, with 90-s intervals between ATP perfusions.

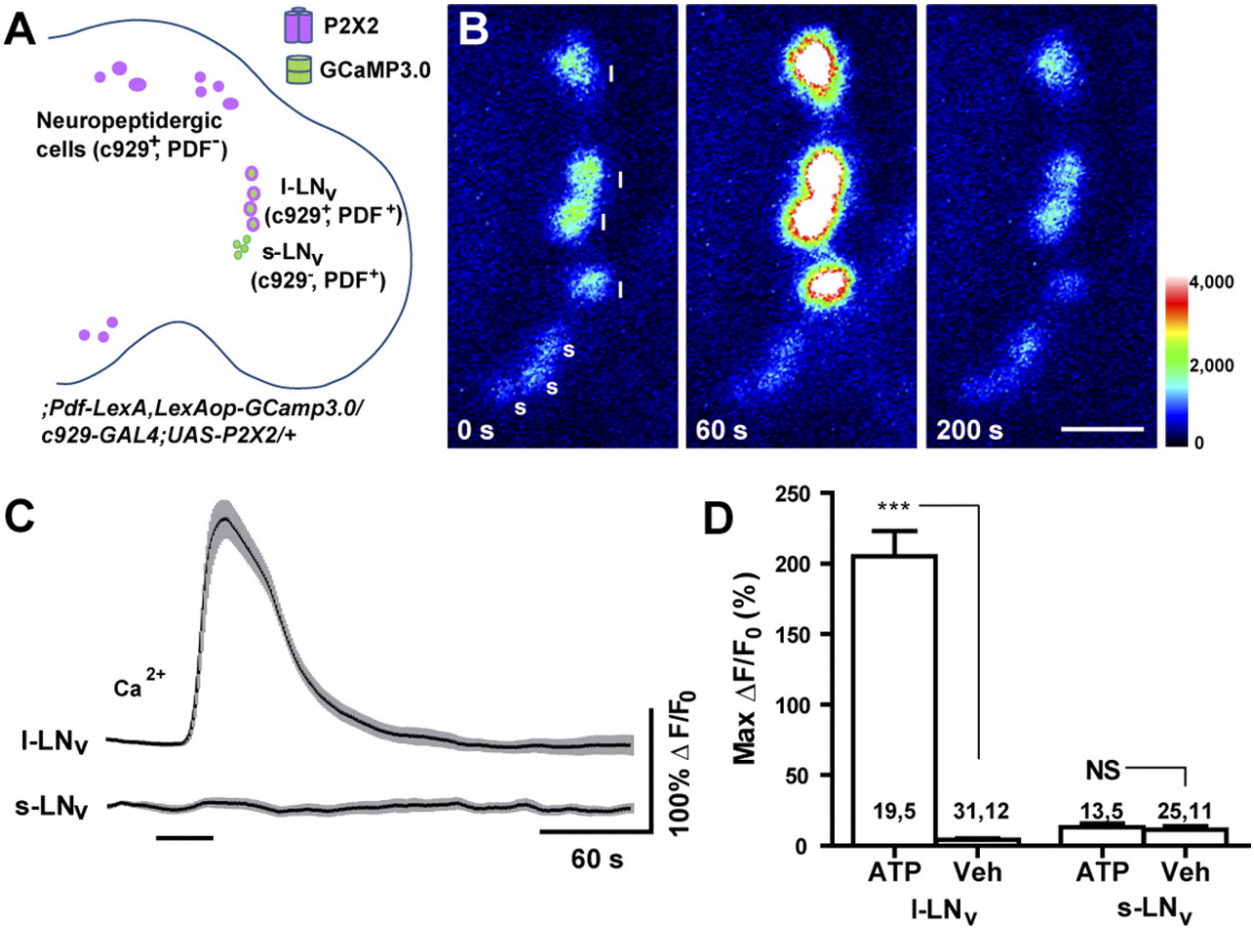

Figure 2.5 Independent expression of P2X2 and genetically encoded sensor in the fly brain by dual binary systems supports the excitation of specific neuronal subsets.
A: schematic diagram showing the expression patterns of P2X2 (magenta) and GCaMP3.0 sensor (green) in the experimental fly brain, whose full genotype is shown.*B*: intensity-mapped stills of l-LN_v and s-LN_v GCaMP3.0 fluorescence before (T = 0 s), during (T = 60 s), and after (T = 200 s) perfusion of 1 mM ATP. The l-LN_vs but not the s-LN_vs responded to ATP. The colors of the legend indicate pixel intensity values. Each "l" indicates a l-LN_v and each "s" indicates a s-LN_v. *C*: mean GCaMP3.0 fluorescence traces of l-LN_vs and s-LN_vs to 30-s perfusions of 1 mM ATP (indicated by the bar under the plots). Sample sizes for these plots are shown in *D*. The *gray-shaded* regions surrounding the mean plots indicate SE. *D*: summary of maximum GCaMP3.0 fluorescence increases displayed by the l-LN_v and s-LN_v to bath-applied ATP and vehicle (Veh). *** indicates a significant difference between ATP and Veh ($P < 0.001$) and NS indicates nonsignificance by Mann—Whitney *U* test. The two numbers displayed within or above each bar of the histogram indicate the number of neurons and the number of brains examined, respectively.

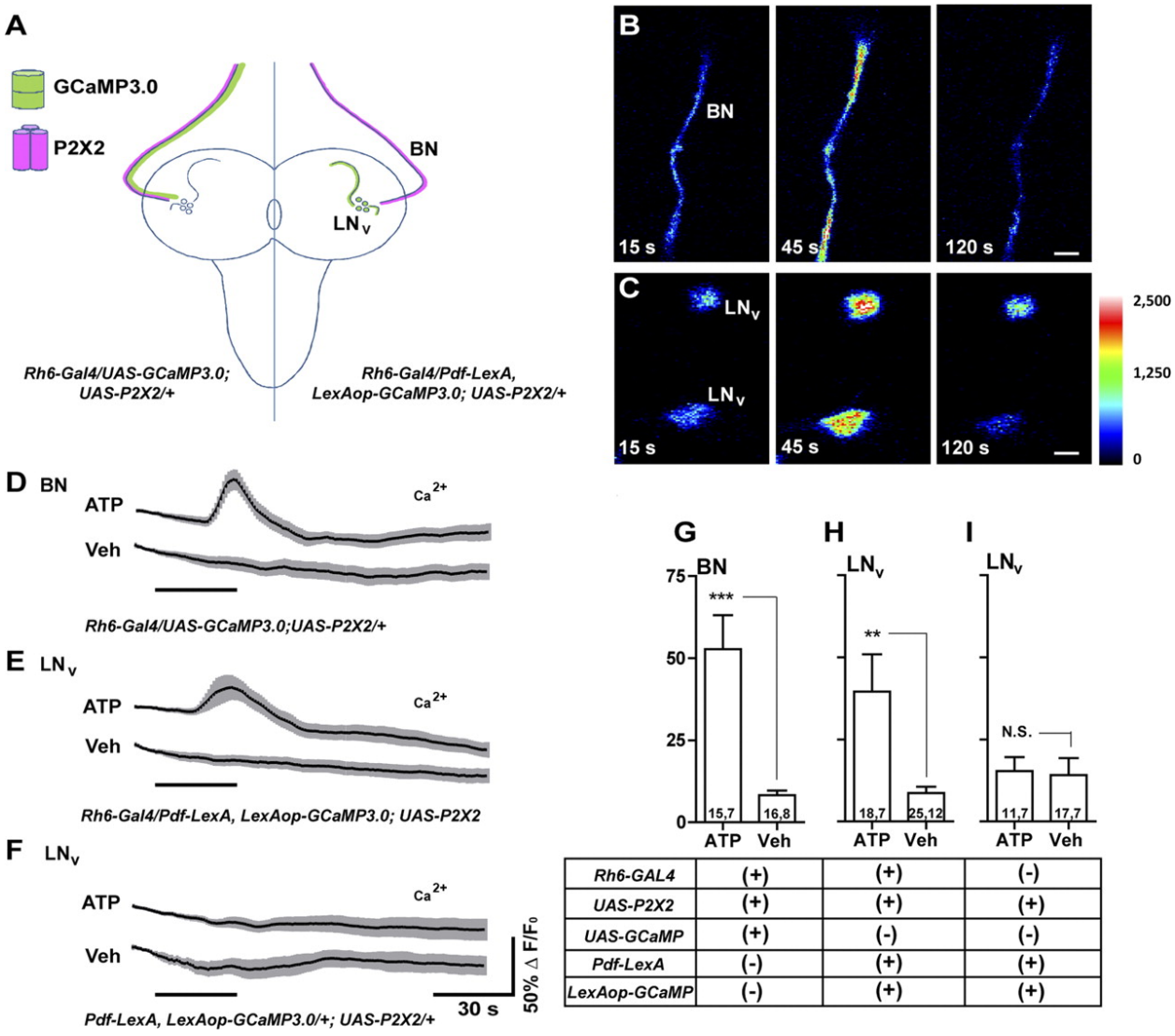

Figure 2.6 Gal4-based excitation and LexA-based live imaging for an established excitatory connection in the larval brain.

A: schematic diagram of Bolwig's Nerve (BN) and larval LN_v anatomy. The expression of GCaMP3.0 (green) and P2X2 (magenta) are indicated for two experimental genotypes. *B*: ATP/P2X2 excitation of BN. Single-plane intensity mapped confocal images of GCaMP3.0 fluorescence in the BN of an *Rh6-Gal4/UAS-GCaMP3.0;UAS-P2X2*/+ larva before (15 s), during (45 s), and after (120 s) the start of 30-s 5 mM ATP perfusion. *C*: single-plane intensity mapped confocal images of GCaMP3.0 fluorescence in two larval LN_vs of a *Pdf-LexA,LexAop-GCaMP3.0/Rh6-Gal4;UAS-P2X2*/+ larva before (15 s), during (45 s), and after (120 s) their response to BN excitation. The look-up table represents pixel intensity values for both *B* and *C*. *D*: mean GCaMP3.0 fluorescence traces for BNs of ;*Rh6-gal4/UAS-GCaMP3.0;UAS-P2X2*/+ larval brains treated with 30-s perfusions (black bar) of 5 mM ATP or vehicle (Veh). *E*: mean GCaMP3.0 fluorescence traces recorded from the LN_vs of *Pdf-LexA,LexAop-GCaMP3.0/Rh6-Gal4;UAS-P2X2*/+ larval brains in response to 30-s perfusions of 5 mM ATP or Veh. *F*: mean GCaMP3.0 fluorescence traces recorded from the LN_vs of *Pdf-LexA,LexAop-GCaMP3.0*/+;*UAS-*

P2X2/+ larval brains in response to 30-s perfusions of 5 mM ATP or Veh. For *D–F*, error bars indicate SE. *G–I*: summary histograms of the maximum GCaMP3.0 fluorescence increases displayed by the BNs (*G*) and s-LN_vs (*H* and *I*) of the genotypes shown in *D–F*. The two numbers displayed within each bar of the histogram indicate the number of neurons and the number of brains examined, respectively. Asterisks indicate a significant difference in maximum fluorescence increase between ATP and Veh treatments and "N.S." indicates no significant difference by Mann—Whitney *U* test (***$P < 0.001$ and **$P < 0.01$). The error bars in *G* represent the SE.

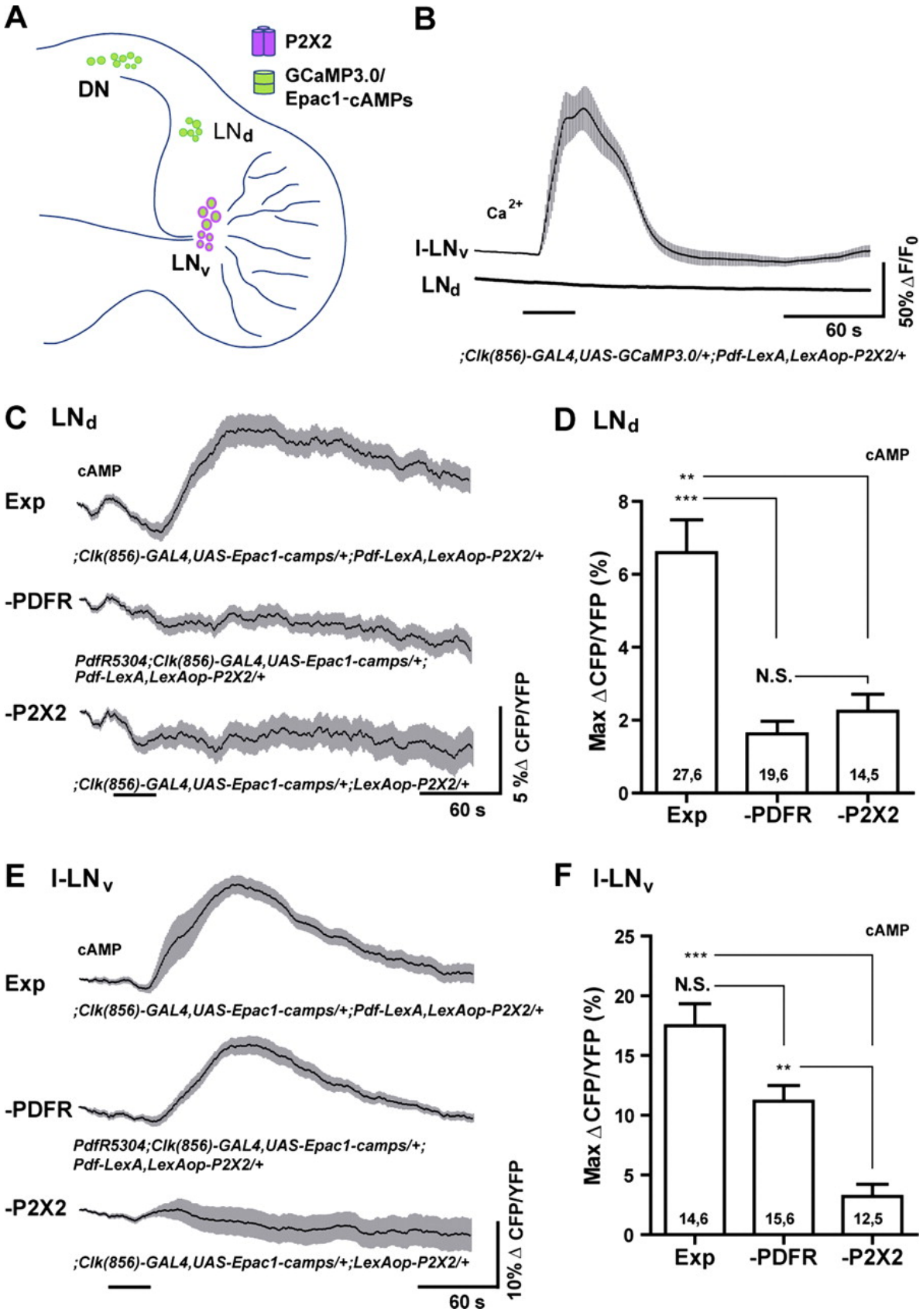
A
P2X2
GCaMP3.0/
Epac1-cAMPs
DN
LNd
LNv
B
Ca2+
l-LNv
LNd
50% ΔF/F0
60 s
;Clk(856)-GAL4,UAS-GCaMP3.0/+;Pdf-LexA,LexAop-P2X2/+
C LNd
cAMP
Exp
;Clk(856)-GAL4,UAS-Epac1-camps/+;Pdf-LexA,LexAop-P2X2/+
-PDFR
PdfR5304;Clk(856)-GAL4,UAS-Epac1-camps/+;
Pdf-LexA,LexAop-P2X2/+
-P2X2
;Clk(856)-GAL4,UAS-Epac1-camps/+;LexAop-P2X2/+
5 %Δ CFP/YFP
60 s
D LNd
cAMP
**
***
Max ΔCFP/YFP (%)
N.S.
27,6
19,6
14,5
Exp
-PDFR
-P2X2
E l-LNv
cAMP
Exp
;Clk(856)-GAL4,UAS-Epac1-camps/+;Pdf-LexA,LexAop-P2X2/+
-PDFR
PdfR5304;Clk(856)-GAL4,UAS-Epac1-camps/+;
Pdf-LexA,LexAop-P2X2/+
-P2X2
;Clk(856)-GAL4,UAS-Epac1-camps/+;LexAop-P2X2/+
10% Δ CFP/YFP
60 s
F l-LNv
cAMP
***
N.S.
**
Max ΔCFP/YFP (%)
14,6
15,6
12,5
Exp
-PDFR
-P2X2

Figure 2.7 LexA-based excitation and GAL4-based live imaging to test a predicted peptidergic connection deep within the adult brain.
A: schematic diagram showing the expression of P2X2 and genetically encoded sensors in the experimental brain for testing the predicted physiologic connection between the LN_v and the LN_d clock neurons. *B*: mean GCaMP3.0 fluorescence traces of the l-LN_vs and LN_ds during their responses to a 30-s bath application of 1 mM ATP (indicated by the bar under the plots). l-LN_v and LN_d plots were recorded simultaneously from the same optical sections of a *;Clock(856)-GAL4,UAS-GCaMP3.0/+;Pdf-LexA,LexAop-P2X2*/+ brain. Shaded regions surrounding the mean plots indicate SE. Excitation of the LN_vs had no measurable effects on GCaMP3.0 fluorescence in the LN_ds. For l-LN_vs, *N* = 14 neurons from 6 brains (14,6). For s-LN_vs, *N* = 17,6. *C*: mean Epac1-camps inverse FRET traces of the LN_ds during excitation of the LN_vs in *;Clock(856)-GAL4,UAS-Epac1-camps*/+;*Pdf-LexA,LexAop-P2X2*/+ brains ("Exp"). LN_v excitation resulted in increases in cAMP in the LN_ds. This response was absent in *$PdfR^{5304}$;Clock(856)-GAL4,UAS-Epac1-camps*/+;*Pdf-LexA,LexAop-P2X2*/+ brains ("—PDFR"), which lacked PDF receptor function, and in*;Clock(856)-GAL4,UAS-Epac1-camps*/+;*LexAop-P2X2*/+ brains, which lacked a LexA driver for the P2X2 element ("—P2X2"). *D*: summary histogram of the mean maximum increases in Epac1-camps inverse FRET for the LN_d data shown in *C*. *E*: mean Epac1-camps inverse FRET traces for l-LN_vs imaged simultaneously with the LN_ds shown in *C*. Plots displayed as for *C*. ATP/P2X2 excitation of the LN_vs resulted in cAMP increases in both wild type ("Exp") and *$PdfR^{5304}$* ("—PDF") backgrounds. The l-LN_vs showed no cAMP increases in response to ATP in the absence of a LexA driver for the P2X2 element ("—P2X2"). *F*: summary histogram of maximum increases in Epac1-camps inverse FRET for the l-LN_v data shown in *E*. For *D* and *F*, the two numbers within or above each bar of the histogram indicate the number of neurons and the number of brains examined respectively. ***$P < 0.001$; **$P < 0.01$; NS, nonsignificance by Kruskal—Wallis one-way ANOVA and Dunn's multiple comparisons test. The mean plots in *C* and *E* were corrected for spontaneous FRET drift by subtracting the mean inverse FRET traces of l-LN_v and LN_d neurons from vehicle treated *;Clock(856)-GAL4,UAS-Epac1-camps*/+;*Pdf-LexA,LexAop-P2X2*/+ ("Exp") brains (seemethods for details).

2.5 Discussion

Animal behavior is an emergent property of neural networks and is shaped by the pattern and nature of the connections between their constituent neurons. Connectivity is therefore an abiding problem in neuroscience, and understanding how it governs complex behavior is a fundamental goal of the field (Lichtman and Sanes 2008). Here we have introduced a method for addressing the physiologic connections between discrete neuronal classes in *Drosophila*. We have shown that the independent dual binary expression of the vertebrate purinergic P2X2 receptor and genetically encoded sensors makes possible the specific excitation of neuronal classes of interest while simultaneously imaging Ca^{2+} and cAMP dynamics within putative follower neurons. Our proof of principle experiments establish this "physiogenetic" approach as a technically facile method of investigating physiologic connections between electrophysiologically inaccessible neuronal classes of the *Drosophila* CNS.

Although the method we introduce here makes possible the detection of neural connections in regions of the brain where multielectrode electrophysiologic experiments are not possible, it is important to note its limitations relative to electrophysiologic techniques. For example, the use of bath-applied ATP to excite P2X2-expressing neurons does not offer the fine temporal control associated with the depolarization of neurons by brief current injections (Fig. 2.1). Likewise, genetically encoded sensors of neural signaling have not yet attained the sensitivity and temporal resolution of electrodes for detecting small changes in membrane voltage or modest excitatory/inhibitory responses. Thus, connections producing subthreshold excitatory input or only very weak excitation in follower neurons might be missed using the approach we have described. Furthermore, some inhibitory connections may not be detectable using existing genetically encoded sensors (e.g., Lelito and Shafer 2012). Thus, for any pair of

neuronal classes, the absence of both cAMP and Ca^{2+} responses in a putative follower neuron is not in itself compelling evidence for a complete lack of connection. Despite these limitations, the work presented here establishes that our method of addressing functional connectivity is sufficiently sensitive to detect both excitatory and modulatory connections between electrophysiologically inaccessible neuronal classes within the adult fly brain, thereby allowing for the analysis of functional connectivity in regions of the brain where electrodes cannot be used. We therefore believe that this method will be immediately useful for the investigation of connectivity within a variety of electrophysiologically inaccessible networks in the fly brain.

The ultimate cellular resolution afforded by this approach is currently limited by the number of available highly specific LexA and Gal4 drivers for directed P2X2 expression. This is no less true for the widespread use of these same drivers for the experimental manipulation of neuronal function and behavior, a limitation that has not prevented the field from learning a great deal about the neuronal classes underlying a wide range of behaviors (Simpson and Stephen 2009). Nevertheless, the current supply of specific drivers allows for many hypothesized connections between neuronal classes to be experimentally tested using the approach we have described, and the production of highly specific genetic drivers continues apace (e.g., Bohm et al. 2010; Luan and White 2007; Pfeiffer et al. 2008, 2010). Furthermore, in instances when sufficiently specific drivers prove unattainable, increased specificity of ATP/P2X2 excitation can be realized through localized puffing of ATP (Hu et al. 2010;Huang et al. 2010) or through the focal liberation of caged ATP using focused laser light (Z. Yao and O.T. Shafer, unpublished observations).

Although the methods described here allow for connections between discrete neuronal classes to be detected and characterized, they do not currently allow for a differentiation between

monosynaptic (direct) and polysynaptic (indirect) connections. This limitation does not preclude the usefulness of the technique, which can nevertheless reveal the presence and physiologic nature of connections between defined neuronal classes, whether monosynaptic or polysynaptic. Furthermore, it may be possible in the future to adapt established pharmacologic methods for determining if a given downstream response to ATP/P2X2 excitation is monosynaptic or polysynaptic. For example, the use of bathing saline containing high concentrations of divalent cations (e.g., Kandel et al. 1967) or tetrodotoxin (e.g., Mizunami 1990) to block the synaptic release from or the firing of interposed neurons could be compatible with this technique if P2X2, a nonselective cation channel, can drive sufficiently high Ca^{2+} in the presynaptic terminals of P2X2-expressing neurons in the presence of these manipulations. We are currently investigating these possibilities in multiple neuronal types.

Although other methods to detect physiologic connectivity have recently been used in the fly brain (e.g., Hu et al. 2010; Ruta et al. 2010), we feel that the approach outlined here has the virtue of a relative technical simplicity, requiring only standard confocal or epifluorescent microscopy and a means of delivering controlled perfusions of ATP solutions. Thus, the LexAop-driven P2X2, GCaMP3.0, and Epac1-camps elements we describe here, in combination with the large number of available Gal4, UAS, and LexA elements, constitute a flexible and technically facile toolkit for the interrogation of central neuronal networks in the fly. These tools can now be used to address functional connectivity within neuronal networks governing a wide range of behaviors in *Drosophila*. Furthermore, *Drosophila* photoreceptors and ligand-gated receptors have been successfully introduced into mammalian neurons (Morita et al. 2006; Zemelman et al. 2002), suggesting that an approach similar to the one described here using

appropriate heterologous receptors could be used to investigate the physiologic connections between neuronal ensembles within other model systems.

2.6 Acknowledgments

This work was supported by a National Institutes of Health Pathway to Independence Award (National Institute of Neurological Disorders and Stroke Grant R00-NS-62953) to O. T. Shafer. We thank Gero Miesenböck, Paul Taghert, Vivek Jayaraman, Michael Rosbash, Nick Glossop, Paul Hardin, Patrick Emery, and the Bloomington Drosophila Stock Center for providing fly stocks used in this study; Bing Yi and Jerry Rubin for sharing LexA and LexAop plasmids; and Robert Denver and John Kuwada for helpful comments on the manuscript.

2.7 References

Bohm RA, Welch WP, Goodnight LK, Cox LW, Henry LG, Gunter TC, Bao H, Zhang B. A genetic mosaic approach for neural circuit mapping in *Drosophila*. Proc Natl Acad Sci USA 107: 16378–16383, 2010[PMC free article] [PubMed]

Börner S, Schwede F, Schlipp A, Berisha F, Calebiro D, Lohse MJ, Nikolaev VO. FRET measurements of intracellular cAMP concentrations and cAMP analog permeability in intact cells. Nat Protocols 6: 427–438, 2011 [PubMed]

Brand A, Perrimon N. Targeted gene expression as a means of altering cell fates and generating dominant phenotypes. Development 118: 401–415, 1993 [PubMed]

Cao G, Nitabach MN. Circadian control of membrane excitability in *Drosophila melanogaster* lateral ventral clock neurons. J Neurosci 28: 6493–6501, 2008 [PMC free article] [PubMed]

Crocker A, Sehgal A. Genetic analysis of sleep. Genes Dev 24: 1220–1235, 2010 [PMC free article][PubMed]

Dickson BJ. Wired for sex: the neurobiology of Drosophila mating decisions. Science 322: 904–909, 2008 [PubMed]

Garczynski SF, Crim JW, Brown MR. Characterization and expression of the short neuropeptide F receptor in the African malaria mosquito, *Anopheles gambiae*. Peptides 28: 109–118, 2007 [PMC free article][PubMed]

Grima B, Chelot E, Xia R, Rouyer F. Morning and evening peaks of activity rely on different clock neurons of the *Drosophila* brain. Nature 431: 869–873, 2004 [PubMed]

Gummadova JO, Coutts GA, Glossop NRJ. Analysis of the *Drosophila* clock promoter reveals heterogeneity in expression between subgroups of central oscillator cells and identifies a novel enhancer region. J Biol Rhythms 24: 353–367, 2009 [PubMed]

Guo ZV, Hart AC, Ramanathan S. Optical interrogation of neural circuits in *Caenorhabditis elegans*. Nat Methods 6: 891–896, 2009 [PMC free article] [PubMed]

Helfrich-Förster C. The period clock gene is expressed in central nervous system neurons which also produce a neuropeptide that reveals the projections of circadian pacemaker cells within the brain of*Drosophila melanogaster*. Proc Natl Acad Sci USA 92: 612–616, 1995 [PMC free article] [PubMed]

Helfrich-Förster C, Edwards T, Yasuyama K, Wisotzki B, Schneuwly S, Stanewsky R, Meinertzhagen IA, Hofbauer A. The extraretinal eyelet of *Drosophila*: development, ultrastructure, and putative circadian function. J Neurosci 22: 9255–9266, 2002 [PubMed]

Helfrich-Förster C, Shafer OT, Wulbeck C, Grieshaber E, Rieger D, Taghert P. Development and morphology of the clock-gene-expressing lateral neurons of *Drosophila melanogaster*. J Comp Neurol500: 47–70, 2007 [PubMed]

Hewes RS, Schaefer AM, Taghert PH. The cryptocephal gene (ATF4) encodes multiple basic-leucine zipper proteins controlling molting and metamorphosis in *Drosophila*. Genetics 155: 1711–1723, 2000 [PMC free article] [PubMed]

Hu A, Zhang W, Wang Z. Functional feedback from mushroom bodies to antennal lobes in the *Drosophila*olfactory pathway. Proc Natl Acad Sci USA 107: 10262–10267, 2010 [PMC free article] [PubMed]

Huang J, Zhang W, Qiao W, Hu A, Wang Z. Functional connectivity and selective odor responses of excitatory local interneurons in *Drosophila* antennal lobe. Neuron 67: 1021–1033, 2010 [PubMed]

Hyun S, Lee Y, Hong ST, Bang S, Paik D, Kang J, Shin J, Lee J, Jeon K, Hwang S, Bae E, Kim J.Drosophila GPCR Han is a receptor for the circadian clock neuropeptide PDF. Neuron 48: 267–278, 2005 [PubMed]

Im SH, Taghert PH. PDF receptor expression reveals direct interactions between circadian oscillators in*Drosophila*. J Comp Neurol 518: 1925–1945, 2010 [PMC free article] [PubMed]

Johard HAD, Yoishii T, Dircksen H, Cusumano P, Rouyer F, Helfrich-Förster C, Nässel DR. Peptidergic clock neurons in *Drosophila*: ion transport peptide and short neuropeptide F in subsets of dorsal and ventral lateral neurons. J Comp Neurol 516: 59–73, 2009 [PubMed]

Kandel ER. Cellular Basis of Behavior: An Introduction to Behavioral Neurobiology. San Francisco: Freeman, 1976, p. 727

Kandel ER, Frazier WT, Waziri R, Coggeshall RE. Direct and common connections among identified neurons in *Aplysia*. J Neurophysiol 30: 1352–1376, 1967 [PubMed]

Kaneko M, Hall JC. Neuroanatomy of cells expressing clock genes in *Drosophila*: transgenic manipulation of the period and timeless genes to mark the perikarya of circadian pacemaker neurons and their projections. J Comp Neurol 422: 66–94, 2000 [PubMed]

Keene AC, Mazzoni EO, Zhen J, Younger MA, Yamaguchi S, Blau J, Desplan C, Sprecher SG. Distinct visual pathways mediate *Drosophila* larval light avoidance and circadian clock entrainment. J Neurosci31: 6527–6534, 2011 [PMC free article] [PubMed]

Kim SK, Rulifson EJ. Conserved mechanisms of glucose sensing and regulation by Drosophila corpora cardiaca cells. Nature 431: 316–320, 2004 [PubMed]

Lai SL, Lee T. Genetic mosaic with dual binary transcriptional systems in *Drosophila*. Nat Neurosci 9: 703–709, 2006 [PubMed]

Lear BC, Merrill CE, Lin JM, Schroeder A, Zhang L, Allada R. A G protein-coupled receptor, groom-of-PDF, is required for PDF neuron action in circadian behavior. Neuron 48: 221–227, 2005 [PubMed]

Lelito KR, Shafer OT., 3rd Reciprocal cholinergic and GABAergic modulation of the small ventrolateral pacemaker neurons of *Drosophila*'s circadian clock neuron network. J Neurophysiol 107: 2096–2108, 2012 [PMC free article] [PubMed]

Lichtman JW, Sanes JR. Ome sweet ome: what can the genome tell us about the connectome? Curr Opin Neurobiol 18: 346–353, 2008 [PMC free article] [PubMed]

Lima SQ, Miesenböck G. Remote control of behavior through genetically targeted photostimulation of neurons. Cell 121: 141–152, 2005 [PubMed]

Lin Y, Stormo GD, Taghert PH. The neuropeptide pigment-dispersing factor coordinates pacemaker interactions in the *Drosophila* circadian system. J Neurosci 24: 7951–7957, 2004 [PubMed]

Lissandron V, Rossetto MG, Erbguth K, Fiala A, Daga A, Zaccolo M. Transgenic fruit-flies expressing a FRET-based sensor for in vivo imaging of cAMP dynamics. Cell Signal19: 2296–2303, 2007

Littleton JT, Ganetzky B. Ion channels and synaptic organization: analysis of the Drosophila genome. Neuron 26: 35–43, 2000 [PubMed]

Luan H, White BH. Combinatorial methods for refined neuronal gene targeting. Curr Opin Neurobiol 17: 572–580, 2007 [PubMed]

Malpel S, Klarsfeld A, Rouyer F. Larval optic nerve and adult extra-retinal photoreceptors sequentially associate with clock neurons during *Drosophila* brain development. Development 129: 1443–1453, 2002 [PubMed]

Marella S, Fischler W, Kong P, Asgarian S, Rueckert E, Scott K. Imaging taste responses in the fly brain reveals a functional map of taste category and behavior. Neuron 49: 285–295, 2006 [PubMed]

McGuire SE, Deshazer M, Davis RL. Thirty years of olfactory learning and memory research in*Drosophila melanogaster*. Prog Neurobiol 76: 328–347, 2005 [PubMed]

Melcher C, Bader R, Pankratz MJ. Amino acids, taste circuits, and feeding behavior in *Drosophila*: towards understanding the psychology of feeding in flies and man. J Endocrinol 192: 467–472, 2007[PubMed]

Mertens I, Meeusen T, Huybrechts R, De Loof A, Schoofs L. Characterization of the short neuropeptide F receptor from *Drosophila melanogaster*. Biochem Biophys Res Commun 297: 1140–1148, 2002[PubMed]

Mertens I, Vandingenen A, Johnson EC, Shafer OT, Li W, Trigg JS, De Loof A, Schoofs L, Taghert PH.PDF receptor signaling in *Drosophila* contributes to both circadian and geotactic behaviors. Neuron 48: 213–219, 2005 [PubMed]

Mizunami M. Nonlinear signal transmission between second- and third-order neurons of cockroach ocelli.J Gen Physiol 95: 297–317, 1990 [PMC free article] [PubMed]

Morita M, Susuki J, Amino H, Yoshiki F, Moizumi S, Kudo Y. Use of the exogenous *Drosophila*octopamine receptor gene to study Gq-coupled receptor-mediated responses in mammalian neurons.Neuroscience 137: 545–553, 2006 [PubMed]

Nikolaev VO, Bünemann M, Hein L, Hannawacker A, Lohse MJ. Novel single chain cAMP sensors for receptor-induced signal propagation. J Biol Chem 279: 37215–37218, 2004 [PubMed]

Nitabach MN, Taghert PH. Organization of the *Drosophila* circadian control circuit. Curr Biol 18: R84—37215–R93, 2008 [PubMed]

Parisky KM, Agosto J, Pulver SR, Shang Y, Kuklin E, Hodge JJL, Kang K, Liu X, Garrity PA, Rosbash M, Griffith LC. PDF cells are a GABA-responsive wake-promoting component of the Drosophila sleep circuit. Neuron 60: 672–682, 2008 [PMC free article] [PubMed]

Peabody NC, Pohl JB, Diao F, Vreede AP, Sandstrom DJ, Wang H, Zelensky PK, White BH.Characterization of the decision network for wing expansion in *Drosophila* using targeted expression of the TRPM8 channel. J Neurosci 29: 3343–3353, 2009 [PMC free article] [PubMed]

Pfeiffer BD, Jenett A, Hammonds AS, Ngo TTB, Misra S, Murphy C, Scully A, Carlson JW, Wan KH, Laverty TR, Mungall C, Svirskas R, Kadonaga JT, Doe CQ, Eisen MB, Celniker SE, Rubin GM. Tools for neuroanatomy and neurogenetics in *Drosophila*. Proc Natl Acad Sci USA 105: 9715–9720, 2008[PMC free article] [PubMed]

Pfeiffer BD, Ngo TTB, Hibbard KL, Murphy C, Jenett A, Truman JW, Rubin GM. Refinement of tools for targeted gene expression in *Drosophila*. Genetics 186: 735–755, 2010 [PMC free article] [PubMed]

Pichaud F, Desplan C. A new visualization approach for identifying mutations that affect differentiation and organization of the Drosophila ommatidia. Development 128: 815–826, 2001 [PubMed]

Potter CJ, Tasic B, Russler EV, Liang L, Luo L. The Q system: a repressible binary system for transgene expression, lineage tracing, and mosaic analysis. Cell 141: 536–548, 2010 [PMC free article] [PubMed]

Pulver SR, Pashkovski SL, Hornstein NJ, Garrity PA, Griffith LC. Temporal dynamics of neuronal activation by channelrhodopsin-2 and TRPA1 determine behavioral output in Drosophila larvae. J Neurophysiol 101: 3075–3088, 2009 [PMC free article] [PubMed]

Reale V, Chatwin HM, Evans PD. The activation of G-protein gated inwardly rectifying K^+ channels by a cloned *Drosophila melanogaster* neuropeptide F-like receptor. Eur J Neurosci 19: 570–576, 2004[PubMed]

Renn SCP, Park JH, Rosbash M, Hall JC, Taghert PH. A PDF neuropeptide gene mutation and ablation of PDF neurons each cause severe abnormalities of behavioral circadian rhythms in *Drosophila*. Cell 99: 791–802, 1999 [PubMed]

Ruta V, Datta SR, Vasconcelos ML, Freeland J, Looger LL, Axel R. A dimorphic pheromone circuit in*Drosophila* from sensory input to descending output. Nature 468: 686–690, 2010 [PubMed]

Salvaterra PM, Kitamoto T. *Drosophila* cholinergic neurons and processes visualized with Gal4/UAS-GFP.Gene Expr Patterns 1: 73–82, 2001 [PubMed]

Schroll C, Riemensperger T, Bucher D, Ehmer J, Vlˆler T, Erbguth K, Gerber B, Hendel T, Nagel G, Buchner E, Fiala A. Light-induced activation of distinct modulatory neurons triggers appetitive or aversive learning in *Drosophila* larvae. Curr Biol 16: 1741–1747, 2006 [PubMed]

Shafer OT, Kim DJ, Dunbar-Yaffe R, Nikolaev VO, Lohse MJ, Taghert PH. Widespread receptivity to neuropeptide PDF throughout the neuronal circadian clock network of *Drosophila* revealed by real-time cyclic AMP imaging. Neuron 58: 223–237, 2008 [PMC free article] [PubMed]

Shafer OT, Taghert PH. RNA-interference knockdown of *Drosophila* pigment dispersing factor in neuronal subsets: the anatomical basis of a neuropeptide's circadian functions. PLoS ONE 4: e8298, 2009[PMC free article] [PubMed]

Shang Y, Griffith L, Rosbash M. Light-arousal and circadian photoreception circuits intersect at the large PDF cells of the *Drosophila* brain. Proc Natl Acad Sci USA 105: 19587–19594, 2008[PMC free article] [PubMed]

Sheeba V, Fogle KJ, Kaneko M, Rashid S, Chou YT, Sharma VK, Holmes TC. Large ventral lateral neurons modulate arousal and sleep in *Drosophila*. Curr Biol 18: 1537–1545, 2008 [PMC free article][PubMed]

Simpson JH, Stephen FG. Mapping and manipulating neural circuits in the fly brain. In: Advances in Genetics. Waltham, MA: Elsevier/Academic Press, 2009, p. 79–143 [PubMed]

Stoleru D, Peng Y, Agosto J, Rosbash M. Coupled oscillators control morning and evening locomotor behaviour of *Drosophila*. Nature 431: 862–868, 2004 [PubMed]

Tian L, Hires SA, Mao T, Huber D, Chiappe ME, Chalasani SH, Petreanu L, Akerboom J, McKinney SA, Schreiter ER, Bargmann CI, Jayaraman V, Svoboda K, Looger LL. Imaging neural activity in worms, flies and mice with improved GCaMP calcium indicators. Nat Methods 6: 875–881, 2009[PMC free article] [PubMed]

Tomchik SM, Davis RL. Dynamics of learning-related cAMP signaling and stimulus integration in the *Drosophila* olfactory pathway. Neuron 64(4): 510–21, 2009

Venken KJT, Simpson JH, Bellen HJ. Genetic manipulation of genes and cells in the nervous system of the fruit fly. Neuron 72: 202–230, 2011 [PMC free article] [PubMed]

Villella A, Hall JC, Jeffrey CH. Neurogenetics of courtship and mating in *Drosophila*. In: Advances in Genetics. Waltham, MA: Elsevier/Academic Press, 2008, p. 67–184 [PubMed]

Wang JW, Wong AM, Flores J, Vosshall LB, Axel R. Two-photon calcium imaging reveals an odor-evoked map of activity in the fly brain. Cell 112(2): 271–82, 2003

Wegener C, Hamasaka Y, Nässel DR. Acetylcholine increases intracellular Ca^{2+} via nicotinic receptors in cultured PDF-containing clock neurons of *Drosophila*. J Neurophysiol 91: 912–923, 2004 [PubMed]

Weiner J. Time, Love, Memory. New York: Vintage Books, 1999

Willemse M, Janssen E, Lange FD, Wieringa B, Fransen J. ATP and FRET: a cautionary note. Nat Biotech25: 170–172, 2007 [PubMed]

Willows AOD, Hoyle G. Neuronal network triggering a fixed action pattern. Science 166: 1549–1551, 1969 [PubMed]

Yasuyama K, Salvaterra PM. Localization of choline acetyltransferase-expressing neurons in *Drosophila*nervous system. Microsc Res Tech 45: 65–79, 1999 [PubMed]

Yizhar O, Fenno LE, Davidson TJ, Mogri M, Deisseroth K. Optogenetics in neural systems. Neuron 71: 9–34, 2011 [PubMed]

Yu D, Baird GS, Tsien RY, Davis RL. Detection of calcium transients in *Drosophila* mushroom body neurons with camgaroo reporters. J Neurosci 23(1): 64–72, 2003

Yuan Q, Xiang Y, Yan Z, Han C, Jan LY, Jan YN. Light-induced structural and functional plasticity in*Drosophila* larval visual system. Science 333: 1458–1462, 2011 [PMC free article] [PubMed]

Zemelman BV, Lee GA, Ng M, Miesenböck G. Selective photostimulation of genetically charged neurons.Neuron 33: 15–22, 2002 [PubMed]

Zhang L, Chung BY, Lear BC, Kilman VL, Liu Y, Mahesh G, Meissner RA, Hardin PE, Allada R. DN1p circadian neurons coordinate acute light and PDF inputs to produce robust daily behavior in*Drosophila*. Curr Biol 20: 591–599, 2010a [PMC free article] [PubMed]

Zhang Y, Liu Y, Bilodeau-Wentworth D, Hardin PE, Emery P. Light and temperature control the contribution of specific DN1 neurons to *Drosophila* circadian behavior. Curr Biol 20: 600–605, 2010b[PMC free article] [PubMed]

Zhao Y, Araki S, Wu J, Teramoto T, Chang YF, Nakano M, Abdelfattah AS, Fujiwara M, Ishihara T, Nagai T, Campbell RE. An expanded palette of genetically encoded Ca^{2+} indicators. Science 333: 1888–1891, 2011 [PMC free article] [PubMed]

Zimmermann G, Wang Lp Vaughan AG, Manoli DS, Zhang F, Deisseroth K, Baker BS, Scott MP.Manipulation of an innate escape response in *Drosophila*: photoexcitation of acj6 neurons induces the escape response. PLoS ONE 4: e5100, 2009 [PMC free article] [PubMed]

CHAPTER 3. GABAergic and glutamatergic inhibition of the lateral clock neurons differentially regulates daytime and nighttime sleep in *Drosophila*[2]

3.1 Abstract

Networks of circadian clock neurons orchestrate daily rhythms in sleep and activity. *Drosophila* displays two peaks of daily activity, the morning and evening peaks. Here, we provide an electrophysiological characterization of the dorsal lateral neurons (LN_ds), the so-called "evening oscillator". We find that the LN_ds are excited by acetylcholine and inhibited by GABA and glutamate. Furthermore, we provide evidence that the $DN1_p$ clock neurons inhibit the LN_ds. Our results reveal that while GABAergic inhibition of the lateral clock neuron network promotes sleep at night, glutamatergic inhibition via GluClα promotes wakefulness during the day. Our work demonstrates how fast synaptic inputs onto the lateral clock neurons orchestrate daily rhythms in sleep and activity. Most surprisingly, our results reveal that, within the clock network of *Drosophila*, the morning oscillator not only promotes morning activity but also promotes evening sleep, while the evening oscillator promotes evening activity and morning sleep.

[2] A manuscript comprising this chapter is in preparation for publication, with authors listed as Zepeng Yao, Richard I. Hume, and Orie T. Shafer.

3.2 Introduction

Daily rhythms in activity and sleep are timed by an endogenous clock, the so-called circadian clock. The central circadian clock consists of a network of clock neurons, each of which contains a molecular clock that generates gene expression oscillations with a period of approximately 24 hours (Herzog, 2007). Clock neurons are organized into functionally distinct subclasses that cooperate to support coordinated rhythms in behaviors and physiology (Vansteensel et al., 2008; Welsh et al., 2010). *Drosophila melanogaster* offers an excellent model to study the distinct roles of different clock neuron classes in circadian timekeeping and the mechanisms through which they are coordinated. The *Drosophila* clock network consists of about 150 clock neurons, radically fewer than the tens of thousands of neurons in the mammalian clock centers (Herzog, 2007). The fly's clock neurons are relatively dispersed throughout the brain and are highly stereotypic in their location and morphology, making each subclass of clock neurons easily identifiable (Helfrich-Förster, 2005). Despite this relative simplicity, flies display robust circadian rhythms in highly conserved behaviors, including sleep (Hendricks et al., 2000; Shaw et al., 2000; Huber et al., 2004).

Genetic rescue and neuronal ablation experiments have led to a widely accepted dual-oscillator model of clock network function in *Drosophila*. In this model, the ventral lateral neurons (LN_vs) function collectively as a "morning oscillator" that promotes activity around dawn, whereas the dorsal lateral neurons (LN_ds) function collectively as an "evening oscillator" that promotes activity around dusk (Grima et al., 2004; Stoleru et al., 2004). The LN_vs express a neuropeptide called pigment-dispersing factor (PDF), which is required for robust endogenous timekeeping in the absence of environmental cues and for the proper coordination of molecular and physiological rhythms among the various clock neuron classes (Helfrich-Förster, 1995; Renn

et al., 1999; Peng et al., 2003; Lin et al., 2004; Shafer et al., 2008; Yao and Shafer, 2014). A subset of the LN_vs, the large-LN_vs (l-LN_vs), functions as an arousal center to promote wakefulness(Shang et al., 2008; Sheeba et al., 2008a). Owing to their large size and anatomical accessibility, the electrophysiological properties of the l-LN_vs have been characterized by several groups. The l-LN_vs are receptive to several fast neurotransmitters (McCarthy et al., 2011), fire both tonic and bursting patterns of action potentials (Sheeba et al., 2008b; Muraro and Ceriani, 2015), and display a daily rhythm in firing rate (Cao and Nitabach, 2008; Sheeba et al., 2008b). In contrast, the electrophysiological properties of the LN_ds are unknown. These critical clock neurons are responsible for generating increased levels of activity around dusk (Grima et al., 2004; Stoleru et al., 2004), which is the most prominent peak of daily activity in flies, and are thought to be the dominant pacemakers of the clock network in the presence of light (Picot et al., 2007; Stoleru et al., 2007). The LN_ds also integrate visual inputs mediated by PDF and direct light inputs via the cell-autonomous photoreceptor Cryptochrome (CRY) (Cusumano et al., 2009) and are important for adjusting the fly's daily activity rhythms to environmental light:dark schedules (Yoshii et al., 2015). In addition to their circadian functions, the LN_ds are likely involved in olfactory associative learning (Chen et al., 2012) and plasticity in mating behaviors (Kim et al., 2013). Despite their importance for circadian timekeeping and behavioral plasticity, the LN_ds remain un-characterized electrophysiologically, presumably due to technical difficulties caused by their size and location within the brain.

Here we report for the first time an electrophysiological analysis of the LN_ds. We find that these critical clock neurons receive multiple fast neurotransmitter inputs, including excitatory cholinergic input mediated by nicotinic acetylcholine receptors, and inhibitory GABAergic (γ-aminobutyric acid) and glutamatergic inputs, both of which are mediated by

ligand-gated chloride channels. We also find that a subset of glutamatergic clock neurons, the posterior dorsal neurons group 1 ($DN1_p$s), inhibits the LN_ds. Furthermore, although GABA and glutamate both inhibit the LN_ds, the actions of these two neurotransmitters on the LN_ds differentially regulate daytime and nighttime sleep. Surprisingly, our results predict that the LN_vs which promote activity in the morning (Grima et al., 2004; Stoleru et al., 2004) also promote sleep in the evening, while the LN_ds which promote activity in the evening (Grima et al., 2004; Stoleru et al., 2004) also promote sleep in the morning. Our work provides the first electrophysiological characterization of the critical LN_ds, and reveals how the various clock neuron classes integrate distinct fast synaptic inputs to orchestrate daily rhythms in sleep and activity.

3.3 Results

3.3.1 The LN_ds fire spontaneous tonic and bursting patterns of action potentials.

Of the various clock neuron classes, only three groups of clock neurons have been recorded electrophysiologically, the l-LN_vs, the s-LN_vs, and the $DN1_p$s. The l-LN_vs have been recorded by multiple groups and been shown to fire both tonic and bursting patterns of action potentials (Park and Griffith, 2006; Cao and Nitabach, 2008; Sheeba et al., 2008b; McCarthy et al., 2011; Muraro and Ceriani, 2015). The s-LN_vs have only been recorded by Cao and Nitabach, with less than 20% of the recorded cells displaying spontaneous firing (Cao and Nitabach, 2008). The $DN1_p$s appear to fire tonic action potentials only (Seluzicki et al., 2014; Flourakis et al., 2015). We therefore sought to determine if the LN_ds fire spontaneous action potentials and if so what firing patterns they display. The LN_ds are heterogeneous in their neurochemistry(reviewed by Hermann-Luibl and Helfrich-Förster, 2015). In this study, we have focused on the three pairs

of LN_ds that co-express the circadian photoreceptor Cryptochrome (CRY) and the receptor for pigment-dispersing factor (PDFR) (Yoshii et al., 2008; Im and Taghert, 2010; Im et al., 2011). These neurons are important for the anticipatory peak of activity at dusk, for the light entrainment of circadian rhythms, and are important targets of the PDF signaling (Grima et al., 2004; Stoleru et al., 2004; Shafer et al., 2008; Cusumano et al., 2009; Yao and Shafer, 2014; Yoshii et al., 2015). We expressed the enhanced green fluorescent protein (EGFP) in these CRY^+/$PDFR^+$ LN_ds using the *Mai179-GAL4* driver (Grima et al., 2004; Yoshii et al., 2008), and made targeted patch-clamp recordings from these neurons in whole-brain explants. All the recordings were done during the light period of a 12hr:12hr light:dark (LD) cycle (see Materials and Methods for details).

We have recorded a total of seven LN_ds in cell-attached configuration. All of the recorded LN_ds fired spontaneous action potentials (Figure 3.1A-B). Four out of seven LN_ds fired tonic action potentials exclusively (Figure 3.1A), while three out of seven LN_ds displayed both bursting and tonic firing (Figure 3.1B). All bursting LN_ds also displayed tonic firing during the course of recording. The overall average firing frequency of the LN_ds in cell-attached configuration is 4.63 ± 1.39 Hz (mean ± SEM, n=7). When firing tonically, the average firing frequency is 3.59 ± 0.98 Hz (n=7). When firing in bursts, the average firing frequency is 12.01 ± 3.79 Hz (n=3).

We also made current-clamp recordings of the LN_ds in whole-cell configuration. The LN_ds have a membrane capacitance of 3.97 ± 0.13 pF (n=40) and a membrane resistance of 1.16 ± 0.07 GΩ (n=40) (Figure 3.1–figure supplement 1). The access resistance of most recordings is under 20 MΩ (Figure 3.1–figure supplement 1). Because of the high membrane resistance of the LN_ds, the seal current is expected to substantially depolarize the membrane potential in current-

clamp mode (Gouwens and Wilson, 2009). We therefore injected a constant hyperpolarizing current (typically -10 to -20 pA) into the recorded cell in order to compensate for the depolarizing effect of the seal current and bring the membrane potential to between -50 to -70 mV. Under these conditions, the LN_ds maintained stable firing rates. However, due to the need for the introduction of hyperpolarizing currents, we were not able to accurately measure the endogenous firing rate or the resting membrane potential of the LN_ds in whole-cell current-clamp recordings, nor any time-of-day effects on these metrics. Of the 40 LN_ds recorded in whole-cell configuration, 18 cells fired tonic action potentials exclusively (Figure 3.1C); 10 cells fired both tonic and bursting patterns of action potentials, alternating between the two firing modes during recording (Figure 3.1D-F); the remaining 12 cells were silent. It is unclear why some LN_ds were silent in whole-cell current-clamp mode. One possibility is that the spike initiation zone or part of the neural processes of the recorded cell was damaged even though the cell membrane appeared to be healthy.

3.3.2 Nicotinic acetylcholine receptors mediate excitatory inputs onto the LN_ds.

Given that acetylcholine (ACh) is the most prevalent fast excitatory neurotransmitter in insect brains (reviewed in Restifo and White, 1990), we first tested the LN_ds' receptivity to cholinergic agonists. In whole-cell current-clamp mode, 30s perfusion of 1 mM carbamoylcholine (CCh), a structural homolog of acetylcholine that is resistant to the action of cholinesterases, induced a burst of action potentials that lasted for approximately eight seconds and a strong depolarization of the membrane potential to about -30 mV in the LN_ds (Figure 3.2A,C,E). Following washout, the cell remained depolarized for tens of seconds, then gradually repolarized and resumed firing (Figure 3.2A). As in mammals, two types of cholinergic receptors exist in *Drosophila*, the ionotropic nicotinic acetylcholine receptors (nAChRs) and the

metabotropic muscarinic acetylcholine receptors (mAChR) (Littleton and Ganetzky, 2000). We utilized the nAChR-specific agonist, nicotine, to ask if LN_ds received nicotinic cholinergic input. 20s perfusion of 100 μM nicotine in current-clamp mode induced bursts of action potentials and strong depolarizations in the LN_ds, very similar to those seen in response to CCh perfusion (Figure 3.2B,D,E). We also performed voltage-clamp recordings to directly measure the currents induced by nicotine. When the LN_d membrane potential was held at -68 mV, perfusion of nicotine induced large inward currents (Figure 3.2–figure supplement 1). When brains were placed in a low calcium bath solution containing 1/10th the normal calcium to reduce network activity, the nicotine-induced currents persisted, indicating that these currents are largely independent of network activity (Figure 3.2–figure supplement 1). Lastly, we used a voltage ramp protocol, wherein the holding potential was changed linearly from -113 mV to +47 mV, to characterize how the nicotine-induced current changed as a function of the membrane potential (see Materials and Methods for details). We observed a nearly linear relationship between the nicotine-induced current and the membrane potential, with a reversal potential of -19.5 ± 5.2 mV (n=4) (Figure 3.2F), which is approximately the average of the sodium and the potassium equilibrium potentials, +49 mV and -91 mV, respectively at 25 °C. This suggests that the nicotine-induced currents are conducted by non-selective cation channels, consistent with the notion that they are conducted by nAChRs. We therefore conclude that nAChRs mediate excitatory synaptic inputs onto the LN_ds.

3.3.3 $GABA_A$ receptors and glutamate-gated chloride channels mediate inhibitory inputs onto the LN_ds.

Next, we tested the LN_ds' receptivity to GABA (γ-aminobutyric acid), the major fast inhibitory neurotransmitter in the fly brain (reviewed in Restifo and White, 1990). In whole-cell

current-clamp recordings, perfusion of 1 mM GABA induced hyperpolarization of the LN_d membrane potential and completely suppressed spontaneous firing (Figure 3.3A-B). The inward GABA-induced currents, measured in voltage-clamp mode with a holding potential of -113 mV, persist in low calcium bath solution, suggesting that the LN_ds are directly responsive to GABA (Figure 3.3–figure supplement 1). Voltage ramp experiments revealed that the reversal potential for the GABA-induced currents was -68.5 ± 6.6 mV (n=3) (Figure 3.2C). This is more negative than but still close to the predicted equilibrium potential for chloride (-49 mV at 25 °C), suggesting that these currents may be at least partially conducted by chloride channels. The $GABA_A$ receptors ($GABA_A$Rs) are chloride-conducting ion channels gated by GABA (reviewed by Macdonald and Olsen, 1994). The presence of 100μM picrotoxin, a potent $GABA_A$R antagonist (Macdonald and Olsen, 1994), almost completely suppressed the GABA-induced currents when measured at a holding potential of -113 mV (Figure 3.3D-E). We conclude that $GABA_A$ receptors mediate inhibitory synaptic inputs onto the LN_ds.

We next tested the LN_ds' receptivity to a third fast neurotransmitter, glutamate. Glutamatergic neurons are widespread in the *Drosophila* central nervous system (Daniels et al., 2008), but the physiological functions of glutamatergic signaling in the central brain are not well understood. The fly genome encodes a glutamate-gated chloride channel, GluClα, which is not present in mammals, suggesting that glutamate can be an inhibitory neurotransmitter in the fly brain (Cully et al., 1996). Indeed, glutamate acts as an inhibitory neurotransmitter in the fly olfactory system (Liu and Wilson, 2013) and mediates inhibition of the l-LN_vs (McCarthy et al., 2011), clock neurons important for arousal in flies (Shang et al., 2008; Sheeba et al., 2008a). Furthermore, glutamate is expressed by a subset of dorsal clock neurons (Hamasaka et al., 2007; Guo et al., 2016) where it may function as a synchronizing factor for the clock neuron network

(Collins et al., 2014). We therefore wondered if the LN_ds would respond to exogenously applied glutamate. Perfusion of 1 mM glutamate resulted in hyperpolarization of the LN_ds and complete suppression of the LN_d firing in current-clamp mode (Figure 3.4A-B). When the LN_d membrane potential was held at -113 mV in voltage-clamp mode, glutamate induced inward currents in the LN_ds that persisted under low calcium conditions, consistent with glutamate having direct effects on the LN_ds (Figure 3.4–figure supplement 1). Voltage ramp experiments revealed that the glutamate-induced current reversed at -58.3 ± 2.6 mV (n=6), close to the predicted chloride equilibrium potential (-49 mV at 25 °C), suggesting that theses currents are conducted by GluClα channels (Figure 3.4C). Because of the lack of highly specific antagonists for GluClα channels, we took a genetic approach, knocking down *GluClα* expression in the LN_ds using RNAi. The knock-down of *GluClα* in the LN_ds significantly reduced the currents induced by glutamate perfusion (Figure 3.4D-E). As an additional control, we showed that the *GluClα* knock-down did not affect the LN_d's response to GABA (Figure 3.4E), indicating that the RNAi against *GluClα* is specific. Thus, the LN_ds are inhibited by glutamate through the action of the glutamate-gated chloride channel GluClα.

3.3.4 The $DN1_p$s provide inhibitory synaptic input onto the LN_ds.

Our results indicate that GABA and glutamate provide inhibitory synaptic inputs onto the LN_ds through chloride channels (Figures 3.3-3.4). None of the various classes of clock neuron in *Drosophila* are GABAergic (Hamasaka et al., 2005), whereas some of the dorsal clock neurons including the dorsal neurons group 1 (DN1s) and dorsal neurons group 3 (DN3s) are glutamatergic (Hamasaka et al., 2007; Guo et al., 2016). The neurites of DN1s and LN_ds intermingle in the dorsal protocerebrum, and a subset of the posterior DN1s ($DN1_p$s) project ventrally and terminate in proximity to the LN_ds (Kaneko and Hall, 2000; Zhang et al., 2010b),

suggesting potential synaptic connections between the $DN1_p$s and the LN_ds. To test this hypothesis, we expressed the mammalian ATP-gated nonselective cation channel P2X2, which is not present in the fly genome (Littleton and Ganetzky, 2000; Lima and Miesenböck, 2005), in the $DN1_p$s to render them excitable by exogenously applied ATP, while simultaneously monitoring LN_d membrane currents using whole-cell voltage-clamp recordings. We found that perfusion of 250 μM ATP consistently and near-maximally excites the P2X2-expressing $DN1_p$s in our experimental conditions (Figure 3.5–figure supplement 1). At a holding potential of -113 mV, perfusion of 250 μM ATP induced inward currents in the LN_ds that are significantly different from those of vehicle controls (Figure 3.5A,D). These ATP-induced currents in the LN_ds depend on P2X2 expression in the $DN1_p$s and therefore the excitation of $DN1_p$s (Figure 3.5C). Voltage ramp experiments reveal that the $DN1_p$-to-LN_d current appears to be outwardly rectifying, with a reversal potential of -72.0 ± 4.2 mV (n=5) (Figure 3.5B), which is in between the chloride and potassium equilibrium potentials, -49 mV and -91 mV, respectively at 25 °C. This suggests that these currents are likely a mixture of chloride and potassium currents, which would normally act to hyperpolarize the LN_ds. We therefore conclude that the $DN1_p$s provide inhibitory synaptic input onto the LN_ds, presumably via glutamate.

As mentioned above, another class of clock neurons, the l-LN_vs, are also inhibited by glutamate (McCarthy et al., 2011). We therefore asked if the l-LN_vs are also inhibited by the $DN1_p$s. P2X2-mediated excitation of the $DN1_p$s induced significant but relatively small inward currents in the l-LN_vs when their membrane potential was held at -113 mV (Figure 3.5E-F). Exciting all the glutamatergic neurons induced larger inward currents in the l-LN_vs (Figure 3.5G), suggesting that the l-LN_vs receive additional glutamatergic inputs from neurons other than the $DN1_p$s.

3.3.5 GABAergic and glutamatergic inputs to the clock network differentially regulate sleep.

A functional molecular clock in the LN_ds is sufficient to generate increased levels of locomotor activity in anticipation of lights-off, indicating that the LN_ds promote locomotor activity around dusk (Grima et al., 2004). A recent study found that the LN_ds display daily rhythms in their intracellular calcium concentration, with the highest calcium levels in the late afternoon, a few hours before the fly's activity peak at dusk (Liang et al., 2016). These results further support the notion that the LN_ds promote locomotor activity in the evening. We therefore reasoned that a properly-timed suppression of LN_d neuronal activity would be important for the fly's normal timing of activity quiescence and sleep. Given that GABA and glutamate inhibit LN_d neuronal activity via $GABA_A$Rs and GluClα respectively (Figures 3.3-3.4), we wondered if the disruption of these inhibitory inputs would have effects on the fly's rhythm of activity and sleep.

When we knocked down *$GABA_AR$* expression in the LN_ds (along with various non-clock neurons) using the combination of *Mai179-GAL4* and *Pdf-GAL80* (Grima et al., 2004; Stoleru et al., 2004; Yoshii et al., 2008), we observed a reduction of total sleep amount specifically in the nighttime of a light/dark cycle, but not in the daytime (Figure 3.6A-B). The same effects were observed when we knocked down *$GABA_AR$* in the LN_ds using a different driver, *R78G02-GAL4*, which is expressed in the $CRY^+/PDFR^+$ LN_ds but not in the $CRY^-/PDFR^-$ LN_ds or the PDF-expressing LN_vs (Dr. C. Helfrich-Förster, personal communication) (Figure 3.6C-D). These phenotypes were also observed when we used different *RNAi* lines targeting different regions of the *$GABA_AR$* transcripts (Liu et al., 2007) (Figure 3.6C-D and Figure 3.6–figure supplement 1A-D). These results indicate that $GABA_A$R-mediated inhibition of the LN_ds normally promotes

sleep at night. Interestingly, it had previously been reported that $GABA_AR$-mediated inhibition of the other class of lateral clock neurons, the LN_vs also promotes sleep at night (Parisky et al., 2008; Chung et al., 2009) (Figure 3.6–figure supplement 1E-F). Therefore, GABA suppresses the neuronal activity of both sets of lateral neurons to promote nighttime sleep.

In contrast, knocking down *GluClα* expression in the LN_ds resulted in an increased daytime sleep, without significantly affecting the amount of nighttime sleep (Figure 3.7A-B). The increase of daytime sleep occurs primarily in the first half of the light period (Figure 3.7B and Figure 3.7–figure supplement 1A). The LN_vs also express *GluClα* (McCarthy et al., 2011; Collins et al., 2012). When we knocked down *GluClα* in the LN_vs, we also observed an increase in the amount of daytime sleep, but not of nighttime sleep (Figure 3.7C-D). However, when *GluClα* was knocked down in the LN_vs, the increase of daytime sleep occurs primarily in the second half of the light period (Figure 3.7D and Figure 3.7–figure supplement 1B). Finally, when *GluClα* was knocked down in both the LN_ds and the LN_vs, the amount of sleep was increased in both the first half and the second half of the light period (Figure 3.7E-F and Figure 3.7–figure supplement 1C). Taken together, our results suggest that the glutamatergic inhibition of lateral clock neurons normally functions to suppress sleep during the day, with GluClα-mediated inhibition of the LN_ds suppressing sleep in the morning and GluClα-mediated inhibition of the LN_vs suppressing sleep in the afternoon. This result was quite surprising, as it predicts that the LN_vs which promote activity in the morning (Grima et al., 2004; Stoleru et al., 2004) also promote sleep in the afternoon, while the LN_ds which promote activity in the afternoon (Grima et al., 2004; Stoleru et al., 2004) also promote sleep in the morning (Figure 3.8).

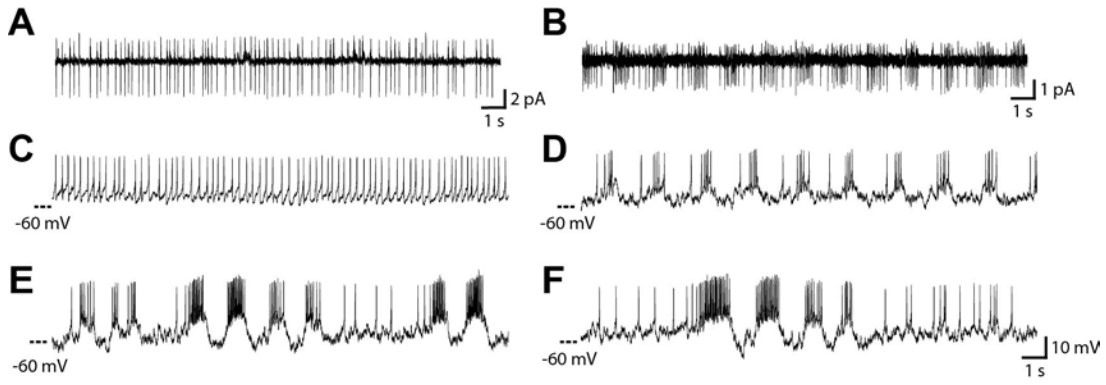

Figure 3.1. Spontaneous tonic and burst firing of the LN_ds.
(**A-B**) Representative cell-attached voltage-clamp recordings of the LN_ds. The pipette potential was 0 mV. The LN_d in (**A**) is displaying tonic firing, while the LN_d in (**B**) is bursting. (**C-F**) Representative whole-cell current-clamp recordings of the LN_ds. A constant hyperpolarizing current was injected to counteract the depolarizing seal current (*see Materials and Methods for details*). Panel (**C**) shows an LN_d displaying tonic firing; Panel (**D**) shows a bursting LN_d. Panels (**E-F**) display examples of LN_ds alternating between tonic and burst firing.

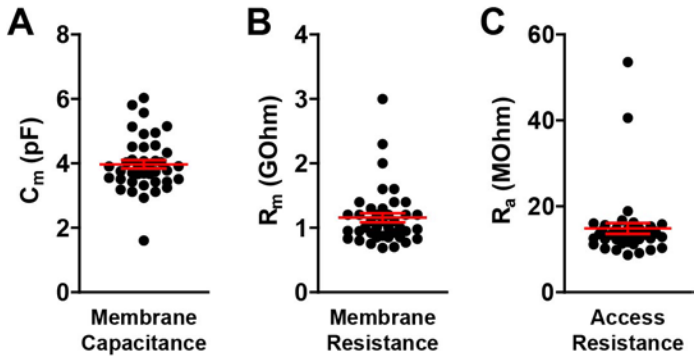

Figure 3.1–figure supplement 1. Electrophyiological parameters of whole-cell LN_d recordings.
(**A**) Membrane capacitance, (**B**) membrane resistance, and (**C**) access resistance for whole-cell LN_d recordings. Graphs report values for a total of 40 LN_ds from 40 male *Mai179>EGFP* brains. Lines represent mean ± SEM (standard error of the mean).

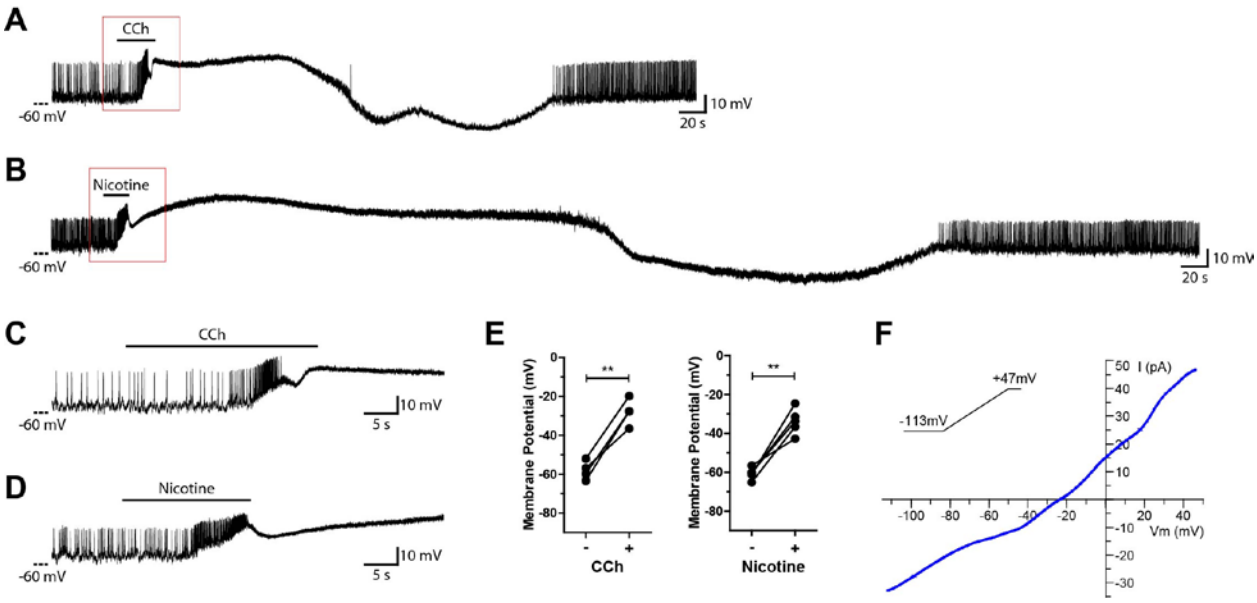

Figure 3.2 Nicotinic acetylcholine receptor agonists excite the LN_ds.
(**A**) Representative whole-cell current-clamp recording of an LN_d responding to the perfusion of 1 mM carbamoylcholine (CCh), a structural homolog of acetylcholine. CCh induced strong depolarization of the LN_d membrane. (**B**) Representative whole-cell current-clamp recording of an LN_d responding to the perfusion of 100 μM nicotine, a nAChR-specific agonist. Nicotine induced a depolarization of the LN_d membrane similar to that observed for CCh in (**A**). (**C-D**) Magnified views of the boxed regions in panel (**A**) and panel (**B**), respectively. The black bars above the traces in (**A-D**) indicate the perfusion time of the indicated chemicals. (**E**) Quantification of the LN_d membrane potential before and after CCh (left) and nicotine (right) treatments. ** $P < 0.01$, by paired t test. (**F**) The current-voltage relationship of the nicotine-induced current in a representative LN_d, measured by a voltage ramp protocol (*see Materials and Methods for details*). The reversal potential is approximately -25 mV, suggesting that the current is conducted by nonselective cation channels.

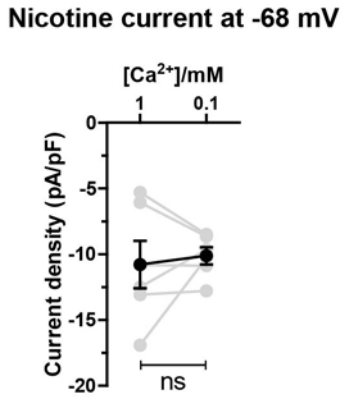

Figure 3.2–figure supplement 1. The nicotine-induced LN_d currents are largely network-independent.
Currents induced by nicotine were measured in the same LN_ds in both normal Ca^{2+} (1 mM) and low Ca^{2+} (0.1 mM) saline at a holding potential of -68 mV. Data for individual LN_ds are shown in light gray. Average values are shown in black. Error bars represent SEM. 'ns', not significant, by paired t test.

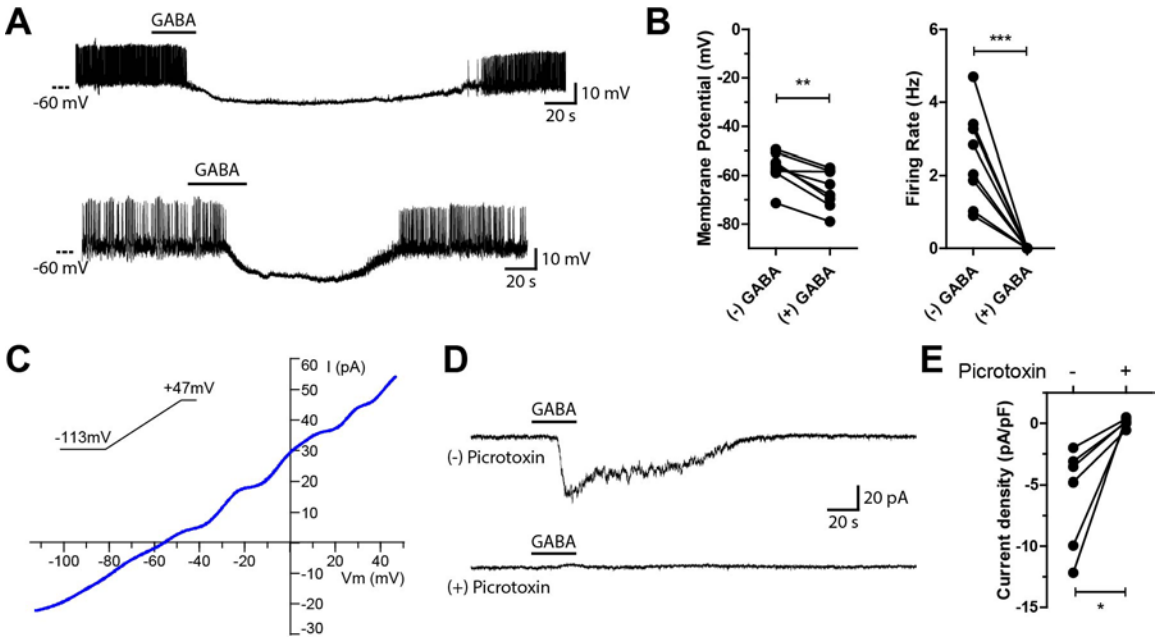

Figure 3.3. GABA inhibits the LN_ds through $GABA_A$ receptors.
(**A**) Representative whole-cell current-clamp recordings of two LN_ds responding to perfusion of 1 mM GABA. GABA induced hyperpolarization of the LN_d membrane potential and completely suppressed the LN_d firing. (**B**) Quantification of the LN_d membrane potential (left) and firing rate (right) before and after GABA treatment. ** $P < 0.01$, *** $P < 0.001$, by paired t test. (**C**) The current-voltage relationship of the GABA-induced current in a representative LN_d, measured by a voltage ramp protocol (*see Materials and Methods for details*). (**D**) Representative whole-cell voltage-clamp recording of an LN_d responding to GABA perfusion in the absence (top) or presence (bottom) of 100 µM picrotoxin, a potent $GABA_AR$ antagonist. The holding potential was -113 mV. In (**A**) and (**D**) the perfusion time of GABA is indicated by the black bars above the traces. (**E**) Current density induced by GABA in the absence or presence of picrotoxin at a holding potential of -113 mV. * $P < 0.05$, by paired t test.

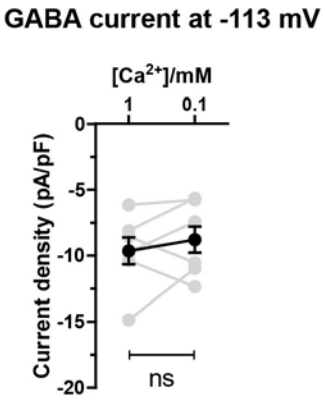

Figure 3.3–figure supplement 1. The GABA-induced LN_d currents are largely network-independent.
Currents induced by GABA were measured in the same LN_ds in both normal Ca^{2+} (1 mM) and low Ca^{2+} (0.1 mM) saline at a holding potential of -113 mV. Data for individual LN_ds are shown in light gray. Average values are shown in black. Error bars represent SEM. 'ns', not significant, by paired t test.

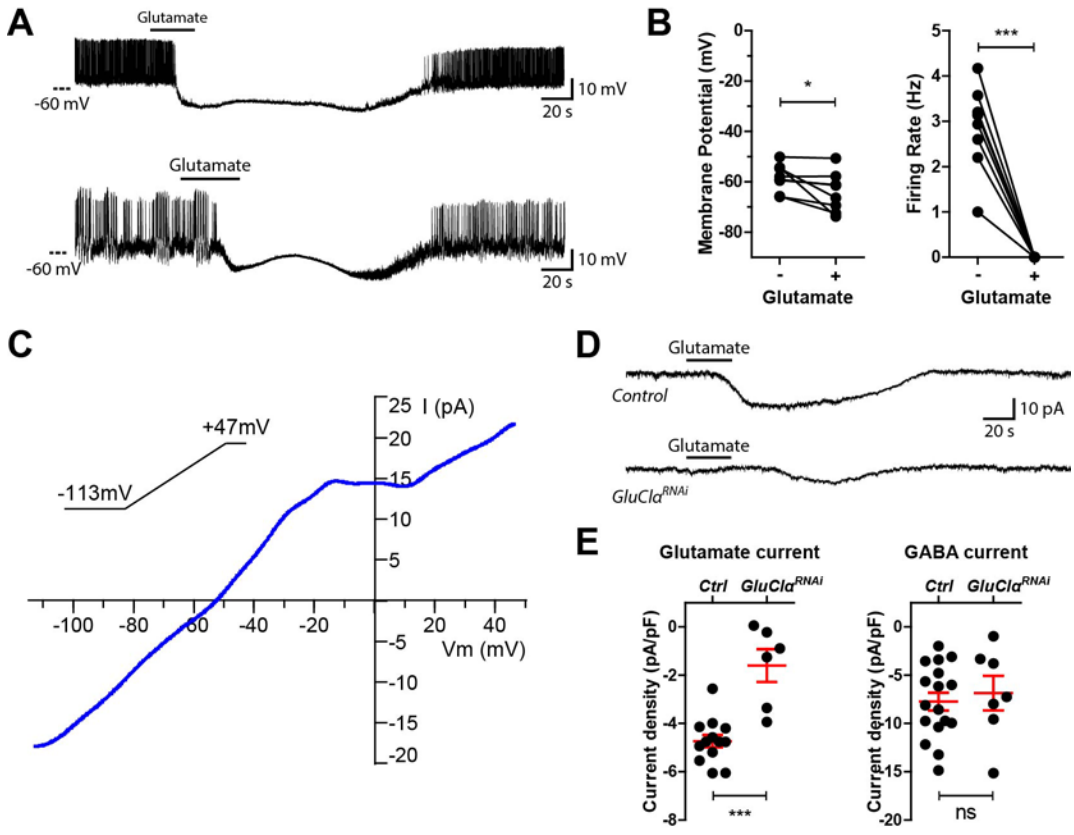

Figure 3.4. Glutamate inhibits the LN_ds through the glutamate-gated chloride channel GluClα.

(**A**) Representative whole-cell current-clamp recordings of two LN_ds responding to perfusion of 1 mM glutamate. Glutamate induced hyperpolarization of the LN_d membrane potential and completely suppressed the LN_d firing. (**B**) Quantification of the LN_d membrane potential (left) and firing rate (right) before and after glutamate treatment. * $P < 0.05$, *** $P < 0.001$, by paired t test. (**C**) The current-voltage relationship of the glutamate-induced current in a representative LN_d, measured by a voltage ramp protocol (*see Materials and Methods for details*). (**D**) Representative glutamate-induced currents in a control LN_d (top) and in an LN_d in which *GluClα* has been knocked down (bottom), both measured at a holding potential of -113 mV. The genotypes are *;Mai179-GAL4/UAS-EGFP;* for the control, and *;Mai179-GAL4,UAS-EGFP/UAS-Dcr-2;UAS-GluClα^{RNAi}/+* for the *GluClα* knock-down. In (**A**) and (**D**) the perfusion time of glutamate is indicated by the black bars above the traces. (**E**) Current density induced by glutamate (left graph) and GABA (right graph) in control LN_ds and *GluClα* knock-down LN_ds at a holding potential of -113 mV. Lines represent mean ± SEM. *** $P < 0.001$, 'ns', not significant, by unpaired t test.

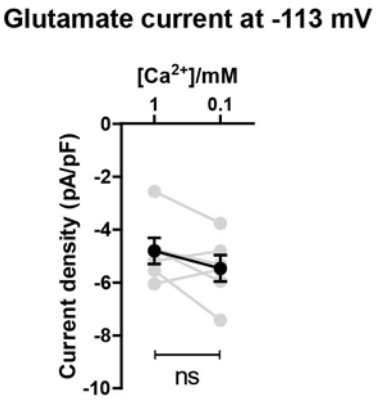

Figure 3.4–figure supplement 1. The glutamate-induced currents in the LN_ds are largely network-independent.

Glutamate induced currents were measured in the same LN_ds in both normal Ca^{2+} (1 mM) and low Ca^{2+} (0.1 mM) external saline at a holding potential of -113 mV. Data for individual LN_ds are shown in light gray. Average values are shown in black. Error bars represent SEM. 'ns', not significant, by paired t test.

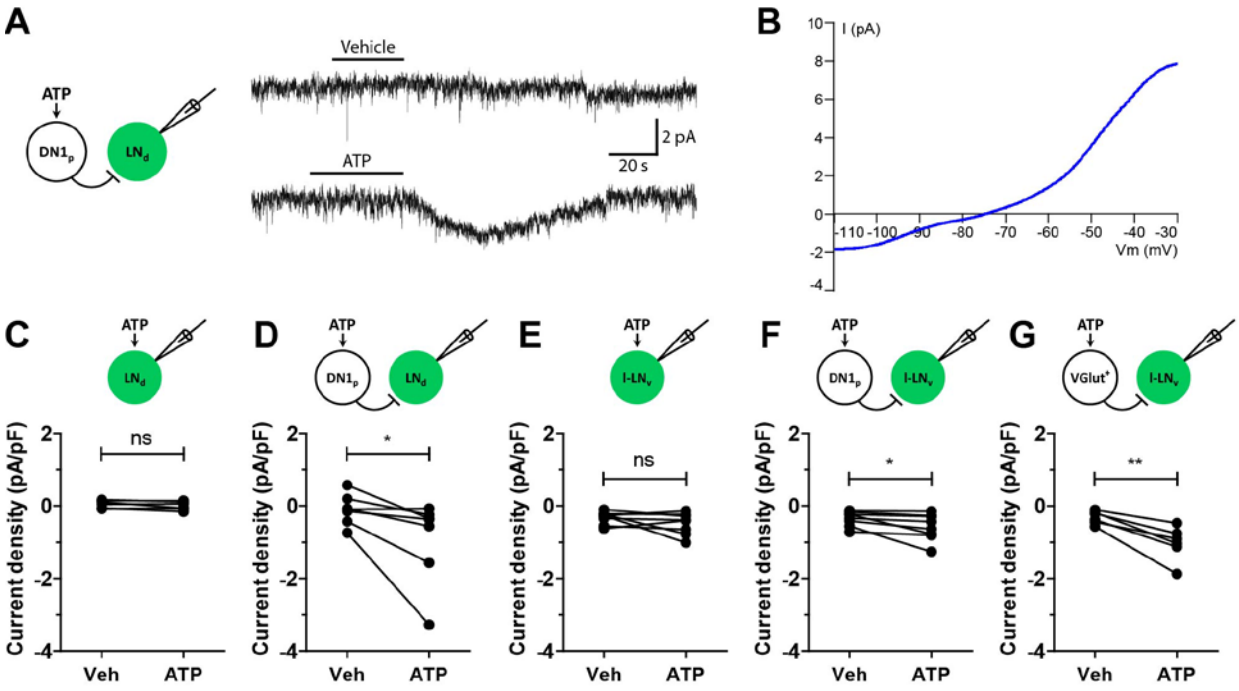

Figure 3.5. The $DN1_p$s inhibit the LN_ds.
(**A**) Left: a diagram of the experimental strategy: P2X2 was expressed in the $DN1_p$s to render them excitable by ATP while the postsynaptic response in an LN_d was simultaneously monitored using patch-clamp recording. Right: representative whole-cell voltage-clamp recordings of LN_ds responding to vehicle (top) and 250 µM ATP (bottom). The perfusion time is indicated by the black bars above the traces. The excitation of $DN1_p$s by ATP induced an inward current in the recorded LN_d at a holding potential of -113 mV. (**B**) Representative current-voltage relationship of the $DN1_p$-to-LN_d current induced by ATP treatment, measured by a voltage ramp protocol. (**C-D**) LN_d current density induced by vehicle and ATP perfusion of control (**C**) and experimental (**D**) flies. The genotypes are *;Mai179-GAL4/UAS-EGFP;LexAop-P2X2/+* for control (**C**) and *;Mai179-GAL4/UAS-EGFP;Clk4.1M-LexA/LexAop-P2X2* for experimental flies (**D**). (**E-G**) l-LN_v current density induced by vehicle and ATP perfusion for the following genotypes: *;Pdf-LexA,LexAop-Epac1-camps/+;UAS-P2X2/+* (**E**), *;Pdf-LexA,LexAop-Epac1-camps/+;Clk4.1M-GAL4/UAS-P2X2* (**F**), and *;Pdf-LexA,LexAop-Epac1-camps/+;VGlut-GAL4/UAS-P2X2* (**G**). * $P < 0.05$, ** $P < 0.01$, 'ns', not significant, by paired t test.

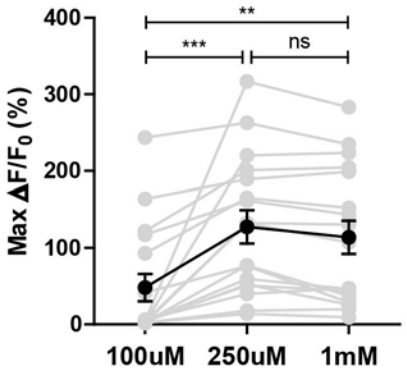

Figure 3.5–figure supplement 1. Perfusion of 250 µM ATP results in consistent and near-maximal excitation of the P2X2-expressing DN1$_p$s.
Calcium imaging was performed to assess the extent of excitation of P2X2-expressing DN1$_p$s by different concentrations of ATP (*see Materials and Methods for details*). 17 DN1$_p$s from 3 brains dissected from *LexAop-GCaMP3.0/Sco;Clk4.1M-LexA/LexAop-P2X2* flies were sequentially treated by 100 µM, 250 µM, and 1 mM of ATP. The Ca^{2+} responses (quantified as maximum percent GCaMP3.0 fluorescence increase over baseline) of individual DN1$_p$s are shown in light gray. Average responses are shown in black. Error bars represent SEM. ** $P < 0.01$, *** $P < 0.001$, 'ns', not significant, by the Friedman one-way ANOVA and Dunn's multiple comparison test.

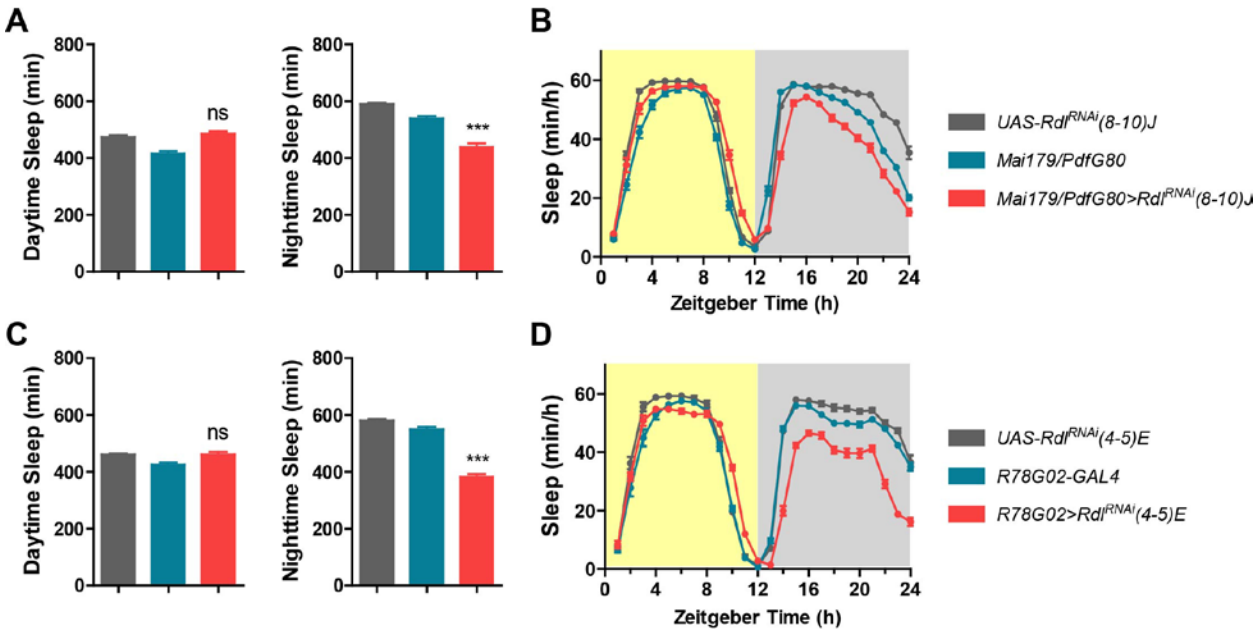

Figure 3.6. RNAi-mediated knock-down of *GABA$_A$R* expression in the LN$_d$s results in reduced nighttime sleep.
(**A, C**) The total amount of daytime sleep (left) and nighttime sleep (right) of the genotypes indicated on the far right of the figure. *GABA$_A$R* (also known as *Rdl* in flies) expression was knocked down in the LN$_d$s using the *Mai179-GAL4/Pdf-GAL80* combination in (**A**) and the *R78G02-GAL4* driver in (**C**). *** P < 0.001, 'ns', not significant. See *Materials and Methods* for details of the statistics. (**B, D**) Population averaged sleep profiles of the indicated genotypes. Yellow indicates the light period and gray indicates the dark period. All data are presented as mean ± SEM.

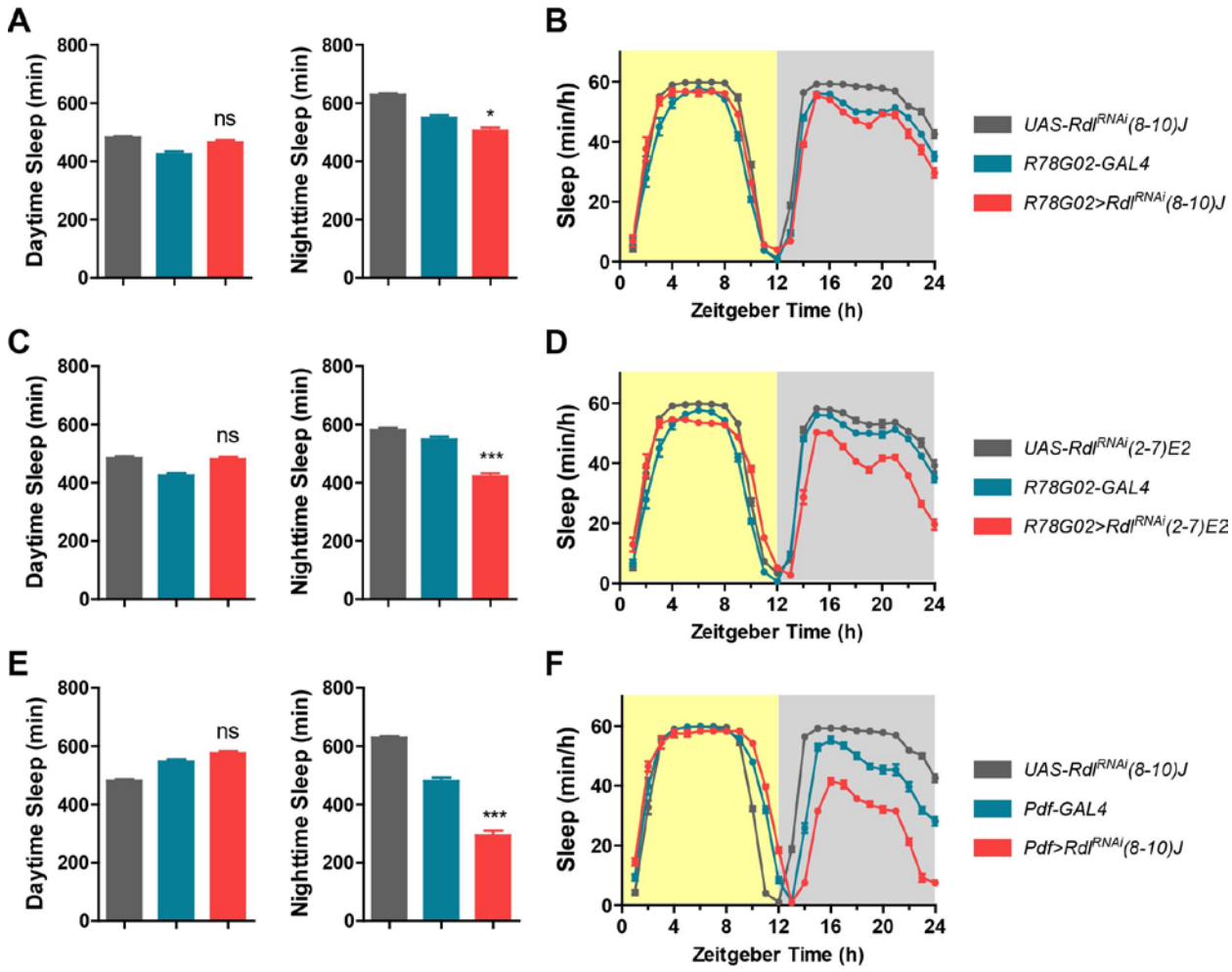

Figure 3.6–figure supplement 1. RNAi-mediated knock-down of *GABA$_A$R* expression in the lateral clock neurons results in reduced nighttime sleep.
(**A, C, E**) The total amount of daytime sleep (left) and nighttime sleep (right) of the genotypes indicated on the far right of the figure. *GABA$_A$R* expression was knocked down in the LN$_d$s using the *R78G02-GAL4* driver and two different RNAi lines (**A, C**), and in the LN$_v$s using the *Pdf-GAL4* driver (**E**). * $P < 0.05$, *** $P < 0.001$, 'ns', not significant. See *Materials and Methods* for details of the statistics. (**B, D, F**) Population averaged sleep profiles of the indicated genotypes. Yellow indicates the light period and gray indicates the dark period. All data are presented as mean ± SEM.

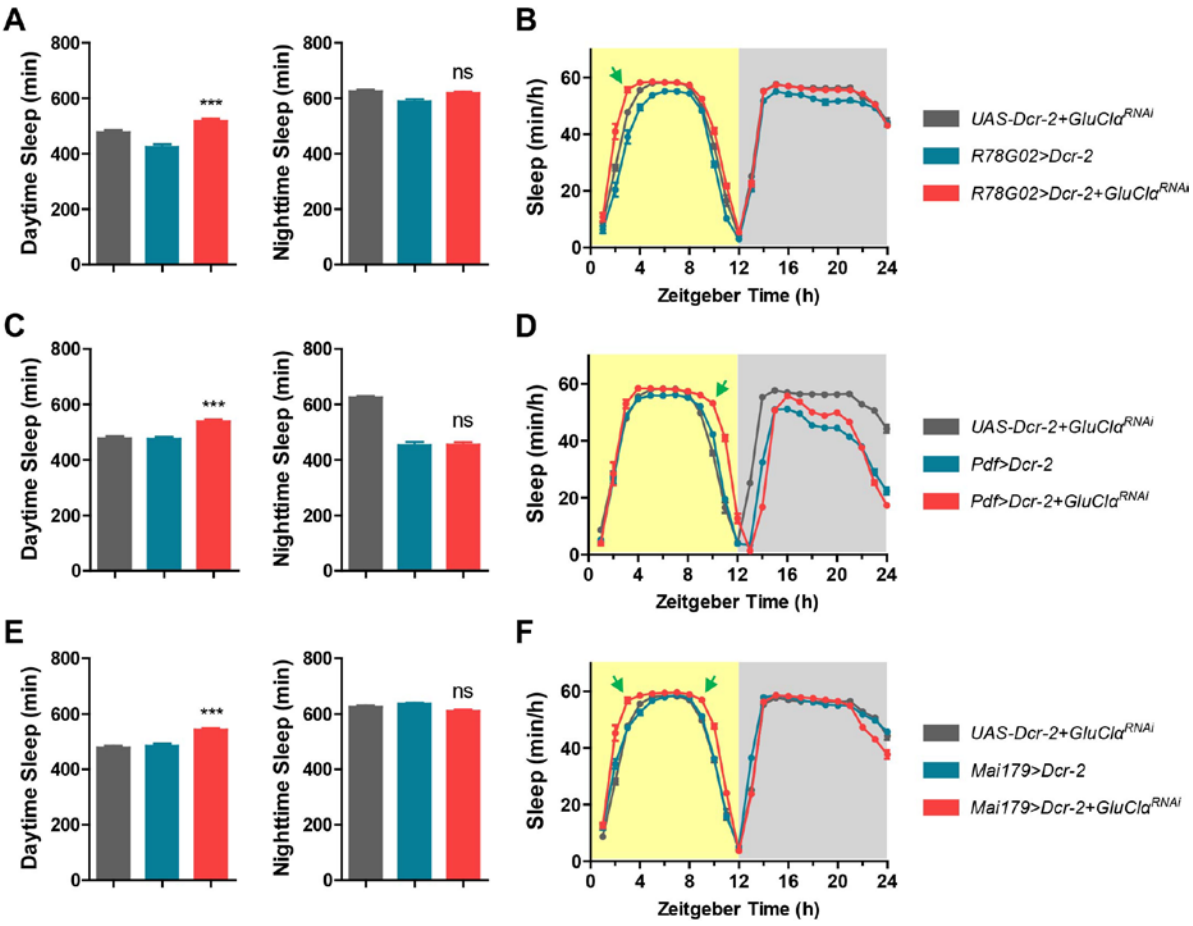

Figure 3.7. RNAi-mediated knock-down of *GluClα* expression in the lateral clock neurons results in increased daytime sleep.
(**A, C, E**) The total amount of daytime sleep (left) and nighttime sleep (right) of the genotypes indicated on the far right of the figure. *GluClα* expression was knocked down in the LN_ds in (**A**), in the LN_vs in (**C**), and in both the LN_ds and the LN_vs in (**E**). *** $P < 0.001$, 'ns', not significant. See *Materials and Methods* for details of the statistics. (**B, D, F**) Population averaged sleep profiles of the indicated genotypes. Yellow indicates the light period and gray indicates the dark period. Green arrows mark the increased daytime sleep in the experimental genotypes. All data are presented as mean ± SEM.

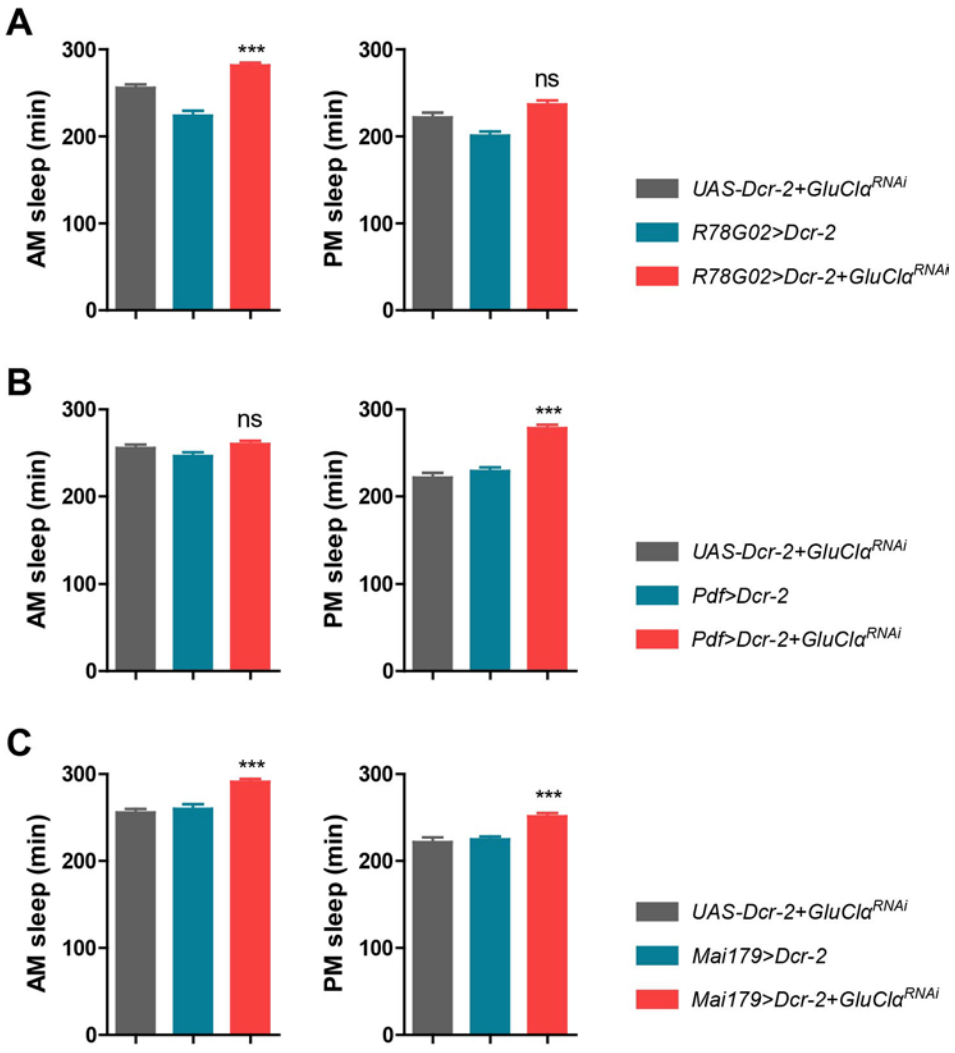

Figure 3.7–figure supplement 1. RNAi-mediated knock-down of *GluClα* expression in the LN_ds and the LN_vs differentially affects daytime sleep.
(**A-C**) The total amount of daytime sleep that occurs in the first 6 hours of the light period (AM sleep, left) and that occurring in the last 6 hours of the light period (PM sleep, right) of the indicated genotypes. Knock-down of *GluClα* expression in the LN_ds results in increased AM sleep (**A**), while knock-down of *GluClα* expression in the LN_vs results in increased PM sleep (**B**). Knock-down of *GluClα* expression in the LN_ds and LN_vs simultaneously results in increases in both AM sleep and PM sleep (**C**). *** $P < 0.001$, 'ns', not significant. See *Materials and Methods* for details of the statistics. All data are presented as mean ± SEM.

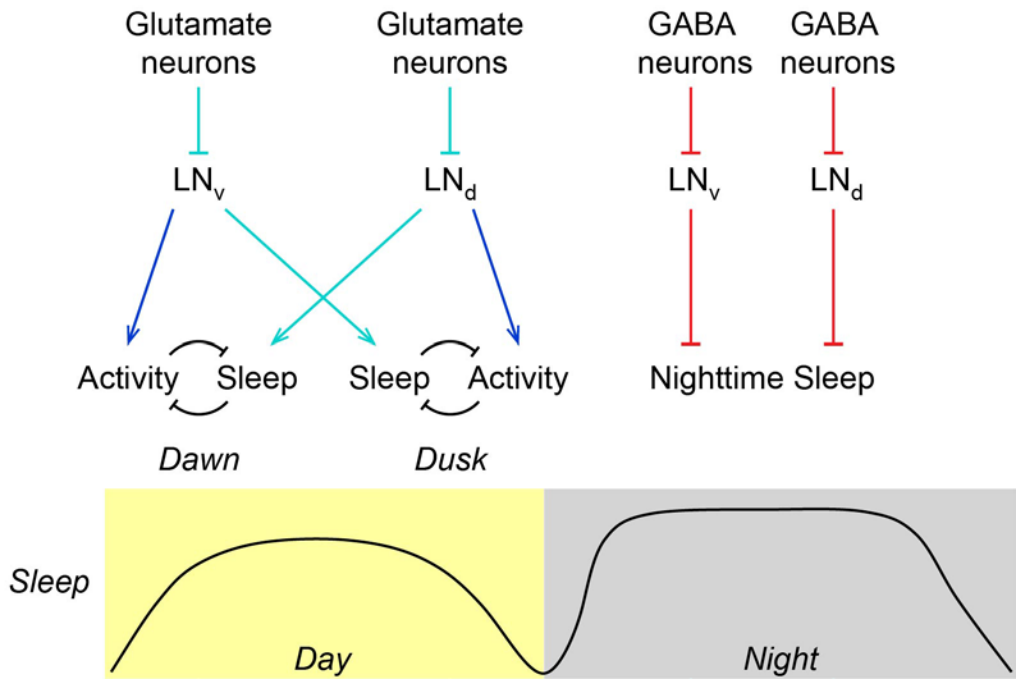

Figure 3.8. A summary model for the differential regulation of daytime and nighttime sleep by GABAergic and glutamatergic inhibition of the lateral clock neurons.
Previous studies have indicated that the LN_vs promote activity around dawn and the LN_ds promote activity around dusk (pathways illustrated in blue) (Grima et al., 2004; Stoleru et al., 2004). Based on our results, GABAergic inhibition promotes nighttime sleep through the suppression of LN_v and LN_d neuronal activity (pathways illustrated in red), whereas glutamatergic inhibition of the lateral clock neurons promotes wakefulness during the day (pathways illustrated in cyan). Impaired suppression of the LN_v activity by glutamate leads to increased sleep around dusk, while impaired suppression of the LN_d activity by glutamate leads to increased sleep around dawn. These results suggest a potential antagonism between the LN_vs and the LN_ds. "→" indicates promotion and "—|" indicates suppression. See text for more details.

3.4 Discussion

3.4.1 Fast synaptic inputs to LN_ds

Using whole-cell patch-clamp recordings, we have characterized the LN_ds' responsiveness to several classical fast neurotransmitters. Acetylcholine is the major excitatory neurotransmitter in the fly brain (reviewed in Restifo and White, 1990). Our results revealed that acetylcholine provides excitatory synaptic inputs to the LN_ds via ionotropic nAChRs. However, our results do not preclude the expression of metabotropic mAChRs in the LN_ds. In addition, we found that GABA and glutamate both provide fast inhibitory synaptic inputs onto the LN_ds via ligand-gated chloride channels, $GABA_AR$ and GluClα, respectively. The residual glutamate currents in the *GluClα RNAi* flies (Figure 3.4D-E) were most likely due to an incomplete knock-down of the *GluClα* expression in the LN_ds, but it is also possible that they are mediated other glutamate receptors, the *Drosophila* metabotropic glutamate receptor mGluR for example. Indeed, a recent study found that *mGluR* is rhythmically expressed in the LN_ds (Guo et al., 2016). Taken together, these results identify for the first time the neurochemical modulators of the critical LN_d clock neurons.

3.4.2 Connectivity in the clock neuron network

The anatomy of *Drosophila*'s clock neuron classes has been well characterized. The neural processes of many clock neurons are intermingled within the dorsal protocerebrum and the accessory medulla of the ventral lateral brain (reviewed by Helfrich-Förster, 2005), suggesting the presence of synaptic connections between clock neuron classes. Despite the longstanding assumption of synaptic contacts between the various classes of clock neurons, physiological connectivity within the clock network has remained largely uncharacterized. We previously developed a means of addressing functional connectivity in the adult fly brain, and

used it to characterize a long predicted modulatory connection between the LN_vs and the LN_ds mediated by PDF (Yao et al., 2012). Based on our finding that the LN_ds are inhibited by glutamate, we wondered if the glutamatergic $DN1_p$ clock neurons might provide inhibitory input onto the LN_ds. Indeed, acute excitation of the $DN1_p$s revealed an inhibitory connection from the $DN1_p$s to the LN_ds, which is likely mediated by both chloride and potassium conductance. Recent work by Guo and colleagues using P2X2-mediated excitation of the $DN1_p$s in conjunction with calcium imaging within the LN_ds revealed that $DN1_p$ excitation results in calcium decreases in the LN_ds (Guo et al., 2016), consistent with an inhibitory connection between the $DN1_p$s and the LN_ds. Guo and colleagues have suggested that this connection is mediated by the *Drosophila* metabotropic glutamate receptor mGluR (Guo et al., 2016). This is consistent with our finding of LN_d potassium conductance following $DN1_p$ excitation, as mGluR is known to activate potassium channels when expressed exogenously in *Xenopus* oocytes (Raymond et al., 1999). However, the presence of chloride conductance suggests that the ionotropic glutamate receptor GluClα also contributes to the inhibitory connection between the $DN1_p$s and the LN_ds.

Given that the l-LN_vs are also inhibited by glutamate (McCarthy et al., 2011), we asked if there is a functional inhibitory connection between the $DN1_p$s and the l-LN_vs. $DN1_p$ excitation produced significant but relatively small currents in l-LN_vs, suggesting that the $DN1_p$s inhibit both the l-LN_vs and LN_ds but with a stronger connection with the latter clock neuron class. This is consistent with recent findings by Guo and colleagues (Guo et al., 2016). These results are also consistent with the finding that the ventral projections of the $DN1_p$s typically terminate within the dorsal protocerebrum and only occasionally extend ventrally to regions of the brain containing l-LN_v projections (Zhang et al., 2010b). An extension of this experimental approach

should make it possible to identify the physiological connectivity between other groups of clock neurons, and between clock neurons and potential input and output pathways.

3.4.3 Differential regulation of daytime and nighttime sleep by GABAergic and glutamatergic inhibition of the lateral clock neurons

Male flies display a characteristic pattern of activity and sleep under a 12:12 light:dark cycle. They are active around dawn and dusk, display a midday siesta, and sleep throughout the night. It has been known for more than a decade that the daily activity peaks around dawn and dusk are controlled by the LN_vs and the LN_ds, respectively (Grima et al., 2004; Stoleru et al., 2004). Less is known about the circadian control of sleep patterns and sleep amount. Studies have found that GABA promotes nighttime sleep through suppressing the neuronal activity of the LN_vs (Parisky et al., 2008; Chung et al., 2009). Here, we extend these findings by showing that GABA also suppresses the neuronal activity of the LN_ds to promote nighttime sleep (Figure 3.6 and Figure 3.8). This fits nicely with the recent finding that the LN_ds are most active in the late afternoon (Liang et al., 2016) to promote a major peak of activity around dusk. Thus, a timely suppression of their neuronal activity would be required for the animal's activity quiescence and consolidated sleep at night.

While conducting these studies we became aware of work by Guo and colleagues revealing that the $DN1_p$s promote sleep through the glutamatergic inhibition of lateral clock neurons (Guo et al., 2016). This work proposed that this inhibition was mediated by the metabotropic glutamate receptor mGluR (Guo et al., 2016). The use of electrophysiological methods has allowed us to identify a second glutamate receptor, GluClα, in the lateral neurons and we show that this ionotropic glutamate receptor mediates a function distinct from mGluR in these cells in the control of sleep. Whereas Guo and colleagues have shown that lateral neuron

mGluR is important for promoting midday sleep, we show that GluClα-mediated inhibition of the lateral clock neurons controls sleep in a fundamentally different and unexpected manner. Though both the LN_vs and the LN_ds promote activity during specific times of the day (Grima et al., 2004; Stoleru et al., 2004; Guo et al., 2016), the glutamatergic inhibition of these neurons via GluClα promotes wakefulness during the daytime, as disruption of GluClα in the lateral clock neurons increased the levels of daytime sleep (Figure 3.7). Even more surprisingly, impairing GluClα-mediated inhibition of the LN_vs (i.e, the morning oscillator) leads to increased sleep *in the late afternoon* while impairing GluClα-mediated inhibition of the LN_ds (i.e., the evening oscillator) leads to increased sleep *in the early morning* (Figure 3.7B,D,F and Figure 3.7–figure supplement 1). Thus, the LN_vs, which have long been thought to drive morning activity (Grima et al., 2004; Stoleru et al., 2004), also promote sleep in the afternoon, and the LN_ds, which drive activity in the afternoon (Grima et al., 2004; Stoleru et al., 2004), also promote sleep in the morning (Figure 3.8).

Given that the LN_vs and LN_ds promote activity around dawn and dusk, respectively, and that activity and sleep are mutually exclusive behavioral states, these results reveal a striking antagonism between the morning and evening oscillators (Figure 3.8). Reciprocal inhibition is a core feature of almost all known central pattern generators, neuronal circuits that generate rhythmic motor patterns endogenously even in the absence of rhythmic inputs (reviewed by Marder and Bucher, 2001). Based on our results, we wonder if similar principles are at play in the circadian timekeeping network, which produces rhythmic outputs over a ~24-hour time-course. While it might be counterintuitive that the LN_vs and LN_ds can promote both activity and sleep, we note that it is likely that these neurons promote sleep indirectly. If there is reciprocal inhibition between the LN_vs and the LN_ds, an increase in LN_v neuronal activity would result in a

greater suppression of LN_d neuronal activity, which would effectively suppress or delay the activity around dusk and therefore lead to an increase in rest or sleep. Alternatively, the LN_vs and the LN_ds may have separate output pathways through which they control activity and sleep. In summary, our results reveal that although GABA and glutamate both provide fast inhibitory synaptic inputs to the lateral clock neurons, the GABAergic input functions to promote sleep at night while the glutamatergic input functions to promote wakefulness during the day. Perhaps most surprisingly, our results reveal that, within the clock neuron network of *Drosophila*, the morning oscillator not only promotes activity in the morning but also promotes sleep in the evening, while the evening oscillator promotes activity in the evening and sleep in the morning.

3.5 Materials and Methods

3.5.1 Fly strains

Flies were reared on cornmeal-sucrose-yeast media under a 12hr:12hr light:dark cycle at 25 °C or under the diurnal conditions of the lab. The following fly lines were used: *Mai179-GAL4* (Siegmund and Korge, 2001; Grima et al., 2004; Stoleru et al., 2004); *Pdf-GAL4* (Renn et al., 1999; Park et al., 2000); *Pdf-LexA* (Shang et al., 2008); *Pdf-GAL80* (Stoleru et al., 2004); *R78G02-GAL4* (Bloomington Stock # 40010); *Clk4.1M-GAL4* (Zhang et al., 2010a, 2010b); *Clk4.1M-LexA* (Cavanaugh et al., 2014); *VGlut-GAL4* (Daniels et al., 2008); *UAS-EGFP* (Bloomington Stock # 5431); *LexAop-GCaMP3.0(4B), LexAop-Epac1-camps(1A), LexAop-P2X2(1)* (Yao et al., 2012); *UAS-P2X2* (Lima and Miesenböck, 2005); *$GABA_AR$ RNAi* lines *UAS-Rdli(8-10)J, UAS-Rdli(4-5)E, UAS-Rdli(2-7)E2* (Liu et al., 2007); *UAS-Dicer-2(III)* (Bloomington Stock # 24651), *UAS-GluClα^{RNAi}* (Vienna *Drosophila* Resource Center ID 105754) (Dietzl et al., 2007; Collins et al., 2012).

3.5.2 Electrophysiology

Brain dissection:

All of the brain dissections and electrophysiological recordings were done in the light phase of a 12:12 LD cycle. Brains from adult male flies (about 3-10 days old) were dissected into the external saline containing 101 mM NaCl, 3 mM KCl, 1 mM $CaCl_2$, 4 mM $MgCl_2$, 1.25 mM NaH_2PO_4, 5 mM glucose, and 20.7 mM $NaHCO_3$ (pH 7.2, 250 mOsm), pre-oxygenated with 95% O_2/5% CO_2 (Gu and O'Dowd, 2006). The dissected brain was placed in a drop of external saline containing 2 mg/mL protease XIV (Sigma-Aldrich, St. Louis, MO) for 30 to 60 seconds to weaken the perineural sheath. The brain was then returned to fresh external saline without protease XIV, and the perineural sheath was carefully removed with fine forceps. Because the LN_d soma are a few cell-layers beneath the surface of the brain, tissues above the LN_d soma were carefully removed with fine forceps to make the LN_d soma accessible to electrodes. The preparation was discarded if the LN_ds were visibly damaged. The dissected brain was placed ventral side up on the floor of an RC-26G perfusion chamber and secured using an SHD-26GH/10 slice anchor (Warner Instruments, Hamden, CT). The brain was allowed to recover from dissection in continuously flowing oxygenated external saline (95% O_2/5% CO_2) for a minimum of 10 minutes. Perfusion with oxygenated external saline was continued throughout the recording period, at a flow rate of approximately 1-2 mL/min.

Drug application:

All drugs were delivered by bath perfusion. The time of solution exchange in the recording chamber was approximately 20-30 seconds. For picrotoxin and low Ca^{2+} solution treatments, the preparation was bathed in 100 µM picrotoxin (in normal external saline) or in low Ca^{2+} external saline (0.1 mM Ca^{2+}/4.9 mM Mg^{2+}) for a minimum of 5 minutes before drugs were

applied. Picrotoxin was purchased from Tocris Bioscience (Bristol, United Kingdom). Carbamoylcholine, nicotine, GABA, glutamate, and ATP were purchased from Sigma-Aldrich (St. Louis, MO).

Whole-cell patch-clamp recordings:

Whole-cell patch-clamp recordings were performed using borosilicate standard wall capillary glass pipettes (World Precision Instruments, Sarasota, FL), with a resistance of 10-14 MΩ after fire polishing. Recording pipettes were filled with internal saline containing 102 mM potassium gluconate, 17 mM NaCl, 0.085 mM $CaCl_2$, 4 mM Mg-ATP, 0.5 mM Na-GTP, 0.94 mM EGTA, and 8.5 mM HEPES (pH 7.2, 235 mOsm) (Cao and Nitabach, 2008). All recordings were corrected for the 13 mV liquid junction potential generated in these solutions. The preparations were visualized using an Olympus BX51WI fixed stage upright microscope equipped with an Olympus LUMPlanFl 40×/0.8 W water-immersion objective (Olympus, Center Valley, PA). The LN_ds and l-LN_vs were identified by their anatomical locations and their expression of fluorescent proteins. Giga-Ohm seals were achieved before breaking in to whole-cell configuration. The identity of the recorded cells was visually confirmed by adding 10 µM Alexa Fluor 594 biocytin (Thermo Fisher Scientific, Waltham, MA) into the internal solution, as previously described (Flourakis and Allada, 2015). Recordings were done using an Axopatch 200 patch-clamp amplifier, a Digidata 1440A digitizer, and the pClamp 10 Clampex software (Molecular Devices, Sunnyvale, CA). Only cells with a membrane resistance higher than 500 MΩ were used for recordings.

Current-clamp recordings were low-pass filtered at 5 kHz before digitization at 10 kHz. Because of the high membrane resistance of many fly neurons, the seal current may substantially depolarize the membrane potential in current-clamp recordings (Gouwens and Wilson, 2009).

We therefore injected a constant hyperpolarizing current (typically -10 to -20 pA) into the recorded cell in order to compensate for the depolarizing effect of the seal current and bring the membrane potential to between -50 and -70 mV.

Voltage-clamp recordings were low-pass filtered at 1 kHz before digitization at 2 kHz. For voltage ramp experiments, the holding potential was changed linearly over 500 ms from -113 mV to +47 mV for each voltage ramp, and ramps were applied every five seconds. Six ramps were applied before drug treatment to obtain an average baseline current. The average baseline current before treatment was subtracted from the recorded current after the drug was applied, such that the resulting current represents current induced by the drug. For steady-state voltage-clamp recordings, the membrane potential was held at -68 mV for nicotine treatments, and at -113 mV for all the other treatments. The recorded current traces were further low-pass filtered at 10 Hz before being displayed in the figures. Analyses of both the current-clamp and the voltage-clamp data were done using the pClamp 10 Clampfit software (Molecular Devices, Sunnyvale, CA).

Cell-attached recordings:

For cell-attached recordings, the recording pipette was filled with external saline. Giga-Ohm seals were achieved before recording in cell-attached configuration in voltage-clamp mode, with the holding potential set at 0 mV. Signals were low-pass filtered at 1 kHz before digitization at 10 kHz, and were further low-pass filtered after recording at 200 Hz before being displayed in the figures.

Neural circuit analysis:

Two modifications were made for the experiments that analyzed functional neuronal connections (Figure 3.5). First, brain dissection and desheathing were performed in ice-cold low

Ca^{2+} external saline (0.1 mM Ca^{2+}/4.9 mM Mg^{2+}) to reduce neurotransmitter release during these procedures. The dissected brain was then returned to normal Ca^{2+} external saline and allowed to rest for a minimum of 10 minutes before recording. Second, the 4 mM ATP in the internal saline was replaced by 4 mM phosphocreatine to avoid ATP leaking from the recording pipette into the bath, which may potentially depolarize the P2X2-expressing cells before measurements took place. All the other procedures were the same as those described above.

3.5.3 Calcium imaging

Calcium imaging experiments were performed to determine the concentration of ATP to be used to excite the P2X2 $DN1_p$s (Figure 3.5–figure supplement 1). Brains from male *w/Y;LexAop-GCaMP3.0(4B)/Sco;Clk4.1M-LexA/LexAop-P2X2(1)* flies were dissected and desheathed in external saline as described above. Calcium imaging was performed as previously described (Yao et al., 2012) using an Olympus Fluoview 1000 laser-scanning confocal microscope equipped with an Olympus LUMFL N 60×/1.10 W water-immersion objective (Olympus, Center Valley, PA). Regions of interest (ROIs) were selected over single somata of the $DN1_p$s using Olympus Fluoview software (Olympus, Center Valley, PA), and the GCaMP3.0 fluorescent intensity was sampled at 1 Hz with a 488-nm laser. Each preparation was sequentially treated with ~30-second perfusions of 100 μM, 250 μM, and 1 mM of ATP, with approximately 10 minutes between treatments. Raw GCaMP3.0 intensity traces were filtered with a 10-point moving average filter, and the maximum percent change in fluorescence over baseline was determined for each trace using custom software developed in Matlab (MathWorks, Natick, MA).

3.5.4 Sleep recording and analysis

Flies aged a week or less were placed individually in recording glass tubes containing 2% agar-4% sucrose food at one end and these were loaded onto the DAM2 *Drosophila* Activity Monitors (TriKinetics, Waltham, MA) for locomotor activity recording. Flies were tested under a 12:12 LD cycle for a minimum of 5 days at a constant temperature of 25°C, and their activity counts were collected in 1-minute bins. Sleep was defined as uninterrupted inactivity lasting for five minutes or more, as previously described (Hendricks et al., 2000; Shaw et al., 2000; Huber et al., 2004). Sleep bouts and the amount of sleep of individual flies were analyzed using the Counting Macro, an Excel-based program, which has been described in detail previously (Pfeiffenberger et al., 2010). The total amount of sleep was determined for each desired period of time (e.g., the first 6 hours of the light period, or the 12-hour dark period) and averaged for the last 4 days. The total sleep amount of an experimental genotype was compared to those of the corresponding *GAL4* and *UAS* controls using the Kruskal-Wallis one-way ANOVA and Dunn's multiple comparison test. Significance was reported only if the experimental group differed significantly from both controls in the same direction, and only the smaller significance value was reported in the figures. For the population average sleep profile (also known as "sleep eduction"), the population average amount of sleep was determined for each hour for the last 4 days, which was then averaged across days to generate a single-day sleep profile.

3.6 Acknowledgements

This work was supported by the NIH (NINDS) grant R01NS077933 and the NSF (IOS) grant 1354046 to OTS. ZY was further supported by the Rackham Predoctoral Fellowship (University of Michigan). We thank P. H. Taghert, M. Rosbash, L.C. Griffith, P. E. Hardin, P.

Emery, F. Rouyer, J. Blau, A. Sehgal, R.L Davis, G. Miesenböck, C. A. Collins, the Bloomington *Drosophila* Stock Center, and the Vienna *Drosophila* Resource Center for providing fly stocks. We thank R. Allada for providing the Counting Macro for sleep analysis. We thank M. Rosbash and C. Helfrich-Förster for communicating results before publication.

3.7 References

Cao, G., and Nitabach, M.N. (2008). Circadian control of membrane excitability in Drosophila melanogaster lateral ventral clock neurons. J. Neurosci. *28*, 6493–6501.

Cavanaugh, D.J., Geratowski, J.D., Wooltorton, J.R.A., Spaethling, J.M., Hector, C.E., Zheng, X., Johnson, E.C., Eberwine, J.H., and Sehgal, A. (2014). Identification of a circadian output circuit for rest: Activity rhythms in drosophila. Cell *157*, 689–701.

Chen, C.-C., Wu, J.-K., Lin, H.-W., Pai, T.-P., Fu, T.-F., Wu, C.-L., Tully, T., and Chiang, A.-S. (2012). Visualizing long-term memory formation in two neurons of the Drosophila brain. Science *335*, 678–685.

Chung, B.Y., Kilman, V.L., Keath, J.R., Pitman, J.L., and Allada, R. (2009). The GABAA Receptor RDL Acts in Peptidergic PDF Neurons to Promote Sleep in Drosophila. Curr. Biol. *19*, 386–390.

Collins, B., Kane, E.A., Reeves, D.C., Akabas, M.H., and Blau, J. (2012). Balance of Activity between LNvs and Glutamatergic Dorsal Clock Neurons Promotes Robust Circadian Rhythms in Drosophila. Neuron *74*, 706–718.

Collins, B., Kaplan, H.S., Cavey, M., Lelito, K.R., Bahle, A.H., Zhu, Z., Macara, A.M., Roman, G., Shafer, O.T., and Blau, J. (2014). Differentially Timed Extracellular Signals Synchronize Pacemaker Neuron Clocks. PLoS Biol. *12*, e1001959.

Cully, D.F., Paress, P.S., Liu, K.K., Schaeffer, J.M., and Arena, J.P. (1996). Identification of a Drosophila melanogaster glutamate-gated chloride channel sensitive to the antiparasitic agent avermectin. J. Biol. Chem. *271*, 20187–20191.

Cusumano, P., Klarsfeld, A., Chélot, E., Picot, M., Richier, B., and Rouyer, F. (2009). PDF-modulated visual inputs and cryptochrome define diurnal behavior in Drosophila. Nat. Neurosci. *12*, 1431–1437.

Daniels, R.W., Gelfand, M. V., Collins, C.A., and DiAntonio, A. (2008). Visualizing glutamatergic cell bodies and synapses in Drosophila larval and adult CNS. J. Comp. Neurol. *508*, 131–152.

Dietzl, G., Chen, D., Schnorrer, F., Su, K.-C., Barinova, Y., Fellner, M., Gasser, B., Kinsey, K., Oppel, S., Scheiblauer, S., et al. (2007). A genome-wide transgenic RNAi library for conditional gene inactivation in Drosophila. Nature *448*, 151–156.

Flourakis, M., and Allada, R. (2015). Patch-clamp electrophysiology in Drosophila circadian pacemaker neurons. In Methods in Enzymology, (Elsevier Inc.), pp. 23–44.

Flourakis, M., Kula-Eversole, E., Hutchison, A.L., Han, T.H., Aranda, K., Moose, D.L., White, K.P., Dinner, A.R., Lear, B.C., Ren, D., et al. (2015). A Conserved Bicycle Model for Circadian Clock Control of Membrane Excitability. Cell *162*, 836–848.

Gouwens, N.W., and Wilson, R.I. (2009). Signal propagation in Drosophila central neurons. J. Neurosci. *29*, 6239–6249.

Grima, B., Chélot, E., Xia, R., and Rouyer, F. (2004). Morning and evening peaks of activity rely on different clock neurons of the Drosophila brain. Nature *431*, 869–873.

Gu, H., and O'Dowd, D.K. (2006). Cholinergic Synaptic Transmission in Adult Drosophila Kenyon Cells In Situ. J. Neurosci. *26*, 265–272.

Guo, F., Yu, J.Y., Jung, H.J., Abruzzi, K.C., Luo, W.L., Griffith, L.C., and Rosbash, M. (2016). Circadian Neuron Feedback Controls the Drosophila Sleep-Activity Profile. Nature *in press*.

Hamasaka, Y., Wegener, C., and Nässel, D.R. (2005). GABA modulates Drosophila circadian clock neurons via GABAB receptors and decreases in calcium. J. Neurobiol. *65*, 225–240.

Hamasaka, Y., Rieger, D., Parmentier, M.-L., Grau, Y., Helfrich-Förster, C., and Nässel, D.R. (2007). Glutamate and its metabotropic receptor in Drosophila clock neuron circuits. J. Comp. Neurol. *505*, 32–45.

Helfrich-Förster, C. (1995). The period clock gene is expressed in central nervous system neurons which also produce a neuropeptide that reveals the projections of circadian pacemaker cells within the brain of Drosophila melanogaster. Proc. Natl. Acad. Sci. U. S. A. *92*, 612–616.

Helfrich-Förster, C. (2005). Neurobiology of the fruit fly's circadian clock. Genes. Brain. Behav. *4*, 65–76.

Hendricks, J.C., Finn, S.M., Panckeri, K. a, Chavkin, J., Williams, J. a, Sehgal, A., and Pack, A.I. (2000). Rest in Drosophila Is a Sleep-like State. Neuron *25*, 129–138.

Hermann-Luibl, C., and Helfrich-Förster, C. (2015). Clock network in Drosophila. Curr. Opin. Insect Sci. *7*, 65–70.

Herzog, E.D. (2007). Neurons and networks in daily rhythms. Nat. Rev. Neurosci. *8*, 790–802.

Huber, R., Hill, S.L., Holladay, C., Biesiadecki, M., Tononi, G., and Cirelli, C. (2004). Sleep homeostasis in Drosophila melanogaster. Sleep *27*, 628–639.

Im, S.H., and Taghert, P.H. (2010). PDF receptor expression reveals direct interactions between circadian oscillators in Drosophila. J. Comp. Neurol. *518*, 1925–1945.

Im, S.H., Li, W., and Taghert, P.H. (2011). PDFR and CRY signaling converge in a subset of clock neurons to modulate the amplitude and phase of circadian behavior in Drosophila. PLoS One *6*, e18974.

Kaneko, M., and Hall, J.C. (2000). Neuroanatomy of cells expressing clock genes in Drosophila: transgenic manipulation of the period and timeless genes to mark the perikarya of circadian pacemaker neurons and their projections. J. Comp. Neurol. *422*, 66–94.

Kim, W.J., Jan, L.Y., and Jan, Y.N. (2013). A PDF/NPF neuropeptide signaling circuitry of male Drosophila melanogaster controls rival-induced prolonged mating. Neuron *80*, 1190–1205.

Liang, X., Holy, T.E., and Taghert, P.H. (2016). Synchronous Drosophila circadian pacemakers display nonsynchronous Ca2+ rhythms in vivo. Science *351*, 976–981.

Lima, S.Q., and Miesenböck, G. (2005). Remote control of behavior through genetically targeted photostimulation of neurons. Cell *121*, 141–152.

Lin, Y., Stormo, G.D., and Taghert, P.H. (2004). The neuropeptide pigment-dispersing factor coordinates pacemaker interactions in the Drosophila circadian system. J. Neurosci. *24*, 7951–7957.

Littleton, J.T., and Ganetzky, B. (2000). Ion Channels and Synaptic Organization: Analysis of the Drosophila Genome. Neuron *26*, 35–43.

Liu, W.W., and Wilson, R.I. (2013). Glutamate is an inhibitory neurotransmitter in the Drosophila olfactory system. Proc. Natl. Acad. Sci. *110*, 10294–10299.

Liu, X., Krause, W.C., and Davis, R.L. (2007). GABAA Receptor RDL Inhibits Drosophila Olfactory Associative Learning. Neuron *56*, 1090–1102.

Macdonald, R.L., and Olsen, R.W. (1994). GABA $_A$ Receptor Channels. Annu. Rev. Neurosci. *17*, 569–602.

Marder, E., and Bucher, D. (2001). Central pattern generators and the control of rhythmic movements. Curr. Biol. *11*, R986–R996.

McCarthy, E. V, Wu, Y., Decarvalho, T., Brandt, C., Cao, G., and Nitabach, M.N. (2011). Synchronized bilateral synaptic inputs to Drosophila melanogaster neuropeptidergic rest/arousal neurons. J. Neurosci. *31*, 8181–8193.

Muraro, N., and Ceriani, F. (2015). Acetylcholine from visual circuits modulates the activity of arousal neurons in Drosophila. Submitted *35*, 16315–16327.

Parisky, K.M., Agosto, J., Pulver, S.R., Shang, Y., Kuklin, E., Hodge, J.J.L., Kang, K., Kang, K., Liu, X., Garrity, P. a, et al. (2008). PDF cells are a GABA-responsive wake-promoting component of the Drosophila sleep circuit. Neuron *60*, 672–682.

Park, D., and Griffith, L.C. (2006). Electrophysiological and anatomical characterization of PDF-positive clock neurons in the intact adult Drosophila brain. J. Neurophysiol. *95*, 3955–3960.

Park, J.H., Helfrich-Förster, C., Lee, G., Liu, L., Rosbash, M., and Hall, J.C. (2000). Differential regulation of circadian pacemaker output by separate clock genes in Drosophila. Proc. Natl. Acad. Sci. U. S. A. *97*, 3608–3613.

Peng, Y., Stoleru, D., Levine, J.D., Hall, J.C., and Rosbash, M. (2003). Drosophila free-running rhythms require intercellular communication. PLoS Biol. *1*, E13.

Pfeiffenberger, C., Lear, B.C., Keegan, K.P., and Allada, R. (2010). Processing sleep data created with the Drosophila activity monitoring (DAM) system. Cold Spring Harb. Protoc. *5*, 1251–1257.

Picot, M., Cusumano, P., Klarsfeld, A., Ueda, R., and Rouyer, F. (2007). Light activates output from evening neurons and inhibits output from morning neurons in the Drosophila circadian clock. PLoS Biol. *5*, 2513–2521.

Raymond, V., Hamon, A., Grau, Y., and Lapied, B. (1999). DmGluRA, a Drosophila metabotropic glutamate receptor, activates G-protein inwardly rectifying potassium channels in Xenopus oocytes. Neurosci. Lett. *269*, 1–4.

Renn, S.C., Park, J.H., Rosbash, M., Hall, J.C., and Taghert, P.H. (1999). A pdf neuropeptide gene mutation and ablation of PDF neurons each cause severe abnormalities of behavioral circadian rhythms in Drosophila. Cell *99*, 791–802.

Restifo, L.L., and White, K. (1990). Molecular and Genetic Approaches to Neurotransmitter and Neuromodulator Systems in Drosophila. Adv. In Insect Phys. *22*, 115–219.

Seluzicki, A., Flourakis, M., Kula-Eversole, E., Zhang, L., Kilman, V., and Allada, R. (2014). Dual PDF signaling pathways reset clocks via TIMELESS and acutely excite target neurons to control circadian behavior. PLoS Biol. *12*, e1001810.

Shafer, O.T., Kim, D.J., Dunbar-Yaffe, R., Nikolaev, V.O., Lohse, M.J., and Taghert, P.H. (2008). Widespread receptivity to neuropeptide PDF throughout the neuronal circadian clock network of Drosophila revealed by real-time cyclic AMP imaging. Neuron *58*, 223–237.

Shang, Y., Griffith, L.C., and Rosbash, M. (2008). Light-arousal and circadian photoreception circuits intersect at the large PDF cells of the Drosophila brain. Proc. Natl. Acad. Sci. U. S. A. *105*, 19587–19594.

Shaw, P.J., Cirelli, C., Greenspan, R.J., and Tononi, G. (2000). Correlates of sleep and waking in Drosophila melanogaster. Science *287*, 1834–1837.

Sheeba, V., Fogle, K.J., Kaneko, M., Rashid, S., Chou, Y.-T., Sharma, V.K., and Holmes, T.C. (2008a). Large ventral lateral neurons modulate arousal and sleep in Drosophila. Curr. Biol. *18*, 1537–1545.

Sheeba, V., Gu, H., Sharma, V.K., O'Dowd, D.K., and Holmes, T.C. (2008b). Circadian- and light-dependent regulation of resting membrane potential and spontaneous action potential firing of Drosophila circadian pacemaker neurons. J. Neurophysiol. *99*, 976–988.

Siegmund, T., and Korge, G. (2001). Innervation of the ring gland of drosophila melanogaster. J. Comp. Neurol. *431*, 481–491.

Stoleru, D., Peng, Y., Agosto, J., and Rosbash, M. (2004). Coupled oscillators control morning and evening locomotor behaviour of Drosophila. Nature *431*, 862–868.

Stoleru, D., Nawathean, P., Fernández, M.D.L.P., Menet, J.S., Ceriani, M.F., and Rosbash, M. (2007). The Drosophila circadian network is a seasonal timer. Cell *129*, 207–219.

Vansteensel, M.J., Michel, S., and Meijer, J.H. (2008). Organization of cell and tissue circadian pacemakers: A comparison among species. Brain Res. Rev. *58*, 18–47.

Welsh, D.K., Takahashi, J.S., and Kay, S.A. (2010). Suprachiasmatic nucleus: cell autonomy and network properties. Annu. Rev. Physiol. *72*, 551–577.

Yao, Z., and Shafer, O.T. (2014). The Drosophila circadian clock is a variably coupled network of multiple peptidergic units. Science *343*, 1516–1520.

Yao, Z., Macara, A.M., Lelito, K.R., Minosyan, T.Y., and Shafer, O.T. (2012). Analysis of functional neuronal connectivity in the Drosophila brain. J. Neurophysiol. *108*, 684–696.

Yoshii, T., Todo, T., Wülbeck, C., Stanewsky, R., and Helfrich-Förster, C. (2008). Cryptochrome is present in the compound eyes and a subset of Drosophila's clock neurons. J. Comp. Neurol. *508*, 952–966.

Yoshii, T., Hermann-Luibl, C., Kistenpfennig, C.R., Schmid, B., Tomioka, K., and Helfrich-Förster, C. (2015). Cryptochrome-Dependent and -Independent Circadian Entrainment Circuits in Drosophila. J. Neurosci. *35*, 6131–6141.

Zhang, L., Chung, B.Y., Lear, B.C., Kilman, V.L., Liu, Y., Mahesh, G., Meissner, R.A., Hardin, P.E., and Allada, R. (2010a). DN1p Circadian Neurons Coordinate Acute Light and PDF Inputs to Produce Robust Daily Behavior in Drosophila. Curr. Biol. *20*, 591–599.

Zhang, Y., Liu, Y., Bilodeau-Wentworth, D., Hardin, P.E., and Emery, P. (2010b). Light and temperature control the contribution of specific DN1 neurons to Drosophila circadian behavior. Curr. Biol. *20*, 600–605.

CHAPTER 4. The *Drosophila* circadian clock is a variably coupled network of multiple peptidergic units[3]

4.1 Abstract

Daily rhythms in behavior emerge from networks of neurons that express molecular clocks. *Drosophila's* clock neuron network consists of a diversity of cell types, yet is modeled as two hierarchically organized groups, one of which serves as a master pacemaker. Here we establish that the fly's clock neuron network consists of multiple units of independent neuronal oscillators, each unified by its neuropeptide transmitter and mode of coupling to other units. Our work reveals that the circadian clock neuron network is not orchestrated by a small group of master pacemakers but rather consists of multiple independent oscillators, each of which drives rhythms in activity.

4.2 Results

Molecular clocks drive circadian rhythms in animals (1). Most circadian rhythms follow from clocks located in small islands of brain tissue (2) and connections within networks of clock neurons produce a robustness in circadian timekeeping uncharacteristic of rhythms driven by isolated neurons or non-neuronal clocks (3, 4). Here we study the clock neuron network

[3] From Yao Z, Shafer OT (2014). The *Drosophila* circadian clock is a variably coupled network of multiple peptidergic units. *Science*. 343(6178):1516-20. doi: 10.1126/science.1251285. Reprinted with permission from AAAS.

of *Drosophila*, similar to yet simpler than that of mammals (5), to learn how networks of clock neurons produce circadian rhythms.

The *Drosophila* brain contains ~150 clock neurons, of which 11 bilateral pairs of lateral neurons are necessary and sufficient for the insect's normal activity rhythms (6) (Fig. 4.S1). Current models suggest that this network is organized into two coupled oscillators: the pigment-dispersing factor (PDF) expressing lateral neurons that control the morning peak of activity and the remaining lateral neurons that control the evening peak of activity (6, 7) (Fig. 4.S1). The dual-oscillator model predicts that the PDF positive neurons serve as master pacemakers that reset the PDF negative neurons daily, thereby dictating the pace of behavioral rhythms in the absence of environmental time cues (8). We tested this prediction by introducing various clock speed discrepancies between the PDF positive and negative clock neurons.

The intrinsic speed of the molecular clock can be manipulated through the activity of the kinases Doubletime (DBT) and Shaggy (SGG) (9, 10) (Fig. 4.1A, Fig. 4.S2, and Table 4.S1). Manipulating these kinases only in the PDF positive clock neurons resulted in a coherent change in clock speed in these neurons (Fig. 4.S3), thereby creating clock speed discrepancies between PDF positive and negative neurons. When these discrepancies were small, activity rhythms were strong and coherent with periodicities determined by the speed of the PDF neurons (Fig. 4.1B, Figs. 4.S4 and 4.S5, and Table 4.S2). When speed discrepancies were larger, flies displayed variable free-running periods, reduced rhythm amplitudes, and a higher incidence of arrhythmicity (Fig. 4.1B, Figs. 4.S4 and 4.S5, and Table 4.S2). Flies with large discrepancies often displayed two periodicities simultaneously, one corresponding to the period of the PDF neurons and the other to that of the PDF negative neurons (Fig. 4.1B, Figs. 4.S4 and 4.S5). In flies lacking PDF receptor (PDFR) the speed of PDF neurons had no influence over activity

rhythms (Fig. 4.1C, Fig. 4.S6, and Table 4.S3), indicating that PDFR signaling is required for PDF neuron control over the network. We conclude that the clock neuron network can produce coherent activity rhythms only when the mismatch between the PDF positive and negative neurons is less than approximately 2.5 hours.

The presence of near 24-hour periodicities despite altered PDF neuron speed suggested that, contrary to the prevailing model, PDF negative clock neurons have independent control of activity rhythms under constant darkness and temperature (DD) (6-8, 11, 12). When we altered the clock speed of PDF negative neurons, flies displayed increased arrhythmicity and desynchronization and reduced rhythm amplitudes (Fig. 4.S7), though the effects were less severe than those seen when PDF positive neurons were manipulated (Fig. 4.2A,Fig. 4.S8, and Table 4.S4)(8). In the absence of PDFR signaling the PDF negative neurons determined the pace of free-running rhythms (Fig. 4.2B, Fig. 4.S8, and Table 4.S4).

We hypothesized that the phenotypes caused by large clock speed discrepancies (Fig. 4.1B and Figs. 4.S4, 4.S5, and 4.S7) were caused by conflicts between PDF positive and negative clock neurons, both of which drive rhythms. PDF neurons alone are sufficient to drive activity rhythms (6). We predicted that in the absence of clocks in PDF negative neurons PDF neurons could coherently drive strong behavioral rhythms at any speed. We restored *period* (*per*) expression only in the PDF neurons of per^{01} mutants (6) (Fig. 4.2, C and E). When such *per*-rescued PDF neurons overexpressed DBT^{S}, flies displayed a strong ~17 h period and showed improved rhythmicity, coherence and rhythm amplitude relative to DBT^{S} overexpression in a *wild-type* background (Fig. 4.2, C and F, and Table 4.S5). Such improvements were also apparent for DBT^{L}overexpression in *per*-rescued PDF positive neurons (Fig. 4.S9 and Table 4.S5). We conclude that the ~24 h periodicities displayed by desynchronized per^{+} individuals

with fast- or slow-running PDF neurons (Fig. 4.2D and Fig. 4.S4) were driven by PDF negative neurons.

PDF signaling is required for the PDF neurons to influence the pace of behavioral rhythms (Fig. 4.1C and Fig. 4.S6), presumably through the resetting of molecular clocks within PDF negative neurons (8), but only about half of the PDF negative clock neurons are predicted to express PDFR (13, 14). Thus, the limited control of the PDF neurons over activity rhythms might be due to a lack of PDF receptivity among PDF negative neurons. We examined PDF receptivity within the PDF negative lateral neurons, a 5th small ventral lateral neuron (5th s-LN$_v$) and six dorsal lateral neurons (LN$_d$s) per hemisphere (Fig. 4.S1). The 5th s-LN$_v$ responds to bath-applied PDF with cAMP increases (15). Using the cAMP sensor Epac1-camps (15), (16) we found that approximately half the LN$_d$s do not display cAMP increases in response to PDF, observing both responding and non-responding LN$_d$s within the same brains (Fig. 4.3, A to D, and G). Restricting the expression of cAMP sensor to the PDFR$^+$ LN$_d$s (14, 17) or the PDFR$^-$ LN$_d$s (7), we found that all PDFR$^+$ LN$_d$s (18 neurons from 7 brains) displayed cAMP responses to PDF (Fig. 4.3, E and G), while none of the PDFR$^-$ LN$_d$s (11 neurons from 6 brains) responded (Fig. 4.3, F and G). All LN$_d$s responded to forskolin, an activator of adenylyl cyclases (Fig. 4.3H) (18). Thus, PDF modulates only subsets of PDF negative neurons.

Given such differential receptivity to PDF, we hypothesized that PDF positive neurons reset the molecular clocks only in subsets of PDF negative lateral neurons. We visualized PERIOD (PER) protein rhythms in the lateral neuron network of control flies and flies with a large clock speed discrepancy, in this case flies with the PDF neurons slowed down through expression of *DBT^L*. We chose this manipulation because the internal desynchronization in these flies was usually not accompanied by arrhythmicity (Table 4.S2). In control flies, the PDF

positive and negative lateral neurons all displayed similar phases of PER accumulation on day four of constant darkness (DD4) (Fig. 4.4, A and D). In contrast, there were differences in PER expression between PDF positive and most PDF negative lateral neurons in flies with slow PDF neurons (Fig. 4.4, B and E). Only two LN_ds per hemisphere were synchronized with the PDF neurons (Fig. 4.4B). These were the two $PDFR^+$ LN_ds that express short neuropeptide F (sNPF) (Fig. 4.4, G to J, and Fig. 4.S10) (19). Synchronization of these two neurons to PDF neurons required PDFR signaling (Fig. 4.4, C and F). Thus, most PDF negative lateral neurons were not reset by the slow PDF neurons (Fig. 4.4, B and E). These uncoupled neurons were likely responsible for the wild-type periodicities displayed by these flies (Fig. 4.1B, Figs. 4.S4, 4.S5, and 4.S11). Two of the $PDFR^+$ lateral neurons, a single LN_d and the 5^{th}s-LN_v, both of which express ion transport peptide (ITP) (Fig. 4.S11) (19), were synchronized not with the PDF neurons, but rather with the $PDFR^-$ LN_ds (Fig. 4.4, B and E), despite their receptivity to PDF. Thus, the slowed PDF neurons reset only two of the seven PDF negative lateral neurons per hemisphere, despite the fact that four out of seven of these neurons are receptive to PDF, revealing that physiological connections between PDF positive and negative neurons do not insure the coupling of their molecular oscillations.

Our results reveal that the PDF negative lateral neurons consist of at least three functionally and neurochemically distinct oscillatory units: Two pairs of $sNPF^+/PDFR^+$ neurons that are strongly coupled to PDF neurons, two pairs of $ITP^+/PDFR^+$ neurons that are less strongly coupled to PDF neurons, and three pairs of $PDFR^-$ neurons that are not directly coupled to PDF neurons (Fig. 4.S11). Each of these oscillatory units is unified by its neuropeptide output and characterized by a distinct mode of coupling to the other oscillatory units (Fig. 4.S11). We conclude that the clock neuron network consists of multiple independent oscillators, each

capable of orchestrating bouts of activity (Fig 4.S11) and that behavioral rhythms emerge from the interactions of many independent oscillators rather than from a unique group of master pacemakers.

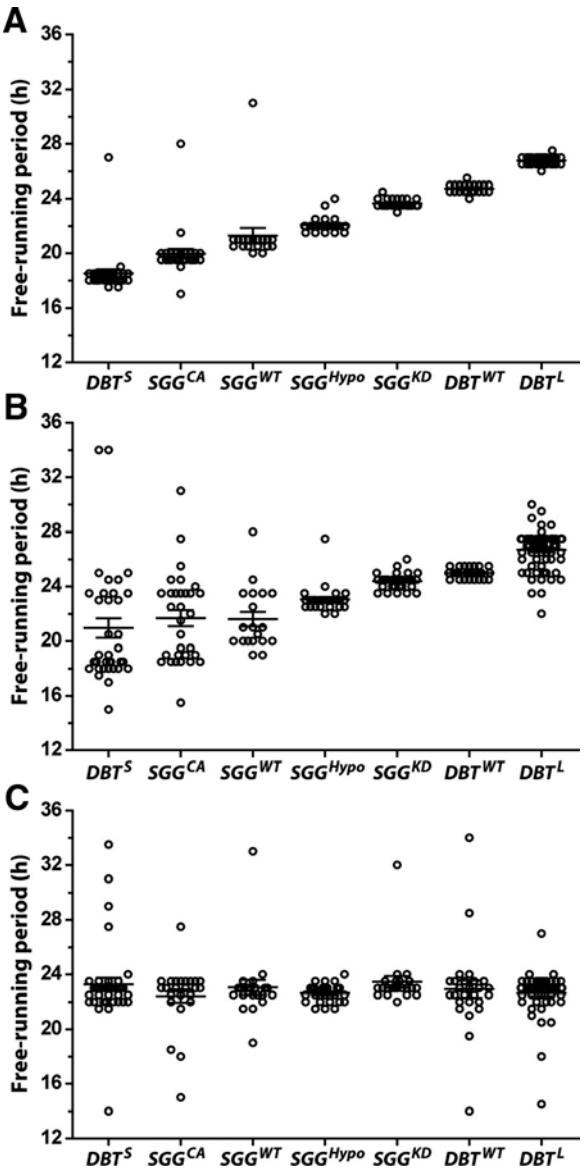

Figure 4.1. The PDF positive clock neurons coherently set free-running periods via PDF signaling over a limited temporal range.
(**A** to **C**) Scatter plots of the predominant free-running periods of rhythmic flies overexpressing different forms of *DBT* or *SGG*in both PDF-positive and -negative clock neurons (driven by*Clk-GAL4*) (A), or in only the PDF-positive neurons (driven by*Pdf-GAL4*) of WT flies (B) or $Pdfr^{-}$ mutants (C). Circles indicate the highest-amplitude free-running period for individual rhythmic flies; lines represent mean ± SEM (error bars). DBT^{S}, DBT^{Short}; SGG^{CA}, constitutively active *SGG*; SGG^{WT}, WT *SGG*; SGG^{Hypo}, hypomorphic *SGG*; SGG^{KD}, kinase-dead *SGG*; DBT^{WT}, WT *DBT*; DBT^{L}, DBT^{Long}. Kruskal-Wallis one-way analysis of variance (ANOVA) reveals a significant difference among groups in (A) and (B) ($P < 0.0001$ for both), but no significant difference among groups in (C) ($P = 0.4829$). h, hours.

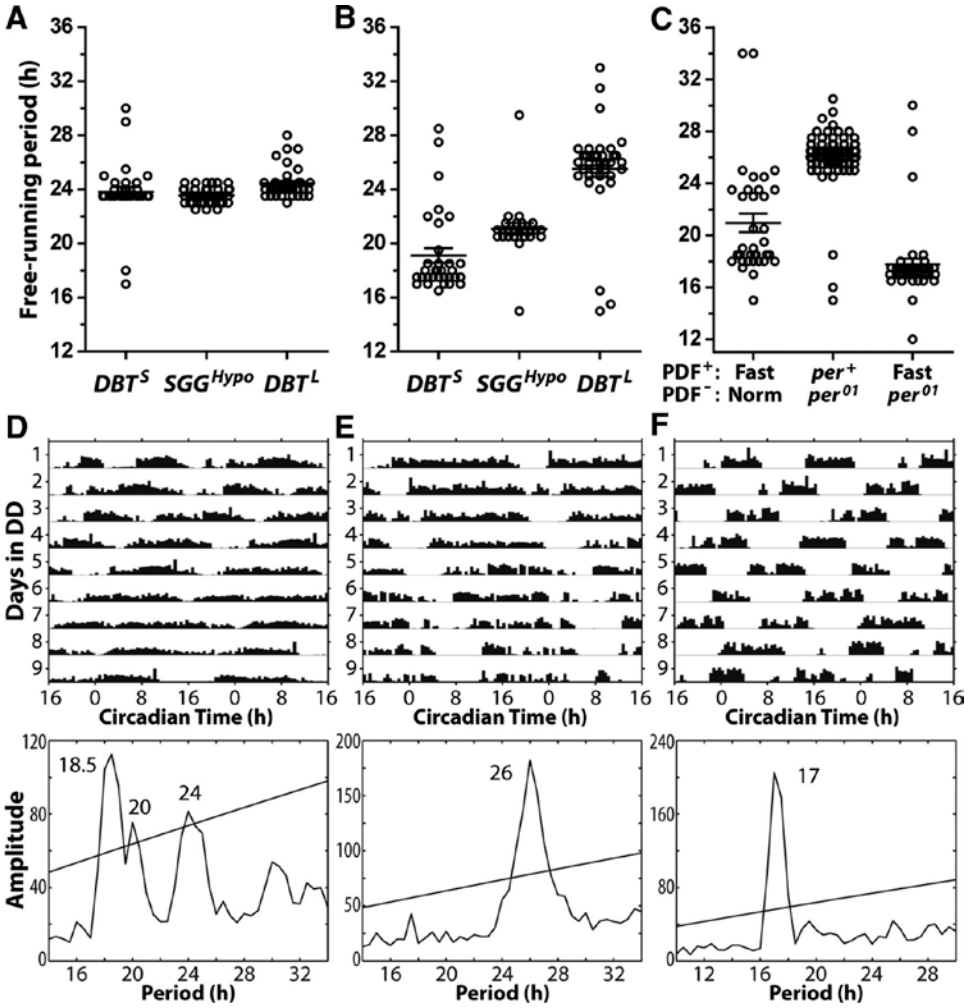

Figure 4.2 The PDF negative clock neurons exert independent control over free-running activity rhythms.

(**A** and **B**) Scatter plots of the predominant free-running periods of rhythmic flies overexpressing DBT^S, SGG^{Hypo}, or DBT^L only in the PDF-negative neurons (driven by *Clk-GAL4/Pdf-GAL80*) of WT flies (A) or $Pdfr^-$ mutants (B). Kruskal-Wallis one-way ANOVA reveals a significant difference among groups in both (A) and (B) ($P < 0.0001$ for both). (**C**) Scatter plots of the predominant free-running periods of rhythmic flies with different compositions of PDF-positive and -negative clock neurons. Specific genotypes are: per^+, $Pdf>DBT^S$ for "Fast PDF^+, normal (Norm) PDF^-"; per^{01}, *Pdf>PER* for "per^+ PDF^+, per^{01} PDF^-"; and per^{01}, $Pdf>PER+DBT^S$ for "Fast PDF^+, per^{01} PDF^-." (**D** to **F**) Representative actograms (upper panels) and χ-square periodograms (lower panels) of individual flies with different compositions of PDF-positive and -negative neurons under constant darkness. Genotypes are as follows: (D) per^+, $Pdf>DBT^S$; (E) per^{01}, *Pdf>PER*; and (F) per^{01}, $Pdf>PER+DBT^S$.

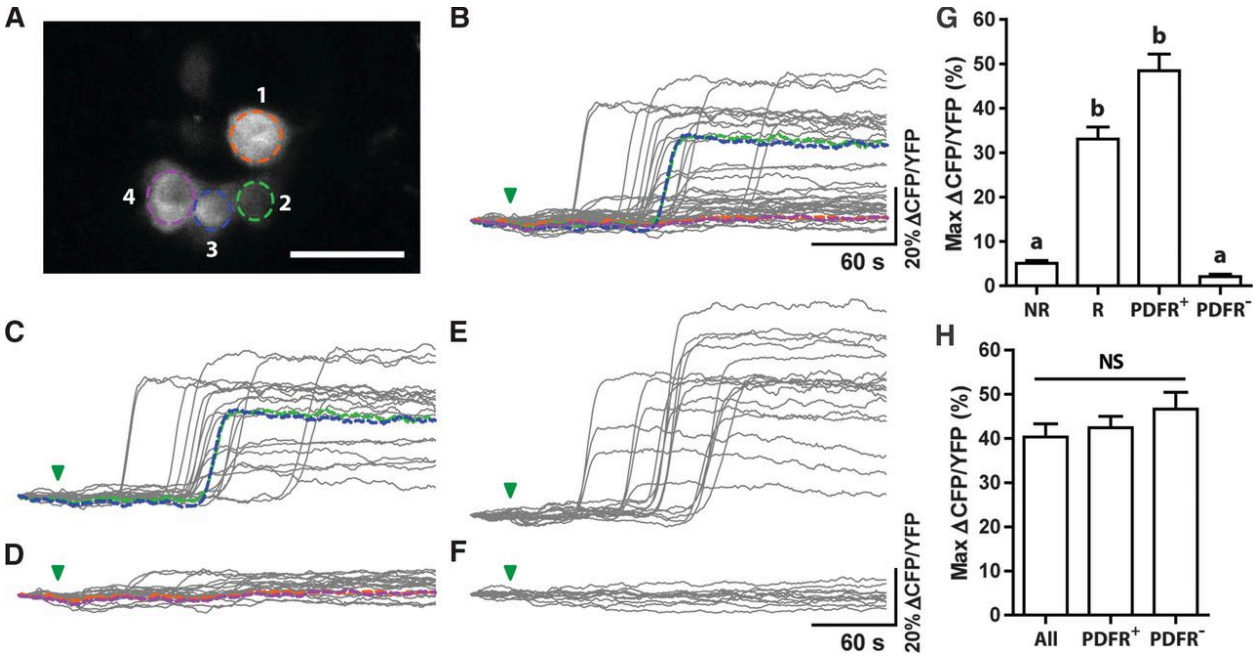

Figure 4.3. Pigment-dispersing factor modulates only half of the PDF-negative dorsal lateral neurons.

(**A**) A representative micrograph showing the dorsal lateral neurons (LN_ds) from a *Clk>Epac1-camps* fly brain. Four of the six LN_ds (labeled 1 to 4) were present in the optical section. Scale bar, 5 μm. (**B** to **F**) cAMP dynamics of LN_ds in response to bath-applied 10^{-5} M PDF peptide (green triangles). Responses of 45 LN_ds imaged from 13*Clk>Epac1-camps* brains shown in (B) fell into two classes: responsive LN_ds [22 out of 45 (22/45)] that displayed large cAMP increases (>10% change in CFP/YFP ratio) (C) and nonresponsive LN_ds (23/45) (<10% changes) (D). The colored traces in (B) to (D) are from the LN_ds shown in (A) circled with the same color as their plots. All $PDFR^+$ LN_ds (18 neurons imaged from seven *Mai179>Epac1-camps*brains) displayed cAMP increases in response to PDF application (E). None of the $PDFR^-$ LN_ds (11 neurons imaged from six *Clk/cry-GAL80>Epac1-camps* brains) displayed cAMP increases (F). CFP, cyan fluorescent protein; YFP, yellow fluorescent protein. (**G**) Summary of maximum cAMP responses of LN_ds to 10^{-5} M PDF. NR, nonresponsive LN_ds from (D); R, responsive LN_ds from (C); $PDFR^+$ and $PDFR^-$ are from (E) and (F), respectively. The letters “a” and “b” denote significantly different groups ($P< 0.0001$) by Kruskal-Wallis one-way ANOVA and Dunn’s multiple comparisons test. (**H**) cAMP responses of LN_ds to bath-applied 10^{-5} M forskolin, a direct activator of adenylyl cyclases. “All” represents forskolin responses of LN_ds recorded from *Clk>Epac1-camps* brains, in which the cAMP sensor was expressed in both $PDFR^+$ and $PDFR^-$ LN_ds. The numbers of neurons and brains examined were: All (16 neurons, five brains), $PDFR^+$ (12 neurons, five brains), and $PDFR^-$ (10 neurons, six brains). NS, not significant by Kruskal-Wallis one-way ANOVA and Dunn’s multiple comparisons test. For all histograms, data are presented as mean ± SEM (error bars).

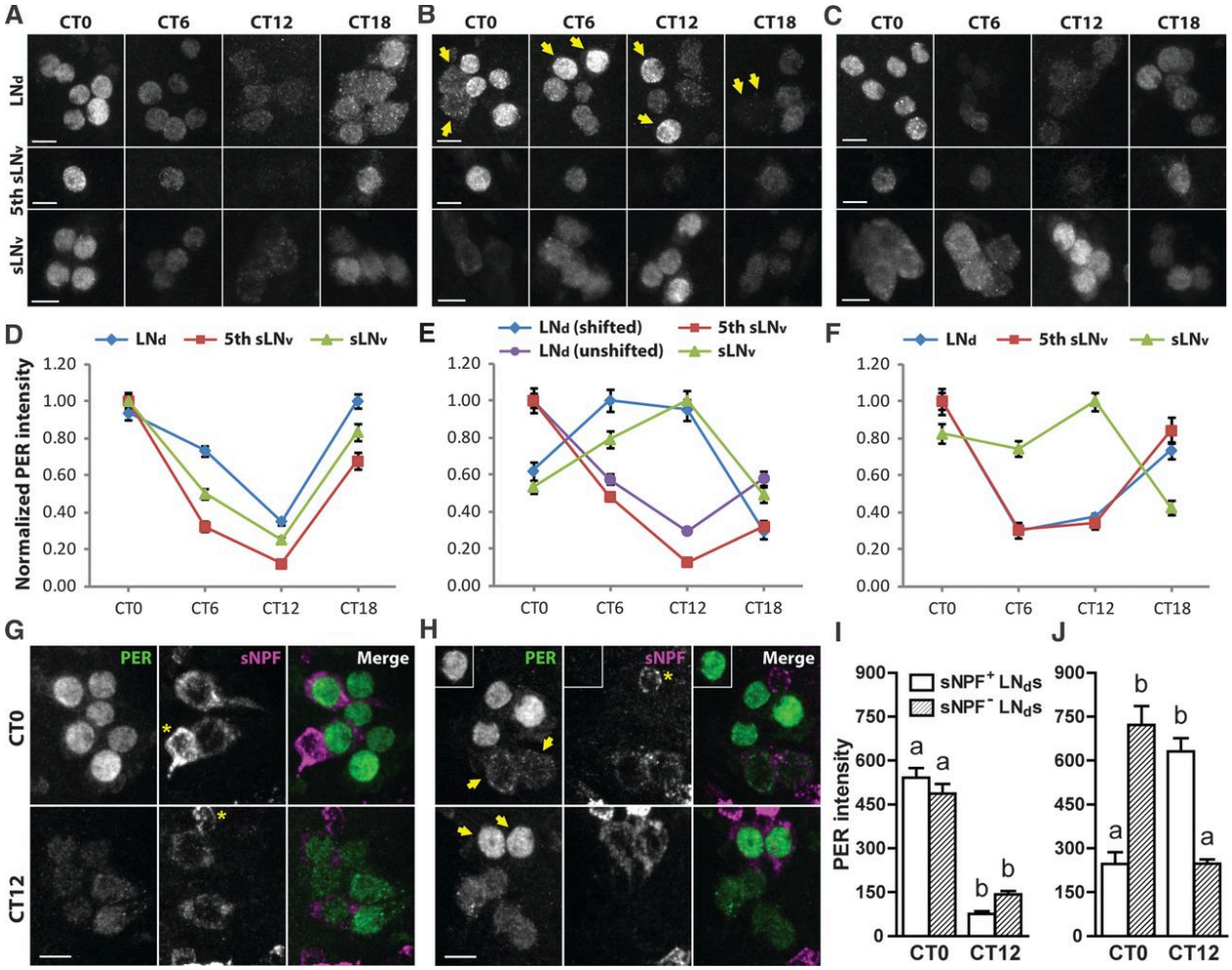

Figure 4.4. Physiological connectivity does not ensure molecular clock coupling in the lateral neuron network.

(**A** to **C**) Immunostaining of PER protein in PDF-positive and -negative lateral neurons across different time points on day 4 of constant darkness (DD4). In *UAS-DBT^{L}* control fly brains, PER accumulated in the PDF-positive (s-LN$_v$s) and -negative (LN$_d$s and fifth s-LN$_v$) neurons with the same phase (A). In *Pdf>DBT^{L}* flies in which the PDF neurons were slowed down, only two LN$_d$s (marked by yellow arrows) were coupled with the s-LN$_v$s, displaying a shifted phase of PER cycling relative to the other LN$_d$s (B). In *Pdfr^{-},Pdf>DBT^{L}* flies, all PDF-negative neurons (LN$_d$s and fifth s-LN$_v$) had similar phases of PER cycling, and none were coupled to the uniformly delayed s-LN$_v$s (C). Scale bars, 5 μm. (**D** to **F**) Quantification of PER immunostaining intensity within lateral neurons of *UAS-DBT^{L}* flies (D),*Pdf>DBT^{L}* flies (E), and *Pdfr^{-}*, *Pdf>DBT^{L}* flies (F). The LN$_d$s in (E) were divided into two groups based on their phase differences and quantified separately: The two LN$_d$s coupled to the s-LN$_v$s were quantified as "LN$_d$ (shifted)" and the others as "LN$_d$ (unshifted)." (**G** to **J**) The two shifted LN$_d$s express neuropeptide sNPF. LN$_d$s were coimmunostained for PER and sNPF at CT0 and CT12 on DD4 (CT0 and CT12 correspond to the light-on and light-off times had the 12 hour:12 hour light:dark cycles continued). In *UAS-DBT^{L}* control flies, the two sNPF^{+} LN$_d$s and four sNPF^{-} LN$_d$s had similar subcellular PER distribution (G) and expression levels (I) at each of these time points. In*Pdf>DBT^{L}* flies, the

$sNPF^+$ LN_ds differ in their PER distribution [(H), yellow arrows] and intensity (J) from the $sNPF^-$ LN_ds. Scale bars, 5 μm. Asterisks in (G) and (H) indicate $sNPF^+$ cells that are not clock neurons (lack of PER expression). The letters "a" and "b" in (I) and (J) denote significantly different groups ($P < 0.0001$ for both) by Kruskal-Wallis one-way ANOVA and Dunn's multiple comparisons test. Sample sizes are reported in Table 4.S6 for (D) to (F) and in Table 4.S7 for (I) and (J). Data are presented as mean ± SEM (error bars).

4.3 Materials and Methods

4.3.1 Fly strains

Flies were reared on cornmeal-yeast-sucrose media at 25 °C under a 12hr: 12hr light: dark cycle or under the diurnal conditions of the lab. All fly strains used in this study have been described previously. These were: *Clk(-856[8/2])-GAL4* (20), *Mai179-GAL4* (6, 21), *Pdf-GAL4* (22), *Pdf-GAL80* and *cry-GAL80* (7), *UAS-Epac1-camps(50A)* (15), *UAS-PER16* (23), per^{01} (also known as per^{0}) (24), the $Pdfr^-$ mutant $Pdfr^{5304}$ (25), the *UAS-Shaggy (SGG)* lines, *UAS-SGG10(wild-type)*, $UAS\text{-}SGG^{S9A}$*(constitutively active)*, $UAS\text{-}SGG^{Y214F}$*(hypomorphic)*, and $UAS\text{-}SGG^{KK83\text{-}84MI}$*(kinase-dead)* (9) (26), and the *UAS-Doubletime (DBT)* lines, $UAS\text{-}DBT^{WT}$*(21M1C)*, $UAS\text{-}DBT^{S}$*(10F5A)*, and $UAS\text{-}DBT^{L}$*(22F1C)* (10).

4.3.2 Live-imaging

The measurement of relative cAMP levels within single neuron soma during bath application of PDF peptide or forskolin was done as previously described (15) with minor modifications. Living brains expressing the cAMP sensor Epac1-camps in neurons of interest were dissected under standard saline consisting of 128 mM NaCl, 2 mM KCl, 4 mM $MgCl_2$, 1.8 mM $CaCl_2$, 36 mM sucrose, and 5 mM HEPES (pH 7.1) (27). Dissected brains were placed in a 35 × 10 mm Falcon Petri Dish containing 1.8 mL standard saline and allowed to settle and

adhere to the bottom of the dish for 5 to 10 minutes before imaging. After 30s of baseline scanning, 0.2 mL of 10^{-4} M PDF peptide or forskolin was gently added into the dish with a micropipette to yield a final peptide or drug concentration of 10^{-5} M. cAMP responses of neurons of interest were monitored for a total of 5 min with an Olympus Fluoview 1000 confocal microscope equipped with the Fluoview software (Olympus, Center Valley, PA, USA). cAMP imaging and data analysis were done as previously described (*28*). *Drosophila* PDF peptide was synthesized by PolyPeptide Laboratories (San Diego, CA, USA), and forskolin was purchased from Sigma (St. Louis, MO, USA).

4.3.3 Analysis of activity rhythms

Adult locomotor activity monitoring and data processing were done as previously described (*29*, *30*) with only the minor modifications described below. Adult male flies were placed individually in glass capillary tubes and these were loaded onto the TriKinetics DAM2 *Drosophila* Activity Monitors (Waltham, MA, USA) for locomotor activity recording. Flies were entrained to 12 hr: 12 hr light: dark cycles at 25 °C for at least 5 days, and then released into constant darkness for at least 7 days. Data analysis and the generation of actograms were done with the ClockLab software from Actimetrics (Wilmette, IL, USA). Rhythmicity and free-running period of individual flies were determined by χ-square periodogram analysis with a confidence level of 0.01 (*31*). The range of free-running periods analyzed for most of the genotypes was from 14 hr to 34 hr, with 0.5 hr intervals, the only exception being for *Pdfr^{-};Clk-GAL4,Pdf-GAL80/+;UAS-DBT^{S}/+* and *per^{01},w;Pdf-GAL4/+;UAS-PER/UAS-DBT^{S}* flies whose free-running periods were analyzed from 10 hr to 30 hr because of the very short periods displayed by these flies. For individuals with more than one significant periodicity, the period with the highest amplitude over significance was used for the determination of average periods.

Flies often displayed secondary peaks at 0.5× and 1.5× the predominant periodicity in the periodogram due to the bimodal organization of their activity rhythms, we therefore did not include these periodicities in our analysis. The “Power” and “Significance” values generated from χ-square analysis were used to calculate “Rhythmic Power” as a measure of the strength of each rhythm. “Power” is the measured periodogram value for an individual fly at the peak periodicity (i.e. the amplitude of the peak in the periodogram), and “Significance” is the minimum periodogram value considered rhythmic at the indicated period based on the confidence level (i.e. the amplitude of the significance line at the peak periodicity). “Rhythmic Power” was calculated as Rhythmic Power = Power – Significance, and therefore represents the amplitude of the peak over significance. The rhythmic power of arrhythmic flies was considered “0” and rhythmic power values of both rhythmic and arrhythmic flies were used in average rhythmic power calculations.

4.3.4 Immunocytochemistry

The immunocytochemistry methods used here have been previously described (*32*). We dissected brains under ice-cold Ca^{2+}-free *Drosophila* Ringer’s solution (182 mM KCl, 46 mM NaCl, 10 mM Tris, pH 7.2) and fixed them in 4% paraformaldehyde in phosphate buffered saline (PBS) for 1 hr at room temperature. We rinsed brains with PBS-TX (PBS with 0.3% Triton X-100), and blocked them with 3% normal goat serum in PBS-TX for 1 hr at room temperature. After a brief rinse with PBS-TX, we incubated brains with primary antibodies diluted in PBS-TX at 4 °C for two nights. Rat anti-PER was provided by Dr. Michael Rosbash (Brandeis University, Waltham, MA, USA) and was used at a dilution of 1:500 (*33*). Rabbit anti-sNPF precursor was provided by Dr. Dick Nässel (Stockholm University, Stockholm, Sweden) and was diluted to 1:1000 (*34*). Mouse monoclonal anti-PDF was obtained from the Developmental Studies

Hybridoma Bank at the University of Iowa (Iowa City, Iowa, USA), and was diluted to 1:200. After five 15-min washes with PBS-TX, we incubated brains in 1:1000 dilutions of Alexa Fluor conjugated secondary antibodies (Invitrogen, Grand Island, NY, USA) at 4 °C overnight. After five washes with PBS-TX (15 min each), followed by two exchanges of PBS, we mounted brains on poly-L-lysine-coated cover slips, dehydrated the mounted brains in a graded glycerol series (30%, 50%, and 70% glycerol in PBS for 5 minutes each) and mounted the cover slips on microscope slides with Vectashield HardSet Mounting Medium (Vector Laboratories, Burlingame, CA, USA). We imaged brains on an Olympus Fluoview 1000 confocal microscope with a 60×/1.10 NA objective (Olympus, Center Valley, PA, USA). We maintained all imaging settings between genotypes for each class of neurons for each experiment, and adjusted settings for each neuronal class to optimize image quality. PER immunostaining intensity of clock neurons was quantified using the ImageJ software (National Institutes of Health, USA) as previously described (*35*). For the comparison of PER subcellular distribution and intensity in $sNPF^+$ and $sNPF^-$ LN_ds, the $sNPF^+$ LN_ds were identified and imaged based on their anatomical positions and co-expression of both PER and sNPF. Only brains in which the $sNPF^+$ LN_ds could be observed were used for these experiments. Specific sample sizes are reported in figure legends and in Table 4.S6 and 4.S7.

4.4 Supplementary Results

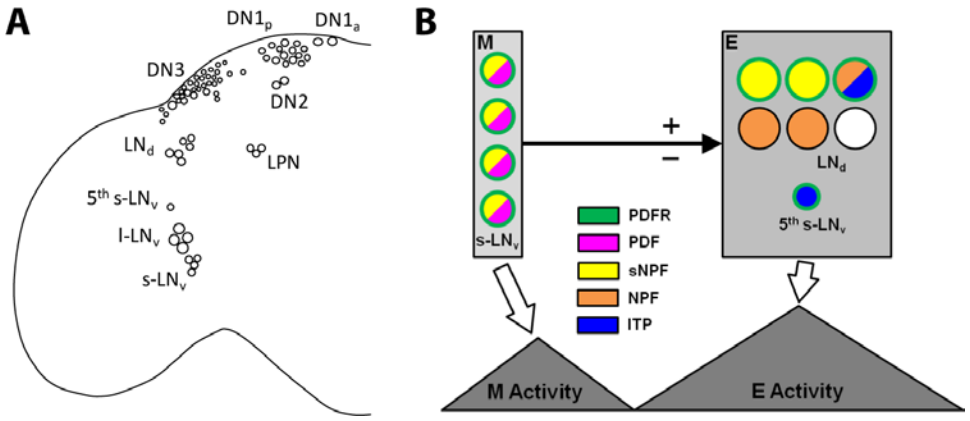

Figure 4.S1. The hierarchical dual-oscillator model of the *Drosophila*'s circadian clock neuron network.
(**A**) A somatic map of the clock neuron network of *Drosophila*. A single hemisphere (left) is shown and the various classes of clock neurons are labeled. The lateral neurons (LN) consist of large ventral lateral neurons (l-LN_vs), small ventral lateral neurons (s-LN_vs), a 5^{th} small ventral lateral neuron (5^{th} s-LN_v), and dorsal lateral neurons (LN_ds). The dorsal neurons (DN) contain $DN1_a$s (anterior), $DN1_p$s (posterior), DN2s, and DN3s. LPN: lateral posterior neurons. The l-LN_vs and s-LN_vs express pigment-dispersing factor (PDF); all other clock neurons are PDF negative. (**B**) The dual-oscillator model of the lateral clock neuron network and its control of activity rhythms. The LN_ds and 5^{th} s-LN_v (evening (E) oscillator) control evening activity. The s-LN_vs (morning (M) oscillator) control morning activity and reset the evening oscillator through daily advances (+) or delays (-), thereby maintaining clock network synchrony under constant conditions. The neuropeptides expressed by the lateral clock neurons are shown. PDF, pigment-dispersing factor; sNPF, short neuropeptide F; NPF, neuropeptide F; ITP, ion transport peptide. Only subsets of the evening oscillator neurons express PDF receptor (PDFR).

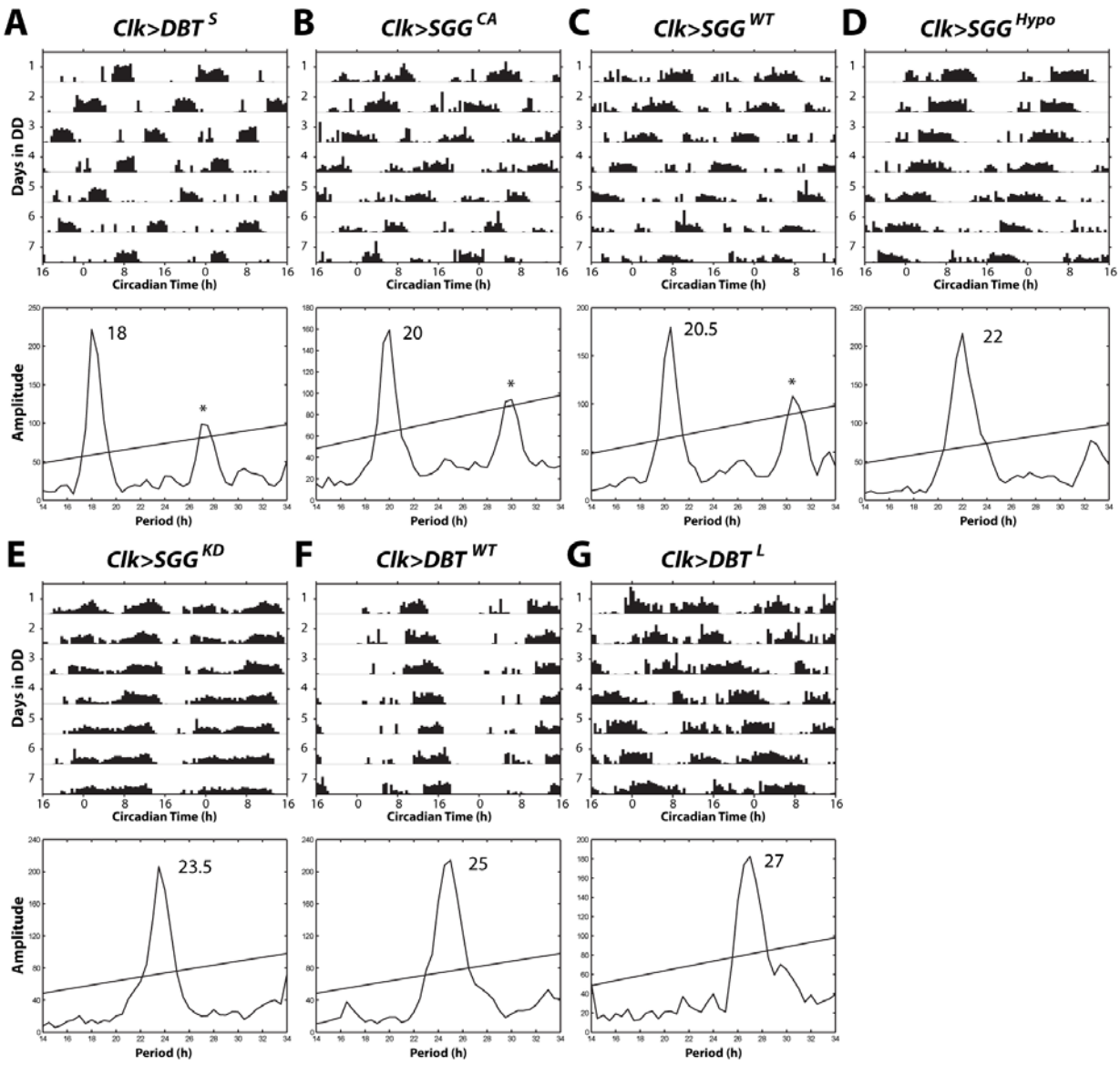

Figure 4.S2. The free-running periods of activity rhythms can be genetically manipulated over a wide temporal range.

(**A** to **G**) Representative actograms (upper panels) and periodograms (lower panels) of individual flies overexpressing different forms of *DBT* or *SGG* in all clock neurons under constant darkness (DD). Genotypes are indicated above the actograms. DBT^{S}, DBT^{Short}; SGG^{CA}, *constitutively active SGG*; SGG^{WT}, *wild-type SGG*; SGG^{Hypo}, *hypomorphic SGG*; SGG^{KD}, *kinase-dead SGG*; DBT^{WT}, *wild-type DBT*; DBT^{L}, DBT^{Long}. Asterisks indicate a secondary peak at 1.5× the predominant peak due to the bimodal organization of the fly's activity rhythms, which is not considered as a real significant periodicity. Note that when overexpressed in all clock neurons, all the *DBT* and *SGG* transgenes support coherent and high-amplitude free-running rhythms.

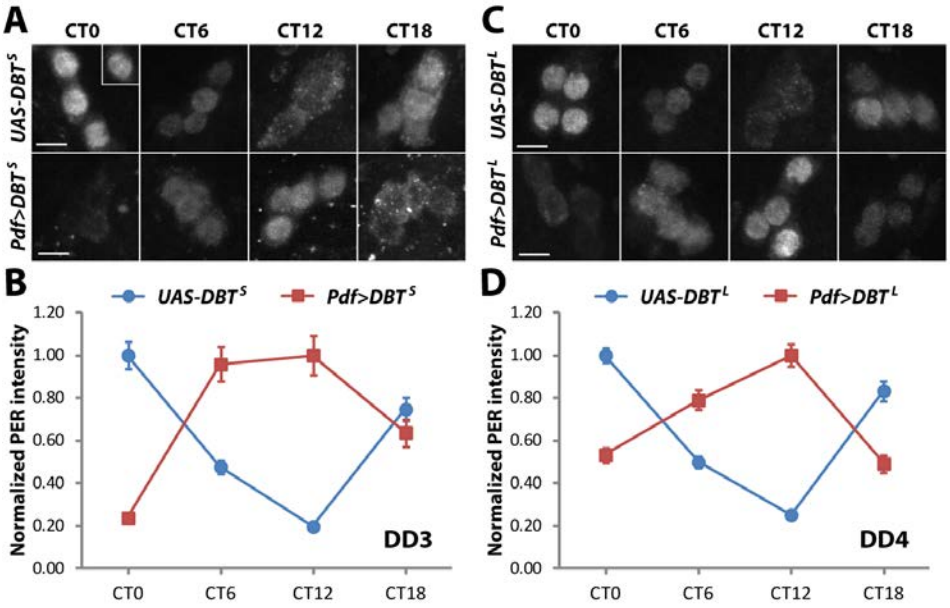

Figure 4.S3. The overexpression of *DBT*^{S} and *DBT*^{L} coherently accelerates and decelerates the molecular clocks of the PDF positive s-LN$_v$s.
(**A**) Representative micrographs of PERIOD (PER) expression in the s-LN$_v$s of control *UAS-DBT*^{S} flies (top row) and experimental *Pdf>DBT*^{S} flies (bottom row) on day 3 of constant darkness (DD3). The overexpression of *DBT*^{S} resulted in a coherent change of phase consistent with a fast-running molecular clock. Scale bars, 5 μm. (**B**) Quantification of PER intensity from the genotypes shown in (A). The numbers of neurons and brains examined for *UAS-DBT*^{S} were CT0 (67, 10), CT6 (70, 11), CT12 (65, 11), CT18 (67, 11), and for *Pdf>DBT*^{S} CT0 (70, 10), CT6 (75, 12), CT12 (65, 10), CT18 (47, 9). (**C**) Representative micrographs of PER expression in the s-LN$_v$s of control *UAS-DBT*^{L} flies (top row) and experimental *Pdf>DBT*^{L} flies (bottom row) on DD4. The overexpression of *DBT*^{L} resulted in a coherent change of phase consistent with a slow-running molecular clock. Scale bars, 5 μm. (**D**) Quantification of PER intensity from the genotypes shown in (C). The numbers of neurons and brains examined for *UAS-DBT*^{L} are CT0 (94, 14), CT6 (80, 11), CT12 (80, 11), CT18 (88, 12), and for *Pdf>DBT*^{L} CT0 (89, 13), CT6 (79, 13), CT12 (80, 12), CT18 (62, 11). Data of (C) and (D) are the same as those in Figure 4.4.

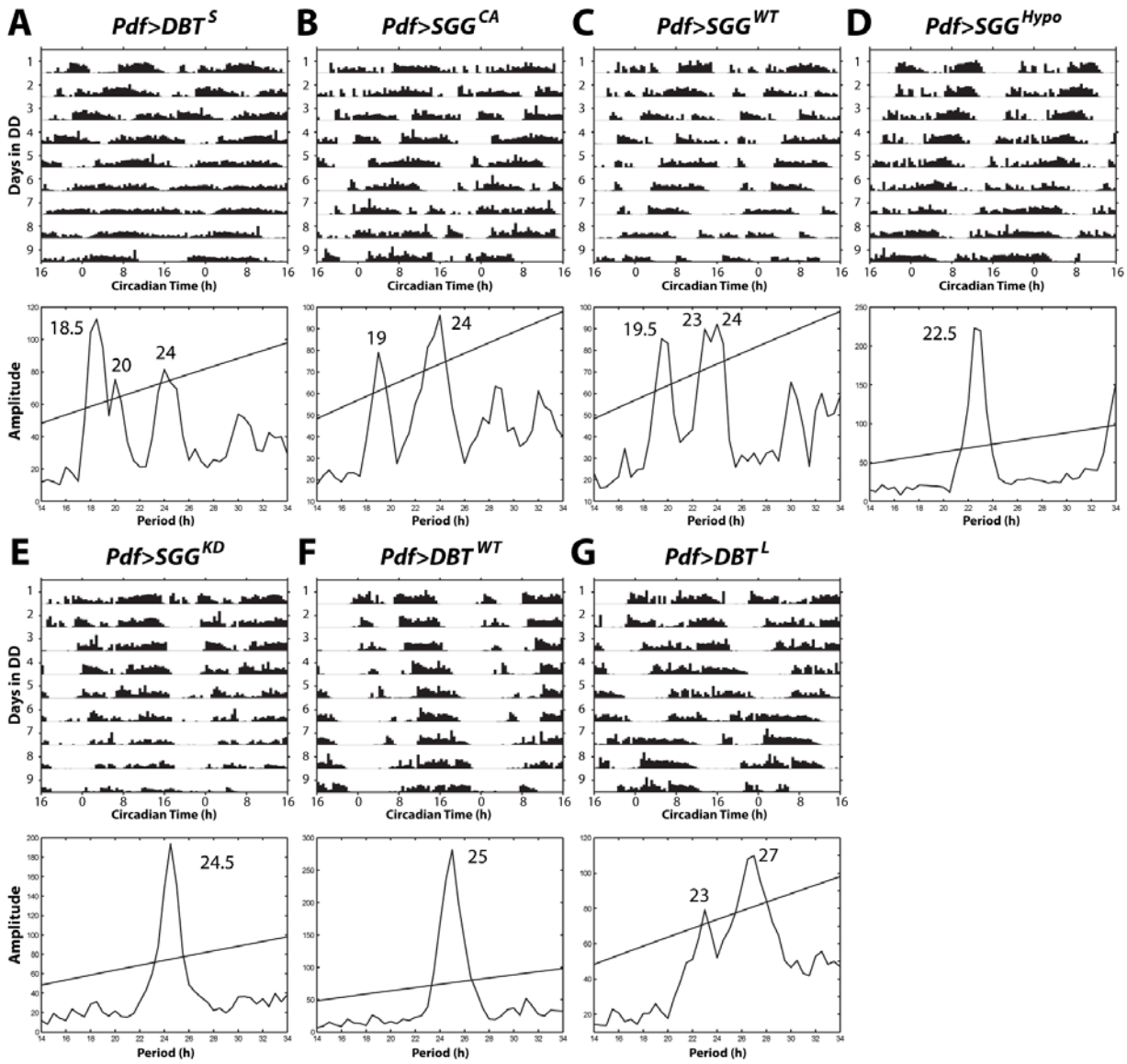

Figure 4.S4. The PDF positive neurons coherently set free-running periods only within a narrow temporal range.

The PDF positive neurons coherently set free-running periods only within a narrow temporal range. (**A** to **G**) Representative actograms (upper panels) and periodograms (lower panels) of individual flies overexpressing different forms of *DBT* or *SGG* only in the PDF positive neurons under DD. Genotypes are indicated above the actograms. When the clock speed discrepancies between PDF positive and negative neurons are small, flies display coherent activity rhythms with single periodicities determined by the speed of the PDF positive neurons (D to F). Large clock speed discrepancies between PDF positive and negative neurons weaken rhythms and often result in internal desynchronization wherein individual flies display multiple significant periodicities in their activity rhythms reflective of both the PDF positive and negative oscillator speed (A to C, and G).

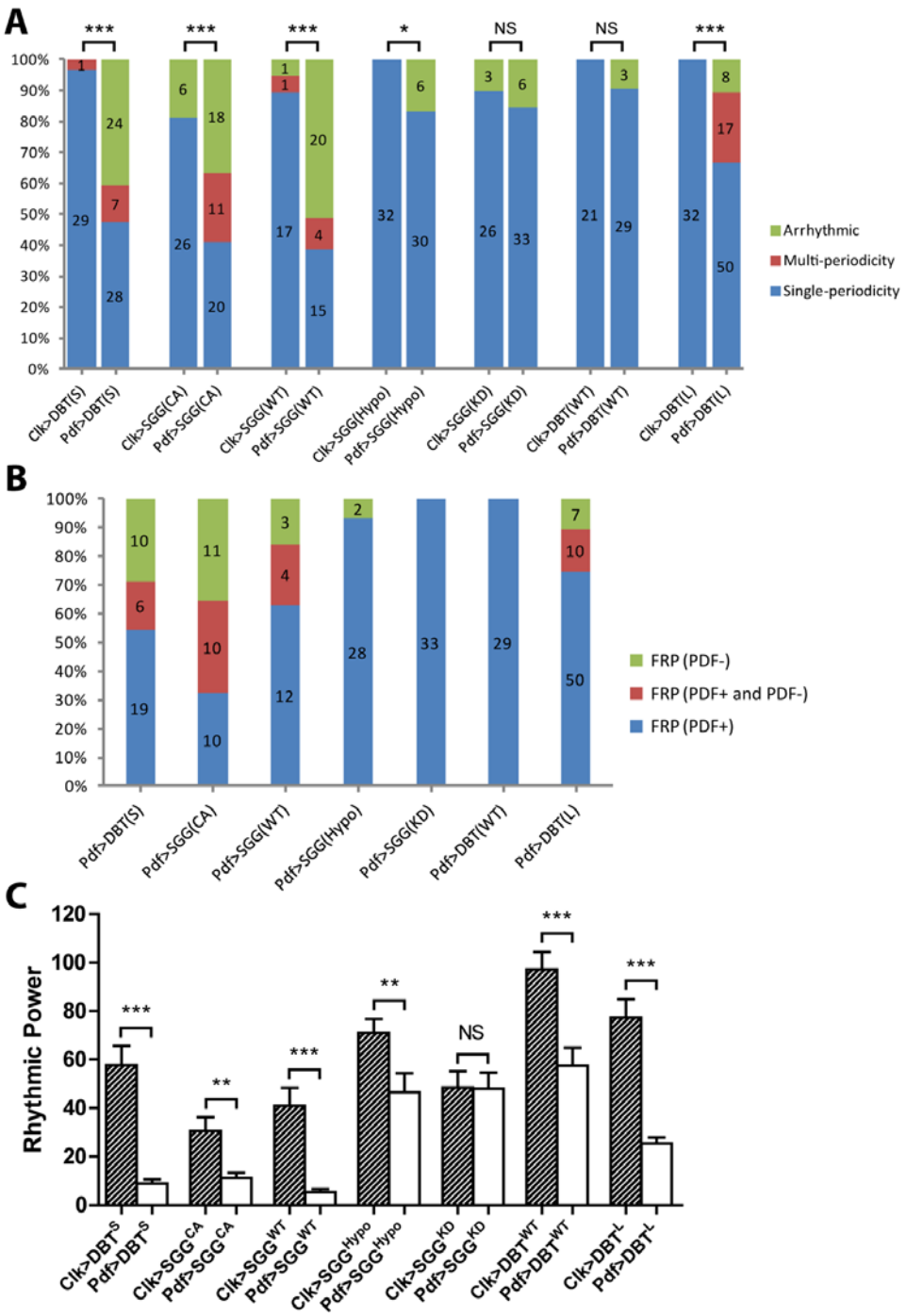

Figure 4.S5. Comparison of rhythmicity, internal desynchronization and rhythmic power between flies overexpressing different forms of *DBT* or *SGG* in both PDF positive and negative clock neurons and in PDF positive neurons only.

(**A**) Pairwise comparison of rhythmicity and internal desynchronization: The percentage of arrhythmic flies and the percentages of rhythmic flies displaying either single or multiple significant periodicities are shown, with the numbers of flies in each category displayed on each

bar of the histogram. * P < 0.05; *** P < 0.001; NS, not significant, by the Freeman-Halton extension of the Fisher's exact test. (**B**) The percentages within the rhythmic subset of flies with modified PDF positive neuron speed displaying a single significant free-running period (FRP) determined by the PDF positive neuron speed (FRP(PDF+)), a single FRP determined by the PDF negative neuron speed (FRP(PDF-)), and multiple FRPs reflective of both PDF positive and negative neuron speeds (FRP(PDF+ and PDF-)). The numbers of flies in each category are displayed on each bar of the histogram. (**C**) Pairwise comparison of rhythmic power between flies overexpressing different forms of *DBT* or *SGG* in both PDF positive and negative neurons and in the PDF positive neurons only. Data are presented as mean ± SEM. ** P < 0.01; *** P < 0.001; NS, not significant, by Mann–Whitney U test.

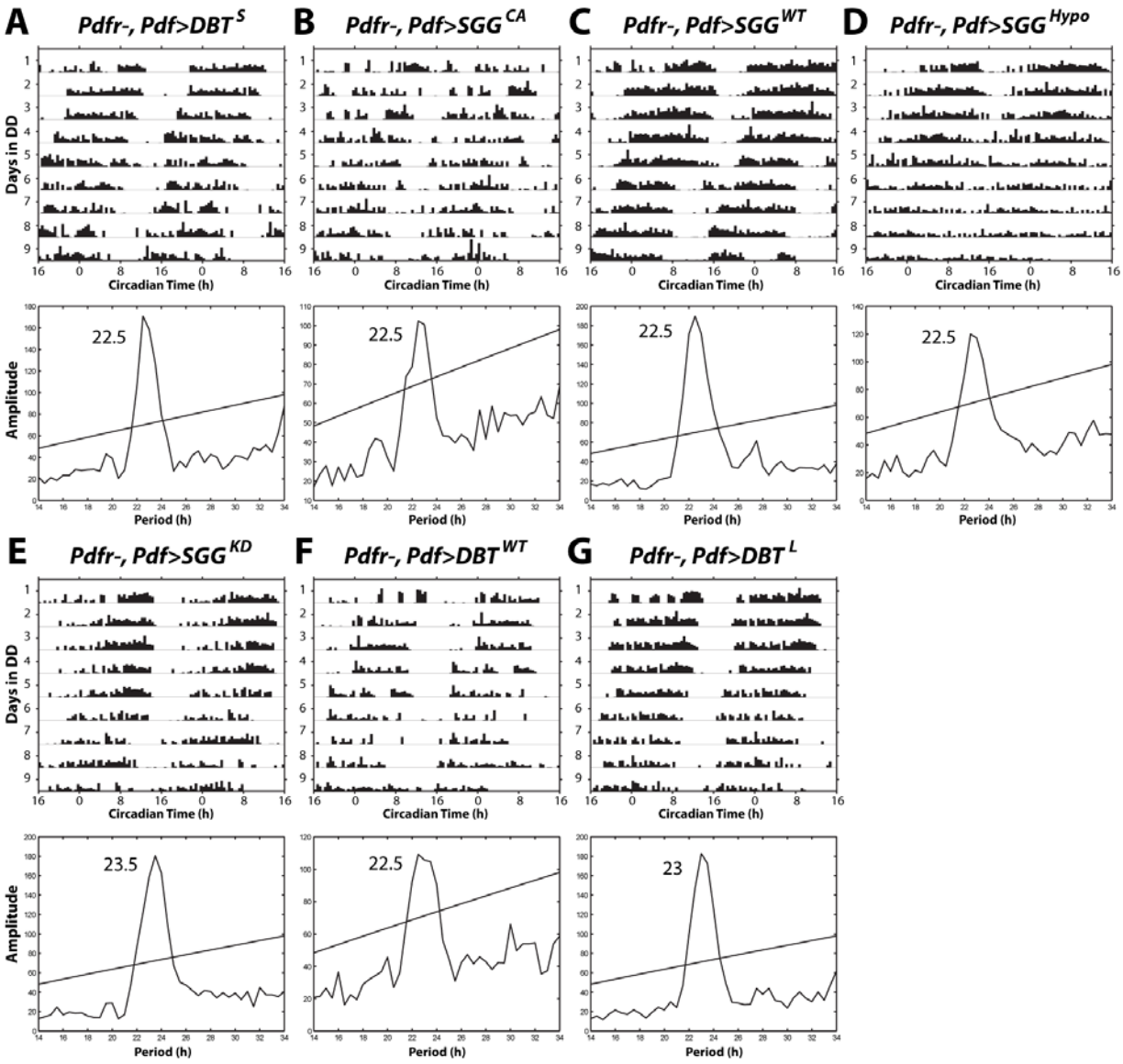

Figure 4.S6. PDFR signaling is required for the PDF neuron influence over free-running periods.

(**A** to **G**) Representative actograms (upper panels) and periodograms (lower panels) of rhythmic *Pdfr*$^{-}$ flies overexpressing different forms of *DBT* or *SGG* only in PDF positive clock neurons under DD. Genotypes are indicated above the actograms. Without a functional PDFR, free-running periods of rhythmic individuals are not influenced by the clock speed of the PDF positive neurons. Note that approximately 40% to 70% of flies containing the loss-of-function *Pdfr* mutation were rhythmic in this study. The proportion of rhythmic *Pdfr* mutants has varied significantly from study to study (e.g., (*14*, *25*, *36*)), and the proportions of rhythmic *Pdfr*^{5304} mutant flies we report here are similar to those reported in previous studies (*14*, *36*).

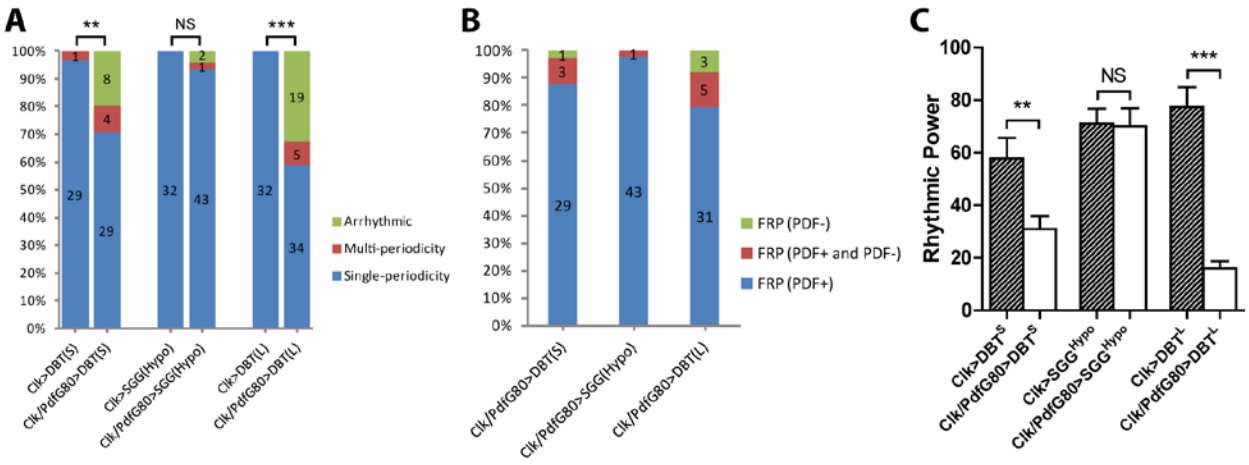

Figure 4.S7. Comparison of rhythmicity, internal desynchronization and rhythmic power between flies overexpressing different forms of *DBT* or *SGG* in both PDF positive and negative clock neurons and in PDF negative clock neurons only.
(**A**) Pairwise comparison of rhythmicity and internal desynchronization: The percentage of arrhythmic flies and the percentages of rhythmic flies with either single or multiple significant periodicities are shown, with the numbers of flies in each category indicated within each bar of the histogram. ** $P < 0.01$; *** $P < 0.001$; NS, not significant, by the Freeman-Halton extension of the Fisher's exact test. (**B**) The percentages within the rhythmic subset of flies with modified PDF negative neuron speed displaying a single significant free-running period (FRP) determined by the PDF negative neuron speed (FRP(PDF-)), a single FRP determined by the PDF positive neuron speed (FRP(PDF+)), and multiple FRPs reflective of both PDF positive and negative neuron speeds (FRP(PDF+ and PDF-)). The numbers of flies in each category are indicated within each bar of the histogram. (**C**) Pairwise comparison of rhythmic power between flies overexpressing DBT^{S}, SGG^{Hypo} or DBT^{L} in both PDF positive and negative neurons and in PDF negative neurons only. Data are presented as mean ± SEM. ** $P < 0.01$; *** $P < 0.001$; NS, not significant, by Mann–Whitney U test.

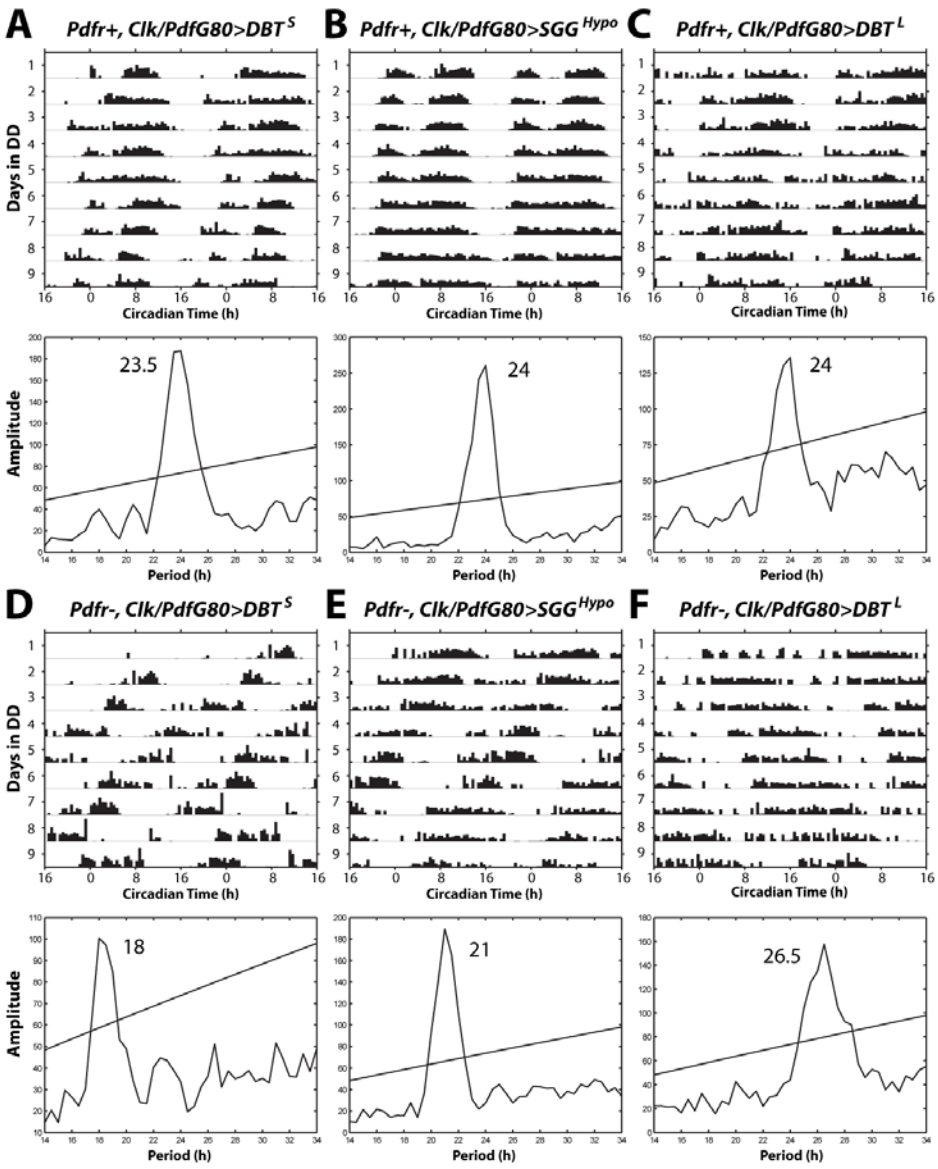

Figure 4.S8. In the absence of PDFR signaling, the PDF negative neurons determine free-running periods.

(**A** to **C**) Representative actograms (upper panels) and periodograms (lower panels) of individual rhythmic flies overexpressing DBT^S (A), SGG^{Hypo} (B), or DBT^L (C) only in the PDF negative clock neurons under DD in a *wild-type* ($Pdfr^+$) background. In this case the PDF negative neurons do not coherently set free-running periods. (**D** to **F**) Representative actograms (upper panels) and periodograms (lower panels) of rhythmic $Pdfr^-$ flies overexpressing DBT^S (D), SGG^{Hypo} (E), or DBT^L (F) only in the PDF negative neurons under DD. Without functional PDFR, the clock speed of PDF negative neurons determines the free-running period of activity rhythms.

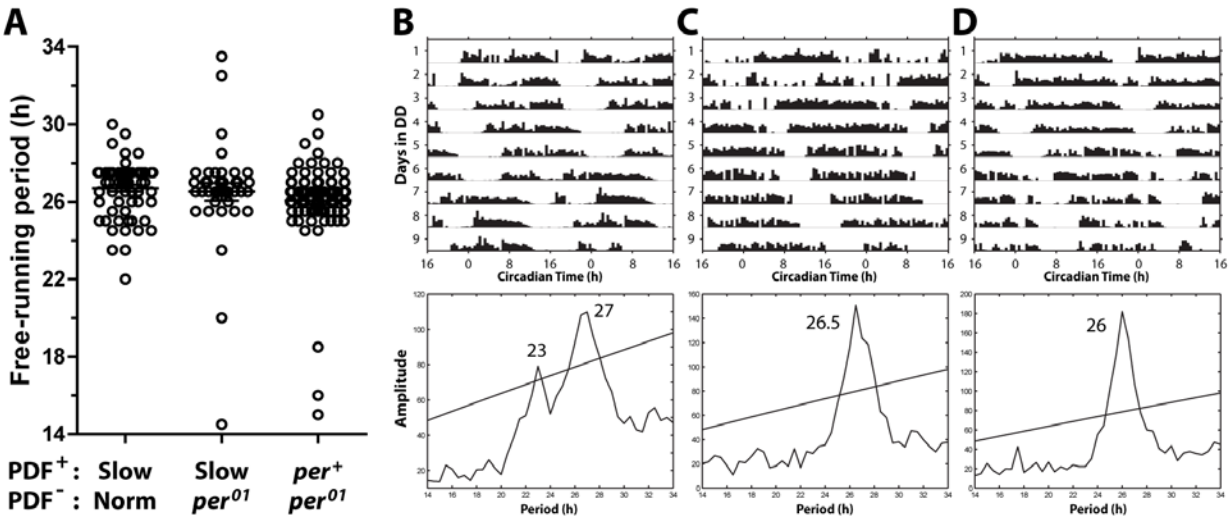

Figure 4.S9. The PDF positive neurons can coherently drive activity rhythms with very long free-running periods in the absence of functional molecular clocks in PDF negative neurons.

(**A**) Scatter plots of the predominant free-running periods of rhythmic flies with different compositions of PDF positive and negative neurons. Specific genotypes are: per^{+}, $Pdf>DBT^{L}$ for "Slow PDF+, Norm PDF-", per^{01}, $Pdf>PER+DBT^{L}$ for "Slow PDF+, per^{01} PDF-", and per^{01}, $Pdf>PER$ for "per^{+} PDF+, per^{01} PDF-". (**B** to **D**) Representative actograms (upper panels) and χ-square periodograms (lower panels) of individual flies with different compositions of PDF positive and negative neurons under constant darkness. Genotypes are as follows: (B) per^{+}, $Pdf>DBT^{L}$, (C) per^{01}, $Pdf>PER+DBT^{L}$, and (D) per^{01}, $Pdf>PER$. (D) is a repeat of Fig. 4.2E.

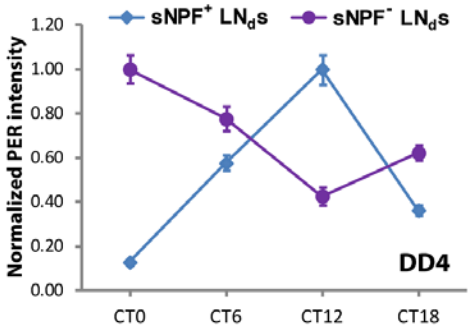

Figure 4.S10. Comparison of PER expression rhythms in sNPF$^+$ and sNPF$^-$ LN$_d$s from flies with slow-running PDF positive neurons (*Pdf>DBT^L*) on DD4.
PER accumulation is delayed in the sNPF$^+$ LN$_d$s, consistent with coupling to the PDF positive neurons (Fig. 4.4, B and E). The numbers of neurons and brains examined for sNPF$^+$ LN$_d$s were CT0 (34, 13), CT6 (38, 12), CT12 (36, 11), CT18 (42, 11), and for sNPF$^-$ LN$_d$s CT0 (69, 13), CT6 (76, 12), CT12 (73, 11), CT18 (82, 11).

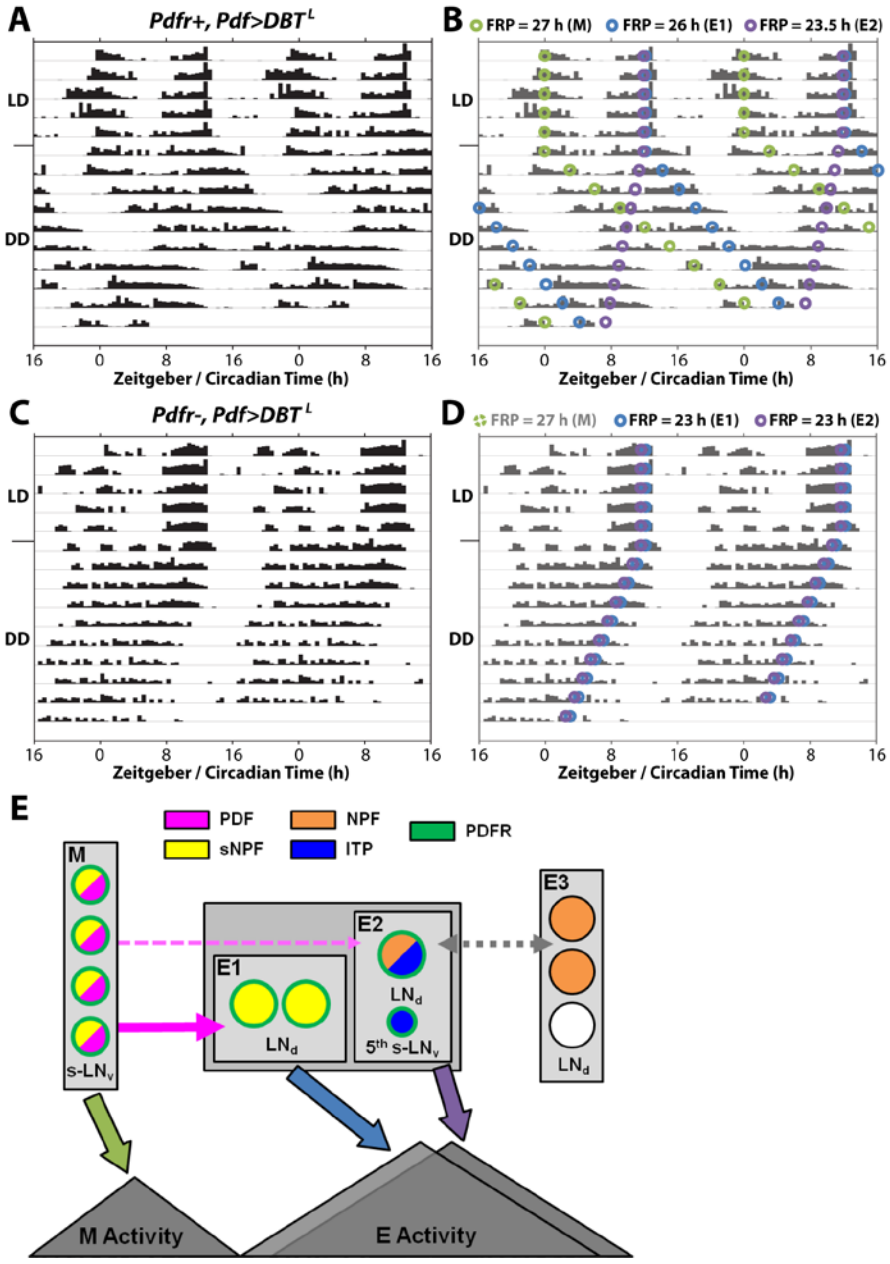

Figure 4.S11. A multi-oscillator interpretation of free-running activity rhythms.
(**A**) A representative actogram of a single *Pdfr*$^{+}$,*Pdf>DBT*^{L} fly. (**B**) A model for the complex rhythm displayed by the individual in (A) based on our PER immunostaining results (Fig. 4.4). In light: dark (LD) conditions, different oscillators are entrained by light: dark cycles and the animal displays a strong and coherent bimodal 24-hour rhythm. Under constant darkness (DD), the slow PDF positive oscillators, the morning (M) oscillators, free-run with an intrinsic free running period (FRP) of ~27 hours (green circles) whereas the PDF negative oscillators, the evening (E) oscillators, split into two components: The E1 oscillators are entrained by the M oscillators and run at a pace slower than their intrinsic clock speed (blue circles, drawn here with

a FRP of ~26 hours). The E2 oscillators are not strongly coupled to the M oscillators and free-run at a pace that is close to their intrinsic clock speed (purple circles, depicted with a FRP of ~23.5 hours). (**C**) A representative actogram of a rhythmic *Pdfr*$^{-}$, *Pdf>DBT*^{L} fly. (**D**) A model for the activity rhythm of the individual in (C). In the absence of PDFR signaling, the E1 and E2 oscillators free-run with their intrinsic clock speeds and remain synchronized in DD (blue and purple circles). The M oscillators free-run with their intrinsic FRP of ~27 hours in DD, but have no apparent influence on behavioral rhythms in the absence of PDFR signaling (dashed green circle above the actogram). (**E**) A summary model for the lateral clock neuron network and its control of activity rhythms. The PDF negative evening (E) oscillator neurons are divided into three functional units. The E3 oscillators (three PDFR^{-} LN$_d$s) are unresponsive to M oscillator outputs, while the E1 (two sNPF^{+}/PDFR^{+} LN$_d$s) and E2 (ITP^{+}/PDFR^{+} LN$_d$ and 5th s-LN$_v$) oscillators both respond to PDF with cAMP increases (magenta arrows). The E1 oscillators are strongly coupled to the M oscillators by PDF signaling (solid magenta arrow), while the E2 oscillators are more strongly coupled with the E3 oscillators (dashed gray arrow). Arrows beneath the oscillators represent output pathways for locomotor activity control.

Table 4.S1. Locomotor activity rhythms of control flies, and flies overexpressing different forms of *DBT* or *SGG* in all the clock neurons in constant darkness.

Genotype	Number of flies	% Rhythmic	% Multi-periodicity*	Period ± SEM (h)	Rhythmic Power ± SEM
w;Clk-GAL4/+;UAS-DBT(S)/+	30	100	3.3	18.5 ± 0.3	57.7 ± 7.9
w;Clk-GAL4/+;UAS-SGG(CA)/+	32	81.2	0	20.0 ± 0.3	30.6 ± 5.7
w;Clk-GAL4/UAS-SGG(WT);	19	94.7	5.6	21.3 ± 0.6	40.9 ± 7.4
w;Clk-GAL4/+;UAS-SGG(Hypo)/+	32	100	0	22.1 ± 0.1	71.0 ± 5.8
w;Clk-GAL4/+;UAS-SGG(KD)/+	29	89.7	0	23.7 ± 0.1	48.5 ± 6.7
w;Clk-GAL4/+;UAS-DBT(WT)/+	21	100	0	24.7 ± 0.1	97.2 ± 7.1
w;Clk-GAL4/+;UAS-DBT(L)/+	32	100	0	26.8 ± 0.1	77.3 ± 7.6
w;Clk-GAL4/+;	47	95.7	6.7	23.8 ± 0.1	45.0 ± 4.9
w;;UAS-DBT(S)/+	16	93.8	0	23.5 ± 0	80.3 ± 11.1
w;;UAS-SGG(CA)/+	16	93.8	13.3	23.8 ± 0.1	50.9 ± 7.4
w;UAS-SGG(WT)/+;	16	100	0	23.8 ± 0.1	61.3 ± 7.6
w;;UAS-SGG(Hypo)/+	15	86.7	0	23.5 ± 0.1	39.1 ± 7.9
w;;UAS-SGG(KD)/+	15	100	13.3	23.4 ± 0.3	32.4 ± 5.7
w;;UAS-DBT(WT)/+	13	100	7.7	23.7 ± 0.1	89.7 ± 11.9
w;;UAS-DBT(L)/+	16	100	6.3	23.7 ± 0.1	102.2 ± 7.4

* % Multi-periodicity indicates the percentage of rhythmic individuals that display more than one significant periodicity.

Table 4.S2. Locomotor activity rhythms of control flies, and flies overexpressing different forms of *DBT* or *SGG* only in the PDF positive clock neurons in constant darkness.

Genotype	Number of flies	% Rhythmic	% Multi-periodicity*	Period ± SEM (h)	Rhythmic Power ± SEM
w;Pdf-GAL4/+;UAS-DBT(S)/+	59	59.3	20.0	21.0 ± 0.7	9.0 ± 1.6
w;Pdf-GAL4/+;UAS-SGG(CA)/+	49	63.3	35.5	21.7 ± 0.6	11.1 ± 2.2
w;Pdf-GAL4/UAS-SGG(WT);	39	48.7	21.1	21.6 ± 0.5	5.3 ± 1.3
w;Pdf-GAL4/+;UAS-SGG(Hypo)/+	36	83.3	0	23.1 ± 0.2	46.6 ± 7.8
w;Pdf-GAL4/+;UAS-SGG(KD)/+	39	84.6	0	24.4 ± 0.1	48.1 ± 6.6
w;Pdf-GAL4/+;UAS-DBT(WT)/+	32	90.6	3.4	25.0 ± 0.1	57.5 ± 7.3
w;Pdf-GAL4/+;UAS-DBT(L)/+	75	89.3	25.4	26.7 ± 0.2	25.4 ± 2.4
w;Pdf-GAL4/+;	16	100	6.3	24.1 ± 0.1	76.2 ± 8.0

* % Multi-periodicity indicates the percentage of rhythmic individuals that display more than one significant periodicity.

Table 4.S3. Locomotor activity rhythms of control flies, and *Pdfr*$^{-}$ mutant flies overexpressing different forms of *DBT* or *SGG* only in the PDF positive neurons in constant darkness.

Genotype	Number of flies	% Rhythmic	% Multi-periodicity*	Period ± SEM (h)	Rhythmic Power ± SEM
Pdfr-;Pdf-GAL4/+;UAS-DBT(S)/+	61	60.7	10.8	23.3 ± 0.5	12.8 ± 2.3
Pdfr-;Pdf-GAL4/+;UAS-SGG(CA)/+	33	72.7	8.3	22.4 ± 0.5	14.1 ± 3.4
Pdfr-;Pdf-GAL4/UAS-SGG(WT);	36	58.3	9.5	23.1 ± 0.5	7.8 ± 2.5
Pdfr-;Pdf-GAL4/+;UAS-SGG(Hypo)/+	46	60.9	14.3	22.6 ± 0.1	8.5 ± 1.7
Pdfr-;Pdf-GAL4/+;UAS-SGG(KD)/+	42	52.4	9.1	23.5 ± 0.4	17.7 ± 4.1
Pdfr-;Pdf-GAL4/+;UAS-DBT(WT)/+	46	56.5	11.5	22.9 ± 0.6	7.7 ± 1.7
Pdfr-;Pdf-GAL4/+;UAS-DBT(L)/+	75	70.7	9.4	22.6 ± 0.2	14.3 ± 2.2
Pdfr-;Pdf-GAL4/+;	32	43.8	0	22.8 ± 0.8	5.5 ± 1.6
Pdfr-;;	46	43.5	20.0	23.1 ± 0.4	7.1 ± 1.8

* % Multi-periodicity indicates the percentage of rhythmic individuals that display more than one significant periodicity.

Table 4.S4. Locomotor activity rhythms of control flies, and flies overexpressing different forms of *DBT* or *SGG* only in the PDF negative clock neurons in constant darkness.

Genotype	Number of flies	% Rhythmic	% Multi-periodicity*	Period ± SEM (h)	Rhythmic Power ± SEM
w;Clk-GAL4,Pdf-GAL80/+;UAS-DBT(S)/+	41	80.5	12.1	23.8 ± 0.4	30.9 ± 5.0
w;Clk-GAL4,Pdf-GAL80/+;UAS-SGG(Hypo)/+	46	95.7	2.3	23.6 ± 0.1	70.0 ± 6.9
w;Clk-GAL4,Pdf-GAL80/+;UAS-DBT(L)/+	58	67.2	12.8	24.5 ± 0.2	16.0 ± 2.7
w;Clk-GAL4,Pdf-GAL80/+;	31	87.1	7.4	23.6 ± 0.1	47.0 ± 7.3
Pdfr-;Clk-GAL4,Pdf-GAL80/+;UAS-DBT(S)/+	65	49.2	12.5	19.1 ± 0.5	10.7 ± 2.7
Pdfr-;Clk-GAL4,Pdf-GAL80/+;UAS-SGG(Hypo)/+	59	42.4	12.0	21.1 ±0.4	9.0 ± 2.2
Pdfr-;Clk-GAL4,Pdf-GAL80/+;UAS-DBT(L)/+	63	55.6	20.0	25.5 ± 0.6	8.5 ± 2.1
Pdfr-;Clk-GAL4,Pdf-GAL80/+;	32	21.9	28.6	23.6 ± 1.5	2.7 ± 1.2

* % Multi-periodicity indicates the percentage of rhythmic individuals that display more than one significant periodicity.

Table 4.S5. Locomotor activity rhythms of control flies, and flies with *period*-rescued PDF positive neurons with or without *DBT* co-overexpression in constant darkness.

Genotype	Number of flies	% Rhythmic	% Multi-periodicity*	Period ± SEM (h)	Rhythmic Power ± SEM
per(01),w;;UAS-PER/+	44	22.7	0	21.4 ± 2.0	1.5 ± 0.5
per(01),w;Pdf-GAL4/+;UAS-PER/+	122	77.9	9.5	26.1 ± 0.2	24.8 ± 2.6
per(01),w;Pdf-GAL4/+;UAS-PER/UAS-DBT(S)	57	77.2	6.8	17.8 ± 0.4	31.3 ± 5.2
per(01),w;Pdf-GAL4/+;UAS-PER/UAS-DBT(L)	44	88.6	15.4	26.5 ± 0.5	14.0 ± 1.9

* % Multi-periodicity indicates the percentage of rhythmic individuals that display more than one significant periodicity.

Table 4.S6. The numbers of neurons and brains examined for PER protein rhythms in Fig. 4.4, D to F.

Genotype	Neuronal class	Time-points on DD4*			
		CT0	CT6	CT12	CT18
Pdfr^{+},*UAS-DBT(L)*	LN_d	152, 14	121, 11	79, 11	141, 12
	5^{th} s-LN_v	25, 13	20, 11	10, 8	23, 12
	s-LN_v	94, 14	80, 11	80, 11	88, 12
Pdfr^{+},*Pdf>DBT(L)*	LN_d (shifted)	44, 13	45, 13	46, 12	26, 11
	LN_d (unshifted)	85, 13	86, 13	85, 12	59, 11
	5^{th} s-LN_v	24, 13	24, 13	12, 9	20, 11
	s-LN_v	89, 13	79, 13	80, 12	62, 11
Pdfr^{-},*Pdf>DBT(L)*	LN_d	105, 10	86, 10	87, 8	85, 8
	5^{th} s-LN_v	18, 10	8, 6	7, 6	12, 8
	s-LN_v	66, 10	63, 10	52, 8	46, 8

* The two numbers within each cell of the table indicate the number of neurons and the number of brains examined respectively.

Table 4.S7. The numbers of neurons and brains examined for PER immunostaining intensity in Fig. 4.4, I and J.

Genotype	Neuronal class	Time-points on DD4*	
		CT0	CT12
UAS-DBT(L)	$sNPF^+$ LN_ds	22, 9	14, 5
	$sNPF^-$ LN_ds	43, 9	28, 5
Pdf>DBT(L)	$sNPF^+$ LN_ds	12, 6	16, 5
	$sNPF^-$ LN_ds	22, 6	29, 5

* The two numbers within each cell of the table indicate the number of neurons and the number of brains examined respectively.

4.5 Acknowledgments

We thank J. L. Price, P. H. Taghert, M. Rosbash, F. Rouyer, N. R. Glossop, and the Bloomington *Drosophila* Stock Center for fly stocks; M. Rosbash for PER antisera, D. R. Nässel for sNPF antibody, the Developmental Studies Hybridoma Bank for PDF antibody, and we thank P. H. Taghert, M. Rosbash, E. D. Herzog, S. J. Aton, and J. Y. Kuwada for helpful comments on the manuscript. We thank M. Rosbash for communicating results before publication. This work was supported by NIH (NINDS) grants R00NS062953 and R01NS077933 to O. T. S.

4.6 References and Notes

1. W. Yu, P. E. Hardin, Circadian oscillators of Drosophila and mammals. *Journal of Cell Science* **119**, 4793 (December 1, 2006).
2. E. D. Herzog, Neurons and networks in daily rhythms. *Nat Rev Neurosci* **8**, 790 (2007).
3. A. C. Liu *et al.*, Intercellular Coupling Confers Robustness against Mutations in the SCN Circadian Clock Network. *Cell* **129**, 605 (2007).
4. S. Yamaguchi *et al.*, Synchronization of Cellular Clocks in the Suprachiasmatic Nucleus. *Science* **302**, 1408 (November 21, 2003).
5. M. J. Vansteensel, S. Michel, J. H. Meijer, Organization of cell and tissue circadian pacemakers: A comparison among species. *Brain Research Reviews* **58**, 18 (2008).
6. B. Grima, E. Chelot, R. Xia, F. Rouyer, Morning and evening peaks of activity rely on different clock neurons of the Drosophila brain. *Nature* **431**, 869 (2004).
7. D. Stoleru, Y. Peng, J. Agosto, M. Rosbash, Coupled oscillators control morning and evening locomotor behaviour of Drosophila. *Nature* **431**, 862 (2004).
8. D. Stoleru, Y. Peng, P. Nawathean, M. Rosbash, A resetting signal between Drosophila pacemakers synchronizes morning and evening activity. *Nature* **438**, 238 (2005).
9. S. Martinek, S. Inonog, A. S. Manoukian, M. W. Young, A Role for the Segment Polarity Gene shaggy/GSK-3 in the Drosophila Circadian Clock. *Cell* **105**, 769 (2001).
10. M. J. Muskus, F. Preuss, J.-Y. Fan, E. S. Bjes, J. L. Price, Drosophila DBT Lacking Protein Kinase Activity Produces Long-Period and Arrhythmic Circadian Behavioral and Molecular Rhythms. *Molecular and Cellular Biology* **27**, 8049 (December 1, 2007).

11. M. Picot, P. Cusumano, A. Klarsfeld, R. Ueda, F. Rouyer, Light Activates Output from Evening Neurons and Inhibits Output from Morning Neurons in the Drosophila Circadian Clock. *PLoS Biol* **5**, e315 (2007).

12. D. Stoleru *et al.*, The Drosophila Circadian Network Is a Seasonal Timer. *Cell* **129**, 207 (2007).

13. S. H. Im, P. H. Taghert, PDF receptor expression reveals direct interactions between circadian oscillators in Drosophila. *The Journal of Comparative Neurology* **518**, 1925 (2010).

14. S. H. Im, W. Li, P. H. Taghert, PDFR and CRY Signaling Converge in a Subset of Clock Neurons to Modulate the Amplitude and Phase of Circadian Behavior in Drosophila. *PLoS ONE* **6**, e18974 (2011).

15. O. T. Shafer *et al.*, Widespread Receptivity to Neuropeptide PDF throughout the Neuronal Circadian Clock Network of Drosophila Revealed by Real-Time Cyclic AMP Imaging. **58**, 223 (2008).

16. V. O. Nikolaev, M. Bünemann, L. Hein, A. Hannawacker, M. J. Lohse, Novel Single Chain cAMP Sensors for Receptor-induced Signal Propagation. *Journal of Biological Chemistry* **279**, 37215 (September 3, 2004).

17. T. Yoshii, T. Todo, C. Wülbeck, R. Stanewsky, C. Helfrich-Förster, Cryptochrome is present in the compound eyes and a subset of Drosophila's clock neurons. *The Journal of Comparative Neurology* **508**, 952 (2008).

18. N. J. De Souza, A. N. Dohadwalla, Ü. Reden, Forskolin: A labdane diterpenoid with antihypertensive, positive inotropic, platelet aggregation inhibitory, and adenylate cyclase activating properties. *Medicinal Research Reviews* **3**, 201 (1983).

19. H. A. D. Johard *et al.*, Peptidergic clock neurons in Drosophila: Ion transport peptide and short neuropeptide F in subsets of dorsal and ventral lateral neurons. *The Journal of Comparative Neurology* **516**, 59 (2009).

20. J. O. Gummadova, G. A. Coutts, N. R. J. Glossop, Analysis of the Drosophila Clock Promoter Reveals Heterogeneity in Expression between Subgroups of Central Oscillator Cells and Identifies a Novel Enhancer Region. *Journal of Biological Rhythms* **24**, 353 (October 1, 2009).

21. T. Siegmund, G. Korge, Innervation of the ring gland of Drosophila melanogaster. *The Journal of Comparative Neurology* **431**, 481 (2001).

22. S. C. P. Renn, J. H. Park, M. Rosbash, J. C. Hall, P. H. Taghert, A pdf Neuropeptide Gene Mutation and Ablation of PDF Neurons Each Cause Severe Abnormalities of Behavioral Circadian Rhythms in Drosophila. *Cell* **99**, 791 (1999).

23. E. Blanchardon *et al.*, Defining the role of Drosophila lateral neurons in the control of circadian rhythms in motor activity and eclosion by targeted genetic ablation and PERIOD protein overexpression. *European Journal of Neuroscience* **13**, 871 (2001).

24. R. J. Konopka, S. Benzer, Clock Mutants of Drosophila melanogaster. *Proceedings of the National Academy of Sciences of the United States of America* **68**, 2112 (1971).

25. S. Hyun *et al.*, Drosophila GPCR Han Is a Receptor for the Circadian Clock Neuropeptide PDF. **48**, 267 (2005).

26. M. Bourouis, Targeted increase in shaggy activity levels blocks wingless signaling. *genesis* **34**, 99 (2002).

27. L. Y. Jan, Y. N. Jan, Properties of the larval neuromuscular junction in Drosophila melanogaster. *The Journal of Physiology* **262**, 189 (October 1, 1976).

28. Z. Yao, A. M. Macara, K. R. Lelito, T. Minosyan, O. T. Shafer, Analysis of Functional Neuronal Connectivity in the Drosophila Brain. *Journal of Neurophysiology*, (April 25, 2012).

29. C. Pfeiffenberger, B. C. Lear, K. P. Keegan, R. Allada, Locomotor Activity Level Monitoring Using the Drosophila Activity Monitoring (DAM) System. *Cold Spring Harbor Protocols* **2010**, pdb.prot5518 (November 1, 2010).

30. C. Pfeiffenberger, B. C. Lear, K. P. Keegan, R. Allada, Processing Circadian Data Collected from the Drosophila Activity Monitoring (DAM) System. *Cold Spring Harbor Protocols* **2010**, pdb.prot5519 (November 1, 2010).

31. P. G. Sokolove, W. N. Bushell, The chi square periodogram: Its utility for analysis of circadian rhythms. *Journal of Theoretical Biology* **72**, 131 (1978).

32. O. T. Shafer, C. Helfrich-Förster, S. C. P. Renn, P. H. Taghert, Reevaluation of Drosophila melanogaster's neuronal circadian pacemakers reveals new neuronal classes. *The Journal of Comparative Neurology* **498**, 180 (2006).

33. X. Liu, L. Lorenz, Q. N. Yu, J. C. Hall, M. Rosbash, Spatial and temporal expression of the period gene in Drosophila melanogaster. *Genes & Development* **2**, 228 (February 1, 1988).

34. H. A. D. Johard *et al.*, Intrinsic neurons of Drosophila mushroom bodies express short neuropeptide F: Relations to extrinsic neurons expressing different neurotransmitters. *The Journal of Comparative Neurology* **507**, 1479 (2008).

35. O. T. Shafer, M. Rosbash, J. W. Truman, Sequential Nuclear Accumulation of the Clock Proteins Period and Timeless in the Pacemaker Neurons of Drosophila melanogaster. *J. Neurosci.* **22**, 5946 (July 15, 2002).

36. L. Zhang *et al.*, DN1p Circadian Neurons Coordinate Acute Light and PDF Inputs to Produce Robust Daily Behavior in Drosophila. *Current Biology* **20**, 591 (2010).

CHAPTER 5. The *Drosophila* circadian clock neuron network features diverse coupling modes and requires network-wide coherence for robust free-running rhythms[4]

5.1 Abstract

In animals, neurons containing molecular clocks communicate through interneuronal connections to form a coherent and robust timekeeping network that orchestrates daily rhythms of activity and sleep. Here, we investigate how the molecular clocks of neurons are coupled and how coordination between clock neuron groups contributes to daily activity rhythms under both light/dark cycles (LD) and constant conditions in the brain of the fly *Drosophila melanogaster*. Upon altering the molecular clock speed specifically in the ventral lateral neurons (LN_vs), we find that the molecular rhythms of the posterior dorsal neurons 1 ($DN1_p$s) are tightly phase-coupled to those of the LN_vs, while the molecular oscillations of two other classes of clock neurons, the dorsal lateral neurons (LN_ds) and the fifth small LN_v (5^{th} s-LN_v), are relatively independent of the LN_vs. Despite the fact that the LN_vs, LN_ds, and 5^{th} s-LN_v collectively determine the timing of daily activity bouts under LD, they are not sufficient to coherently produce activity rhythms under constant conditions when their clocks run at different speeds than the remaining components of the clock network. We find that coordinated free-running rhythms require clock synchrony not only in the LN classes, but also in the $DN1_p$s. These results uncover new and unexpected patterns of coupling in the clock neuron network and reveal that robust free-

[4] A manuscript comprising this chapter is in preparation for publication, with authors listed as Zepeng Yao, Amelia J. Bennett, Jenna L. Clem, and Orie T. Shafer.

running behavioral rhythms require a coherence of molecular oscillations in an unexpectedly large proportion of the clock neuron network.

5.2 Introduction

Most organisms have a circadian clock that orchestrates daily rhythms of physiology and behavior. In animals, the master clock consists of a network of so-called “clock neurons”, each containing a molecular clock that generates molecular oscillations with periods of approximately 24 hours (1). Through interneuronal communication, clock neurons coordinate their molecular clocks to form a coherent clock network that is capable of producing robust circadian timekeeping in various outputs (2) in the absence of environmental time cues. How this coordination occurs is not well understood.

Drosophila melanogaster has proved a valuable model system in which to investigate clock neuron communication and coordination. The *Drosophila* clock network consists of approximately 150 clock neurons, several orders of magnitude fewer than those of mammals, yet it shares both anatomical and functional similarities with the mammalian clock network (3, 4). Studies of the *Drosophila* clock network suggest that it is organized into multiple oscillatory units that are differentially coupled to one another (5, 6). Three divisions of this clock neuron network have been studied most extensively: (i) the ventral lateral neurons (LN_vs), consisting of four pairs of large LN_vs (l-LN_vs) and four pairs of small LN_vs (s-LN_vs), both of which express the neuropeptide pigment-dispersing factor (PDF); (ii) six pairs of dorsal lateral neurons (LN_ds) and one pair of PDF-negative s-LN_vs (also called 5^{th} s-LN_vs); (iii) the posterior dorsal neurons 1 ($DN1_p$s), many of which express a deep-brain blue light photoreceptor Cryptochrome (CRY) (7).

These three groups of neurons are thought to cooperate to produce two daily peaks of activity near dawn and dusk, the so-called morning and evening peaks of activity. The LN_vs are important for the morning peak of activity in anticipation of lights-on, and are therefore considered as a group to be the "Morning Oscillator" (8, 9). The LN_vs are also critical pacemakers that help maintain free-running rhythms in constant environments (10) and the PDF they express is important for inter-clock-neuron coordination (11, 12). The LN_ds and 5^{th} s-LN_v are important for the evening peak of activity in anticipation of lights-off, and as a group are considered the "Evening Oscillator" (8). The CRY-expressing (CRY^+) $DN1_p$s can promote morning or evening activity depending on the specific experimental conditions, and they likely lie downstream of the LN_vs and mediate circadian outputs (13-16). Much of the evidence for assignment of these timekeeping functions is based on genetic rescue experiments that restored molecular clock function in subsets of clock neurons in an otherwise clock-less mutant background (e.g., (8, 13)).

Genetically altering molecular clock speed in clock neurons of interest offers another powerful approach to assess the influence of a specific group of neurons in the context of an otherwise functional clock network. This approach has revealed important features of clock network organization and coordination (5, 17, 18). In addition, the introduction of clock speed discrepancies between neuronal subsets offers a unique chance to experimentally study if and how molecular clocks are coupled between different classes of clock neurons. Here, by genetically altering the molecular clock speed in the LN_vs, LN_ds and 5^{th} s-LN_v, and CRY^+ $DN1_p$s, alone or in combination with other neuronal groups, we investigate the coupling of their molecular clocks, and re-examine their contributions to daily activity peaks and free-running activity rhythms. Our results reveal that clock neuron groups display diverse modes of molecular

clock coupling and that coordinated free-running activity rhythms require coherence of molecular oscillations across an unexpectedly large proportion of the clock network.

5.3 Results

5.3.1 Neuronal clock speed determines the phases of morning and evening peaks in light:dark cycles.

In *Drosophila*, the molecular clock can be cell-autonomously sped-up and slowed-down through the overexpression of two mutant forms of the *Doubletime (DBT)* kinase, DBT^{Short} (DBT^{S}) and DBT^{Long} (DBT^{L}), respectively (19). DBT^{S} overexpression shortens the period of the molecular clock by 5 to 6 hours, while DBT^{L} overexpression lengthens the period of the molecular clock by about 3 hours (19). We overexpressed DBT^{S} and DBT^{L} in all or most clock containing cells using the *Clk(856)-GAL4* driver (Table 5.S1 and Fig. 5.1) to assess the extent to which these kinase manipulations are able to affect the timing of morning and evening peaks of activity under a 12hr:12hr light:dark cycle (LD). DBT^{S} overexpression driven by *Clk(856)-GAL4* advanced the morning peak of activity under LD by about 1.5 hours, and advanced the evening peak of activity by about 2 hours (Fig. 5.1A-B). The overexpression of DBT^{L} with *Clk(856)-GAL4* delayed the evening peak by about an hour, but had no significant effect on the phase of the morning peak (Fig. 5.1A-B). Molecular clocks are expressed not only in the central nervous system, but also in peripheral tissues (reviewed by (20)). When we overexpressed DBT^{S} and DBT^{L} exclusively in the nervous system using the pan-neuronal driver *neuronal synaptobrevin-GAL4* (*nSyb-GAL4*) (Table 5.S1), we observed similar changes in the timing of morning and evening peaks (Fig. 5.1C-D), consistent with the notion that neuronal clocks set the phase of daily activity peaks under LD. We note here that the overexpression of DBT^{L} failed to

measurably delay the morning peak of activity, even when uniformly and strongly expressed throughout the clock neuron network, indicating that a three-hour increase in the period of the molecular clock is not sufficient to delay the morning peak under these LD conditions.

5.3.2 The LN_vs can delay but not advance the phase of evening activity under LD.

We next overexpressed DBT^S and DBT^L specifically in the LN_vs (using *Pdf-GAL4*), and in the LN_ds and 5^{th} s-LN_v (using a combination of *Mai179-GAL4* and *Pdf-GAL80* elements; see Table 5.S1 for details) to evaluate their influence on the phase of activity peaks under LD. Consistent with the previous designation of the LN_ds and 5^{th} s-LN_v as the evening oscillator (8), speeding-up and slowing-down these neurons significantly advanced and delayed the phase of the evening activity peak, respectively, but had no significant effects on the phase of the morning activity peak (Fig. 5.2A-B). Speeding-up the LN_vs advanced the morning peak without affecting the phase of the evening peak (Fig. 5.2C-D), consistent with the previous designation of these neurons as the morning oscillator (8). However, quite unexpectedly, when the LN_v clocks were slowed-down, the evening activity peak was significantly delayed while the phase of the morning peak was unaffected (Fig. 5.2C-D). This result is not predicted by the morning/evening dual-oscillator model of the fly's clock neuron network (8, 9, 17).

5.3.3 A subset of the LN_d clocks displays a delay-specific coupling to the LN_v clocks.

We previously found that the LN_vs can delay the clocks in a subset of the LN_ds through PDF signaling when LN_v clocks were slowed-down (5). This provides an explanation for the delaying of the evening activity peak by the LN_vs (Fig. 5.2C-D). If this is the case, our above finding that the LN_vs are not capable of advancing the evening activity peak (Fig. 5.2C-D) would suggest that the LN_vs are not capable of advancing the molecular clocks in any of the evening oscillator neurons. To test this prediction, we performed time-course immunostaining of the

PERIOD (PER) protein, an essential component of the molecular clock (reviewed by (21)), in the LN_ds and 5^{th} s-LN_v to see if their molecular oscillations were influenced by increasing the speed of the LN_v clocks. In brains in which only the LN_vs were specifically sped-up or slowed-down, the PER rhythms of LN_vs were clearly phase-shifted compared to un-manipulated controls after three or four days in DD (Fig. 5.3A-C). While a subset of LN_ds was phase-coupled to the LN_vs when the LN_v clocks were slowed-down through DBT^L overexpression ((5); replotted in Fig. 5.3B), none of the LN_ds nor the 5^{th} s-LN_v were phase-coupled to the LN_vs when the LN_v clocks were sped-up through DBT^S overexpression (Fig. 5.3C). The LN_ds and 5^{th} s-LN_v failed to couple with the LN_vs, even when the LN_v clocks were sped-up by only about 2 hours per cycle through the overexpression of a hypomorphic allele of the *Shaggy* kinase (5, 22) (in contrast to about 5 to 6 hours per cycle for DBT^S overexpression) (Fig. 5.3D-E). These results are consistent with our observation that the LN_vs were not capable of advancing the evening peak when their molecular clocks were sped-up (Fig. 5.2C-D). Taken together, a subset of LN_ds displays a delay-specific coupling to the LN_vs as their molecular clocks can be slowed-down but not sped-up by the LN_vs, while the clocks of remaining LN_ds and the 5^{th} s-LN_v are independent of LN_v molecular oscillations.

5.3.4 The molecular clocks of CRY-expressing $DN1_p$s are tightly phase-coupled to those of the LN_vs.

Cavanaugh and colleagues have proposed that the CRY^+ $DN1_p$s are postsynaptic to the LN_vs and mediate neuronal output from the clock neuron network to drive activity rhythms (16). We therefore wondered if and how the molecular clocks of the CRY^+ $DN1_p$s are functionally coupled to those of the LN_vs. When the LN_v clocks were sped-up or slowed-down, the PER rhythms of the CRY^+ $DN1_p$s were phase-shifted compared to un-manipulated controls. Indeed,

the molecular clocks of the CRY^+ $DN1_p$s closely followed those of the LN_vs, despite the molecular clocks in the $DN1_p$s not being genetically altered (Fig. 5.4A-C). Therefore, the LN_vs are capable of both advancing and delaying the molecular clocks in the CRY^+ $DN1_p$s under free-running conditions. In contrast to the neurons that make up the relatively independent evening oscillator, the CRY^+ $DN1_p$s are tightly phase-coupled to the LN_vs in their molecular oscillations.

Speeding-up the molecular clocks of the CRY^+ $DN1_p$s advanced the morning peak without affecting the evening peak phase, while slowing-down the molecular clocks in the CRY^+ $DN1_p$s delayed the evening peak without affecting the morning peak phase (Fig. 5.4D-E). These are strikingly similar to the effects of altering the clock speed of the LN_vs (compare Fig. 5.4D-E to Fig. 5.2C-D). Furthermore, altering the clock speed of the LN_vs and the CRY^+ $DN1_p$s simultaneously (using a combination of *Pdf-GAL4* and *Clk4.1M-GAL4* drivers, Table 5.S1) resulted in similar changes in the phase of activity peaks to those of altering the clock speed in either group alone, except that the morning peak was advanced to a greater extent for DBT^S overexpression when the two drivers were used simultaneously (compare Fig. 5.4F-G to Fig. 5.2C-D and Fig. 5.4D-E). These results are consistent with our finding that the molecular oscillations of the CRY^+ $DN1_p$s are tightly phase-coupled to those of the LN_vs.

5.3.5 The lateral neuron classes alone are sufficient for setting the timing of daily activity peaks under LD.

Given the relative independence of the LN_ds and 5^{th} s-LN_v (the evening oscillator) from the LN_vs (the morning oscillator), we asked if simultaneously altering the clock speeds of all of these lateral neuron groups would be sufficient to set the phases of the morning and evening peaks of activity under LD conditions. Overexpressing DBT^S and DBT^L using *Mai179-GAL4*, which is expressed in the 5^{th} s-LN_v and in subsets of the LN_vs and LN_ds (see Table 5.S1 for

details), resulted in a near-complete resetting of the phase of the evening peak, but not the morning peak of activity (compare Fig. 5.5A-B to Fig. 5.1). *DBT*^{S} and *DBT*^{L} overexpression driven by another lateral neuron driver, *DvPdf-GAL4* (Table 5.S1), was also not sufficient to fully reset the phases of activity peaks (Fig. 5.S1). However, when *DBT*^{S} and *DBT*^{L} were overexpressed in all of the lateral neurons, through the combined use of the *Mai179-GAL4* and *DvPdf-GAL4* drivers (see Table 5.S1 for details), the phases of both morning and evening activity peaks were completely reset (compare Fig. 5.5C-D to Fig. 5.1). Thus, the lateral clock neurons can fully control the timing of activity peaks under entrained conditions when their clock speeds are collectively altered.

5.3.6 Coherent free-running activity rhythms require molecular clock coherence between the lateral neurons and dorsal neurons.

We previously showed that the LN_vs are not the only component in the clock network that determines the pace of free-running activity rhythms under constant darkness, i.e., clock neurons other than the LN_vs also have control over such rhythms (5). Here, by genetically altering the clock speed in different combinations of clock neuron classes, we systemically investigate how they contribute to free-running rhythms in the context of an otherwise normally functional clock network. As previously reported, *DBT*^{S} overexpression in all or most clock containing cells using the *Clk(856)-GAL4* driver shortened the free-running period to about 18.5 hours, while *DBT*^{L} overexpression driven by *Clk(856)-GAL4* lengthened the free-running period to about 27 hours, and these “all clock” manipulations resulted in strong, well organized rhythms ((5); Fig. 5.6A and Table 5.S2). Overexpressing *DBT*^{S} and *DBT*^{L} exclusively in the nervous system using the pan-neuronal *nSyb-GAL4* driver also resulted in coherent changes in the free-

running period (Fig. 5.6B, Fig. 5.S2B, and Table 5.S2), supporting the notions that the speed of neuronal clocks determines the pace of free-running rhythms.

The LN_ds/5^{th} s-LN_v and the CRY^+ $DN1_p$s each have minimal influence on the free-running period of the activity rhythm (Fig. 5.6C-D and Table 5.S2), though altering the clock speed in the LN_ds/5^{th} s-LN_v resulted in an increased level of arrhythmicity and an increased incidence of internal desynchrony, wherein single flies displayed complex rhythms with more than one periods (Fig. 5.S3C and Table 5.S2). As reported previously, the LN_vs have a strong influence over free-running activity rhythms in that they are capable of imposing their intrinsic period to the overt activity rhythms (Fig. 5.6E and Table 5.S2), but this was accompanied by increased levels of arrhythmicity and internal desynchrony (Fig. 5.S3E and Table 5.S2;(5, 17, 23)). Altering the clock speed in both the LN_vs and the CRY^+ $DN1_p$s simultaneously resulted in nearly identical effects as those of altering the LN_v clock speed alone (Fig. 5.6F, Fig. 5.S3F, and Table 5.S2), consistent with our finding that the CRY^+ $DN1_p$ clocks are tightly phase-coupled to LN_v clocks.

Surprisingly, even though the lateral clock neurons can fully control the timing of activity peaks under LD when their clock speed is altered (Fig. 5.5C-D), they cannot coherently reset free-running period in DD when other clock cells remain un-manipulated (Fig. 5.6G-I, Fig. 5.S2G-I, Fig. 5.S3G-I, and Table 5.S2). This was the case even when the clock speed of all the lateral neurons was altered (Fig. 5.6I, Fig. 5.S2I, and Table 5.S2). Although our results indicate that the molecular clocks of the CRY^+ $DN1_p$s are tightly phase-coupled to those of the LN_vs (Fig. 5.4A-C), we reasoned that the resetting of the CRY^+ $DN1_p$ clocks by the LN_vs may not always be complete, especially when a large clock speed discrepancy exists between the $DN1_p$s and LN_vs. We therefore wondered if the free-running period would be more coherently reset when the clock

speed of the $DN1_p$s is simultaneously altered with the clocks of all of the lateral neurons. We drove DBT^S and DBT^L expression in the CRY^+ $DN1_p$s along with subsets of the lateral neurons using a combination of *Mai179-GAL4* and *Clk4.1M-GAL4* drivers, or a combination of *DvPdf-GAL4* and *Clk4.1M-GAL4* drivers (see Table 5.S1 for details of expression patterns of each driver). Free-running period was not fully reset in either case, especially when DBT^S expression was driven by these combinations of *GAL4s* (Fig. 5.6J-K, Fig. 5.S2J-K, Fig. 5.S3J-K, and Table 5.S2). Finally, we drove the expression of DBT^S and DBT^L in the CRY^+ $DN1_p$s and in all the lateral neurons using a combination of the *DvPdf-GAL4*, *Mai179-GAL4* and *Clk4.1M-GAL4* drivers (see Table 5.S1 for details). For these flies, the free-running period was almost completely reset (Fig. 5.6L, Fig. 5.S2L, Fig. 5.S4, and Table 5.S2). However, even these flies displayed an increased incidence of arrhythmicity and relatively weak free-running activity rhythms (Fig. 5.S3L and Table 5.S2). Thus, the CRY^+ $DN1_p$s and all the lateral neurons together represent a minimal subset of clock neurons that are capable of resetting free-running period of activity rhythms, albeit with weaker rhythms than those observed when all neuronal clocks are altered.

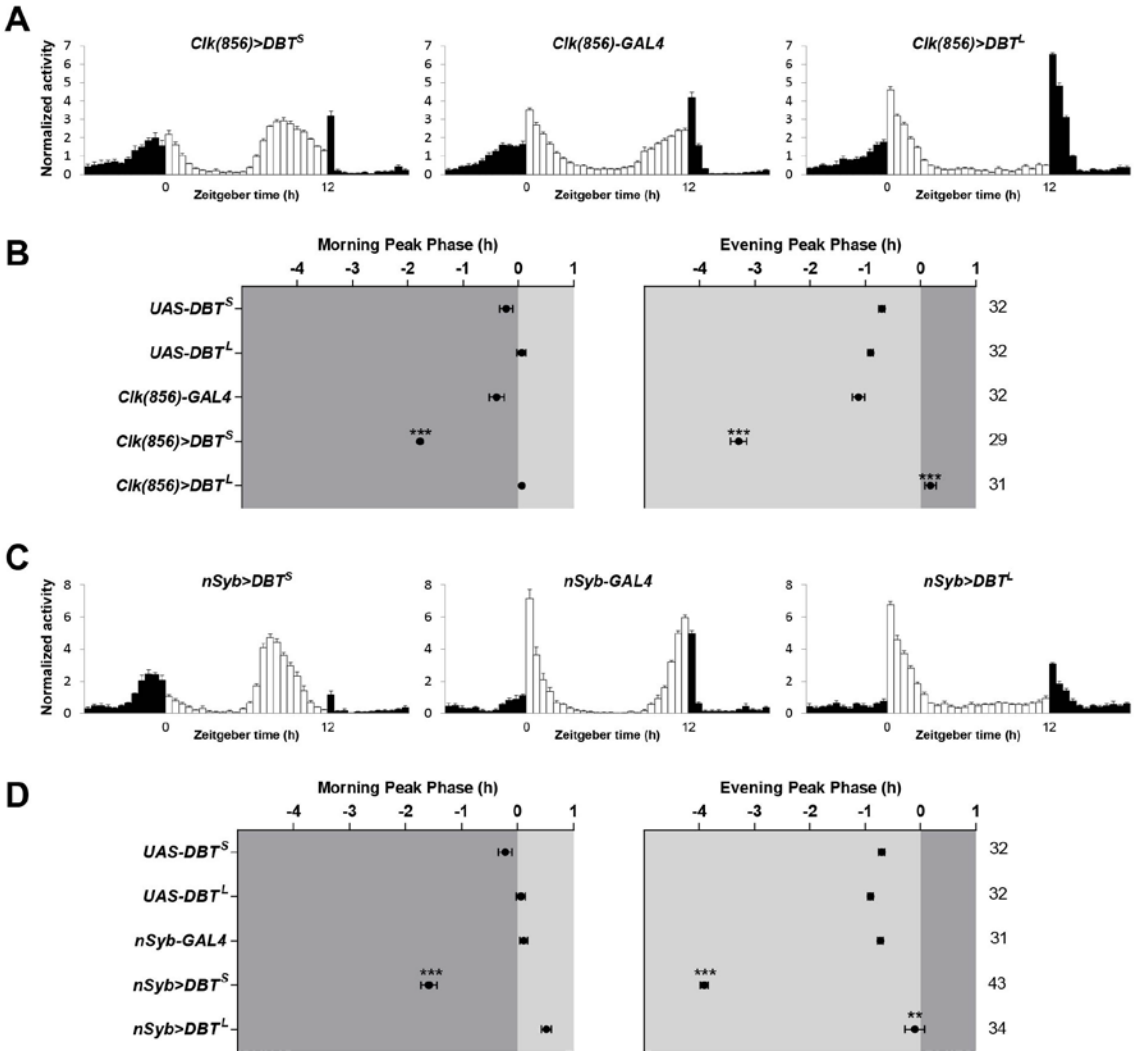

Figure 5.1. Neuronal clock speed determines the phase of activity peaks in LD cycles. (*A,C*) Population averaged activity profiles of DBT^S and DBT^L overexpressing flies and *GAL4* control flies for *Clk(856)-GAL4* (*A*) and *nSyb-GAL4* (*C*) in LD. *(B,D)* The average phases of morning and evening activity peaks in LD of the indicated genotypes. "0" marks the time of lights-on for the left panels and the time of lights-off for the right panels. Dark gray indicates darkness and light gray indicates light. The numbers of flies analyzed are indicated on the right of the phase panels. ** $P < 0.01$; *** $P < 0.001$. Details of statistical analysis are described in *Materials and Methods*. For all the plots, lines represent mean ± SEM (standard error of the mean).

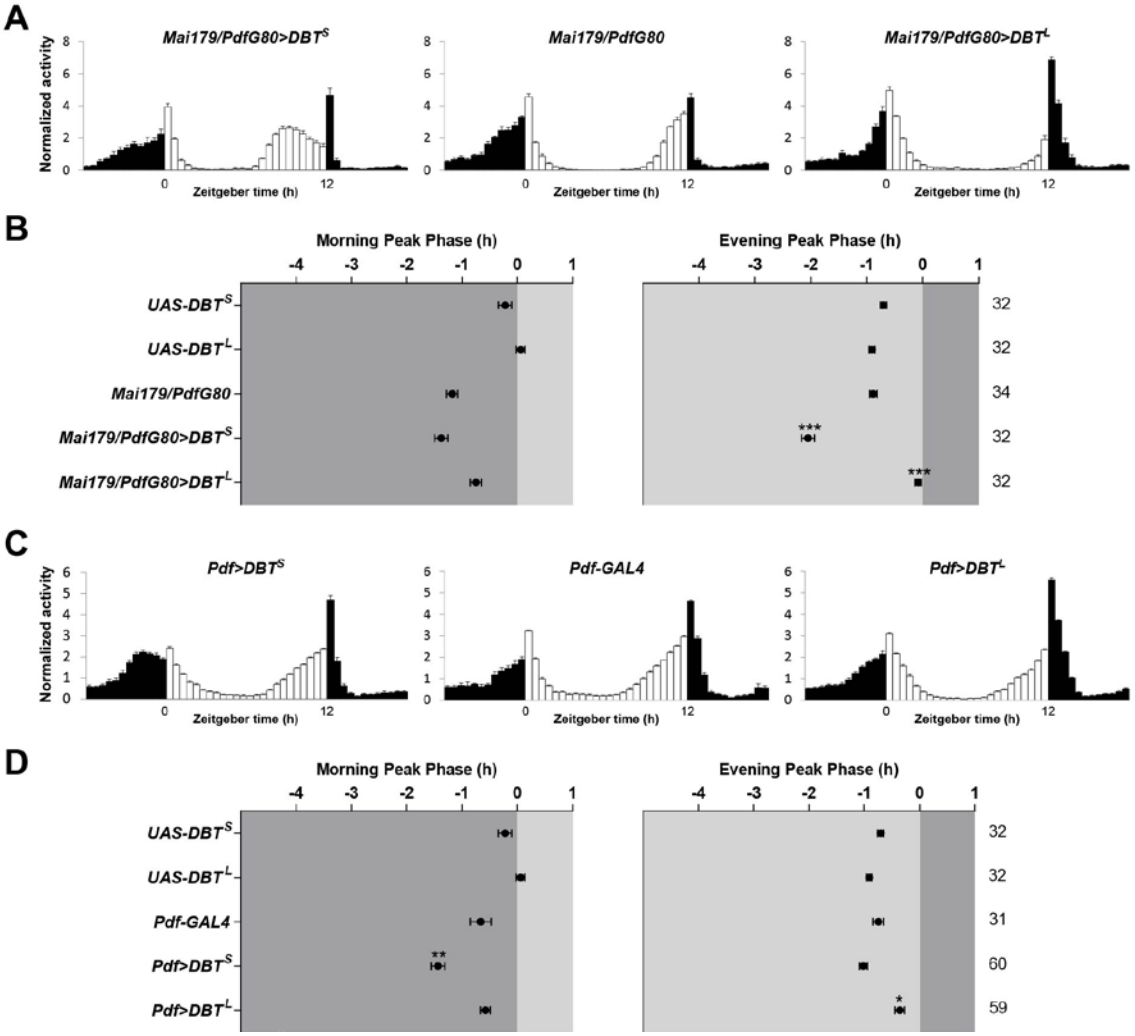

Figure 5.2. Differential influence on the phase of activity peaks in LD by the LN_d/5th s-LN_v clocks and the LN_v clocks.

(*A*,*C*) LD population averaged activity profiles of flies overexpressing *DBT^S* and *DBT^L* in the LN_ds and 5th s-LN_v (*A*), in the LN_vs (*C*), and their respective *GAL4* controls. *(B,D)* The average phases of morning and evening activity peaks under LD of the indicated genotypes. "0" marks the time of lights-on for the left panels and the time of lights-off for the right panels. Dark gray indicates darkness and light gray indicates light. The numbers of flies analyzed are indicated on the right. * $P < 0.05$; ** $P < 0.01$; *** $P < 0.001$. See *Materials and Methods* for details of the statistics. All the data are presented as mean ± SEM.

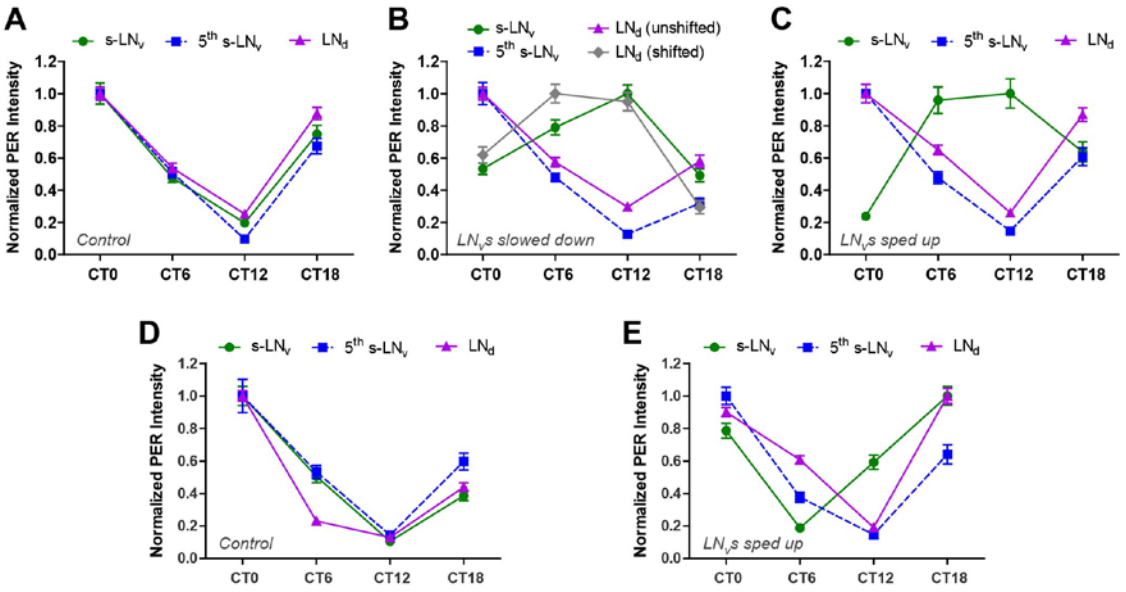

Figure 5.3. A subset of the LN_d clocks displays delay-specific coupling to the LN_v clocks. (*A*) Normalized PER immunostaining intensity of the s-LN_vs, the 5th s-LN_v, and the LN_ds of *UAS-DBT^S* control flies. Similar results were observed for these clock neuron classes in *UAS-DBT^L* control flies (5). (*B,C*) Normalized PER immunostaining intensity of different clock neuron classes of *Pdf>DBT^L* flies (*B*) and *Pdf>DBT^S* flies (*C*). For *Pdf>DBT^L* flies (*B*), the LN_ds were divided into two groups based on their phase differences in PER staining and quantified separately: those phase-coupled to the s-LN_vs were quantified as "LN_d (shifted)", and the others as "LN_d (unshifted)". Results in panel (*B)* are based on data first reported in (5). (*D,E*) Normalized PER immunostaining intensity of different clock neuron classes of *UAS>SGG^{Hypo}* control flies (*D*) and *Pdf>SGG^{Hypo}* flies (*E*). Note that for *UAS>SGG^{Hypo}* flies (*D*), the troughs of PER oscillations in s-LN_v, 5th s-LN_v, and LN_d are all at CT12, whereas for *Pdf>SGG^{Hypo}* flies (*E*), the trough of PER oscillation in s-LN_v is at CT6 while those of 5th s-LN_v and LN_d remain at CT12. All the data are presented as mean ± SEM.

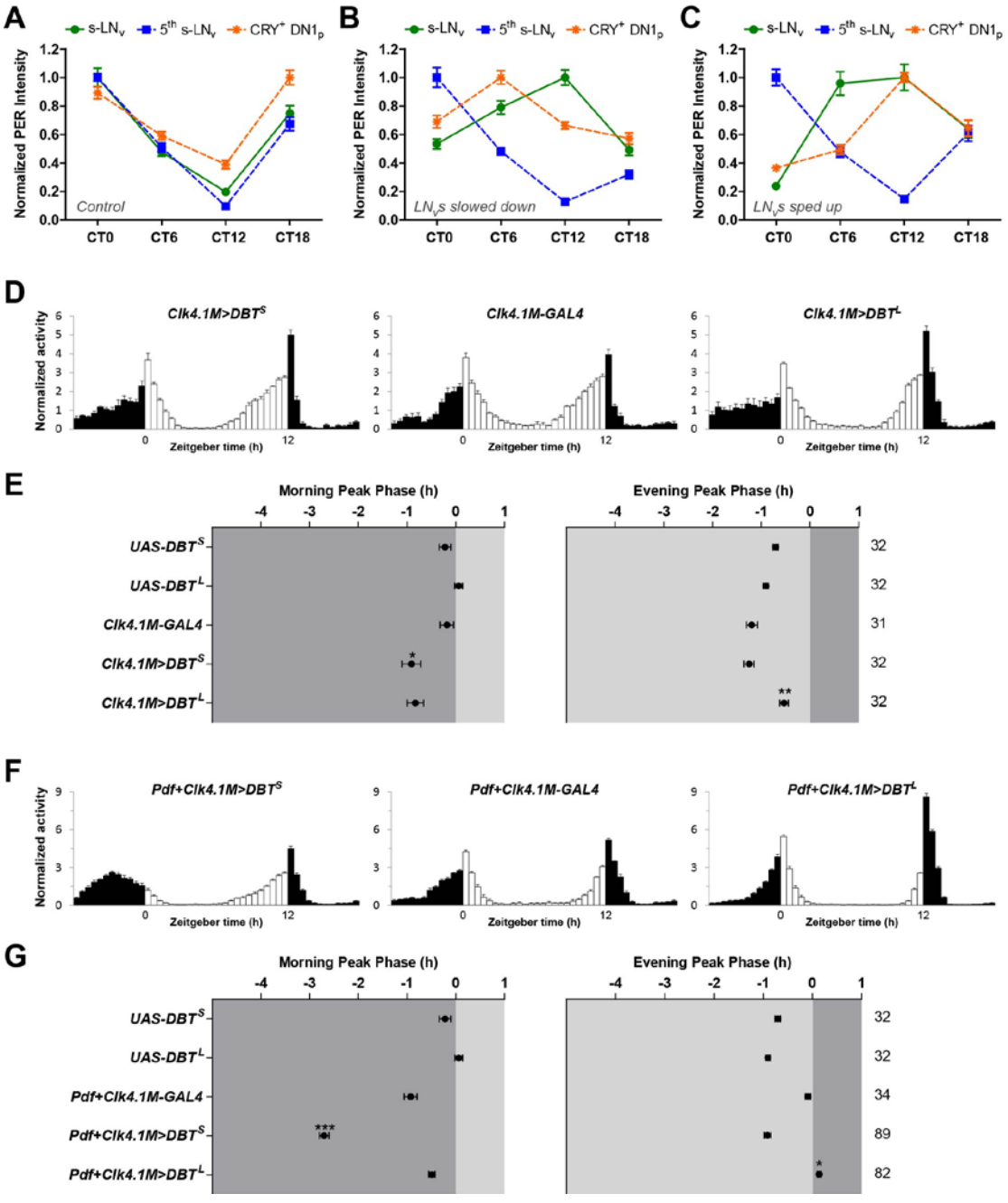

Figure 5.4. The CRY$^+$ DN1$_p$ clocks are tightly phased-coupled to the LN$_v$ clocks.
(*A-C*) Normalized PER immunostaining intensity of the CRY$^+$ DN1$_p$s of *Pdf-GAL4* flies (*A*), *Pdf>DBT^L* flies (*B*), and *Pdf>DBT^S* flies (*C*). The PER rhythms of the s-LN$_v$s and the 5th s-LN$_v$ are shown for comparison, which are the same data as those shown in **Fig. 5.3***A-C*. (*D*,*F*) LD population averaged activity profiles of flies overexpressing *DBT^S* and *DBT^L* in the CRY$^+$ DN1$_p$s only (*D*), in both the LN$_v$s and the CRY$^+$ DN1$_p$s (*F*), and their respective *GAL4* controls. (*E*,*G*) The average phases of morning and evening activity peaks in LD of the indicated genotypes. "0"

marks the time of lights-on for the left panels and the time of lights-off for the right panels. Dark gray indicates darkness and light gray indicates light. The numbers of flies analyzed are indicated on the right. * $P < 0.05$; ** $P < 0.01$; *** $P < 0.001$. See *Materials and Methods* for details of the statistics. All the data are presented as mean ± SEM.

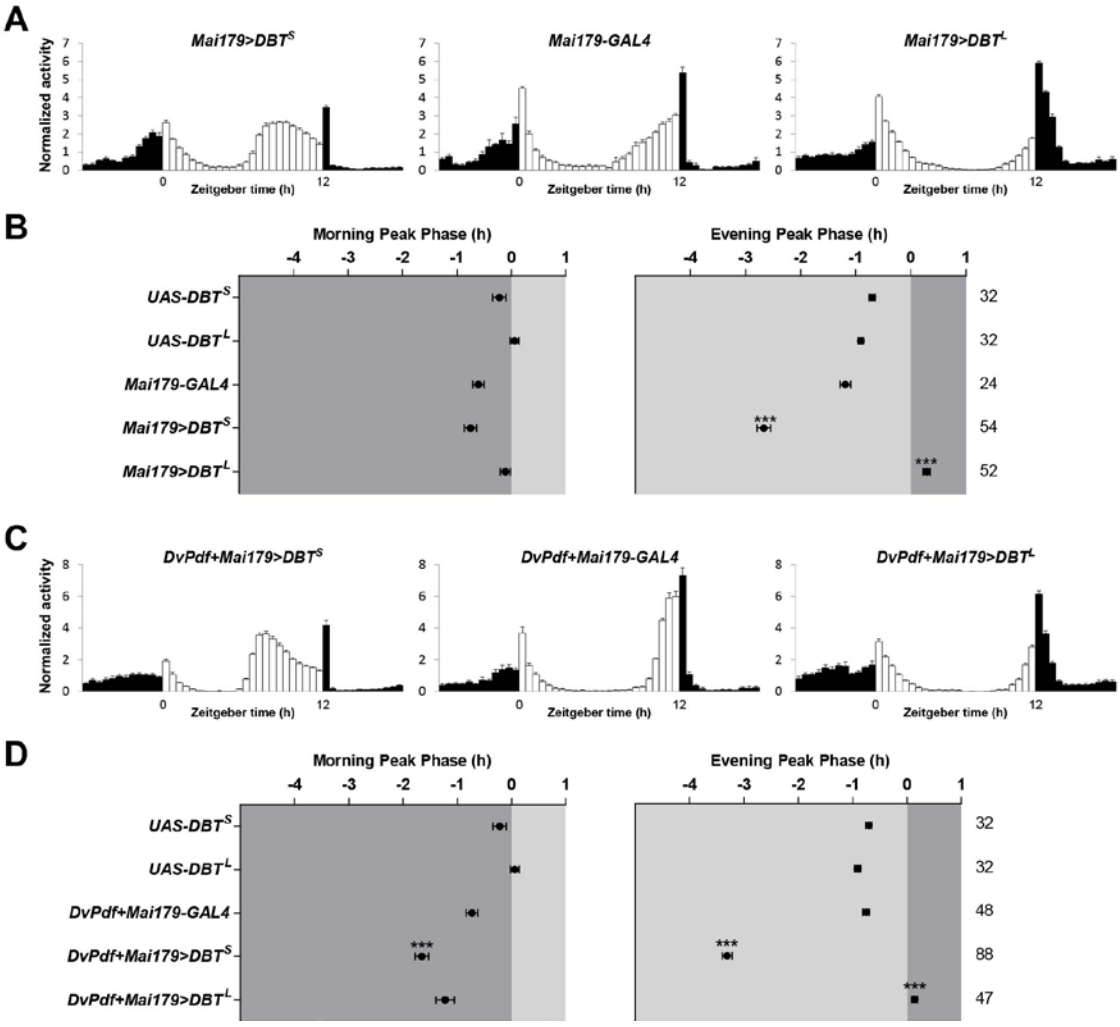

Figure 5.5. The lateral clock neurons are sufficient to set the timing of activity peaks under LD.

(*A*,*C*) LD population averaged activity profiles of control flies and flies overexpressing DBT^S and DBT^L in the lateral clock neurons driven by *Mai179-GAL4* (*A*) or a combination of *Mai179-GAL4* and *DvPdf-GAL4* (*C*). See *Table 5.S1* for details of the expression patterns of these *GAL4* drivers. (*B*,*D*) The average phases of morning and evening activity peaks in LD of the indicated genotypes. "0" marks the time of lights-on for the left panels and the time of lights-off for the right panels. Dark gray indicates darkness and light gray indicates light. The numbers of flies analyzed are indicated on the right. The phases of activity peaks are almost completely reset when DBT^S and DBT^L are expressed in all the lateral clock neurons using a combination of *Mai179-GAL4* and *DvPdf-GAL4* drivers (compare panel (*D*) to **Fig. 5.1***B*). *** $P < 0.001$. Details of statistical analysis are described in *Materials and Methods*. All the data are presented as mean ± SEM.

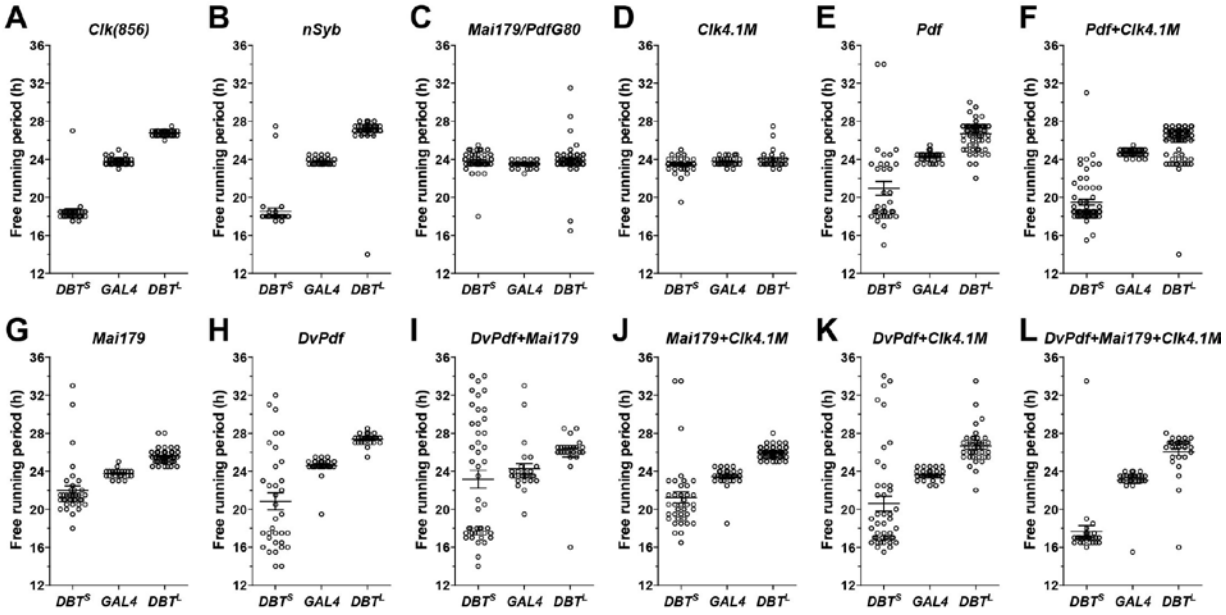

Figure 5.6. Coherent free-running activity rhythms require synchrony in all of the lateral clock neurons as well as the CRY$^+$ DN1$_p$s.
(*A-L*) Scatter plots of the predominant free-running periods of rhythmic *GAL4* control flies and flies overexpressing *DBT^S* and *DBT^L* under the indicated drivers. See *Table 5.S1* for details of the expression pattern of each *GAL4* driver. Results of panel (*A*) and panel (*E*) are based on data first reported in (5). For all the plots, lines represent mean ± SEM.

5.4 Discussion

5.4.1 Diverse modes of phase coupling between clock neuron classes

The genetic alteration of molecular clock speed in a subset of clock neurons results in a desynchronized clock network. This provides a means to address how clock neurons are phase-coupled with respect to their molecular timekeeping. Though such network desynchrony is artificially induced, animals do experience transient desynchrony of similar magnitudes under normal physiological conditions. For example, an abrupt shift of the LD cycle induces transient desynchrony in the rodent circadian center, the suprachiasmatic nuclei (SCN), wherein clock neurons of the ventral SCN adapt to the new light schedule rapidly while those of the dorsal SCN require several days to resynchronize (24, 25). We therefore think that our genetic manipulations are relevant to our understanding of the physiological basis of phase coupling within the clock network.

Here, by genetically speeding-up and slowing-down the molecular clocks in the LN_vs, neurons required for robust circadian timekeeping, we investigated if and how their molecular oscillations are coupled to those of the LN_ds, 5^{th} s-LN_v, and CRY^+ $DN1_p$s. Our results suggest that the molecular oscillations of the CRY^+ $DN1_p$s are tightly phase-coupled to those of the LN_vs – they can be sped-up as well as slowed-down by the LN_vs (Fig. 5.4A-C). This is consistent with a recent study suggesting that the CRY^+ $DN1_p$s are downstream targets of the LN_vs (16). In contrast, the molecular oscillations of the LN_ds and 5^{th} s-LN_v are relatively independent of LN_v molecular oscillations – only the two LN_ds that express short neuropeptide F (sNPF) can be delayed by the LN_vs, but none can be sped-up by the LN_vs (Fig. 5.3, (5)). We have previously established that the delaying of molecular clocks in the two sNPF-positive LN_ds by LN_vs is mediated by PDF signaling (5). The coupling of CRY^+ $DN1_p$s to the LN_vs is also likely to

depend on PDF signaling, as a subset of the former expresses PDF receptor and responds physiologically to synthetic PDF peptide (26-28). Given that PDF is required for molecular clock oscillations in the CRY^+ $DN1_p$s under constant conditions (29), we could not experimentally address this possibility. Our analysis reveals that various clock neuron classes are differentially coupled to the LN_vs. An extension of our experimental approach will make it possible to address coupling between other pairs of clock neuron groups, determine their modes of coupling (i.e., unidirectional or bidirectional), and uncover the mechanisms underlying differential coupling among the various clock neuron groups.

5.4.2 Control of the anticipatory morning and evening peaks of activity under LD cycles

Under LD cycles, *Drosophila* displays an anticipatory morning peak and an anticipatory evening peak of activity, both of which are under circadian control (reviewed by (30)). Previous work employing cell ablation and genetic rescue approaches established that the LN_vs function as a "morning oscillator" that generates the morning peak of activity, and the LN_ds and 5^{th} s-LN_v collectively function as an "evening oscillator" that generates the evening peak of activity (8). Similar experimental approaches revealed that the CRY^+ $DN1_p$s promote both morning and evening activity, depending on the experimental conditions (13, 15). Here, we have re-evaluated the roles of these three groups of clock neurons in the control of morning and evening bouts of activity in the context of an otherwise fully functional clock network, by genetically accelerating or decelerating the LN_v, LN_d, and CRY^+ $DN1_p$ molecular clocks and examining the effects on the timing of morning and evening activity bouts.

Consistent with their previous designation as the "evening oscillator", speeding-up and slowing-down the molecular clocks of LN_ds and 5^{th} s-LN_v resulted in significantly advanced and delayed evening peaks, respectively, without significant influence on the phase of the morning

peak (Fig. 5.2A-B). Quite unexpectedly, we found that both the LN_vs and the CRY^+ $DN1_p$s advanced the morning peak but not the evening peak when their clocks were sped-up, and delayed the evening peak but not the morning peak when their clocks were slowed-down (Fig. 5.2C-D and Fig. 5.4D-G). This result is not predicted by current models, which predict that under a 12:12 bright LD cycle at 25°C the LN_vs and the CRY^+ $DN1_p$s should only contribute to the timing of the morning peak of activity (8, 9, 13). Our finding that their clock speed can also affect the timing of the evening peak suggests that they might have direct control over the evening peak as well, or alternatively that they influence the evening peak via the LN_ds and 5^{th} s-LN_v. We consider the latter likely, given our finding that the LN_vs are capable of delaying a subset of the "evening oscillator" neurons, but not advancing any of them (Fig. 5.3). We note that this unexpected influence on the evening peak was apparent only when their molecular clocks were slowed-down, highlighting the importance of bidirectional manipulations of clock speed in the context of clock interactions. The LN_vs and CRY^+ $DN1_p$s were not capable of delaying the morning peak when DBT^L was overexpressed in these neurons, but this was the case even when DBT^L was expressed in all circadian clock expressing cells (Fig. 5.1A-B), suggesting that the three-hour increase in period caused by the manipulation is never enough to overcome the light entrainment and masking of the morning peak. Finally, changing the clock speed only in the lateral neurons (LN_vs, 5^{th} s-LN_v, and LN_ds) is sufficient to reset the phases of morning and evening peaks under LD. This is not in conflict with the contention that the CRY^+ $DN1_p$s contribute to the timing of activity peaks, as we have shown that their molecular clocks would be coupled to those of the LN_vs even when they are not genetically altered. We propose that clock neurons do not act in isolation to control the daily activity peaks. Rather, we propose that coupling and interactions among clock neuron groups influence the timing of activity peaks and

shape activity patterns, and that changes in these interactions are the basis for clock network plasticity in response to environmental changes.

5.4.3 A distributed clock network controls free-running activity rhythms

It has been known for more than a decade that the PDF-expressing LN_vs are critical for free-running activity rhythms. Genetic ablation of the LN_vs, or loss-of-function mutations in *Pdf* or *Pdf receptor* genes result in severely weakened free-running activity rhythms (10, 31-33). Restoring *period* expression only in the LN_vs of the *period* null mutant was sufficient to generate free-running activity rhythms (8). Finally, the LN_vs are capable of imposing their intrinsic period on the overt free-running activity rhythm when their clock speed is genetically altered (5, 17, 23). Nevertheless, clock neurons other than the LN_vs also exert control over free-running activity rhythms (5, 34). For example, the LN_ds and 5^{th} s-LN_v control the evening peak of activity (8), which is largely maintained under constant conditions, and rescuing *period* expression only in the LN_ds and 5^{th} s-LN_v restored free-running rhythms in a large proportion of flies under constant dim light conditions (35).

By genetically changing the clock speed in the LN_vs, the LN_ds and 5^{th} s-LN_v, and the CRY^+ $DN1_p$s, we examined how these three groups of clock neurons, alone or in combination, influence free-running activity rhythm in the context of an otherwise normally functional clock network. When the clock speed is altered in each of the three groups alone, only the LN_vs have significant influence on free-running period, consistent with the longstanding notion that LN_vs have the strongest control on the pace of free-running activity rhythms among these three groups (Fig. 5.6C-E and Table 5.S2). Surprisingly, even though the lateral neurons together are capable of coherently resetting the phase of activity peaks in LD (Fig. 5.5C-D), they are not capable of coherently driving free-running rhythms under DD (Fig. 5.6G-I and Table 5.S2). This is most

apparent when they were sped-up through *DBT*^{S} overexpression. Even when *DBT*^{S} was overexpressed in the CRY^{+} DN1$_{p}$s and a large subset of lateral neurons, the free-running activity rhythm was not coherently reset (Fig. 5.6J-K and Table 5.S2). Only when *DBT*^{S} was overexpressed in the CRY^{+} DN1$_{p}$s and in every lateral neuron, did we observe a nearly complete and coherent resetting of free-running period (Fig. 5.6L and Table 5.S2). Therefore, a strong and coherent free-running activity rhythm requires a surprisingly large proportion of the fly's 150 clock neurons to cycle in synchrony.

Based on our results, we suggest that the lateral neurons plus the CRY^{+} DN1$_{p}$s likely represent the minimal subset of clock neurons that must oscillate in synchrony to drive a coherent free-running rhythm in locomotion. Nevertheless, flies overexpressing *DBT*^{S} in this minimal subset still display weaker rhythms and a higher incidence of arrhythmicity when compared to those overexpressing *DBT*^{S} in all clock cells (Fig. 5.S3L and Table 5.S2), suggesting that some or all of the remaining neurons in the network normally contribute to free-running rhythms. Thus, free-running rhythms in activity are controlled by a larger and more distributed clock network than previously thought.

5.5 Materials and Methods

5.5.1 Fly strains

Flies were reared on cornmeal-sucrose-yeast media at 25 °C under 12-hour light: 12-hour dark (LD) cycles, or at room temperature under the quasi-diurnal conditions of the lab. All of the fly strains used in this study have been described previously, they are: *UAS-DBT*^{S}*(10F5A)* and *UAS-DBT*^{L}*(22F1C)(19)*, *UAS-SGG*^{Y214F}*(hypomorphic SGG mutant)* (Bloomington Stock # 6817)

(5, 36), *nSyb-GAL4* (37), *Clk(856)-GAL4* (38), *Pdf-GAL4* (10, 39), *Clk4.1M-GAL4* (13, 14), *Mai179-GAL4* (8, 40), *Pdf-GAL80* (9), and *DvPdf-GAL4* (41).

5.5.2 Locomotor activity rhythm recording and analysis

Locomotor activity rhythms of adult male flies were recorded using the TriKinetics DAM2 *Drosophila* Activity Monitors (Waltham, MA). Flies aged a week or less were placed individually in recording glass tubes containing 2% agar-4% sucrose food, and these were loaded onto the DAM2 monitors for locomotor activity recording. Flies were entrained to 12:12 LD cycles for at least 5 days, and subsequently released into constant darkness (DD) for at least 7 days, at a constant temperature of 25°C. Activity counts were collected in either 5-minute or 1-minute bins that were subsequently summed into 30-minute bins for time-series analysis.

Averaged population activity profiles (also known as “eduction plots”) of specific genotypes in LD were generated using the Counting Macro, an Excel-based program, which has been described previously (42). First, activity levels were normalized among individual flies, such that for each individual fly the average activity value of all bins for the last four days in LD equals 1. Second, the population average of normalized activity is determined for any given 30-min bin for the last four days in LD. Finally, the population activity for these four days is averaged into a single 24-hour day, and the results are displayed in the figures.

The phases of morning and evening peaks of individual flies were determined as follows. First, activity of the last three days in LD was averaged to generate an average activity profile for each individual fly. This average single-day activity profile was filtered with a zero-phase Butterworth filter to diminish oscillations with periods of less than 20 hours (43). The filtered activity profile was plotted in Matlab (MathWorks, Natick, MAMathworks, Inc.), and the ‘Findpeaks’ function in the Signal Processing Toolbox of Matlab was used to identify the

morning and evening peaks of activity, and their corresponding phases. An experimenter who was blind to the genotypes manually confirmed the accuracy of morning and evening peaks identified by the 'Findpeaks' function. The phases of morning and evening peaks of an experimental genotype were compared to those of the corresponding *GAL4* and *UAS* controls using the Kruskal-Wallis one-way ANOVA and Dunn's multiple comparison test. Significance was only reported if the experimental genotypes differed significantly from both controls in the same direction, and only the smaller significance value is reported in the figures.

The analysis of free-running activity rhythms was done using the ClockLab software from Actimetrics (Wilmette, IL) as previously described (5). In brief, rhythmicity and free-running period of individual flies were determined using the χ-square periodogram function implemented in ClockLab, with a confidence level of 0.01 (44). For all the genotypes, the range of free-running periods analyzed was from 14 hours to 34 hours, with 0.5-hour intervals. For individuals with more than one significant period, only the period with the highest amplitude over significance was used for the scatter plots of free-running periods in the figures and the determination of average periods in Table 5.S2. For each significant period, the χ-square analysis in Clock Lab returns a "Power" value and a "Significance" value. "Rhythmic Power" was calculated as "Rhythmic Power = Power – Significance" for rhythmic flies, and considered "0" for arrhythmic flies, as previously described (5, 42).

5.5.3 Immunocytochemistry

Immunostaining of whole-mount *Drosophila* brains was done as previously described (5). Flies were entrained to LD cycles for a minimum of three days and then released into DD. Flies were collected every six hours for four time points on the third day under DD for DBT^{S} overexpressing flies, and on the fourth day under DD for the other manipulations. Dissected

brains were fixed in 4% paraformaldehyde for 1 hour at room temperature, blocked with 3% normal goat serum for 1 hour at room temperature, and stained with rat anti-PER antibodies (1:500) (provided by Dr. Michael Rosbash, (45)) at 4 °C for two nights and then rinsed in PBS-TX. LN_vs were identified by co-staining the brains with mouse anti-PDF antibodies (1:200) (Developmental Studies Hybridoma Bank, contributed by Dr. Justin Blau). CRY^+ $DN1_p$s were identified by co-staining the brains with rabbit anti-CRY antibodies (1:500) (provided by Dr. Charlotte Helfrich-Förster, (46)). Alexa Fluor conjugated secondary antibodies were used at 1:1000 (Invitrogen, Grand Island, NY) at 4 °C overnight and then rinsed in PBS-TX. Brains were mounted for imaging in Vectashield HardSet Mounting Medium (Vector Laboratories, Burlingame, CA). All samples were imaged on an Olympus Fluoview 1000 confocal microscope with a 60×/1.10 NA objective (Olympus, Center Valley, PA). Imaging settings were tailored for each class of clock neurons, but were kept constant for all time points and genotypes within a neuronal class. PER immunostaining intensity of individual clock neurons was quantified using the ImageJ software (National Institutes of Health, USA) as previously described (47). Both hemispheres of about ten brains were used for quantification at each time point.

5.6 Supplementary Results

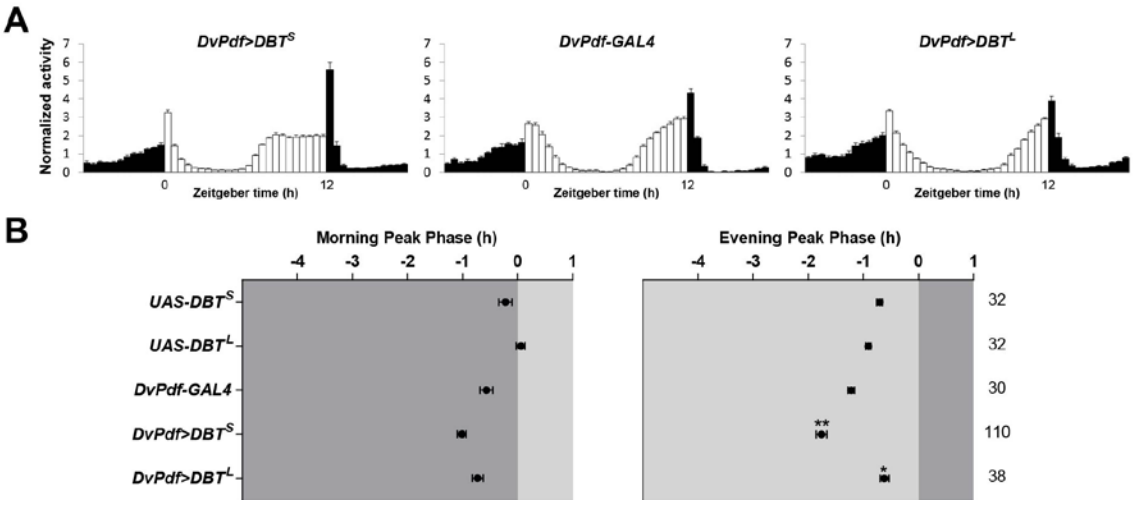

Figure 5.S1. The *DvPdf-GAL4* expressing neurons are not sufficient to fully reset the phases of activity peaks under LD.
(*A*) LD population averaged activity profiles of flies overexpressing DBT^S and DBT^L in subsets of the lateral clock neurons under the *DvPdf-GAL4* driver (*Table 5.S1*) and the *DvPdf-GAL4* control flies. *(B)* The average phases of morning and evening activity peaks under LD of the indicated genotypes. "0" marks the time of lights-on for the left panel and the time of lights-off for the right panel. Dark gray indicates darkness and light gray indicates light. The numbers of flies analyzed are indicated on the right. * $P < 0.05$; ** $P < 0.01$. See *Materials and Methods* for details of the statistics. All the data are presented as mean ± SEM.

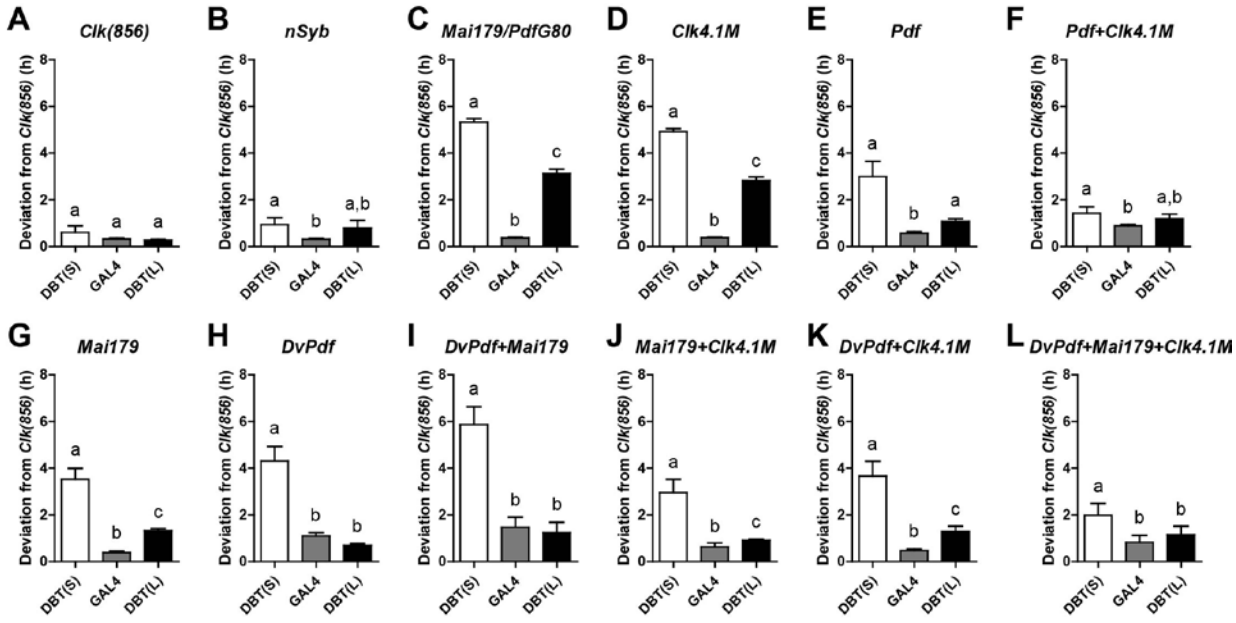

Figure 5.S2. Deviation of free-running periods for each *GAL4* manipulation from the expected free-running periods.

(*A-L*) The absolute deviation of free-running periods from the expected periods for *GAL4* control flies and flies overexpressing DBT^S and DBT^L under the indicated drivers. The means of the free-running periods of the *Clk(856)-GAL4* manipulations are taken as the expected free-running periods, i.e. the expected period for DBT^S overexpression is 18.5h, for DBT^L overexpression 26.8h, and for *GAL4* control 23.8h. For each *GAL4* manipulation, the absolute deviation (without signs) of free-running periods from the respective expected period was calculated and plotted as mean ± SEM in the graphs. A small deviation value indicates that the free-running periods are close to the expected period for that specific manipulation. For each panel, groups that do not share a letter ("a", "b", or "c") are significantly different from each other ($P < 0.05$, by Kruskal-Wallis one-way ANOVA and Dunn's multiple comparisons test).

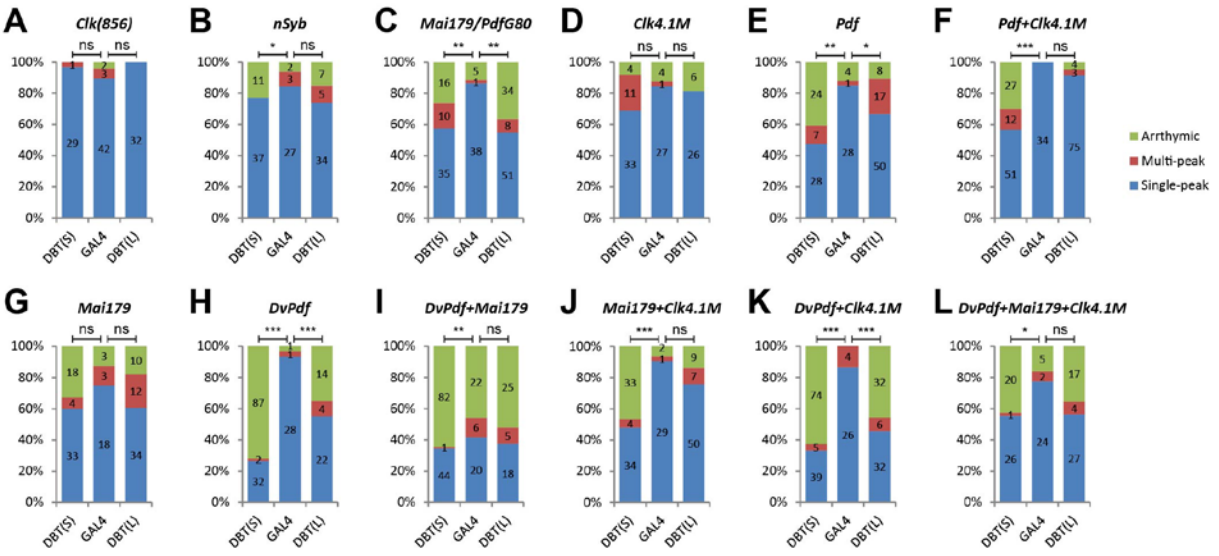

Figure 5.S3. Rhythmicity and internal desynchronization of free-running rhythms for each *GAL4* manipulation.

(*A-L*) The percentages of arrhythmic flies, rhythmic flies displaying a single significant period, and rhythmic flies displaying multiple significant periods for *GAL4* control flies and flies overexpressing DBT^S and DBT^L under the indicated drivers. The numbers of flies in each category are displayed on each bar of the histogram. * P < 0.05; ** P < 0.01; *** P < 0.001; ns, not significant, by the Freeman-Halton extension of the Fisher's exact test.

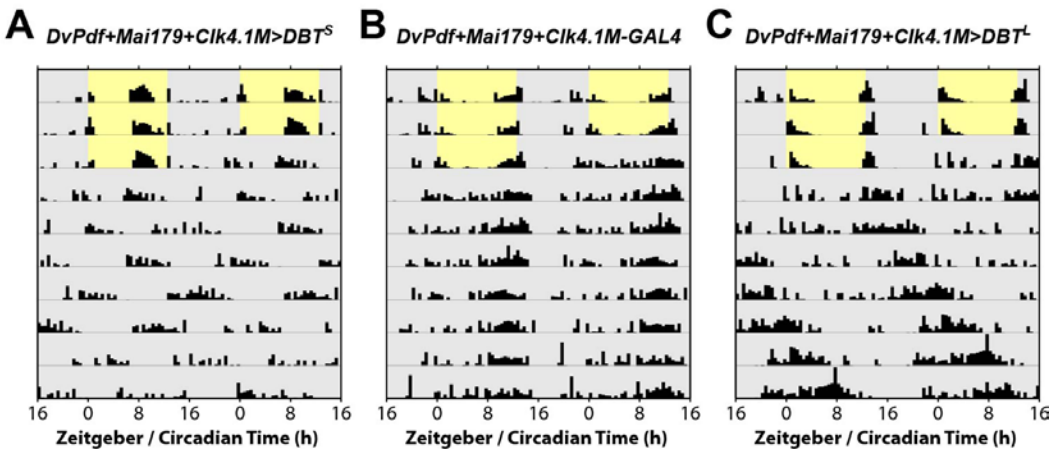

Figure 5.S4. The CRY$^+$ DN1$_p$s and all of the lateral clock neurons together are capable of coherently resetting free-running activity rhythms.
(*A*-*C*) Representative individual actograms of the *GAL4* control (*B*) and flies overexpressing *DBT^S* (*A*) and *DBT^L* (*C*) in the CRY$^+$ DN1$_p$s and all of the lateral clock neurons, through a combined use of *DvPdf-GAL4*, *Mai179-GAL4*, and *Clk4.1M-GAL4* (*Table 5.S1*). The actograms are double-plotted for two consecutive days. Yellow indicates light and gray indicates darkness.

Table 5.S1. Expression patterns of *GAL4* drivers.

GAL4 driver	Expression pattern
nSyb-GAL4	All neurons (37)
Clk(856)-GAL4	All major groups of clock neurons (38)
Pdf-GAL4	l-LN_vs, s-LN_vs (10, 39)
Clk4.1M-GAL4	High expression in ~4-5 $DN1_p$s, weaker expression in another ~4-5 $DN1_p$s; the majority express CRY (13, 14).
Mai179-GAL4	s-LN_vs, 3 CRY^+ LN_ds, 5^{th} s-LN_v, weak and variable expression in l-LN_vs, and many non-clock neurons (8, 46, 48).
Mai179-GAL4/Pdf-GAL80	3 CRY^+ LN_ds, 5^{th} s-LN_v, and many non-clock neurons
DvPdf-GAL4	l-LN_vs, s-LN_vs, 4 LN_ds (1 CRY^+, 3CRY^-), 5^{th} s-LN_v (34, 41)

Table 5.S2. Summary of free-running locomotor activity rhythms.

Genotype	Number of flies	% Rhythmic	% Multi-periodicity*	Period ± SEM (h)	Rhythmic Power ± SEM
;;UAS-DBT(S)/+	37	94.6	0	23.5 ± 0.1	54.4 ± 7.2
;;UAS-DBT(L)/+	44	97.7	7.0	23.6 ± 0.2	72.9 ± 6.2
;Clk(856)-GAL4/+;	47	95.7	6.7	23.8 ± 0.1	45.0 ± 4.9
;Clk(856)-GAL4/+;UAS-DBT(S)/+	30	100	3.3	18.5 ± 0.3	57.7 ± 7.9
;Clk(856)-GAL4/+;UAS-DBT(L)/+	32	100	0	26.8 ± 0.1	77.3 ± 7.6
;;nSyb-GAL4/+	32	93.8	10.0	23.8 ± 0.1	41.7 ± 8.1
;;nSyb-GAL4/UAS-DBT(S)	48	77.1	0	18.5 ± 0.3	21.7 ± 3.7
;;nSyb-GAL4/UAS-DBT(L)	46	84.8	12.8	26.9 ± 0.3	33.6 ± 5.3
;Mai179-GAL4/Pdf-GAL80;	44	88.6	2.6	23.5 ± 0.1	41.0 ± 4.7
;Mai179-GAL4/Pdf-GAL80;UAS-DBT(S)/+	61	73.8	22.2	23.8 ± 0.2	17.8 ± 2.4
;Mai179-GAL4/Pdf-GAL80;UAS-DBT(L)/+	93	63.4	13.6	23.9 ± 0.2	9.8 ± 1.5
;;Clk4.1M-GAL4/+	32	87.5	3.6	23.8 ± 0.1	34.0 ± 4.9
;;Clk4.1M-GAL4/UAS-DBT(S)	48	91.7	25.0	23.4 ± 0.1	31.6 ± 3.3
;;Clk4.1M-GAL4/UAS-DBT(L)	32	81.3	0	24.0 ± 0.2	18.1 ± 2.6
;Pdf-GAL4/+;	33	87.9	3.4	24.2 ± 0.1	59.7 ± 6.9
;Pdf-GAL4/+;UAS-DBT(S)/+	59	59.3	20.0	21.0 ± 0.7	9.0 ± 1.6
;Pdf-GAL4/+;UAS-DBT(L)/+	75	89.3	25.4	26.7 ± 0.2	25.4 ± 2.4
;Pdf-GAL4/+;Clk4.1M-GAL4/+	34	100	0	24.7 ± 0.1	91.8 ± 6.9
;Pdf-GAL4/+;Clk4.1M-GAL4/UAS-DBT(S)	90	70.0	19.0	19.5 ± 0.3	13.7 ±1.7
;Pdf-GAL4/+;Clk4.1M-GAL4/UAS-DBT(L)	82	95.1	3.8	26.0 ± 0.2	55.1 ± 3.7
;Mai179-GAL4/+;	24	87.5	14.3	23.8 ± 0.1	24.5 ± 4.8
;Mai179-GAL4/+;UAS-DBT(S)/+	55	67.3	10.8	22.0 ± 0.5	6.6 ±1.2
;Mai179-GAL4/+;UAS-DBT(L)/+	56	82.1	26.1	25.6 ± 0.1	22.1 ± 2.3
DvPdf-GAL4/Y;;	30	96.7	3.4	24.6 ± 0.2	46.1 ± 4.9
DvPdf-GAL4/Y;;UAS-DBT(S)/+	121	28.1	5.9	20.8 ± 0.9	1.5 ± 0.3
DvPdf-GAL4/Y;;UAS-DBT(L)/+	40	65.0	15.4	27.4 ± 0.1	17.7 ± 3.5
DvPdf-GAL4/Y;Mai179-GAL4/+;	48	54.2	23.1	24.3 ± 0.5	17.6 ± 4.6
DvPdf-GAL4/Y;Mai179-GAL4/+;UAS-DBT(S)/+	127	35.4	2.2	23.2 ± 0.9	2.7 ± 0.5
DvPdf-GAL4/Y;Mai179-GAL4/+;UAS-DBT(L)/+	48	47.9	21.7	26.0 ± 0.5	8.3 ± 2.1
;Mai179-GAL4/+;Clk4.1M-GAL4/+	32	93.8	3.3	23.4 ± 0.2	20.3 ± 3.1
;Mai179-GAL4/+;Clk4.1M-GAL4/UAS-DBT(S)	71	53.5	10.5	21.3 ± 0.6	4.1 ± 0.7
;Mai179-GAL4/+;Clk4.1M-GAL4/UAS-DBT(L)	66	86.4	12.3	26.0 ± 0.1	19.8 ± 2.1

DvPdf-GAL4/Y;;Clk4.1M-GAL4/+	30	100	13.3	23.6 ± 0.1	66.9 ± 7.1
DvPdf-GAL4/Y;;Clk4.1M-GAL4/UAS-DBT(S)	118	37.3	11.4	20.6 ± 0.8	5.3 ± 1.1
DvPdf-GAL4/Y;;Clk4.1M-GAL4/UAS-DBT(L)	70	54.3	15.8	26.6 ± 0.3	8.9 ± 1.6
DvPdf-GAL4/Y;Mai179-GAL4/+;Clk4.1M-GAL4/+	31	83.9	7.7	23.0 ± 0.3	31.8 ± 5.6
DvPdf-GAL4/Y;Mai179-GAL4/+;Clk4.1M-GAL4/UAS-DBT(S)	47	57.4	3.7	17.7 ± 0.6	9.2 ± 1.9
DvPdf-GAL4/Y;Mai179-GAL4/+;Clk4.1M-GAL4/UAS-DBT(L)	48	64.6	12.9	26.0 ± 0.4	12.4 ± 2.9

* % Multi-periodicity indicates the percentage of rhythmic individuals that display more than one significant periodicity.

5.7 Acknowledgements

This work was supported by the NIH (NINDS) grant R01NS077933 to O.T.S. Z.Y. was further supported by the Rackham Predoctoral Fellowship (University of Michigan). We thank J. L. Price, P. H. Taghert, M. Rosbash, F. Rouyer, N. R. Glossop, P. E. Hardin, P. Emery, J. H. Park, and the Bloomington *Drosophila* Stock Center for providing fly stocks. We thank M. Rosbash for the PER antisera, C. Helfrich-Förster for the CRY antisera, and the Developmental Studies Hybridoma Bank for the monoclonal PDF antibodies. We thank J. D. Levine for providing Matlab codes for signal analysis, and R. Allada for providing the Counting Macro. Finally, we thank María de la Paz Fernandez and Paul Taghert for reading and discussing a draft of this manuscript.

5.8 References

1. Herzog ED (2007) Neurons and networks in daily rhythms. *Nat Rev Neurosci* 8(10):790-802.
2. Welsh DK, Takahashi JS, & Kay SA (2010) Suprachiasmatic Nucleus: Cell Autonomy and Network Properties. *Annual Review of Physiology* 72(1):551-577.
3. Nitabach MN & Taghert PH (2008) Organization of the Drosophila Circadian Control Circuit. *Current Biology* 18(2):R84-R93.
4. Vansteensel MJ, Michel S, & Meijer JH (2008) Organization of cell and tissue circadian pacemakers: A comparison among species. *Brain Research Reviews* 58(1):18-47.
5. Yao Z & Shafer OT (2014) The Drosophila circadian clock is a variably coupled network of multiple peptidergic units. *Science* 343(6178):1516-1520.
6. Hermann-Luibl C & Helfrich-Förster C (2015) Clock network in Drosophila. *Current Opinion in Insect Science* 7:65-70.
7. Yoshii T, Rieger D, & Helfrich-Förster C (2012) Two clocks in the brain: An update of the morning and evening oscillator model in Drosophila. *Progress in Brain Research*, eds Andries Kalsbeek MMTR & Russell GF (Elsevier), Vol Volume 199, pp 59-82.
8. Grima B, Chelot E, Xia R, & Rouyer F (2004) Morning and evening peaks of activity rely on different clock neurons of the Drosophila brain. *Nature* 431(7010):869-873.

9. Stoleru D, Peng Y, Agosto J, & Rosbash M (2004) Coupled oscillators control morning and evening locomotor behaviour of Drosophila. *Nature* 431(7010):862-868.

10. Renn SCP, Park JH, Rosbash M, Hall JC, & Taghert PH (1999) A pdf Neuropeptide Gene Mutation and Ablation of PDF Neurons Each Cause Severe Abnormalities of Behavioral Circadian Rhythms in Drosophila. *Cell* 99(7):791-802.

11. Peng Y, Stoleru D, Levine JD, Hall JC, & Rosbash M (2003) Drosophila Free-Running Rhythms Require Intercellular Communication. *PLoS Biol* 1(1):e13.

12. Lin Y, Stormo GD, & Taghert PH (2004) The Neuropeptide Pigment-Dispersing Factor Coordinates Pacemaker Interactions in the Drosophila Circadian System. *J. Neurosci.* 24(36):7951-7957.

13. Zhang Y, Liu Y, Bilodeau-Wentworth D, Hardin PE, & Emery P (2010) Light and Temperature Control the Contribution of Specific DN1 Neurons to Drosophila Circadian Behavior. *Current biology : CB* 20(7):600-605.

14. Zhang L, *et al.* (2010) DN1p Circadian Neurons Coordinate Acute Light and PDF Inputs to Produce Robust Daily Behavior in Drosophila. *Current Biology* 20(7):591-599.

15. Fujii S & Amrein H (2010) Ventral lateral and DN1 clock neurons mediate distinct properties of male sex drive rhythm in Drosophila. *Proceedings of the National Academy of Sciences* 107(23):10590-10595.

16. Cavanaugh DJ, *et al.* (2014) Identification of a circadian output circuit for rest:activity rhythms in Drosophila. *Cell* 157(3):689-701.

17. Stoleru D, Peng Y, Nawathean P, & Rosbash M (2005) A resetting signal between Drosophila pacemakers synchronizes morning and evening activity. *Nature* 438(7065):238-242.

18. Stoleru D, *et al.* (2007) The Drosophila Circadian Network Is a Seasonal Timer. *Cell* 129(1):207-219.

19. Muskus MJ, Preuss F, Fan J-Y, Bjes ES, & Price JL (2007) Drosophila DBT Lacking Protein Kinase Activity Produces Long-Period and Arrhythmic Circadian Behavioral and Molecular Rhythms. *Molecular and Cellular Biology* 27(23):8049-8064.

20. Ito C & Tomioka K (2016) Heterogeneity of the Peripheral Circadian Systems in Drosophila melanogaster: A Review. *Front Physiol* 7:8.

21. Hardin PE (2011) Molecular genetic analysis of circadian timekeeping in Drosophila. *Adv Genet* 74:141-173.

22. Martinek S, Inonog S, Manoukian AS, & Young MW (2001) A Role for the Segment Polarity Gene shaggy/GSK-3 in the Drosophila Circadian Clock. *Cell* 105(6):769-779.

23. Beckwith EJ & Ceriani MF (2015) Experimental assessment of the network properties of the Drosophila circadian clock. *J Comp Neurol* 523(6):982-996.

24. Albus H, Vansteensel MJ, Michel S, Block GD, & Meijer JH (2005) A GABAergic Mechanism Is Necessary for Coupling Dissociable Ventral and Dorsal Regional Oscillators within the Circadian Clock. *Current biology : CB* 15(10):886-893.

25. Nagano M, *et al.* (2003) An abrupt shift in the day/night cycle causes desynchrony in the mammalian circadian center. *J Neurosci* 23(14):6141-6151.

26. Shafer OT, *et al.* (2008) Widespread Receptivity to Neuropeptide PDF throughout the Neuronal Circadian Clock Network of Drosophila Revealed by Real-Time Cyclic AMP Imaging. 58(2):223-237.

27. Im SH & Taghert PH (2010) PDF receptor expression reveals direct interactions between circadian oscillators in Drosophila. *The Journal of Comparative Neurology* 518(11):1925-1945.

28. Seluzicki A, *et al.* (2014) Dual PDF signaling pathways reset clocks via TIMELESS and acutely excite target neurons to control circadian behavior. *PLoS Biol* 12(3):e1001810.

29. Yoshii T, *et al.* (2009) The Neuropeptide Pigment-Dispersing Factor Adjusts Period and Phase of Drosophila's Clock. *The Journal of Neuroscience* 29(8):2597-2610.

30. Hall JC (2003) Genetics and molecular biology of rhythms in Drosophila and other insects. *Adv Genet* 48:1-280.

31. Hyun S, *et al.* (2005) Drosophila GPCR Han Is a Receptor for the Circadian Clock Neuropeptide PDF. 48(2):267-278.

32. Lear BC, *et al.* (2005) A G Protein-Coupled Receptor, groom-of-PDF, Is Required for PDF Neuron Action in Circadian Behavior. 48(2):221-227.

33. Mertens I, *et al.* (2005) PDF Receptor Signaling in Drosophila Contributes to Both Circadian and Geotactic Behaviors. *Neuron* 48(2):213-219.

34. Guo F, Cerullo I, Chen X, & Rosbash M (2014) PDF neuron firing phase-shifts key circadian activity neurons in Drosophila. *Elife* 3.

35. Rieger D, Wülbeck C, Rouyer F, & Helfrich-Förster C (2009) Period Gene Expression in Four Neurons Is Sufficient for Rhythmic Activity of Drosophila melanogaster under Dim Light Conditions. *Journal of Biological Rhythms* 24(4):271-282.

36. Bourouis M (2002) Targeted increase in shaggy activity levels blocks wingless signaling. *genesis* 34(1-2):99-102.

37. Pauli A, *et al.* (2008) Cell-type-specific TEV protease cleavage reveals cohesin functions in Drosophila neurons. *Dev Cell* 14(2):239-251.

38. Gummadova JO, Coutts GA, & Glossop NRJ (2009) Analysis of the Drosophila Clock Promoter Reveals Heterogeneity in Expression between Subgroups of Central Oscillator Cells and Identifies a Novel Enhancer Region. *Journal of Biological Rhythms* 24(5):353-367.

39. Park JH, *et al.* (2000) Differential regulation of circadian pacemaker output by separate clock genes in Drosophila. *Proc Natl Acad Sci U S A* 97(7):3608-3613.

40. Siegmund T & Korge G (2001) Innervation of the ring gland of Drosophila melanogaster. *The Journal of Comparative Neurology* 431(4):481-491.

41. Bahn JH, Lee G, & Park JH (2009) Comparative analysis of Pdf-mediated circadian behaviors between Drosophila melanogaster and D. virilis. *Genetics* 181(3):965-975.

42. Pfeiffenberger C, Lear BC, Keegan KP, & Allada R (2010) Processing Circadian Data Collected from the Drosophila Activity Monitoring (DAM) System. *Cold Spring Harbor Protocols* 2010(11):pdb.prot5519.

43. Levine JD, Funes P, Dowse HB, & Hall JC (2002) Signal analysis of behavioral and molecular cycles. *BMC Neurosci* 3:1.

44. Sokolove PG & Bushell WN (1978) The chi square periodogram: Its utility for analysis of circadian rhythms. *Journal of Theoretical Biology* 72(1):131-160.

45. Liu X, Lorenz L, Yu QN, Hall JC, & Rosbash M (1988) Spatial and temporal expression of the period gene in Drosophila melanogaster. *Genes & Development* 2(2):228-238.

46. Yoshii T, Todo T, Wülbeck C, Stanewsky R, & Helfrich-Förster C (2008) Cryptochrome is present in the compound eyes and a subset of Drosophila's clock neurons. *The Journal of Comparative Neurology* 508(6):952-966.

47. Shafer OT, Rosbash M, & Truman JW (2002) Sequential Nuclear Accumulation of the Clock Proteins Period and Timeless in the Pacemaker Neurons of Drosophila melanogaster. *J. Neurosci.* 22(14):5946-5954.

48. Shafer OT & Taghert PH (2009) RNA-Interference Knockdown of Drosophila Pigment Dispersing Factor in Neuronal Subsets: The Anatomical Basis of a Neuropeptide's Circadian Functions. *PLoS ONE* 4(12):e8298.

CHAPTER 6. Concluding Remarks

Using *Drosophila* as a simple yet conserved model system, my thesis research aims to understand how circadian clock neurons are physiologically connected and how their molecular timekeeping is functionally coordinated to produce robust and coherent circadian rhythms. In support of these aims I first developed a new experimental approach to address physiological connectivity in the *Drosophila* brain, and characterized several important connections within the *Drosophila* clock neuron network using this approach. I have provided the first electrophysiological characterization of the critical LN_d clock neurons and revealed how they integrate distinct fast synaptic inputs to control the daily timing of sleep and activity. Furthermore, I have found that the *Drosophila* clock neuron network features diverse modes of coupling between the various clock neuron classes. Lastly, I revealed that the *Drosophila* clock neuron network consists of multiple independent oscillators and requires network-wide coherence for robust circadian rhythms in activity and sleep. My thesis research greatly advances our understanding of how the circadian clock neuron network is wired, organized, and coordinated. Given that disruption of circadian rhythms is associated with increased risks of a large spectrum of diseases, including obesity, heart diseases, cancer, and mood disorders (Albrecht, 2012), my thesis research may help address the widespread adverse effects of circadian rhythm disorders. Here, I summarize the key findings and implications of my thesis research as follows.

6.1 A new approach to address functional neuronal connectivity in the *Drosophila* brain

Chapter 2 describes a new experimental approach that my colleagues and I developed for analyzing functional neuronal connections in the *Drosophila* brain. In this approach, the mammalian ATP-gated cation channel P2X2 is genetically expressed in neurons of interest to render them excitable by ATP on demand, while genetically encoded fluorescent sensors are simultaneously expressed in putative postsynaptic neurons to monitor their response upon the excitation of P2X2-expressing neurons. This approach has proved powerful, versatile, yet technically facile, and is now being widely used in the field of *Drosophila* neurobiology (e.g., Haynes et al., 2015; Kallman et al., 2015).

6.2 Physiological connectivity within the *Drosophila* clock neuron network

Using the experimental approach my colleagues and I developed for neuronal connectivity analysis, I have confirmed a long predicted peptidergic connection from the LN_vs to the LN_ds mediated by PDF, and showed that it is a modulatory connection that results in cAMP increases without causing acute excitation in the LN_ds (Chapter 2). Furthermore, I show that within the LN_v group, PDF secreted from the l-LN_vs acts to specifically increase cAMP levels but not calcium levels in the s-LN_vs (Fig. 6.1 and Chapter 2). Lastly, using ATP/P2X2-mediated excitation of the glutamatergic $DN1_p$s in conjunction with whole-cell patch-clamp recording of the LN_ds and l-LN_vs, I uncover inhibitory connections from the $DN1_p$s to the LN_ds and to the l-LN_vs (Chapter 3). Together, I have begun to delineate the neuronal connections between important groups of clock neurons. An extension of this experimental approach will allow the characterization of functional connectivity between other groups of clock neurons, and between clock neurons and potential input and output pathways.

6.3 Electrophysiological characterization of the critical LN_d clock neurons

In Chapter 3, I have provided the first electrophysiological analysis of the critical LN_d clock neurons, which are considered collectively as the evening oscillator of the clock neuron network (Grima et al., 2004; Stoleru et al., 2004). I found that the LN_ds fire spontaneous tonic and bursting patterns of action potentials, and that the LN_d neuronal activity is modulated by multiple fast neurotransmitters. Specifically, the LN_ds are excited by acetylcholine via nicotinic acetylcholine receptors, and inhibited by GABA and glutamate via $GABA_A$ receptors and the glutamate-gated chloride channel GluClα, respectively. The LN_ds' receptivity to multiple fast neurotransmitters is in striking similarity to that of the LN_vs (McCarthy et al., 2011; Lelito and Shafer, 2012). Using genetic and behavioral approaches, I found that while GABAergic inhibition of the lateral clock neurons functions to promote sleep at night, glutamatergic inhibition of the same neurons functions to promote wakefulness during specific times of the day. These results advance our understanding of the neurophysiological properties of central clock neurons and reveal how the various clock neuron classes integrate distinct synaptic inputs to orchestrate circadian rhythms in sleep and activity.

6.4 Diverse modes of coupling between the various clock neuron groups

In Chapter 4 and Chapter 5, using a genetic strategy to specifically speed-up or slow-down the LN_v molecular clocks, I experimentally investigated if and how molecular clocks of the various clock neuron classes are coupled to the critical LN_v clocks. I found that the molecular clocks of the 5^{th} s-LN_v and most of the LN_ds are not coupled to the LN_vs, while the two pairs of sNPF-expressing LN_ds can only be delayed but not advanced by the LN_vs. In contrast, the CRY-expressing $DN1_p$s can be both delayed and advanced by the LN_vs. These results reveal that the

various classes of clock neurons do not display a uniform mode of coupling. Rather, they display unique and complex coupling relationships that vary from group to group. This may have important implications in the clock network plasticity in the face of changing environments.

6.5 The *Drosophila* clock neuron network consists of multiple oscillators and requires network-wide coherence for robust free-running rhythms

Despite the fact that the clock neuron network features a diversity of cell types that are anatomically and neurochemically distinct, it has been long modeled as a hierarchical two-oscillator network, in which the morning oscillator (the LN_vs) functions as a master pacemaker in the absence of environmental cues. In Chapter 4, through the genetic speeding-up and slowing-down the LN_v clocks to different extents, I find that the LN_vs can set the pace of the clock network only when their intrinsic period differs less than ~2.5 hours from that of the rest of the network. In contrast to the widely accepted "Master Pacemaker" model, my results demonstrate that the clock network consists of multiple oscillatory units, each of which drives rhythms in activity. Furthermore, I find that each oscillatory unit is unified by its neuropeptide output, which might be a general organizing principle that might apply to the circadian clock neuron networks of other animals. Lastly in Chapter 5, by genetically altering the clock speed in different subsets of clock neurons, I show that coherent free-running activity rhythms require molecular clock synchrony at least in all of the lateral clock neurons as well as the $DN1_p$s, which constitute a much larger proportion of the clock neuron network than previously thought. These findings provide insights into the organization and network coordination of the *Drosophila* circadian clock.

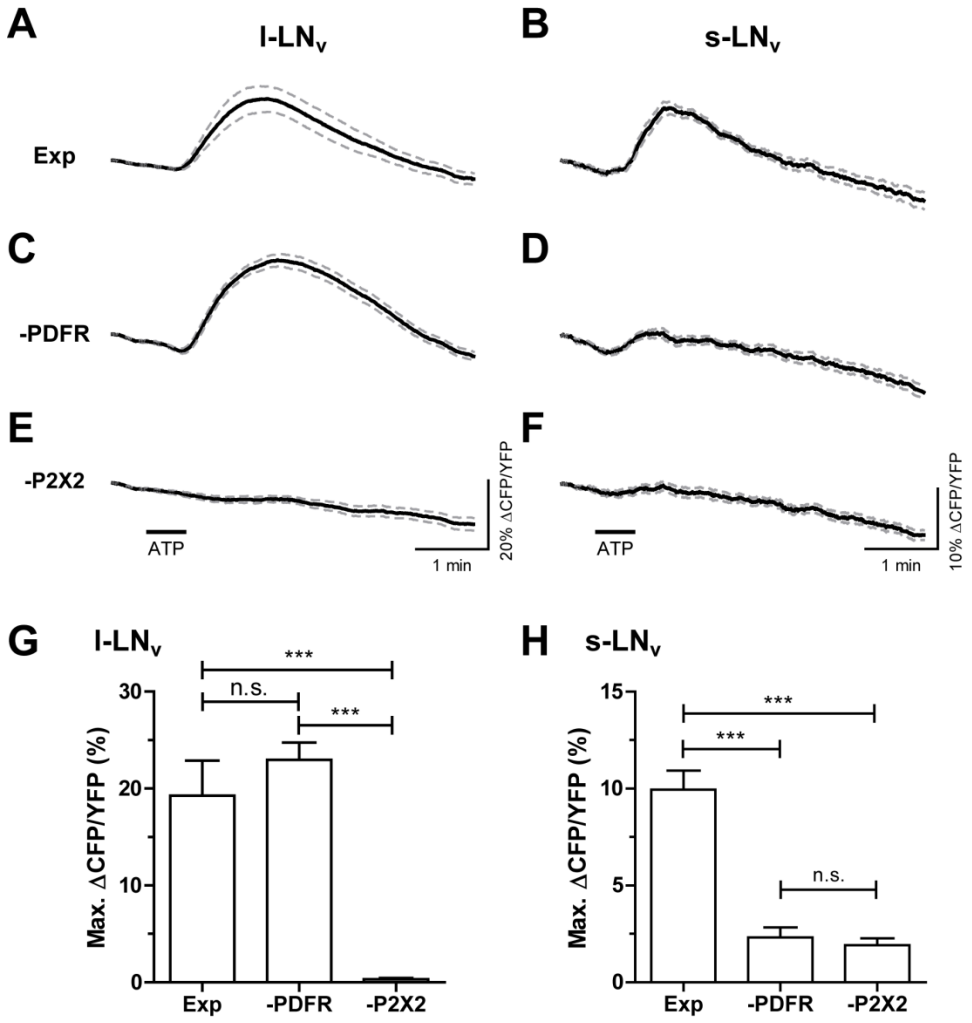

Figure 6.1. The l-LN$_v$s modulate cAMP levels in the s-LN$_v$s.
(**A**) Averaged Epac1-camps inverse FRET plot (±SEM) of l-LN$_v$s imaged in *c929-Gal4/Pdf-LexA,LexAop-Epac1-camps;UAS-P2X2/+* brains, before, during and after 30s perfusion of 1mM ATP (indicated on the bottom plot in each column). ATP/P2X2 mediated excitation caused clear inverse FRET increases. (**B**) Averaged Epac1-camps inverse FRET plot (±SEM) of s-LN$_v$s from the same brains as (A). Excitation of the *c929* network produced inverse FRET increases in the s-LN$_v$s. (**C**) Averaged Epac1-camps inverse FRET plot (±SEM) of l-LN$_v$s imaged in a *Pdfr* mutant background using *han^{5304};c929-GAL4/Pdf-LexA,LexAop-Epac1-camps;UAS-P2X2/+* brains. *c929* network excitation caused clear inverse FRET increases in these neurons. (**D**) Averaged Epac1-camps plot (±SEM) of s-LN$_v$s from the same brains as (C). Excitation of the *c929* network failed to produce inverse FRET increases in the s-LN$_v$s in the absence of PdfR function. (**E**) Averaged Epac1-camps inverse FRET plot (±SEM) of l-LN$_v$s imaged in *Pdf-LexA,LexAop-Epac1-camps/+;UAS-P2X2/+* brains. ATP failed to produce inverse FRET increases in the absence of the *GAL4* driver. The scale bars in (E) also apply to (A) and (C). (**F**) Averaged Epac1-camps inverse FRET plot (±SEM) of s-LN$_v$s from the same brains as (E). ATP

caused no obvious inverse FRET increases. The scale bars in (F) also apply to (B) and (D). (**G**) Comparison of maximum Epac1-camps responses for the l-LN_v data shown in (A), (C), and (E). ATP (1mM) perfusion caused significant inverse FRET increases in both the experimental ("Exp" *c929-GAL4/Pdf-LexA,LexAop-Epac1-camps;UAS-P2X2/+*) and *PdfR* mutant ("-PDFR" *han*^{5304} *;c929-GAL4/Pdf- LexA,LexAop-Epac1-camps;UAS-P2X2/+*) conditions, relative to the negative control lacking the *GAL4* driver for P2X2 expression ("-P2X2" *Pdf-LexA,LexAop-Epac1-camps/+;UAS-P2X2/+*). (**H**) Comparison of maximum Epac1-camps responses for the s-LN_v data shown in (B), (D), and (F). ATP (1mM) perfusion caused significant inverse FRET increases in experimental (Exp) flies relative to both *PdfR* mutant (-PDFR) and -P2X2 controls. Genotypes were identical to those in (G). For (G) and (H), *** indicates $P < 0.001$ and n.s. indicates no significant difference ($P \geq 0.05$), by Kruskal—Wallis one-way ANOVA and Dunn's multiple comparison test. The methods and materials used in this figure are the same as those described in Chapter 2.

6.6 References

Albrecht, U. (2012). Timing to Perfection: The Biology of Central and Peripheral Circadian Clocks. Neuron *74*, 246–260.

Grima, B., Chélot, E., Xia, R., and Rouyer, F. (2004). Morning and evening peaks of activity rely on different clock neurons of the Drosophila brain. Nature *431*, 869–873.

Haynes, P.R., Christmann, B.L., and Griffith, L.C. (2015). A single pair of neurons links sleep to memory consolidation in drosophila melanogaster. Elife *2015*, 1–24.

Kallman, B.R., Kim, H., and Scott, K. (2015). Excitation and inhibition onto central courtship neurons biases Drosophila mate choice. Elife *4*, e11188.

Lelito, K.R., and Shafer, O.T. (2012). Reciprocal cholinergic and GABAergic modulation of the small ventrolateral pacemaker neurons of Drosophila's circadian clock neuron network. J. Neurophysiol. *107*, 2096–2108.

McCarthy, E. V, Wu, Y., Decarvalho, T., Brandt, C., Cao, G., and Nitabach, M.N. (2011). Synchronized bilateral synaptic inputs to Drosophila melanogaster neuropeptidergic rest/arousal neurons. J. Neurosci. *31*, 8181–8193.

Stoleru, D., Peng, Y., Agosto, J., and Rosbash, M. (2004). Coupled oscillators control morning and evening locomotor behaviour of Drosophila. Nature *431*, 862–868.